THE STRUCTURE AND MAGNETIC FABRIC OF THE QUETICO METASEDIMENTARY ROCKS IN THE CALM LAKE - PERCH LAKE AREA, NEAR ATIKOKAN, NORTHWESTERN ONTARIO

by

PERRY SARVAS©

Submitted in partial fulfillment of the
requirements for the degree of
MASTER OF SCIENCE

LAKEHEAD UNIVERSITY, THUNDER BAY, ONTARIO

NOVEMBER, 1987

ProQuest Number: 10611758

All rights reserved

INFORMATION TO ALL USERS
The quality of this reproduction is dependent upon the quality of the copy submitted.

In the unlikely event that the author did not send a complete manuscript
and there are missing pages, these will be noted. Also, if material had to be removed,
a note will indicate the deletion.

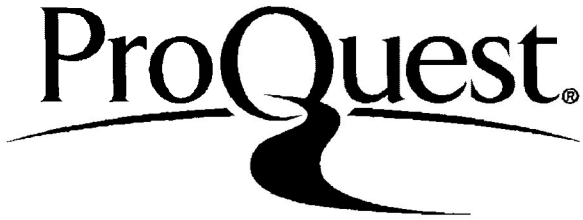

ProQuest 10611758

Published by ProQuest LLC (2017). Copyright of the Dissertation is held by the Author.

All rights reserved.
This work is protected against unauthorized copying under Title 17, United States Code
Microform Edition © ProQuest LLC.

ProQuest LLC.
789 East Eisenhower Parkway
P.O. Box 1346
Ann Arbor, MI 48106 - 1346

Permission has been granted to the National Library of Canada to microfilm this thesis and to lend or sell copies of the film.

The author (copyright owner) has reserved other publication rights, and neither the thesis nor extensive extracts from it may be printed or otherwise reproduced without his/her written permission.

L'autorisation a été accordée à la Bibliothèque nationale du Canada de microfilmer cette thèse et de prêter ou de vendre des exemplaires du film.

L'auteur (titulaire du droit d'auteur) se réserve les autres droits de publication; ni la thèse ni de longs extraits de celle-ci ne doivent être imprimés ou autrement reproduits sans son autorisation écrite.

ISBN 0-315-44793-1

ABSTRACT

The Quetico metasedimentary rocks are the metamorphosed equivalents of a turbidite sequence, comprised of a repetative interstratification of sandstones and mudstones. The rocks are metamorphosed to lower greenschist facies, but metamorphic grade increases progressively from north to south. Anchimetamorphosed phyllites and slates in the north part of the present study area grade progressively into biotite schists in the south part.

Interpretation of structural features in the study area, mainly bedding(S_0) - cleavage(S_1) relationships and structural facing directions, has led to the delineation of a number of major F_1 folds. These are tight to isoclinal, asymmetric *sheath* folds, with axial planes arranged en echelon and slightly oblique to the dominant east-west, vertically-dipping, structural trend. The orientation, geometry and disposition of the F_1 folds suggest the Quectico rocks of the present study area have experienced a regional dextral trans-pressional tectonic evolution, with components of north-south regional shortening and east-west regional dextral shear, with a possible component of vertical (south side up) displacement.

The Quetico metasedimentary rocks have a polymineralllic magnetic mineralogy comprised of significant proportions of a ferrimagnetic (magnetite and pyrrhotite) and a paramagnetic (chlorite, biotite, muscovite) component. The rocks possess a predominantly tectonic magnetic fabric, which consists of a deformational, and a metamorphic, magnetic fabric. In some rocks(especially coarse-grained sandstones with wide-spaced cleavage planes) a depositional magnetic fabric is partially preserved. The complexities involved in having component deformational, metamorphic and depositional magnetic fabrics indicate that the principal magnetic susceptibility directions of the rock's magnetic susceptibility anisotropy cannot be considered reliable indicators of principal finite strain directions in the Quetico metasedimentary rocks. Great care must be taken in interpreting the significance of principal magnetic susceptibility directions.

ACKNOWLEDGEMENTS

This thesis was proposed and supervised by Dr. Graham Borradaile, whose assistance, support, encouragement and criticisms were of substantial contribution. Dr. W. Keeler and Dr. M. Hawton were advisors. I gratefully acknowledge Dr. P. Fralick's comments and ideas, which pertain to the sedimentary features and depositional environment sections of this paper.

Sam Spivak drafted some diagrams, and provided valuable advice on many of the others, in this thesis. Anne Hammond and Diane Crothers provided excellent technical support.

I would like to thank Denver Stone of the A.E.C.L. for sending me copies of his field geology maps relevant to this thesis' study area, and Alan MacTavish, formerly of the Ontario Ministry of Northern Development and Mines, Mines and Minerals Division, for providing some photographic slides of rock outcrops in the study area.

Finally, I would like to thank my family. Their very presence and unfailing support provided me with the confidence I needed to complete this thesis.

This thesis work was funded by NSERC grant A6861 to Dr. Graham Borradaile.

TABLE OF CONTENTS

INTRODUCTION

The Calm Lake - Perch Lake study area is located approximately 240 kilometers west of Thunder Bay and is transected by Ontario provincial highway 11. The study area is underlain by Archean rocks of the Superior structural province of the Canadian Shield. It is at the boundary of the Quetico and Wabigoon subprovinces (Fig. 1). The Quetico metasedimentary rocks of the present area are part of a narrow, continuous strip of anchimetamorphosed clastic sedimentary rocks at the interface of the Quetico and Wabigoon subprovinces.

While the Quetico metasedimentary rocks have been included in a number of geological investigations, only recently has a detailed investigation of structural geology been initiated. Results of these investigations by Borradaile (1982), Dutka (1982), Stubbley (1983) and Stewart (1984) include the delineation of a number of major folds with apparently strongly curvilinear fold axes. Interpretation of the genesis of these folds, however, is hampered by a general paucity of outcrop exposure and a lack of regional strain markers.

A study of the magnetic fabric of the rocks may assist structural interpretation. It has been demonstrated elsewhere that principal directions of the *magnitude ellipsoid of magnetic susceptibility* of deformed rocks can be reliable indicators of finite strain directions.

The purpose of the present study, then, is to investigate the structural geology and magnetic fabric of the Quetico metasedimentary rocks in the Calm Lake - Perch Lake area in order to provide some insight into the tectonic evolution of these rocks at a major subprovince boundary.

CHAPTER ONE
PREVIOUS STUDIES

1-1. Introduction.

The present study area is located at the boundary of two Archean east-west trending lithological belts or subprovinces (Fig. 1). The north belt is termed the Wabigoon subprovince. It is a granite-greenstone terrane comprised of metamorphosed mafic to felsic volcanic and volcanogenic rocks, and associated chemical and clastic metasediments. These are intruded over extensive areas by felsic to intermediate batholiths and plutons. To the south, the Quetico belt consists of metamorphosed lithic arenites, siltstones and slates, with a central axis of schists, paragneisses and migmatites derived from the sedimentary rocks.

Within the present study area, and throughout much of the Quetico-Wabigoon interface, the boundary of the two subprovinces is characterized by a discrete, relatively narrow zone of fault rocks. The rocks define the Quetico fault zone, a major, transcurrent fault with an indeterminant amount of dextral movement. West of Calm Lake (see Fig. 2), the fault apparently bifurcates. The western extension of the Quetico Fault is contained entirely within the Wabigoon subprovince, while the Quetico-Wabigoon belt boundary is defined by another fault, termed the Seine River Fault.

1-2. Previous Studies of General Geology.

The present study area is part of a much wider area that has been involved in a long history of investigation and controversial geological research. Lawson's(1888) first study of the rocks in the

Figure 1. Archean lithological subprovinces of the Canadian Shield with the location of the present study area.

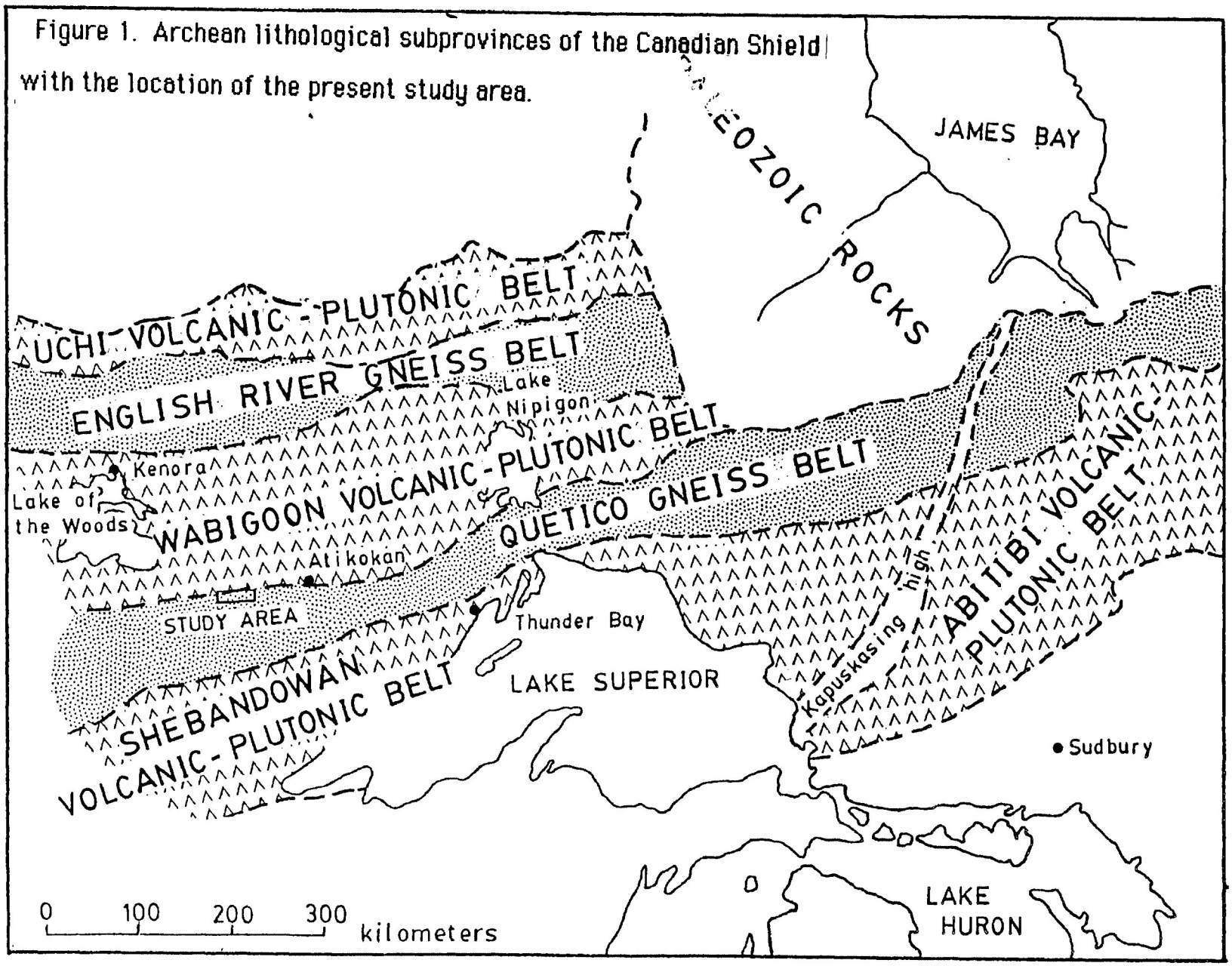

Rainy Lake area (approximately 20 kilometers west of the present study area) led him to establish a Precambrian stratigraphy. Lawson defined the 'Couchiching Series', a southern sequence of sedimentary rocks, the 'Keewatin Series', comprised chiefly of volcanic rocks with subordinate sedimentary rocks, and the 'Laurentian rocks', granites intrusive into both the Couchiching and Keewatin series. Subsequent study by Lawson(1913) eastward in the Bad Vermilion Lake area led to the expansion of his stratigraphic classification to include the 'Seine Series' of sedimentary rocks and a younger group of granitic intrusives which he called the 'Algoman rocks'.

Lawson believed the 'Couchiching Series' to be older than the 'Keewatin Series', and the 'Seine Series' to be superposed upon both or possibly contemporaneous with the Keewatin Series. Studies by U.S.G.S. workers in Minnesota (Adams et. al.,1905) led them to conclude that the Keewatin rocks were older than Couchiching. This sparked a major, long-lived controversy on the stratigraphic relationship between all of the groups defined by Lawson, eventually becoming known as the "Couchiching problem."

The scope of the present study is confined to the structure and magnetic fabrics of the rocks of the northernmost part of the Quetico subprovince(Fig. 1), between their highly metamorphosed equivalents to the south and the Quetico Fault to the north. As such, reiteration of the controversy surrounding the "Couchiching problem" would be redundant. Brief summaries of this controversy are given by Wood(1980) and by Poulsen(1980).

The present study area is part of areas first investigated by Smith(1893) and by McInnes(1899). Lawson also investigated parts of

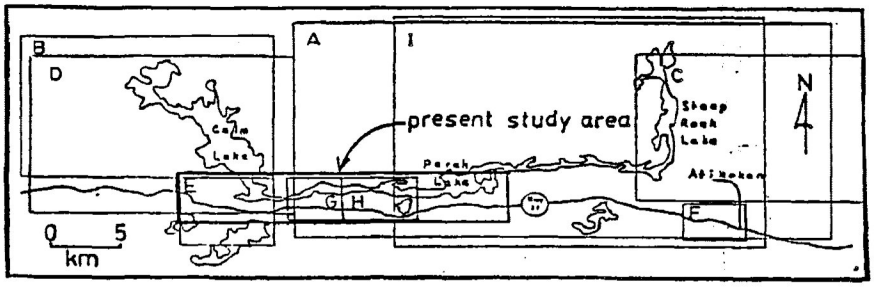

A) MOORE (1939)

B) YOUNG(1960)

C) SHKLANKA(1972)

D) FUMERTON(1980)

E) BORRADAILE(1982)

F) DUTKA(1982)

G) STUBLEY(1983)

H) STEWART(1984)

I) STONE et al. (1986)

Figure 2. Locations of the present study area and of previous geological investigations.

the present study area when he restudied the Rainy Lake region. Grout(1925) and Tanton(1926) first recognized the gneisses and migmatites as more highly metamorphosed equivalents of the adjacent northerly metasediments, as well as the gradational nature of the metamorphic intensification. Subsequent workers, wishing to avoid the stratigraphic implications in the use of Lawson's terms 'Couchiching series' and 'Seine series', refered to the metasedimentary rocks as the "southern sedimentary sequence"(Hawley,1929; Shklanka, 1972). Recently, "Quetico metasedimentary rocks" has come into more common usage(Pirie and Mackasay, 1978; Wood, 1980; Fumerton, 1980; Borradaile, 1982).

1-3. Previous Studies of Structural Geology.

Until only very recently, a detailed investigation of the structural geology of the Quetico metasediments had not been conducted. Early investigations tended to concentrate on the nature of the boundary between the Quetico and Wabigoon subprovinces.

Lawson(1913) interpreted both belt assemblages as regional monoclines, dipping steeply southward. However, Grout(1925) defined a regional syncline with a vertically-dipping axial plane centred in the metasediments.

Tanton(1926) considered the metasedimentary rocks to be part of the north limb of an anticlinorium, with the south limb cut off by the intrusion of a granitic batholith. Tanton based his interpretation on bedding top directions, which he found to be predominantly to the north. Tanton, however, also observed south-directed bed tops and postulated the existence of a number of tightly folded secondary folds

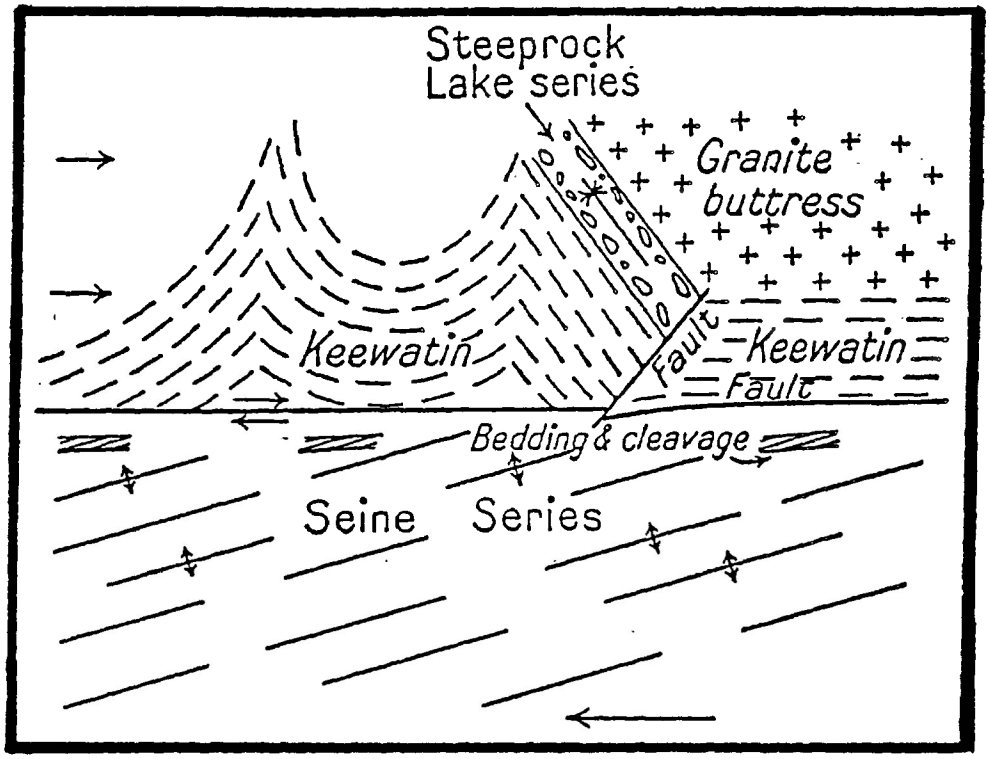

Figure 3. Interpretation by Hawley(1929) of the relationship of faulting along the Quetico fault zone and folding of the Quetico metasedimentary rocks. Hawley postulated that folding concurrent with the strike-slip fault movement led to establishment of a series of en-echelon folds with the dominant trend parallel to the regional extension direction, and with vertically-directed fold axes.

with amplitudes of approximately 300 meters.

Hawley(1929) investigated the same Quetico-Wabigoon boundary zone approximately 30 kilometers eastward of the present study area. Hawley, like Tanton(1926), looked closely at bedding top directions and generally agreed with Tanton's interpretation of a series of tight anticlines and synclines with east-west trending vertical axial planes, arranged in an en-echelon pattern.

Upon observation of a vertically-dipping, highly schistose zone, Hawley(1929) was first to postulate the presence of a major fault (the Quetico Fault) at the Quetico-Wabigoon boundary. Hawley believed the folding to be syntectonic with faulting, formed as a result of horizontal shearing movement associated with the regional wrench fault(Fig. 3). Hawley recognized that folds formed in this manner would be distributed in an en-echelon arrangement with variably-directed fold axes but a dominant trend parallel to the regional extension direction.

Moore(1930) also recorded the presence of small assymetric folds which he believed related to a regional northward thrust of the Quetico metasedimentary sequence over the granitic and volcanogenic rocks of the Wabigoon belt.

Subsequent studies made only cursory examinations of the Quetico metasediments. Shklanka(1972) noted that reversals in younging directions were observed. Fumerton(1980) stated that "foliation is parallel to bedding" and that these have "easterly strike, dip steeply to the north and have consistent tops to the north." Stone et. al.(1986) stated "reversals in younging direction are common within metasediments of the Quetico belt, but the exact locations of fold

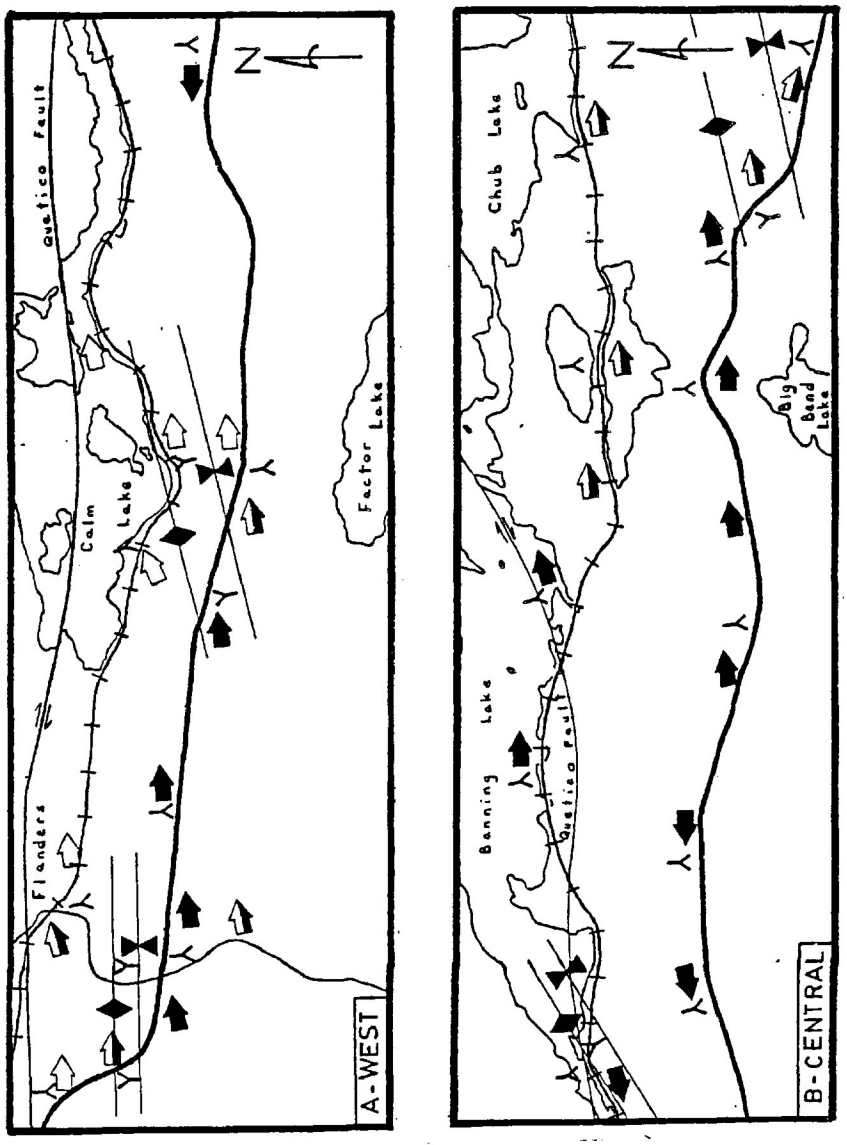

Figure 4. The major structural features of the areas studied by Borradaile(1982), Stubbley(1983) and Stewart(1984).

Local younging direction

Anticlinal/synclinal axial trace

Structural facing direction:
Upward, sideways, downward.

Figure 5. Three-dimensional sketch of the geometry of folds in the Quetico metasedimentary rocks in the Calm Lake - Banning Lake area (from Borradaile, 1982 and Stubbley, 1983).

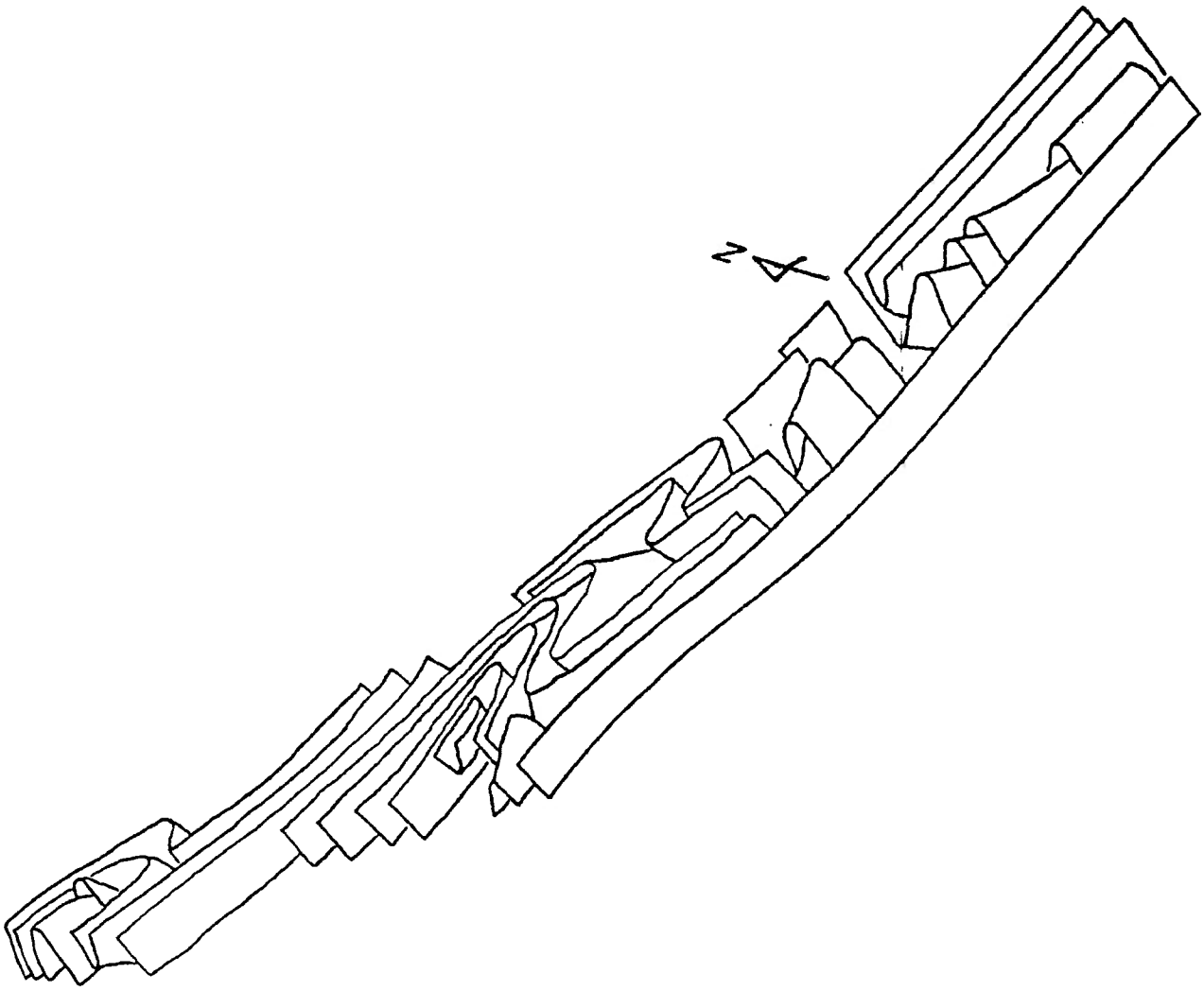

axes are not known everywhere, due to lack of marker units."

1-4. Recent Studies of Structural Geology.

Recently, Borradaile and coworkers initiated a detailed investigation into the structural geology of the Quetico metasedimentary rocks(Borradaile, 1982, Dutka, 1982, Stubley, 1983, Stewart, 1984; see also Poulsen, 1980)(Fig. 2). Structural mapping involved investigation of bedding and cleavage orintations, bedding-cleavage relationships, local younging directions, minor fold asymmetry and structural facing directions(see Borradaile, 1972).

The workers succeeded in delineating a number of regional folds(Fig. 4). These folds are tight to isoclinally folded with axial planes that dip near-vertically and strike approximately east-west. The most surprising aspect of these folds is the strongly curvilinear nature of their fold axes. This is illustrated in Figure 4 by the systematic change in structural facing directions, which alternate from upward-facing through sideways-facing to downward-facing. As such, the folds can be described in various locations as upright synclines and anticlines, sideways-closing or neutral folds, and synformal anticlines and antiformal synclines(Fig. 5).

CHAPTER TWO

PRESENT STUDY

2-1. Introduction.

The non-cylindrical folds delineated by Borradaile(1982), Stubley(1983) and Stewart(1984) (Figs. 4 and 5) present an interesting structural problem. Folds with such strongly curvilinear fold axes can be described as sheath-like in appearance. The genesis of sheath-like folds cannot generally be easily deciphered, and in the Quetico metasedimentary belt this problem is only exacerbated by a general paucity of rock outcrop. Knowledge of the regional strain distribution may be of assistance; unfortunately, the Quetico metasediments have a distinct lack of regional reliable strain markers. Nevertheless, an indication of principal strain directions may be provided by study of the rocks' magnetic fabric.

Magnetic fabric can be defined as the physical arrangement of magnetic minerals within a rock. The magnetic fabric will dictate the shape and orientation of the magnetic susceptibility anisotropy(MSA), or directional variability of magnetic susceptibility. The MSA of a rock can be described by a magnitude ellipsoid of magnetic susceptibility with orthogonal axes defining the three principal magnetic susceptibilties: K_{max}, K_{int}, and K_{min} (the maximum, intermediate and minimum magnetic susceptibilities, respectively).

Many recent workers have attempted comparison of strain ellipsoids and magnetic susceptibility ellipsoids in deformed rocks(Graham, 1966; Hrouda and Janak, 1976; Kligfield et. al., 1982;

Borradaile and Alford, in press). Results of this work have shown that , in most cases, there is a definite correlation between directions of principal strains and principal magnetic susceptibilities, such that minimum susceptibility directions are parallel to directions of greatest shortening, and maximum susceptibility directions are parallel to maximum extension directions, even in only modestly deformed rocks. Such a correlation, however, cannot be applied to magnitudes of principal strains and principal magnetic susceptibilities(Borradaile and Mothersill, 1984, Henry, 1983). In other words, the spatial arrangement of magnetic minerals is generally reflective of the strain distribution within a rock, but there is no simple relationship between a rock's MSA and the amount of strain it experienced.

2-2. Scope of the Present Study.

The present study is a detailed investigation and collation of the structure and magnetic fabric of the Quetico metasedimentary rocks, both on a regional and a mesoscopic scale. Structural investigation involved.

1. A reinvestigation of the areas studied by Borradaile(1982), Stubley(1983) and Stewart(1984)(Fig. 2).
2. Structural mapping and interpretation of a similar, 12-kilometer section of Quetico metasedimentary rocks east of that mapped by Stewart(1984).
3. Observation and analysis of micro- and mesoscopic petrofabrics.

Investigation of the magnetic fabrics of the Quetico metasedimentary rocks involved.

1. Systematic collection of over 200 oriented samples of Quetico rocks from throughout the study area.
2. Systematic, more closely-spaced collection of oriented samples from fold closures and refracted cleavage exposed within the study area.
3. Determination and analysis of the magnetic susceptibility and magnetic susceptibility anisotropy(MSA) of all oriented samples.
4. Determination of the magnetic mineralogy of the Quetico rocks.
5. Correlation of the MSA data with magnetic mineralogy.
6. Correlation of the MSA data with petrofabric.
7. Correlation of the MSA data with structural elements.

The extended mapping of structural geology has added to the knowledge of the location, geometry and nature of folds within the Quetico belt.

The investigation of the magnetic fabric of the Quetico rocks produced some interesting information, including.

1. The polymineralic nature of the magnetic mineralogy and how this could affect both the shape and orientation of the magnitude ellipsoid of magnetic susceptibility.
2. The nature of variation in the magnitude ellipsoid of magnetic susceptibility with variation in lithology, mineralogy and strain, especially from study of the refracted cleavage.

Collation of structural geology, petrofabrics and magnetic fabrics yielded insight into.

1. Regional distribution of principal strain directions in the Quetico metasedimentary belt.
2. The nature of genesis of folds within the Quetico

metasedimentary belt.

2-3. Method of Investigation.

Field Investigations:

Approximately ten weeks, in total, were spent in the field engaged in structural mapping and sample collection.

Structural mapping involved the observation, measurement and recording of bedding and cleavage orientations, bedding-cleavage intersection lineations, minor fold asymmetry and orientation, local younging directions, and other minor structural features, such as local kink zones and ductile shear zones.

Collection of oriented samples was accomplished by either marking the strike and dip of a well-developed cleavage plane, or by marking the north direction on horizontal surfaces. Samples were collected from rock exposures along Highway 11, the C.N.R. railway and the Seine River system, at intervals of approximately 300 meters(Fig. 6). Cores of 2.5 centimeters diameter were also collected in selected locations through use of a back pack drill. In all, 297 samples were collected.

Laboratory Investigations:

Much of the laboratory time was spent in preparing and measuring the oriented samples for MSA, and in determining the magnetic mineralogy of some samples. Experimental procedures for both are described in later sections.

Twenty-five thin sections were prepared and examined to assist in petrographic investigations.

Figure 6. Map of the present study area indicating the locations of the oriented rock samples.

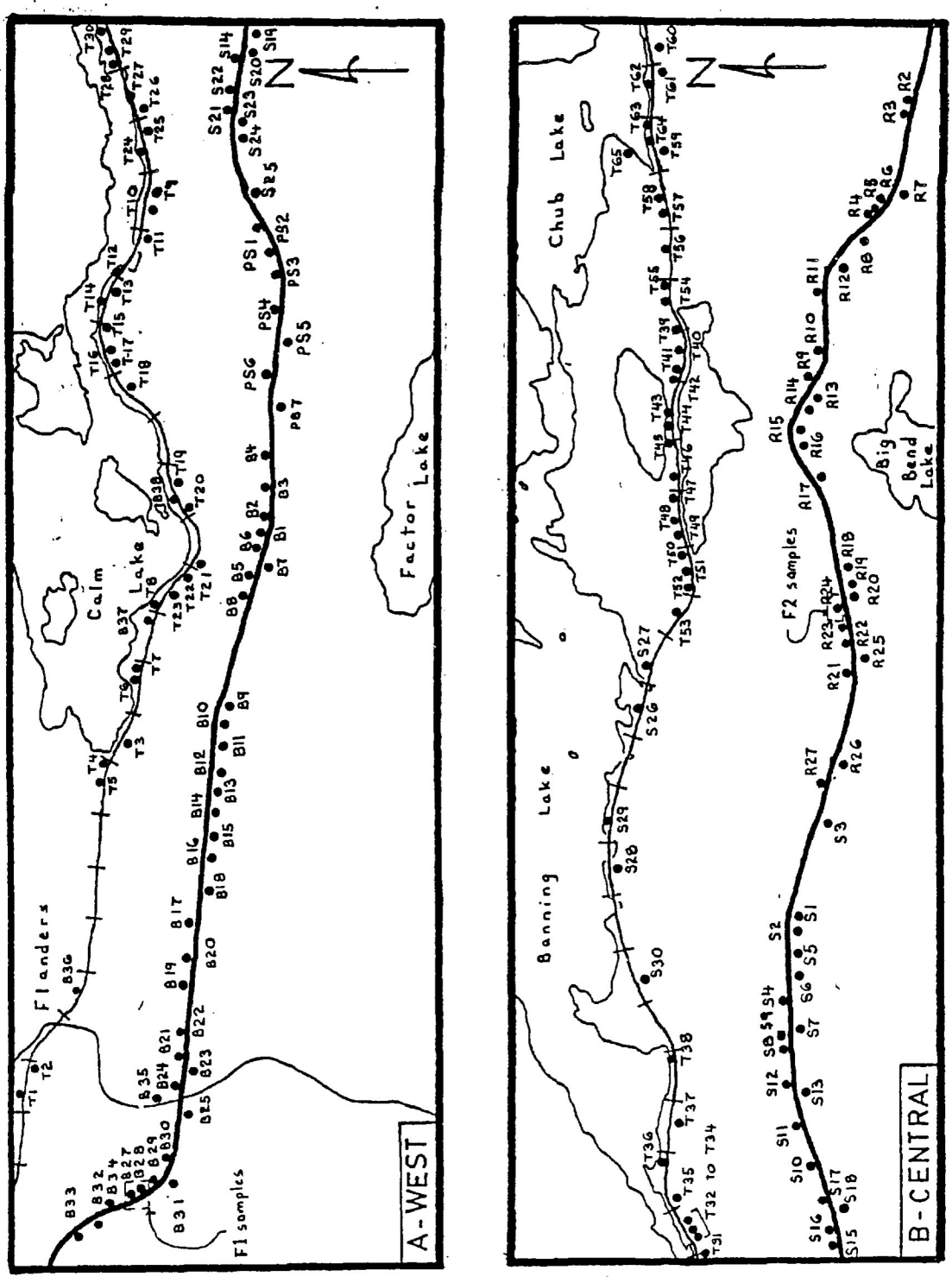

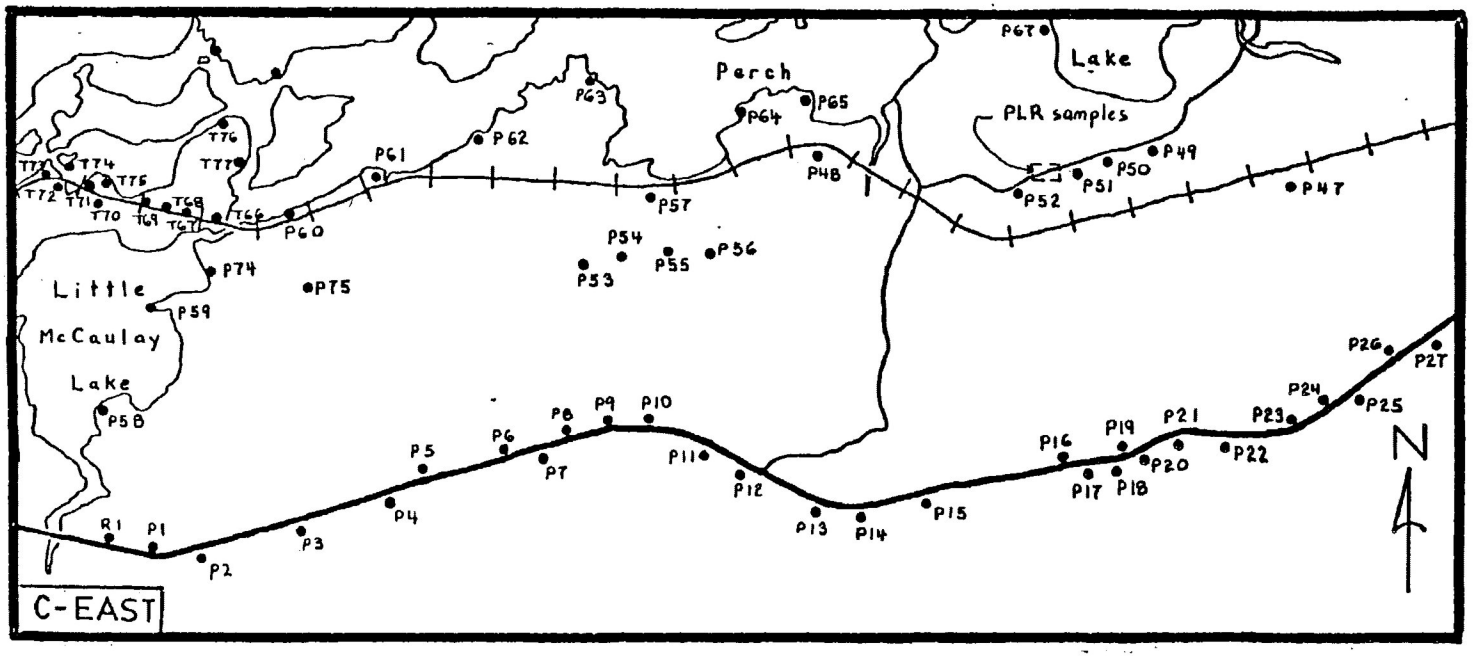

● R23 Sample location and number	Scale 0 1 2 km
Detailed study area	Canadian National Railroad
	Provincial highway 11
	Other road

CHAPTER THREE
LITHOLOGIES AND SEDIMENTARY GEOLOGY

Introduction

The rocks of the study area have undergone a pervasive regional metamorphism, and could be broadly classified as schists and phyllites. Most rocks, however, are also readily recognizable as clastic sedimentary rocks, with many preserved sedimentary structures and textures. The following lithological units are identified in the present study area(the prefix meta- is implied for all rocks):

Clastic sedimentary rocks

Sandstones

Mudstones

Volcanic rocks

Mafic volcanic flows

Felsic to intermediate volcanoclastics

3-2. Lithologies.

Clastic sedimentary rocks

Sandstones

Sandstones are very abundant as massive beds up to one meter wide or interbedded with argillites in thin strata in some places less than one centimeter wide. They are also found as graded beds

completely transitional in grain size to mudstone. The beds are light to medium grey on a fresh surface.

Quartz is easily most abundant of the framework minerals of the sandstones, comprising 50 percent or more of this textural fraction. Grain size rarely exceeds one millimeter, and is completely gradational to less than 0.02 millimeters. Quartz grains typically display undulose extinction and, less commonly, recovery. Ribbon quartz is present in some rocks.

Feldspar is next in abundance of the framework minerals. Most rocks contain 10 to 15 percent of the feldspar clasts, some rocks having up to 25 percent. Sodic plagioclase is the most common feldspar; alkali feldspar is rare. Maximum grain size is slightly less than one millimeter and, like quartz, grain size is completely gradational to less than 0.02 millimeter. Most feldspar grains are saussuritized to varying degrees; some are very extensively altered. Feldspar grains are generally more deformed than quartz grains.

Lithic fragments are a rare component of the sandstones. Fine-grained, intergrown quartz, feldspar, chlorite and sericite, are observed. Patchy aggregates of quartz and chlorite may represent original cherty fragments. Coarser-grained quartzolitic fragments are more rarely observed. Lithic fragments rarely exceed 5 percent of the volume of the framework minerals. They are, however, the most deformed of the components and are commonly extensively altered to fine-grained chlorite and sericite. It is probable that many lithic fragments are now completely altered and represent a large proportion of the pseudomatrix(Plates 1 and 2).

Matrix content of the sandstones is quite variable, from less than 5 percent to over 70 percentof volume. Most sandstones have matrix

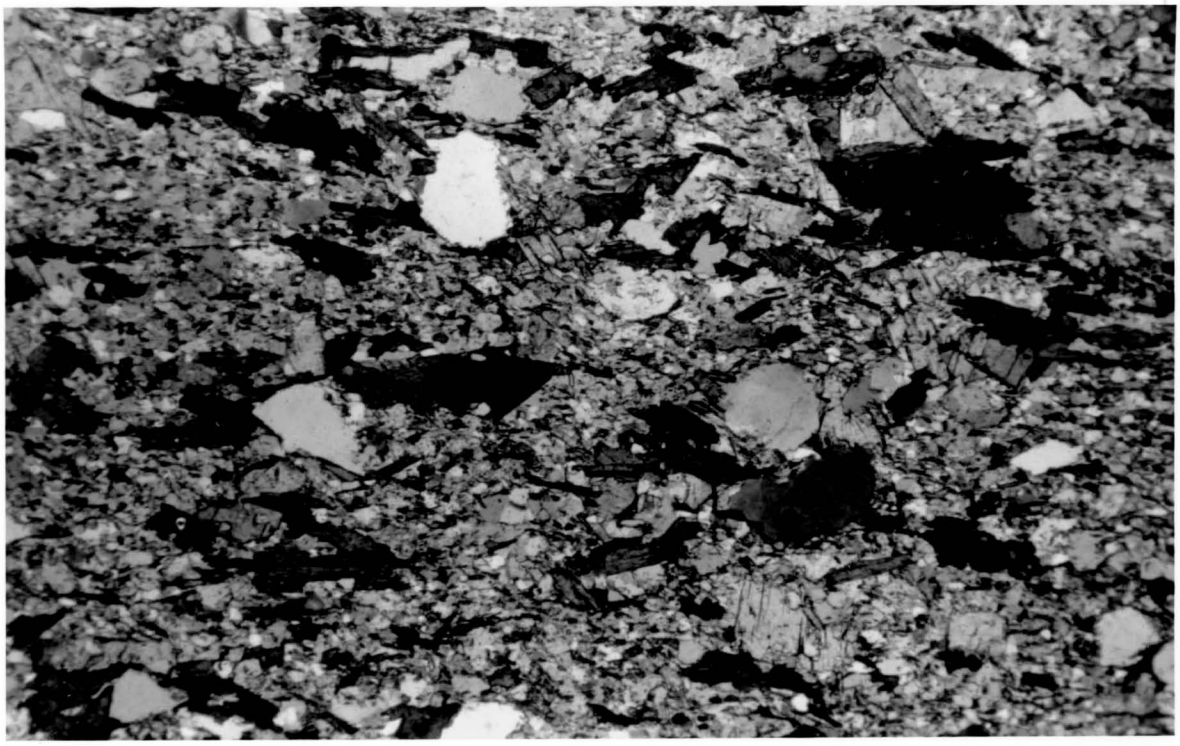

Plate One. Photomicrograph of a biotite schist (metamorphosed sandstone) from the south part of the study area (sample location B08 - see Fig. 6). The slide consists mainly of subrounded quartz clasts and coarse biotite crystals in a matrix of fine-grained quartz and feldspar and phyllosilicates. The rock possesses a typical "greywacke texture", with a significant proportion of the matrix consisting of recrystallized quartz and feldspar, and anchimetamorphosed phyllosilicates. Note the two generations of biotite: a coarse-grained fraction of stubby crystals with ragged crystal outlines, and a fine-grained fraction of elongate crystals with a strong preferred crystallographic orientation. The coarse-grained fraction may represent post-deformation metamorphism, suggesting, perhaps, that metamorphism, at least in this part of the study area, was longer-lived than deformation.
1 cm = 0.2 mm

content in the range of 10 to 30 percent. It is, in some cases, related to grain size. That is, the coarser sandstones typically have a small matrix content. Some graded beds display an increase in matrix content with decrease in grain size. Mineralogy of the very fine-grained matrix is as follows(see Plate 3):

Quartz+chlorite+muscovite+feldspar(±carbonate±biotite)

Accessory epidote, sphene and apatite are also present.

Quartz, chlorite and muscovite comprise over 80 percent of the matrix.

In some rocks, compositional banding, with alternating quartz-rich, and phyllosilicate-rich bands, is present(Plate 4).

Carbonate is a significant mineral in some rocks, forming up to 10 percent of the matrix. It is most abundant in rocks within the north part of the study area. Carbonate is observed replacing framework minerals, within strain shadows of quartz fragments, as a matrix cement, and as patchy grains and lenses.

Opaque mineral phases comprise one to ten percent of the sandstones. Grains generally range in size from 0.05 millimeters to 0.3 millimeters. The dark minerals occur in thin section as pseudomorphs after, or partially replacing framework minerals, as subhedral to euhedral cubic crystals or as strung-together or amorphous lenses. Observations of polished grain mounts under reflected light microscope have identified some of the opaque minerals as pyrite, pyrrhotite and magnetite, in order of abundance.

There are a number of classification systems for sandstones. The one adopted for the Quetico metasandstones in this study is a modified version of Pettijohn, Potter and Siever(1972)(Fig. 10).

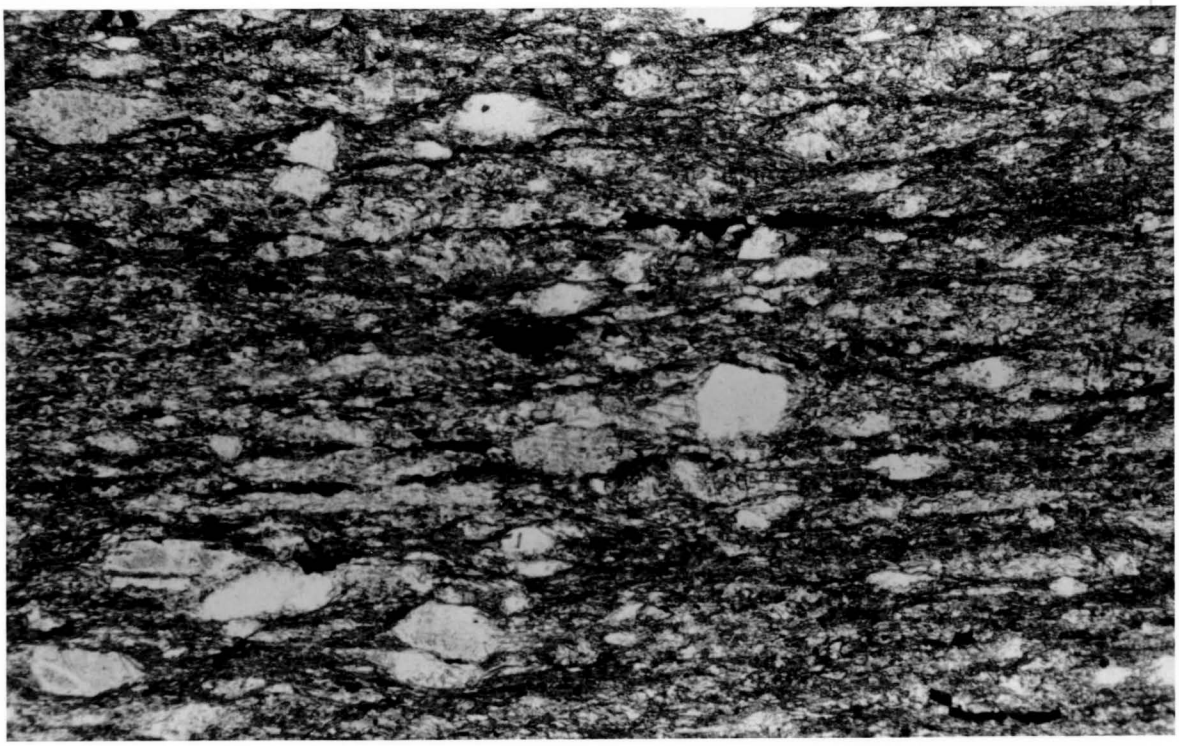

Plate Two. Photomicrograph of a metamorphosed lithic subarkose (sample B34 - see Fig. 6). Quartz (clear) and feldspar (slightly mottled) clasts in a fine-grained matrix comprised of quartz, feldspar, chlorite, muscovite and carbonate. A lense of carbonate can also be seen in the lower left-hand corner of the photograph. The rock possesses a very well-developed planar deformational microfabric. Note the dark bands in the photograph. These bands represent stylolitic cleavage traces.
1 cm = 0.2 mm

According to this system, sandstones with matrix contents of less than 15 percent are termed arenites. Those with matrix contents greater than 15 percent are termed wackes. The sandstones are then further subdivided according to relative abundances of quartz+chert, feldspar, and lithic fragments.

As noted previously, sandstones in the present study area have a variable matrix content. A significant, but largely indeterminate, amount of the matrix consists of altered lithic fragments, highly saussuritized feldspar fragments and dynamically recrystallized quartz fragments and, as such, is of diagenetic or of metamorphic and/or deformational origin.

According to the Pettijohn et. al.(1972) classification, Quetico sandstones could be classified both as arenites and as wackes, but the classification system does not account for pseudomatrix quartz subgrains of metamorphic/deformational derivation. Allowance for these post-depositional effects may require many wackes to be reclassified as arenites.

All sandstones of the present study area are from the same environment of deposition and are probably deposits of essentially the same sedimentary processes.They are designated arenites and classified accordingly(Fig. 10). Modifiers qualitatively indicate matrix content: matrix-poor(<15 percent matrix content), matrix-rich(>15 percent matrix content) and matrix-supported(>75 percent matrix content, individual framework minerals do not touch).

Examples of each of matrix-poor, matrix-rich and matrix-supported arenites are found in the persent study area. Arenites are classified as subarkose and lithic subarkose. One sample examined was a relatively fine-grained quartz arenite. Most of the

Quetico metasandstones are matrix-rich lithic subarkoses.

Mudstones

Mudstones are common, but less abundant than the sandstones, in the present study area. They comprise the top portion of graded beds or are interbedded with sandstones. Bed thickness ranges from 10 centimeters to less than one centimeter.

The mudstones consist of a very fine-grained assemblage of granular, subrounded quartz and plagioclase feldspar with minute laths of chlorite and muscovite with subparallel alignment. Grain sizes are generally less than 0.05 millimeters, but sand-sized fragments of quartz and feldspar make up to 25 percent of some rocks. Compositional banding, with alternating quartz-rich and phyllosilicate-rich bands, is common(Plate 4). Bands are less than one millimeter wide. Carbonate cement and patchy carbonate lenses are observed in some rocks. The mudstones typically contain one to two percent opaque minerals, with grain sizes in the range of 0.04 millimeters to 0.2 millimeters. The subhedral to euhedral cubic outline of many of these opaque minerals suggests pyrite of post-depositional (and post-deformational) origin.

The mudstones are typified by a metamorphic mineralogy (chlorite+muscovite). The sub-parallel alignment of phyllosilicates defines a continuous cleavage which transects depositional surfaces. Thus, the dominant fabric of the mudstones is of metamorphic origin. As such, most workers in the Quetico metasedimentary belt have identified these rocks as slates and phyllites(e.g. Borradaile,1982, Stubbley,1983; Stewart,1984).

Volcanic rocks

Rocks of volcanic derivation are exposed in a limited extent in the extreme north regions of the study area. The rocks are generally considered to be north of, or within the Quetico fault zone, and part of the Wabigoon granite-greenstone belt.

Two volcanic lithologies are identified in the study area: mafic volcanic flow rocks and felsic to intermediate volcanoclatic rocks.

Mafic volcanic flow rocks

Massive mafic flow rocks are exposed in the extreme northwest corner of the study area along the C.N.R. railway west of Flanders, and interbedded with volcanoclastic rocks on the south shore of Banning Lake(Fig. 6). The rocks are dark grey-green to reddish brown on weathered surface and dark to medium green on fresh surfaces. They are massive, medium-grained and possess a moderately well-developed cleavage from preferential orientation of amphiboles and micaceous minerals.

Thin section examination of one sample (Plate 6) shows actinolite, quartz and feldspar phenocrysts in a fine-grained, felted matrix consisting of epidote, chlorite, actinolite, quartz and feldspar. A well-developed continuous cleavage is developed from the strong preferred orientation of matrix minerals. Actinolite phenocrysts are generally polygranular in lath-like or fibrous aggregates. Feldspar phenocrysts are generally highly saussuritized.

Felsic to intermediate volcanoclastic rocks

Volcanoclastic rocks are exposed in the north-central part of the study area, along the C.N.R. railroad and the south shore of Banning

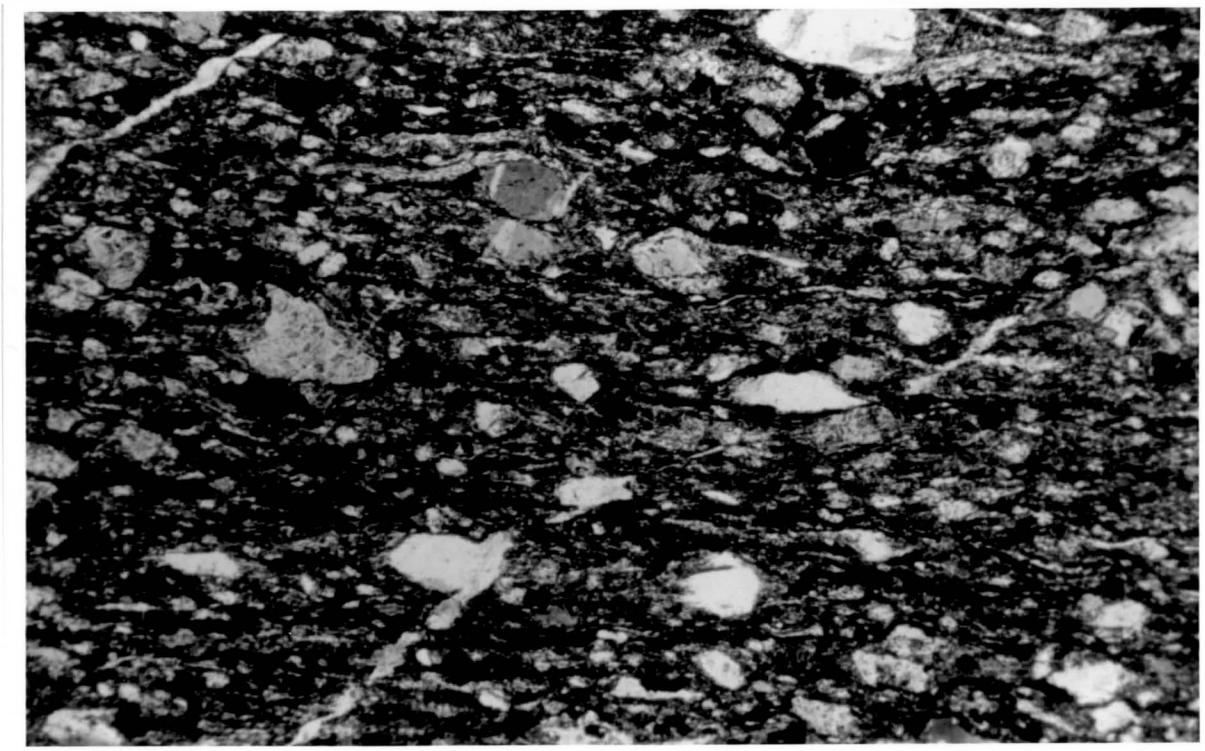

Plate Three. Photomicrograph of a metamorphosed matrix-rich lithic subarkose (sample T13 - see Fig. 6). Quartz (clear) and feldspar (light grey) clasts in a fine-grained matrix of quartz, feldspar, chlorite, muscovite, epidote, sphene and carbonate. The rock has a well-developed tectonic planar fabric. Many of the quartz and feldspar clasts display strain shadows with fine-grained quartz-mica and quartz-mica-carbonate intergrowths in the shadow regions. One feldspar grain (on right-hand side of the photograph) is poikioblastic, with inclusions of epidote.
1 cm = 0.2 mm

Lake near Banning Narrows(Fig. 6). The volcanoclastic rocks are apparently a water-lain sequence, often interlayered with phyllites and sandstones, and, texturally, displaying laminations and well-rounded fragments. Toward the north, both volcanoclastic and sedimentary rocks become transitionally thinner-bedded and subordinate to mafic and intermediate flow rocks.

Felsic volcanoclastic rocks are light buff coloured, with reddish brown alteration products typically along cleavage surfaces. Fairly coarse(up to 4 millimeters) deformed crystal fragments of quartz and feldspar and lithic fragments are imbedded in a very fine-grained, fissile groundmass. The groundmass consists mainly of very fine-grained(less than 0.02 millimeter) quartz and sericite with chlorite, epidote and minor amounts of carbonate and sphene. Quartz crystal fragments are least deformed, displaying undulose extinction or dynamic recrystallization. Feldspar crystal fragments are saussuritized and some grains display mechanical twinning. Lithic fragments are felsic in composition, consisting of a fine-grained, polygranular assemblage of quartz, feldspar, muscovite and chlorite. The lithic fragments are highly deformed(Plate 5).

Intermediate volcanoclastic rocks are dark to medium green on fresh surfaces, and typically reddish brown to dark green on weathered surfaces. Crystal fragments of quartz and feldspar and lithic fragments are elongate and up to 4 millimeters in length, but not abundant. Groundmass of the intermediate volcanoclastic rocks is similar to that of the felsic volcanoclastic rocks, with a greater abundance of chlorite and epidote. Lithic fragments consist of a very fine-grained(0.01 millimeter) assemblage of quartz, feldspar,

chlorite, muscovite and epidote. Some rocks display compositional banding, with alternating quartz-rich and phyllosilicate-rich bands less than one millimeter wide.

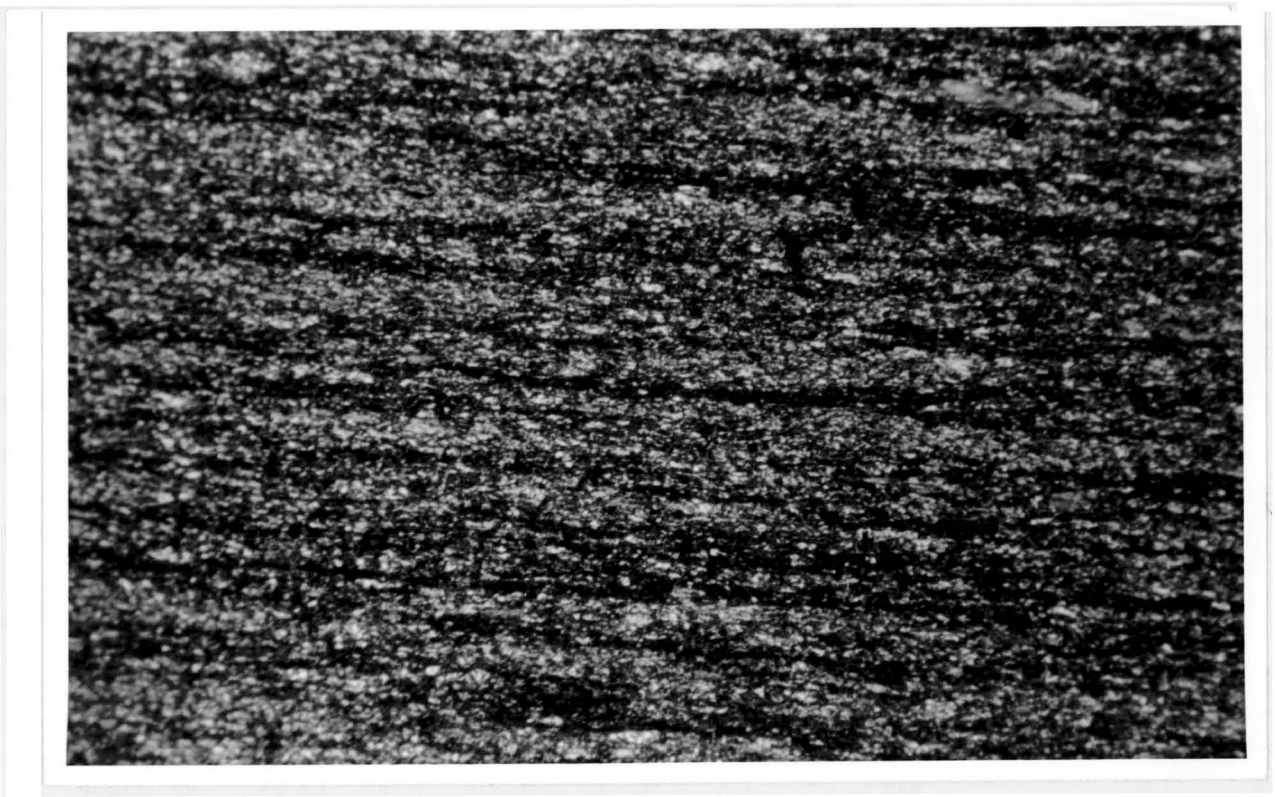

Plate Four. Photomicrograph of metamorphosed mudstone-siltstone laminations (sample T36 - see Fig. 6). The rock consists of a fine-grained assemblage of quartz, chlorite, muscovite and feldspar. Dark phyllosilicate-rich bands and light quartz-rich bands, less than one millimeter wide, indicate mudstone and siltstone laminations, respectively.
1 cm = 0.2 mm

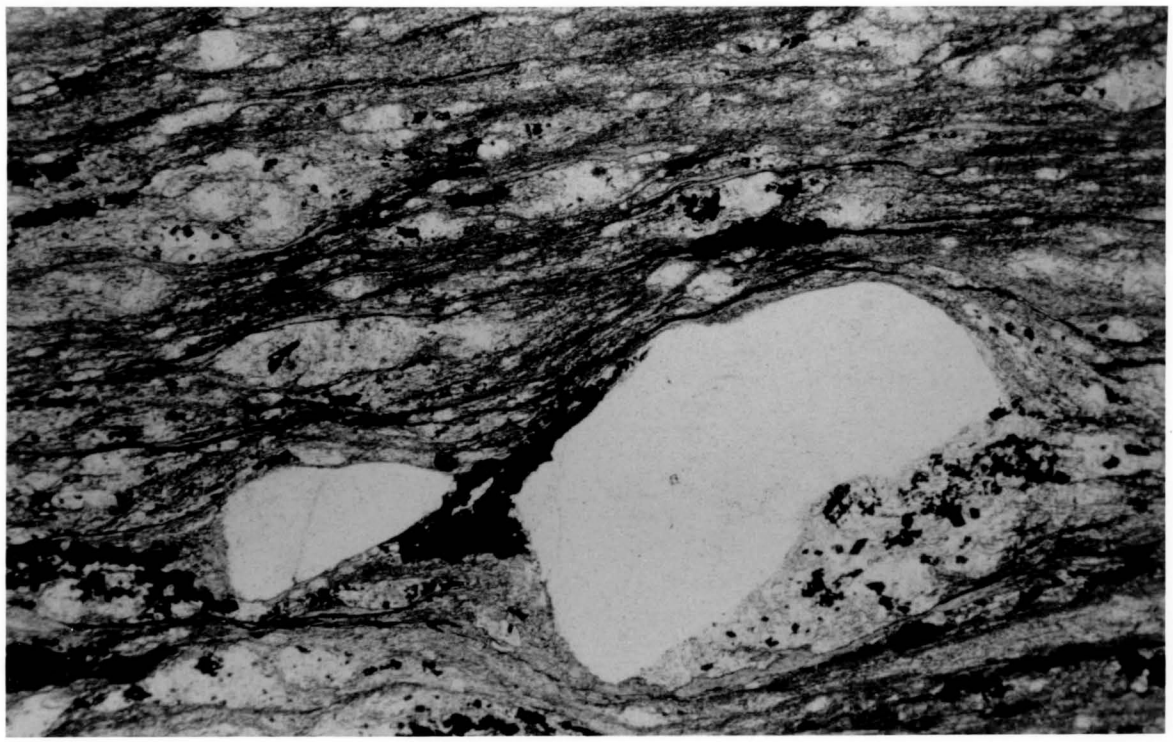

Plate Five. Photomicrograph of a metamorphosed felsic lapilli tuff. Quartz crystal (clear), feldspar crystal (light grey) and lithic fragments (mottled) in a fine-grained matrix of sericite, quartz, chlorite, and opaque minerals. The rock possesses a well-developed tectonic planar fabric, with the dark bands possibly representing stylolitic cleavage traces. The asymmetric distribution of the strain shadows about the coarse quartz crystal suggests a component of rotation in tectonic fabric development.
1 cm = 0.2 mm

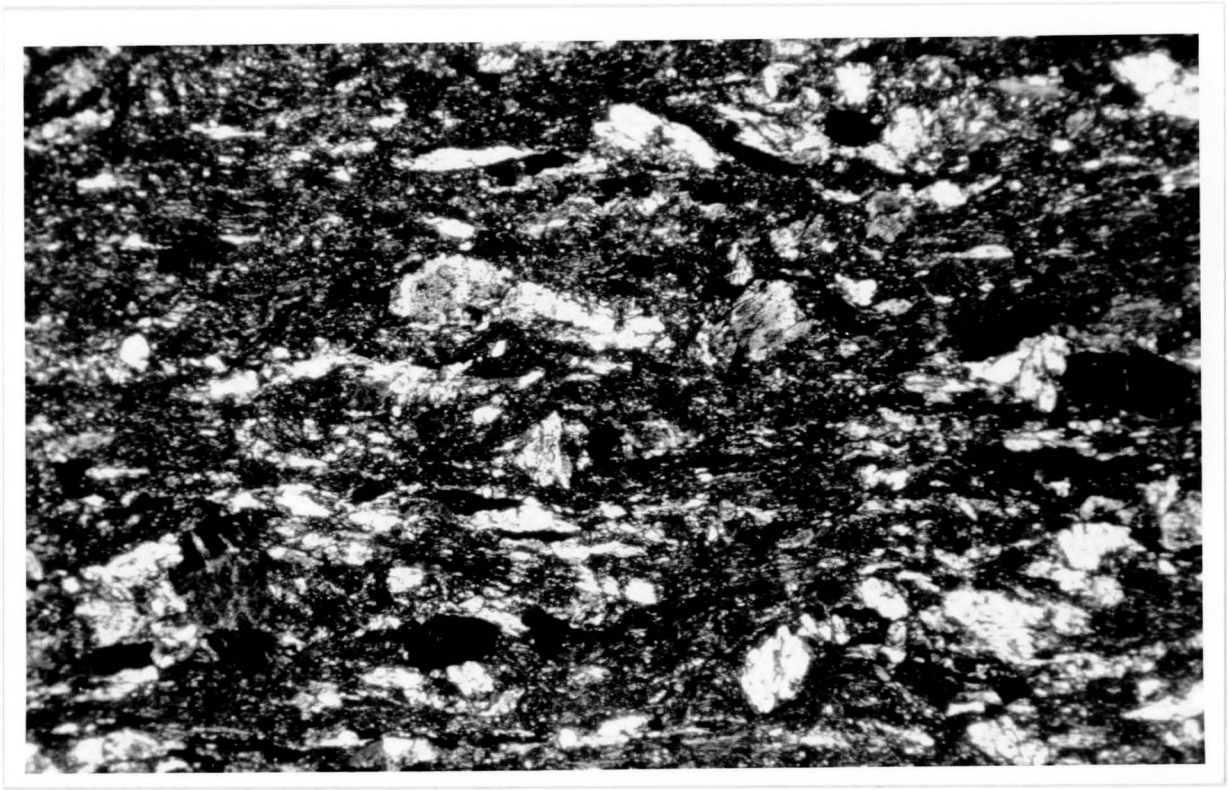

Plate Six. Photomicrograph of a mafic meta-volcanic flow rock (sample T01 - see Fig. 6). The rock consists of actinolite and feldspar phenocrysts in a felted, fine-grained matrix of epidote, chlorite, actinolite, quartz, feldspar and opaque minerals. Feldspar phenocrysts are highly saussuritized. A well-developed continuous cleavage is defined by the preferred orientation of matrix minerals.
1 cm = 0.2 mm

3-3. Sedimentary Features

The Quetico metasedimentary sequence is comprised of a repetitive interstratification of alternating sandstones and mudstones. Bed thickness varies considerably from one meter to less than one centimeter. Mudstone beds are commonly laminated. In thin section, compositional banding of some mudstones is observed, with silt-sized quartz-rich bands and mud-sized phyllosilicate-rich bands less than one millimeter thick.

Beds are laterally continuous. Very few beds are observed to truncate, pinch out or vary greatly in thickness. Bases of sandstone beds are sharply demarked and straight.

Numerous primary sedimentary structures and textures are observed(Fig. 7). Many of these structures indicate local younging directions.

By far the most common sedimentary texture is graded bedding. Graded sandstone beds(Fig. 7A) vary in thickness from nearly one meter to one centimeter. Grain size typically grades from coarse sand upward to finer sand, silt and mud.

Ripple cross-lamination(Fig. 7D) is observed in numerous locations. The cross-laminated beds are less than 5 centimeters thick and are found within sandstone beds and sandstone-mudstone laminations. Tops of the laminations are truncated and foresets gradually curve downward to become parallel with underlying beds.

Load casts(Fig. 7C) and flame structures are present in some locations. In one location, incipient development of a "ball-and-pillow" structure is present(Fig. 7A). Such a structure develops when a competent sand bed begins to sink into a less competent underlying mudstone bed. With progressive development, a

Figure 7. Illustrations of typical primary sedimentary structures observed in the Quetico metasedimentary rocks:

A. Incipient development of a "ball-and-pillow" structure at the contact of a mudstone bed and an overlying graded sandstone bed.

B. Crude cross-stratification in a sandstone bed infilling a scour channel.

C. Bed loading of a sandstone bed overlying mudstone-siltstone laminations.

D. Ripple cross-stratification within a sandstone bed.

E. A possible dewatering pipe at the contact of a sandstone bed and an overlying coarse sandstone bed. Dewatering pipes form when lithostatic loading causes rapid expulsion of water from underlying beds along localized conduits.

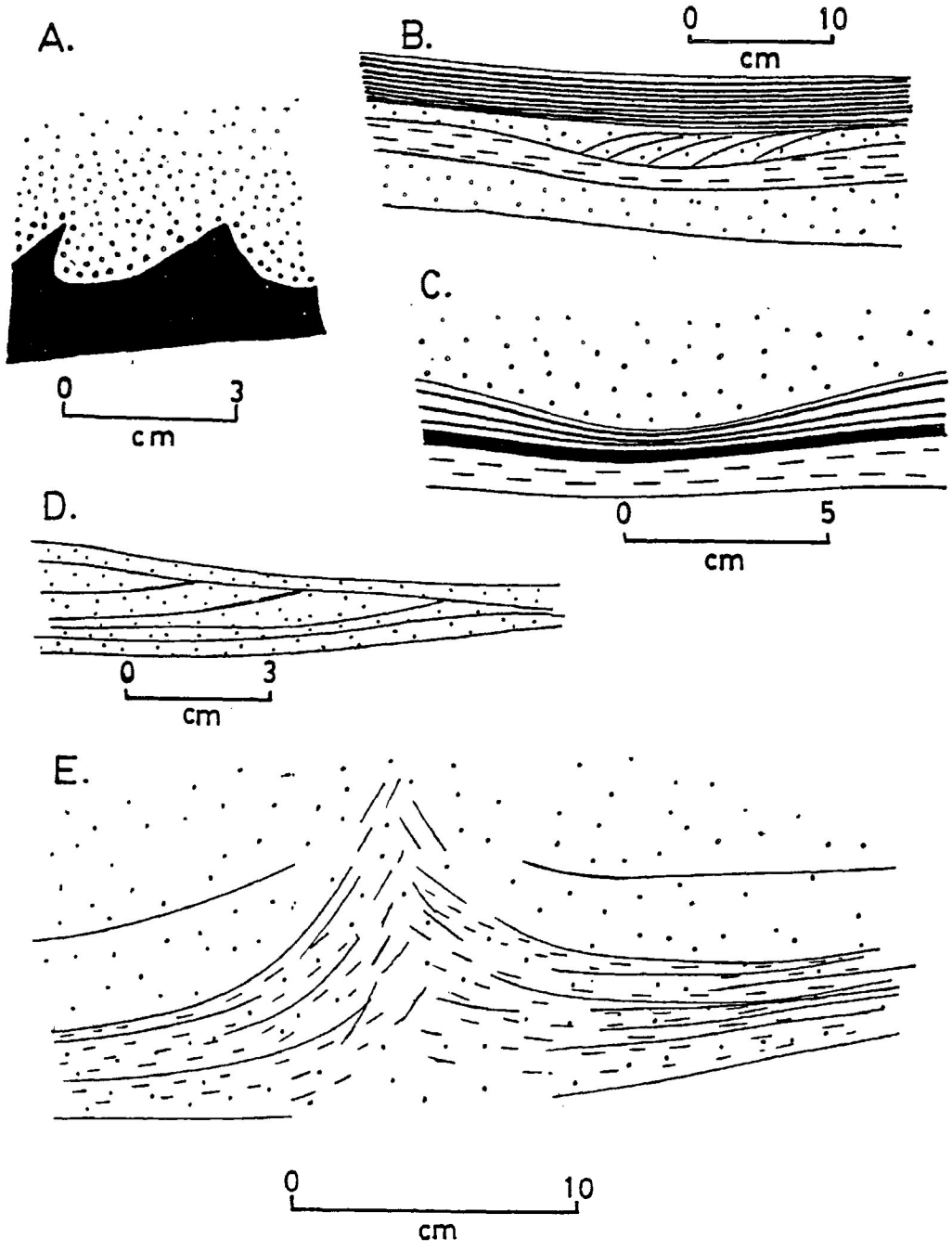
A.
0
3
cm
B.
0
10
cm
C.
0
5
cm
D.
0
3
cm
E.
0
10
cm

lense of sandstone may become detached from the overlying bed and incorporated into the mudstone as a sandstone "ball"

Scour channels and erosional surfaces are rather rarely observed. In some cases, the erosional depression is directionally refilled with coarse debris, forming a crude cross-stratification(Fig. 7B).

A structure resembling a dewatering pipe is observed in one location. Such a pipe forms in sandstone beds when lithostatic loading causes the rapid expulsion of water from underlying beds along localized channels or pipes. The pipes originate from, and are generally perpendicular to, the base of beds. The pipes disrupt sedimentary structures within the beds(Fig. 7E).

3-4. Environment of Deposition

The general sedimentary features of the Quetico metasedimentary rocks can be summarized as follows.

1. Repetitive interlayering of sandstone and mudstone beds.
2. Sandstone beds are laterally continuous, have sharp, abrupt bases and are commonly graded.
3. The most commonly observed sedimentary structuresand textures are graded bedding, parallel laminations and ripple cross-laminations.
4. No evidence for shallow water reworking of the sediments by tidal, wave or storm-wave action.

These general features suggest deeper water deposition of sediments from turbidity currents. Previous workers(e.g. Shklanka,1972, Wood, 1980, Fumerton, 1980, Borradaile, 1982, Dutka, 1982, Stubley, 1983, Stewart, 1984) have also interpreted the Quetico metasediments as a turbidite sequence

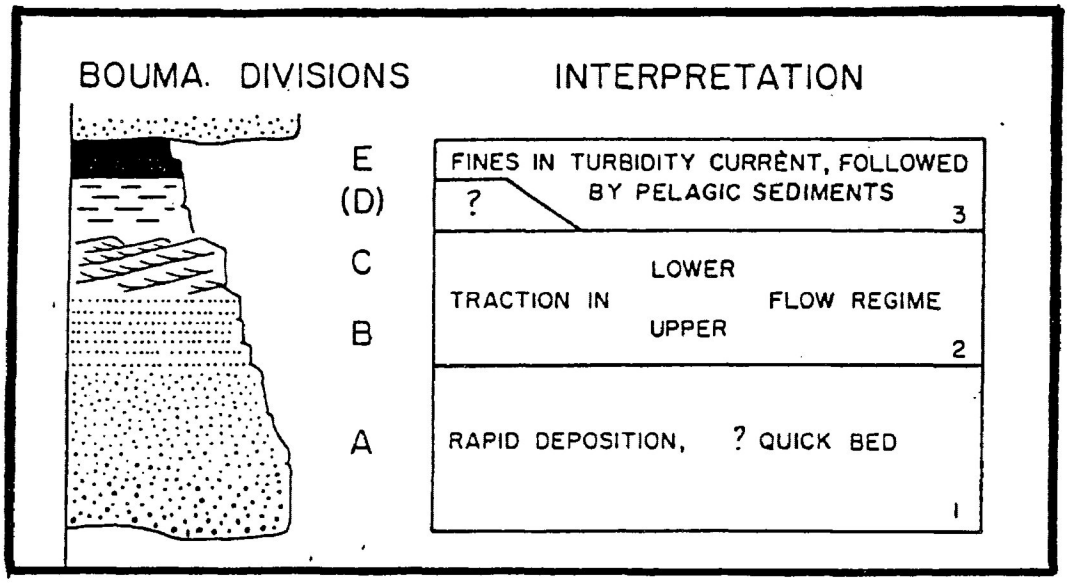

Figure 8. The five horizons of the Bouma sequence for turbidites:

A. Massive or graded sandstone.
B. Parallel laminated sandstone.
C. Ripple cross-laminated fine sandstone.
D. Fine silt and mud laminations.
E. Mudstone.

(from Walker, 1984).

Kuenen and Migliorini(1950) first proposed the concept of sedimentary deposition from turbidity currents. Since then, a wealth of data describing the sedimentary features of turbidites has accumulated. Bouma(1962) described a sequence which represents the idealized sequential accumulation of a single turbidite. This sequence has become generally accepted. The Bouma cycle or sequence consists of five horizons(Fig. 8) from base to top. A) massive or graded sand; B) sandy parallel laminations; C) rippled and/or convoluted laminations; D) fine silt and mud laminations, E) mud.

The Bouma sequence represents all horizons observed in turbidites, and in sequential arrangement. No other horizons have been consistently identified in turbidites. The Bouma sequence, however, is an idealized sequence, and all five horizons are usually not present. One or more horizon can be absent from an entire turbidite succession.

The Bouma sequence does provide a means of easily describing turbidites. For example, a sequence consisting of all five horizons could be termed ABCDE turbidites. A sequence consisting of alternating graded sandstone and shale could be termed AE turbidites.

Sullwold(1960) first interpreted turbidite sequences in terms of submarine fans. Mutti and Ricci Lucchi(1972) proposed facies and facies sequences as a means of describing the depositional environment of the submarine fan. From this concept evolved a number of fan models and turbidite facies. Walker(1984) describes a submarine fan model(Fig. 9) consisting of.

1. Upper fan with a single feeder channel.
2. Mid fan with branching distributary channels feeding

Figure 9. Submarine fan environmental model, showing the typical depositional sequences associated with different depositional environments of the fan. (from Walker, 1984).

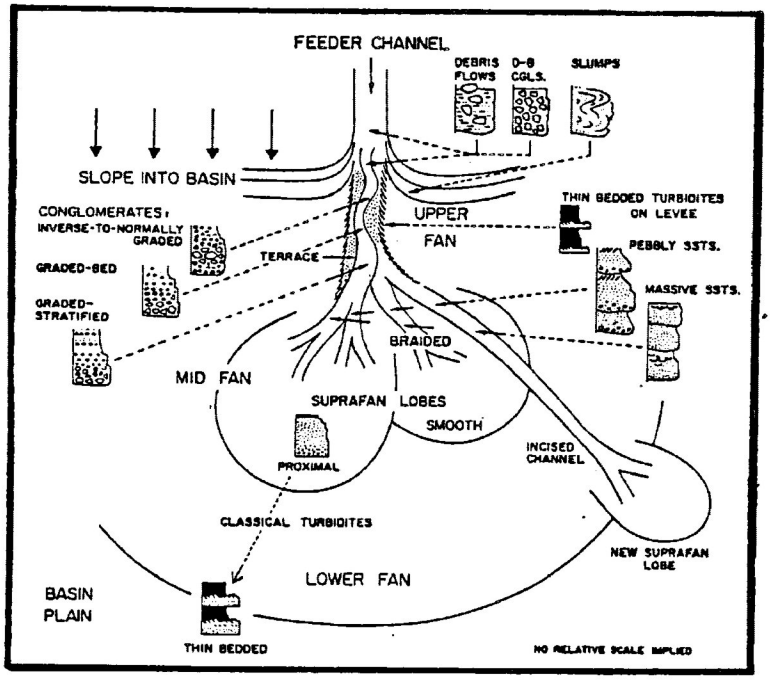

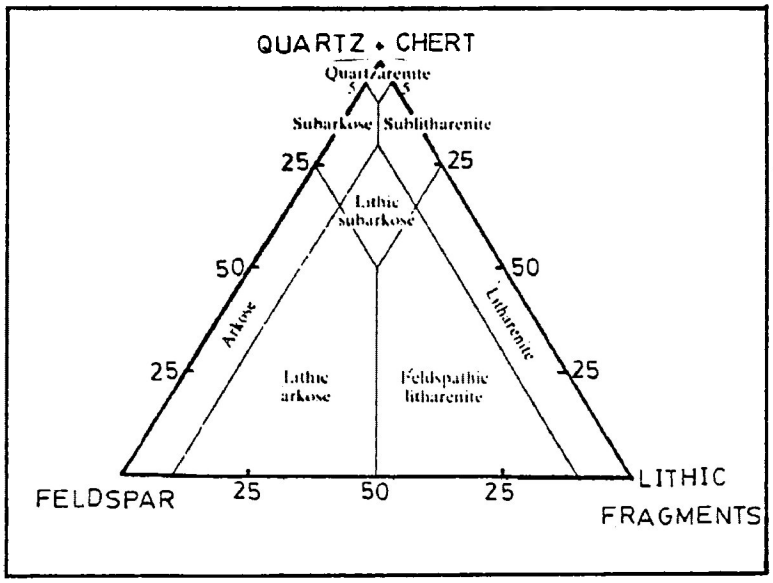

Figure 10. Classification system for sandstones based on relative amounts of quartz fragments, feldspar fragments and lithic fragments. Fragments are >0.02mm. (from Pettijohn et. al., 1972).

depositional lobes.

3. Lower fan.

4. Basin plain.

Using this submarine fan model, turbidites could be placed in a more exact depositional environment(see Fig. 9). For example, AE turbidites would be proximal to the fan-channel in the mid- to upper fan, while thin-bedded BCDE or CDE turbidites would be channel-distal, associated with the lower fan, the basin plain, or interchannel areas..

Walker(1984) describes five facies which account for all depositional sequences of his fan model:

1. Classical turbidites, as described above, with the Bouma sequence as the ideal.
2. Massive sandstones.
3. Pebbly sandstones.
4. Conglomerates.
5. Slumps, slides, debris flows and other exotic facies.

In the present study area, only the classical turbidite facies is observed. This is hardly surprising, since classical turbidites are associated with the mid fan, lower fan and basin plain, and these divisions account for, by far, the most extensive area of the submarine fan environment. Elsewhere within the Quetico metasedimentary belt, pebbly sandstones and conglomerates have been observed to a limited extent(see, e.g., Dutka, 1982).

In the east and west parts of the study area, ABE, ABDE, and BDE turbidites are most commonly observed. In some locations, the entire Bouma sequennce is represented. The A or B horizons are dominant, but all horizons are relatively thin-bedded, rarely exceeding 20

centimeters in thickness. The turbidites of these parts of the study area are interpreted as part of the lower-mid to outer submarine fan depositional environment.

In the central parts of the study area, there is an increase in both proportion and thickness of the A horizon. ABE, BCE and AE turbidites dominate. These are best observed in the series of outcrops along Highway 11 east of Little McCauley Lake(Fig. 6). Here, massive to graded sandstone beds up to one meter thick are common. By comparison, other horizons are thin. Turbidites in the central part of the study area are interpreted as part of the mid fan region of a submarine fan.

A more comprehensive interpretation of the depositional environment of the Quetico metasedimentary rocks is beyond the scope of this study. It should be noted, though, that a general paucity of outcrop and a recognition of the rather complex structural geology of this area would make a more detailed study somewhat difficult.

CHAPTER FOUR

STRUCTURAL GEOLOGY AND METAMORPHISM

4-1. Structural Geology

Part of the present study involved a re-investigation of the structural geology previously reported and interpreted by Borradaile(1982), Stubley(1983) and Stewart(1984)(see Fig. 2). Dutka(1982) also conducted a detailed structural mapping of a section of the Quetico metasedimentary rocks some 10 kilometers east of the present study area, close to Atikokan.

The interpretation of structural geology of the present study is based on data compiled by the three authors, by the re-investigation of the three respective area, and by myself from structural mapping in an area east of and adjacent to the area studied by Stewart(1984) (Fig. 2).

Interpretation of the major structural features of the Quetico rocks is based on the observation and interpretation of the following structural elements in outcrop and handspecimen scale.

1. S-surfaces.
2. Bedding-cleavage intersection lineations.
3. Local younging directions.
4. Asymmetric minor folds.
5. Fold structural facing.

S-surfaces

There are two planar surfaces consistently found in outcrop. sedimentary bedding surfaces(S_0) and cleavage surfaces(S_1)

Numerous bedding (S_0) surfaces are generally exposed in each outcrop. Massive sandstones, graded sandstones, mudstones and mudstone-sandstone laminations vary in thickness from one meter to less than one centimeter.

A single penetrative cleavage is observed in all outcrops and is designated S_1. In thin section, the cleavage is observed to be continuous and defined by the preferred crystallographic orientation of phyllosilicates and, subordinately, by the preferred dimensional orientation of quartz and feldspar. In outcrop, cleavage is observed to be better developed in mudstones than in sandstones. S_1 surfaces are often difficult to see in outcrop in sandstones, and can be measured only by the observation of the orientation of individual coarse phyllosilicates or by discontinuous fracture cleavage surfaces.

In some outcrops(e.g. sample location P51, see Fig. 6), well-developed refracted cleavage is observed(Plate 9). The refracted cleavage is always found in graded sandstone beds. The angle between S_0 and S_1 surface traces on the outcrop surface varies systematically from 55 degrees at the coarse-grained base to less than 10 degrees at the argillaceous top of the graded beds.

Other S-surfaces include minor kink bands and brittle-ductile shear zones. Both structures displace S_0 and S_1 surfaces in the example illustrated.

Kink bands are observed in many outcrops. The bands are generally less than one centimeter in width, irregularly spaced and discontinuous. In some locations(e.g. sample location T43, see Fig. 6), regularly-spaced, asymmetric kink bands are found.

Brittle-ductile shear zones, like kink bands, are observed in many

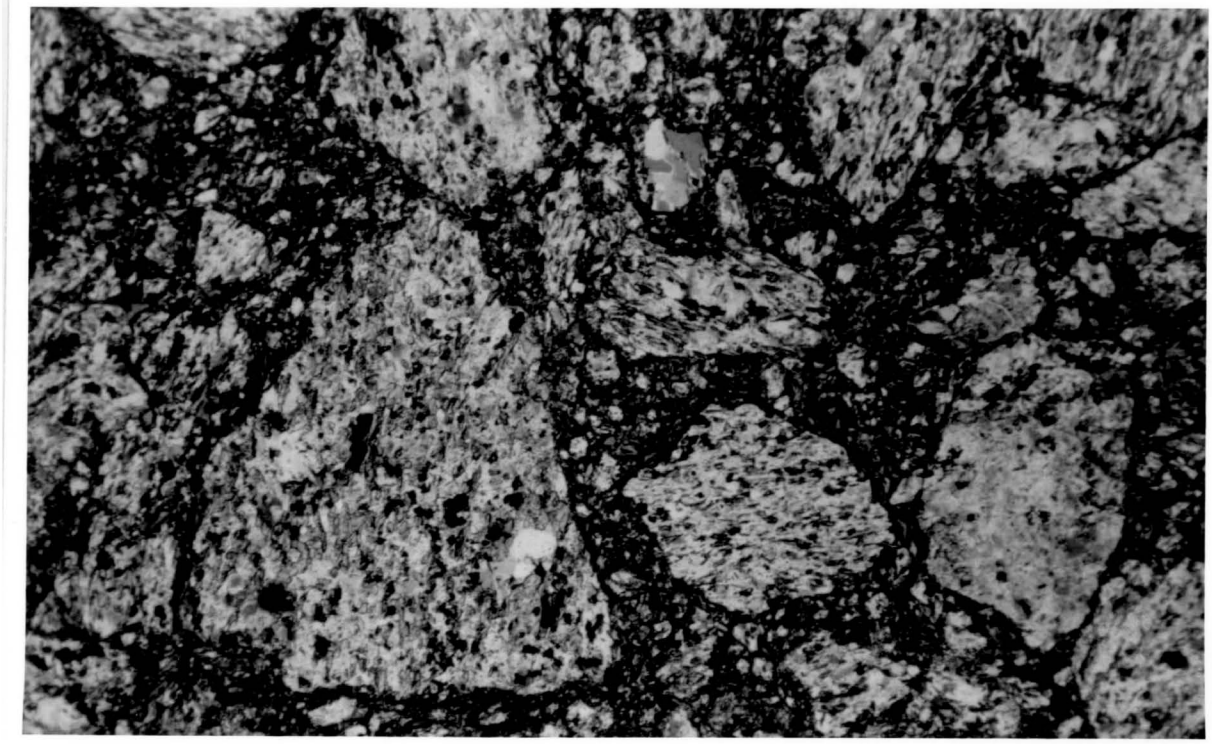

Plate Seven. Photomicrograph of a brecciated metasandstone (sample location P25 - see Fig. 6). The sub-angular to sub-rounded fragments range in size from over one centimeter to less than one millimeter in diameter. Note that the fragments possess well-developed continuous cleavage traces, principally defined by the preferred crystallographic orientation of phyllosilicates. The cleavage traces, however, are differently-oriented in different fragments, indicating that brecciation was a post-S_1 cleavage event.

1 cm = 0.2 mm

Plate Eight. Outcrop surface of brecciated metasandstone (sample location - see Fig. 6). Pocket knife is 7 centimeters long.

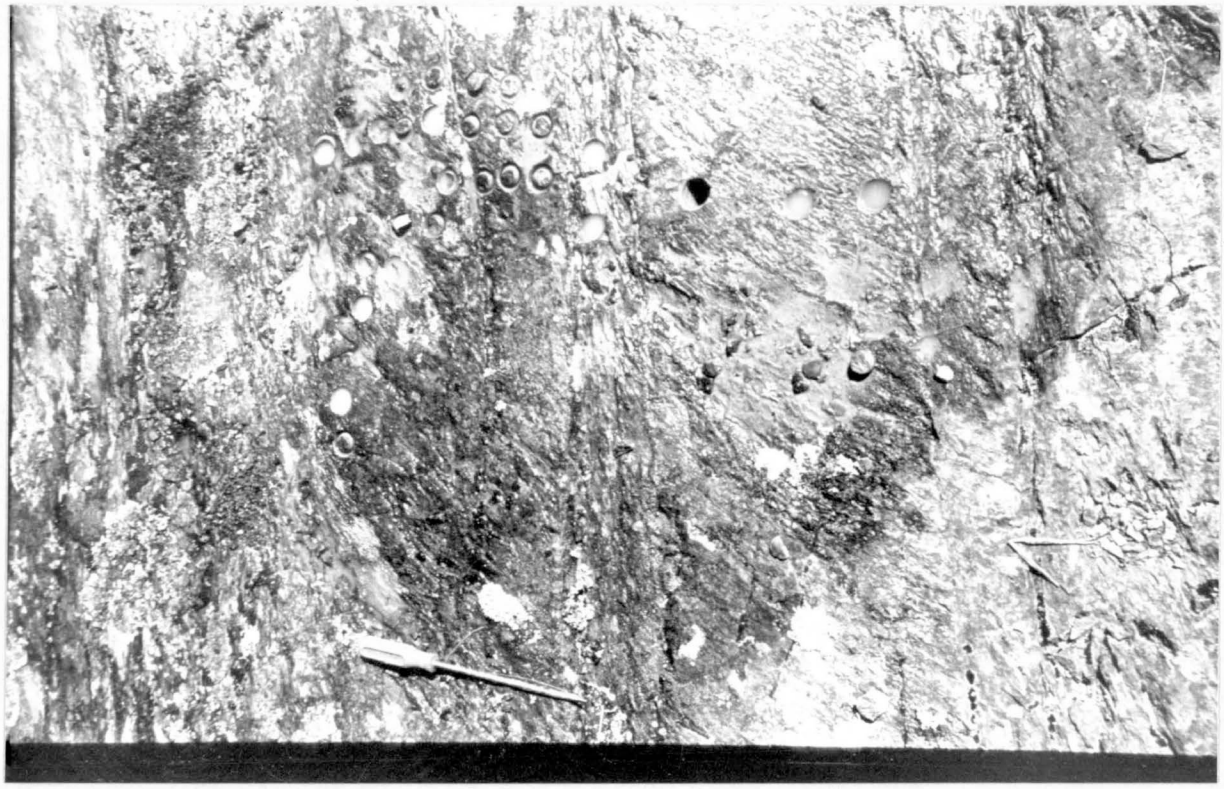

Plate Nine. Well-developed S_1 cleavage refraction in graded sandstone beds with argillaceous tops (PLR samples - see Fig. 6). S_0 bedding planes are oriented at 085-90. S_1 cleavage plane orientation varies from 030-45 at the sandstone base of the beds to 075-70 at the argillaceous top of beds.

Plate Ten. Well-developed bedding-cleavage intersection lineations in Quetico metasedimentary rocks in the face of a mudstone rock exposure next to Highway 11(F2 sample location - see Fig. 6). Note the curvilinear nature of these S_0/S_1 intersection lineations.

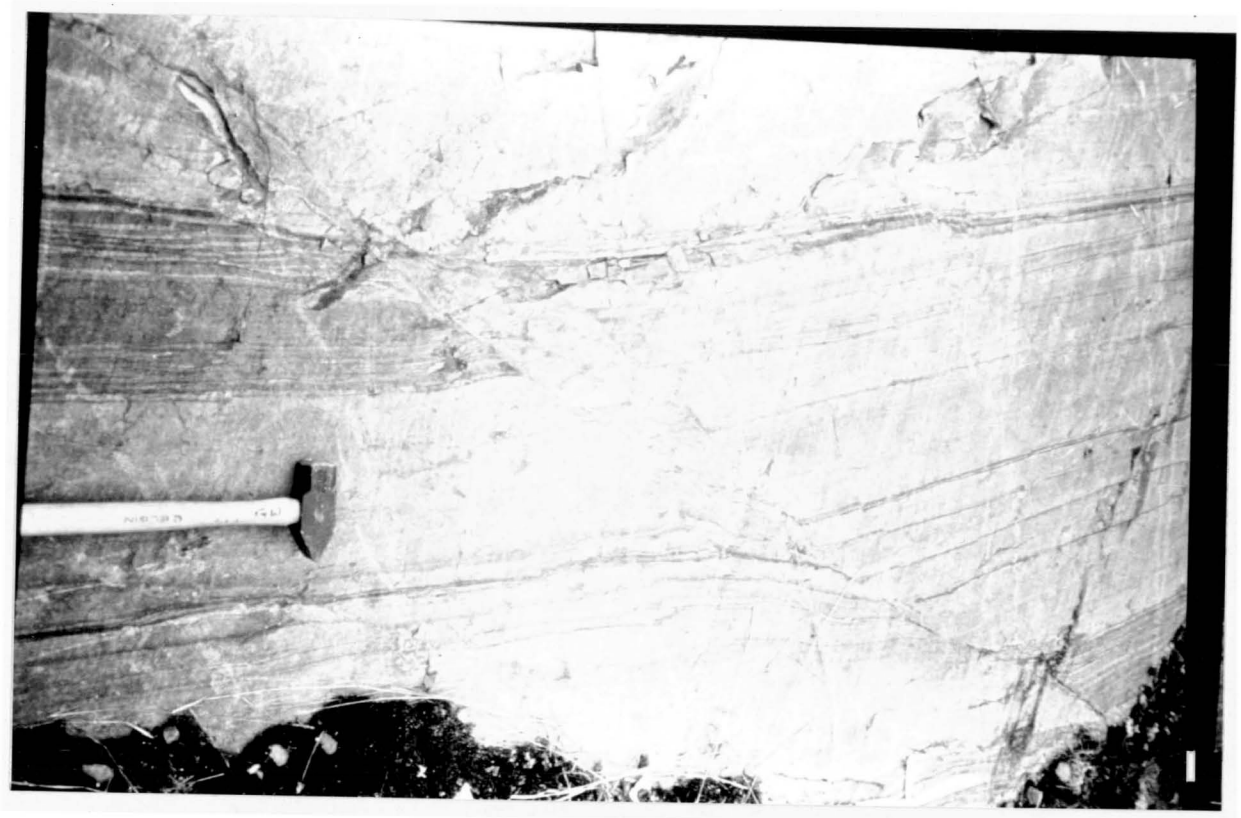

Plate Eleven. Brittle-ductile shear zone (S_2 surface) at the top surface of a Quetico meta-sedimentary rock outcrop next to Highway 11(sample location P36 - see Fig. 6). This S_2 plane is oriented at 100-90 and displays dextral displacement. The hammer is resting on a turbidite bed which displays all five horizons of the ideal Bouma sequence.

outcrops(Plate 11). The shear zones are discontinuous with variable widths up to one meter. The zones are characterized by the bending and/or faulting of S_0 and S_1 surfaces, thinning and boudinage of bedding and intensification of the planar penetrative deformational fabric. Quartz-filled, sigmoidal-shaped tension fractures are present in some shear zones. Displacement of S_0 and S_1 surfaces along the shear zones rarely exceeds 10 centimeters.

Both kink bands and shear zones are oriented in conjugate sets at approximately 035-90 and 120-90. The planes oriented at 035-90 generally display right-lateral displacement; those at 120-90 generally display left-lateral displacement.

The fact that both kink bands and shear zones displace S_0 and S_1 surfaces, that both are oriented at a coincidental set of conjugate attitudes with the same sense of displacement, and the observation that some kink bands progressively change into a gentle bending of S_0 and S_1 surfaces all suggest that the kink bands and brittle-ductile shear zones are related to the same deformational episode. Both are designated S_2 surfaces and are arbitrarily assigned to a D_2 deformational episode for this area. S_2 surfaces are widely- and irregularly-spaced, discontinuous and display very little displacement.

Bedding-cleavage intersection lineations

Only one lineation is consistently observed throughout the study area: the bedding-cleavage intersection lineations(S_0/S_1 linearions). These lineations are most clearly developed in mudstones and fine

sandstones.

Systematic structural mapping of outcrops failed to reveal evidence of consistently-oriented silicate mineral lineations. It is apparent these silicate minerals describe predominantly a flat-shaped fabric in the Quetico metasedimentary rocks.

Local younging directions

There are a number of primary sedimentary features in the present study area which indicate local younging. The most common is graded bedding, representing the A horizon of turbidite sequences. Turbidites are unreworked, deep-water sedimentary deposits and it is believed that graded bedding is a reliable younging indicator, although local coarsening-upward cycles are present. Care must be taken to decide whether a perceived graded bed is, in fact, a single bed.

Cross-stratification is another fairly common younging indicator. Again, care must be taken in the present study area to distinguish cross-stratified foreset beds from sigmoidal-shaped tension fractures which are present in some thin-bedded sandstones.

Other local younging direction indicators include scour channels, bed loads and flame structures.

Asymmetric minor folds

Asymmetric minor folds are only rarely exposed in the present study area. Intrafolial folds are often observed in sandstone-mudstone laminations, but their sense of symmetry is difficult to discern from these folds.

Where possible, the sense of symmetry and the plunge of fold axes of the minor folds have been recorded.

Fold structural facing

Structural facing is an important structural parameter which provides insight into structural style, fold orientation and stratigraphic order of a deformed rock sequence in three dimensions. The term was first used by Cummins and Shackleton(1955). Shackleton(1958) clarified the concept of fold structural facing, defining it as the direction, parallel to a fold's axial plane, and perpendicular to its fold axis, in which progressively younger strata is encountered(Fig. 11A).

Under this definition, structural facing has important stratigraphic implications. In an area of folded strata, local younging directions can vary considerably. The structural facing direction, however, is consistent and indicates the direction in which the stratigraphic succession, as a whole, becomes younger(Fig. 11A). Reversals or strong variations in structural facing directions may, but need not necessarily, indicate polyphase deformation(Fig. 11B).

When folded rocks possess an axial planar cleavage, and when local younging direction is known, the angular relationship of folded layering and axial planar cleavage can be utilized, and fold structural facing direction can be determined at the limbs of a fold(Borradaile, 1976). Axial planar cleavage planes are approximately(though not necessarily strictly) parallel to the axial plane of the folded layering. As well, the intersection lineation between axial planar cleavage and folded layering is approximately parallel to the fold axis(Fig. 11C). Refering to Shackleton's definition, and substituting axial planar cleavage for axial plane and intersection lineation for fold axis, structural facing can be determined at the limb of a fold as the direction, parallel to axial planar cleavage surfaces and perpendicular

Figure 11. The concept of structural facing.

A. Fold structural facing direction (heavy arrows) is the direction, parallel to the axial plane (stippled) and perpendicular to the fold axis, in which progressively younger strata is encountered. Note that, in the series of folds, local younging direction, as indicated by graded bedding, varies considerably from limbs to hinge zones, but structural facing direction is consistent throughout.

B. Reversals in structural facing direction may indicate more than one phase of folding. In this example, a large recumbent fold is refolded into a series of second folds. Reversals of structural facing directions on second cleavage surfaces indicate the location of the first (recumbent) fold axial surface (from Borradaile, 1976).

C. Structural facing may be determined at the limbs of a fold when it can be shown that the fold possesses an axial planar cleavage. Here, structural facing direction (heavy arrow) is the direction, parallel to the axial planar cleavage surfaces and perpendicular to the intersection lineation of the cleavage and folded surface, in which progressively younger strata is encountered.

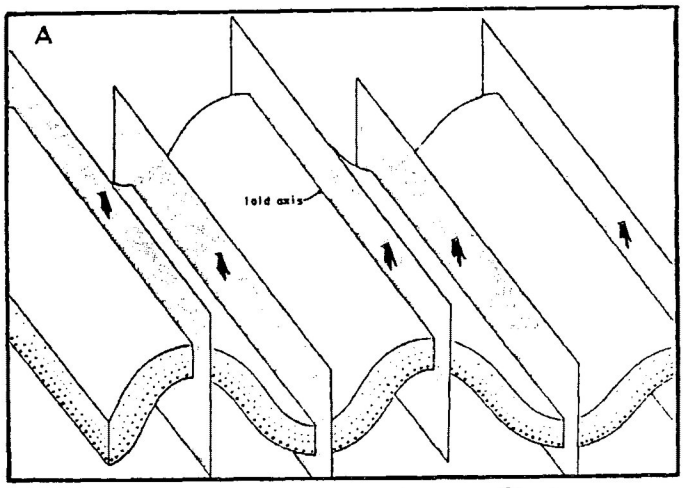
A
fold axis

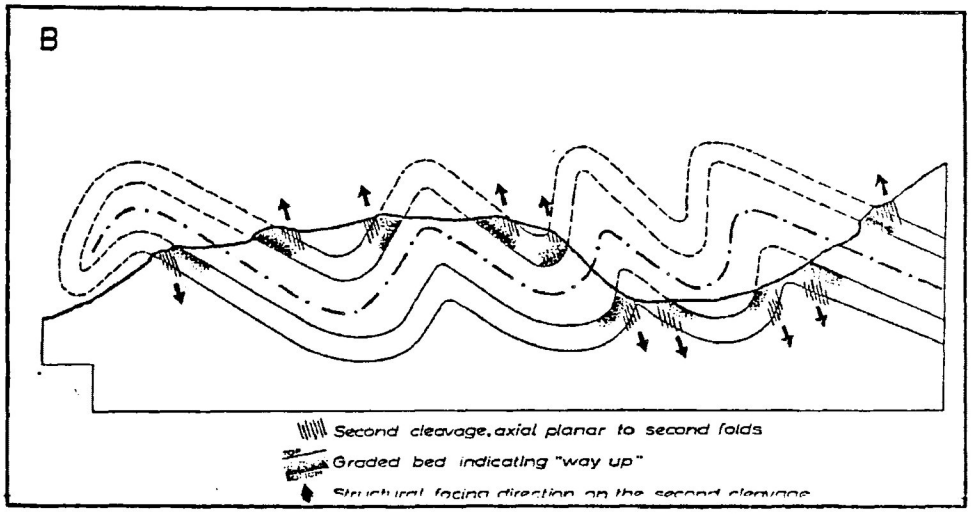
B
Second cleavage, axial planar to second folds
Graded bed indicating "way up"

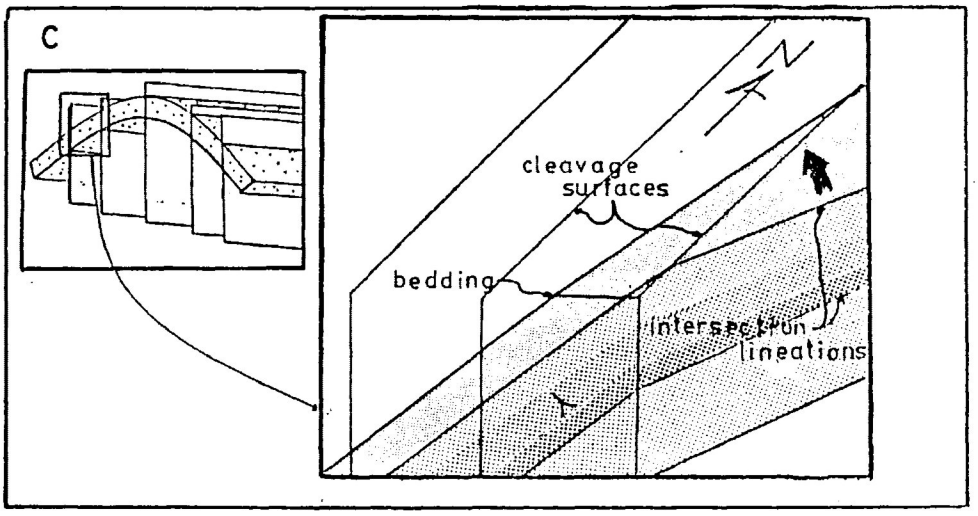
C
cleavage surfaces
bedding
intersection lineations
N

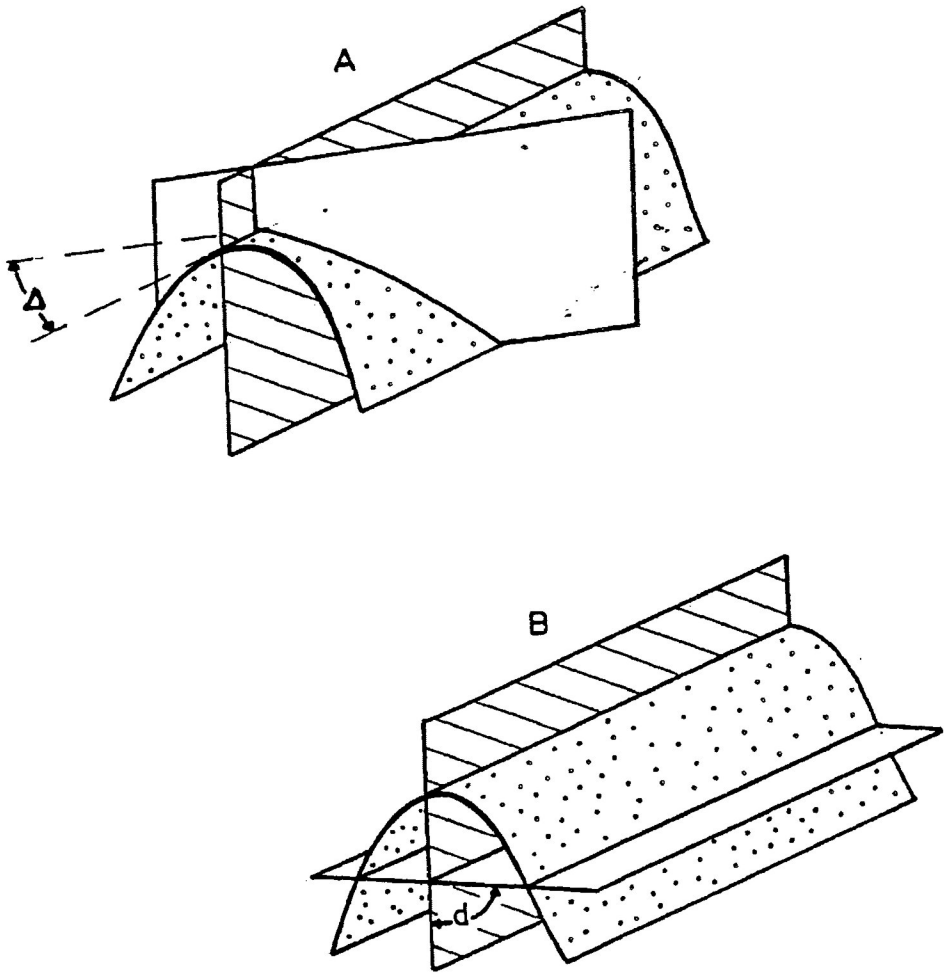

Figure 12. The two extremes of angular relationships between cleavage planes and the axial plane of transected folds, where Δ is the dihedral angle between the cleavage planes and the fold axis, and d is the angle between the cleavage planes and the axial surface of the fold. When $\Delta = d = 0$, cleavage is parallel to the axial plane, and is termed axial planar.

A. $d = 0 \neq \Delta$. Note that cleavage may appear to be axial planar in the fold profile.

B. $\Delta = 0 \neq d$. Note that the intersection lineations between cleavage planes and fold surface are parallel to the fold axis.

to layering-cleavage intersection lineations, in which the layering becomes younger(Fig. 11C).

Determination of structural facing directions at the limbs of folds from bedding-cleavage relationships requires the cleavage to be axial planar. In the overwhelming number of cases of syn-deformational cleavage development, cleavage planes are axial planar to folds generated by that deformation phase. There are, however, rare recorded cases in which cleavage, of both post-deformational and syn-deformational origin, is not axial planar(Borradaile, 1978). Folds with non-axial, synchronous planar cleavage are termed transected folds.

Before determining structural facing directions from bedding-cleavage relationships, then, it is important to establish the relationship, because axial planar cleavage cannot be assumed.

Consider a folded layer containing cleavage planes(Fig. 12). Where Δ is the dihedral angle between the cleavage planes and the fold axis, and d is the angle between cleavage and the axial surface of a fold in the fold profile, cleavage is axial planar when Δ=d=0. Borradaile (1978) suggests that these conditions should be confirmed in a number of well-exposed dominant fold hinges or in minor folds accompanying the dominant folds to establish axial planar cleavage in an area of folded layering.

In the Quetico metasedimentary rocks of the present study area, this angular relationship has been examined in a number of asymmetric minor folds and in a major fold closure exposed beside Highway 11 near Flanders(sample location B28, Fig. 6). In all cases, the conditions Δ=d=0 are satisfied and cleavage can be considered axial planar(see Figs. 13 and 14).

It seems safe, then, to conclude that S_1 cleavage planes are axial

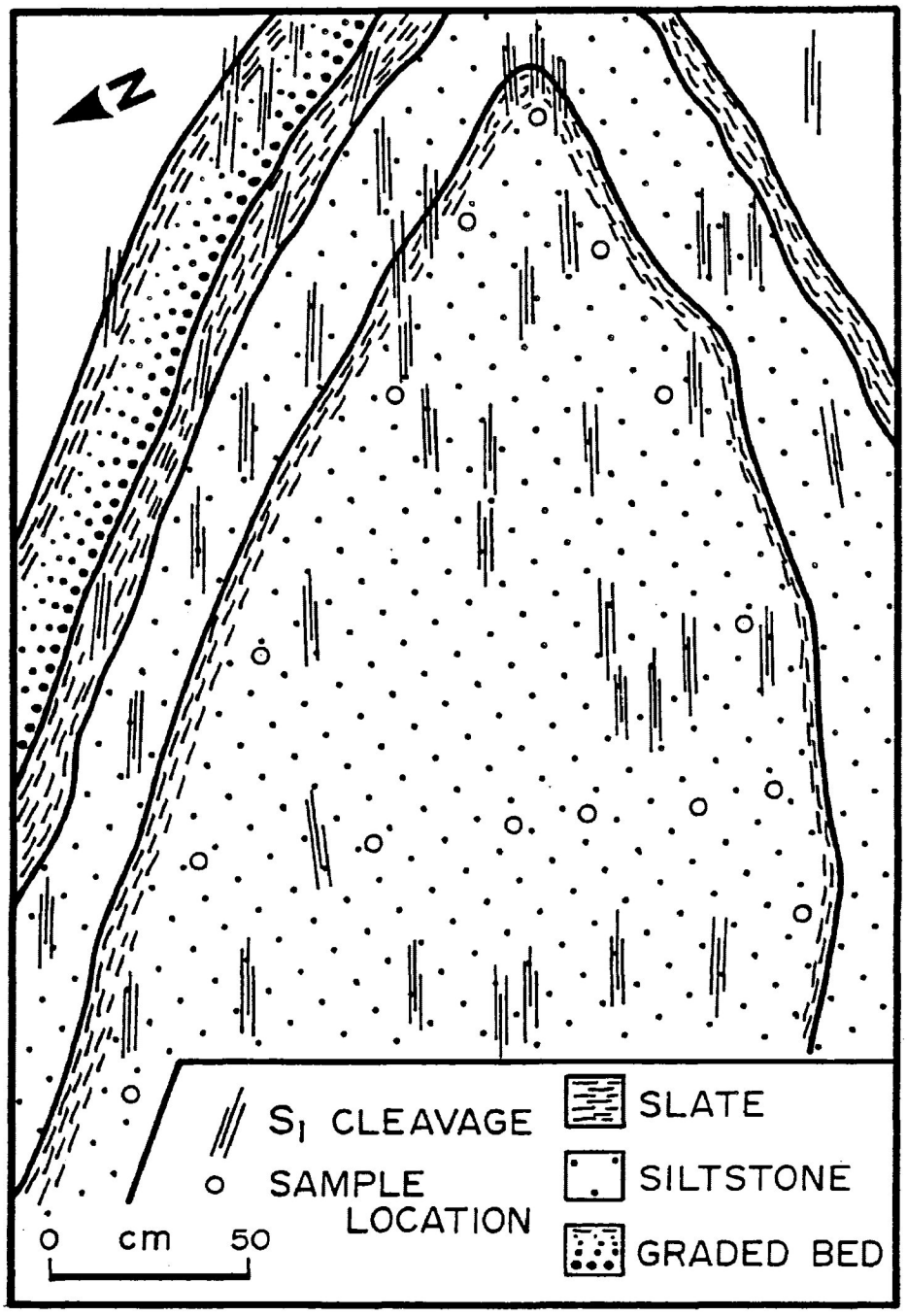

Figure 13. Sketch of near-profile view of a major F_1 fold closure at sample location B28 (see Fig. 6). Note the bedding-cleavage relationship. S_1 cleavage planes are axial planar to the folded S_0 beds.

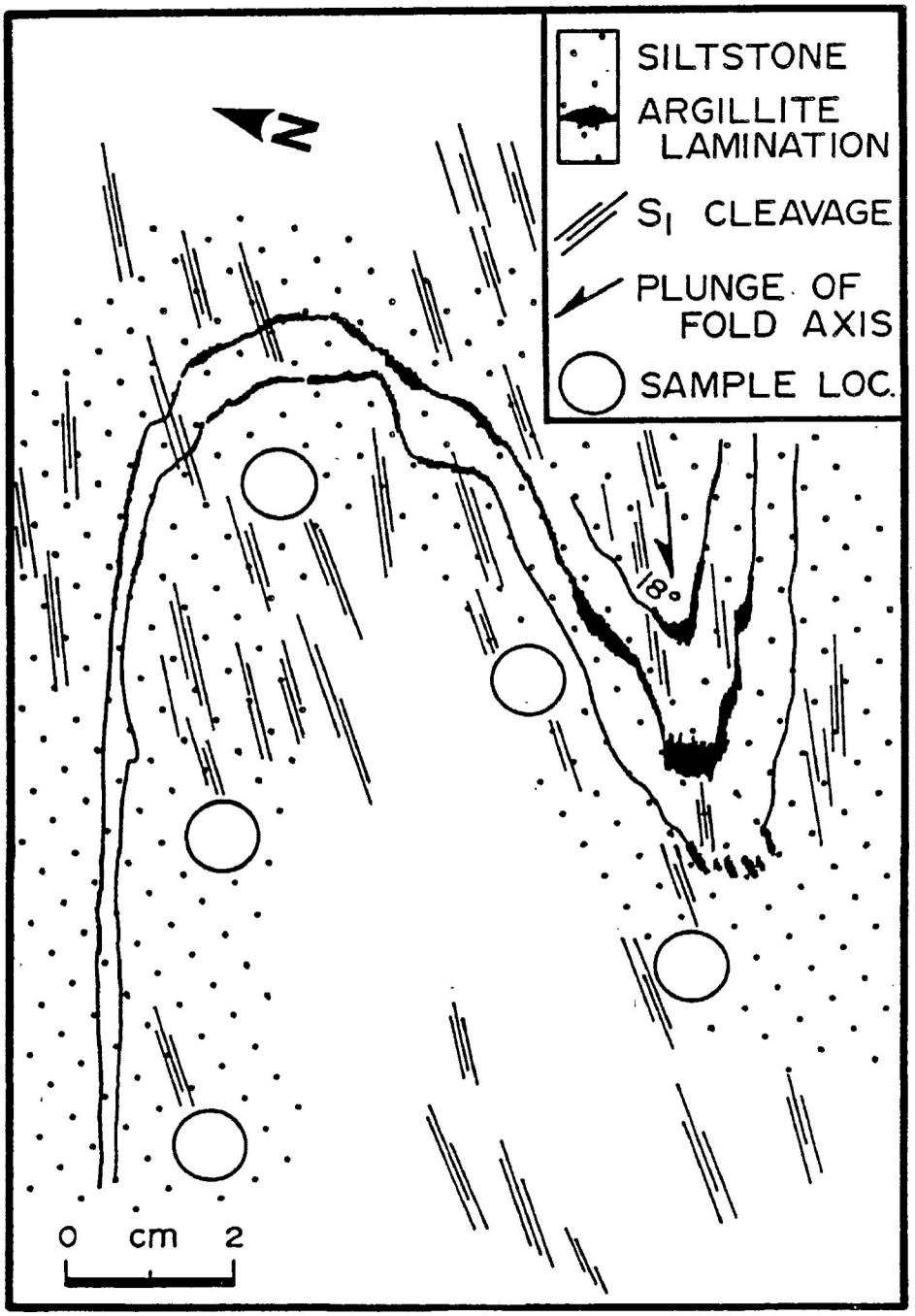

Figure 14. Sketch of near-profile view of a minor, asymmetric F_1 fold at sample location R24 (see Fig. 6). S_1 cleavage planes are axial planar to the minor F_1 fold.

planar to major folds in the Quetico metasedimentary rock sequences, and bedding-cleavage relationships can be used to indicate location and sense of closure of folds and to determine structural facing directions.

Major structural features

Analysis and delineation of major structures is based on careful investigation and interpretation of related minor structural features observable in outcrop scale: S-surface relationships, local younging directions, structural facing directions and asymmetric minor fold orientations.

From these features, two deformational episodes have been delineated.

Figure 15 provides a summary of minor and major structural features of the present study area. The structural geology map in the inside flap of the back cover of this thesis provides a more detailed representation of structural data.

S_0 bedding surfaces are relatively consistently oriented, varying little from an average strike of approximately 080 degrees, and usually dipping very steeply toward the north or south.

S_1 cleavage surfaces, like S_0 surfaces, display a relatively consistent orientation throughout the study area. The average S_1 surface strikes at approximately 075 degrees and dips near-vertically or occasionally steeply to the north or south.

S_0/S_1 intersection lineations have variable orientations within a plane approximately parallel to S_0 and S_1 planes, and this can be observed even in outcrop scale. A contoured stereograph of S_0/S_1

Figure 15. Map of the major structural features of the Quetico metasedimentary rocks in the Calm Lake - Perch Lake area.

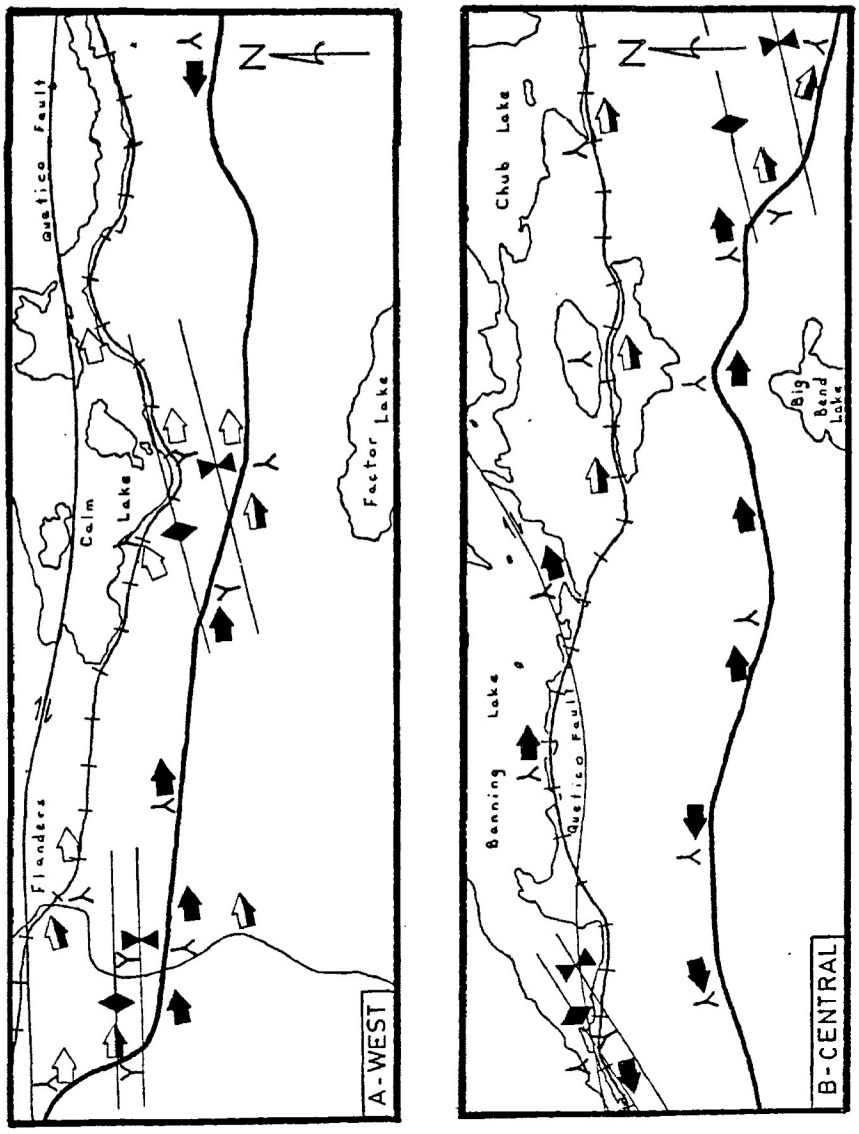

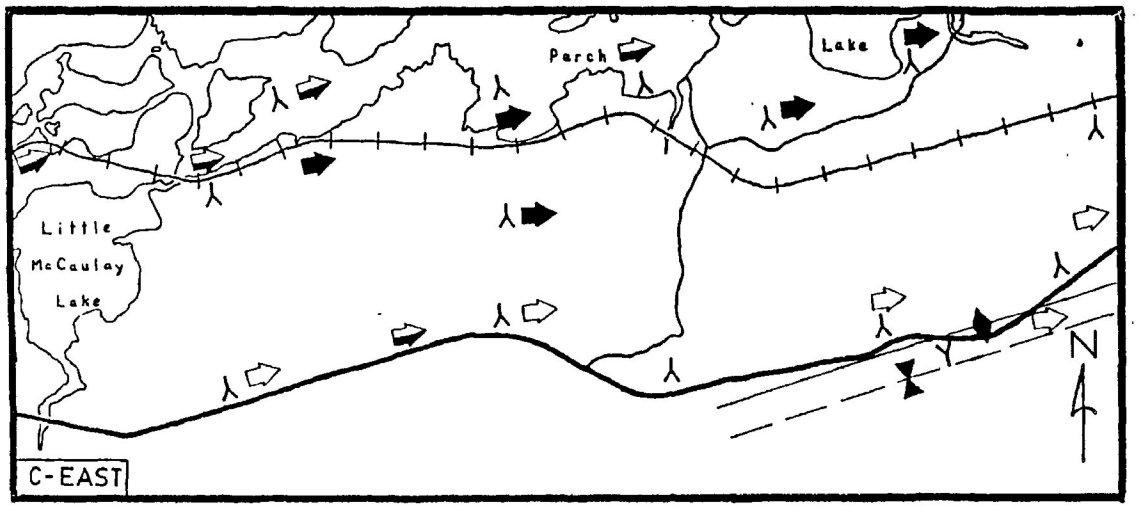

Major F_1 axial trace:
Syncline
Anticline

Structural facing directions:
Upward
Sideward
Downward

Local younging directions: top

Scale 0 1 2 km

Canadian National Railroad

Provincial highway 11

Other road

lineations defines a number of density maxima(Fig. 16B).

Most local younging directions are toward the north(Fig. 15). There are some locations, however, where local younging directions are toward the south. These are invariably accompanied by a change in bedding-cleavage relationship although the structural facing direction remains constant. Such reversals in the local younging direction help to bracket the locations of major F_1 fold axial traces(Fig. 15).

Structural facing directions, like S_0/S_1 intersection lineations,have a wide range of orientations and often vary systematically from upward- through sideways- to downward-facing over a distance of approximately three kilometers in the prominent structural strike direction. Most structural facing directions, however, have an east-facing component(Fig. 15).

The characteristics of the outcrop scale structural elements have the following implications for the geometry and attitude of the major F_1 folds:

1. The rather consistent orientation of S_0 planes indicates F_1 folds are tight to isoclinal with long limbs and hinge zones of relatively small volume in narrow zones.
2. The preponderance of northward younging directions indicates that the major F_1 folds are asymmetric with long north-younging limbs alternating with short south-younging limbs.
3. The strong variation in directions of both structural facing and bedding-cleavage intersection lineations indicates that the fold axes of the major F_1 folds are strongly curvilinear, possibly

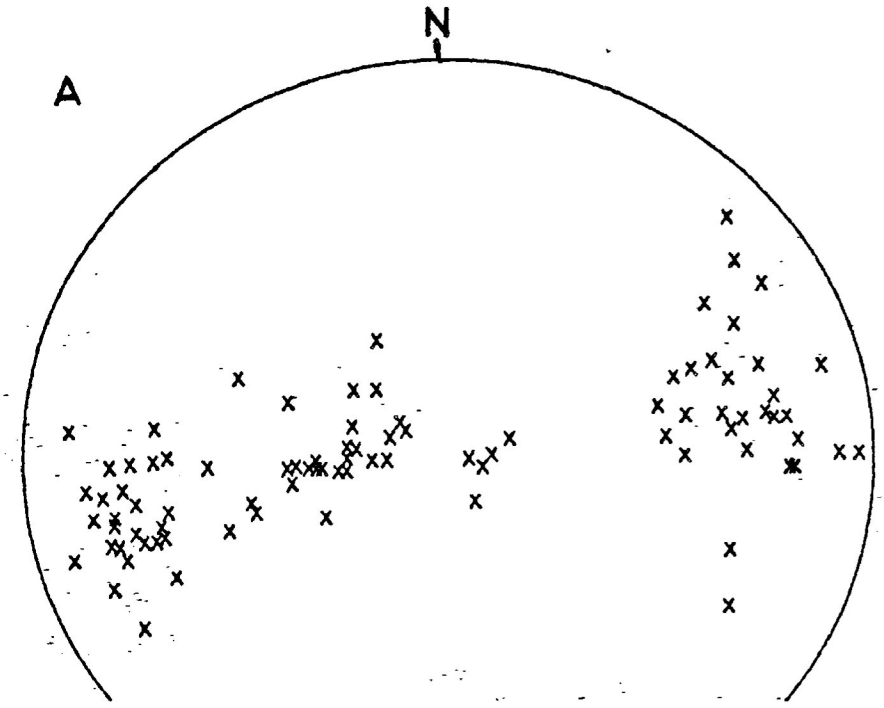

Figure 16A. Stereographic projection of orientations of bedding-cleavage (S0/S1) intersection lineations in the Quetico metasedimentary rocks of the present study area.

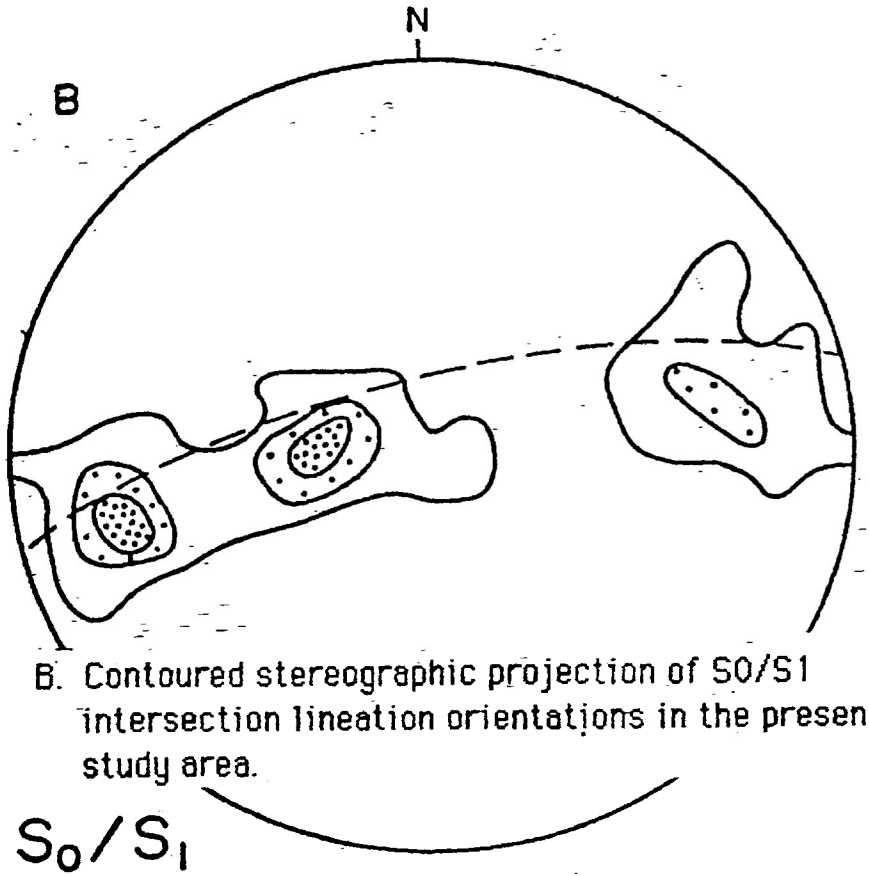

B. Contoured stereographic projection of S0/S1 intersection lineation orientations in the present study area.

"sheath-like".

In summary, the structural geology of the Quetico metasedimentary rocks of the present study area is characterized by a number of major F_1 folds. The F_1 folds are tight to isoclinal and asymmetric. They are also non-cylindrical. The fold axes are so strongly curvilinear that, in various locations, folds can be described as upright synclines and anticlines, elsewhere as sideways-closing folds and in still other locations as antiformal synclines and synformal anticlines. The pairs of axial planes of the asymmetric F_1 folds are spaced approximately three to four kilometers apart in roughly en echelon arrangment subparallel to the dominant east-west structural trend(Figs. 15 and 17).

In one location(sample location P26, see Fig. 6), a zone of brecciation is present. The breccia zone is composed of lithified sub-angular to sub-rounded fragments of gradational size range from over one centimeter to less than one millimeter in diameter(Plates 7 and 8). The zone boundary is irregular, varying from sharp to gradational. At one point, the zone boundary is characterized by the bending of S_0 and S_1 surfaces, followed by incipient fracture and brecciation, then brecciation toward the central part of the zone Careful examination reveals that the sub-angular, variably-oriented breccia fragments possess S_1 cleavage surfaces, indicating the brecciation is a post-cleavage deformation phase. Elsewhere, S_2 shear zones are observed displacing the breccia zone

The breccia zone may represent a late-stage brittle deformation phase of the D_1 deformation episode (the same episode that earlier

generated the S_1 cleavage and the major F_1 folds).

The final phase of deformation observable throughout the present study area is represented by the conjugate set of S_2 kink bands and brittle-ductile shear zones, oriented at approximately 035-90 and 120-90, displaying right-lateral and left-lateral displacement, respectively. Displacement along these surfaces rarely exceeds ten centimeters. The S_2 surfaces represent the structural features of the local D_2 deformational episode. The S_2 surfaces are generally irregularly-spaced and discontinuous, and have an insignificant effect on the structural features and trends of the D_1 deformational episode.

Table 1 summarizes the sequence and structural features of the two deformational episodes.

Table 1. Sequence and features of the D_1 and D_2 deformational episodes affecting the Quetico metasedimentary rocks in the Calm Lake - Perch Lake area.

D_2 episode	Development of conjugate sets of minor, irregularly-spaced, discontinuous kink bands and brittle-ductile shear zones. The S_2 surfaces are oriented at approximately 035-90 and 120-90, and display right-lateral and left-lateral displacement, respectively, of less than one meter.
D1 episode	Late-stage brittle deformation forms local, discontinuous brecciation zones.
	Development of major F1 folds in roughly en echelon arrangement along a dominant east-west structural trend. F1 folds are tight to isoclinal, asymmetrical and non-cylindrical. Axial planes trend east-west and dip near-vertically, but fold axes are strongly curvilinear. Contemporaneous development of pervasive, continuous axial planar cleavage, and asymmetric minor folds.

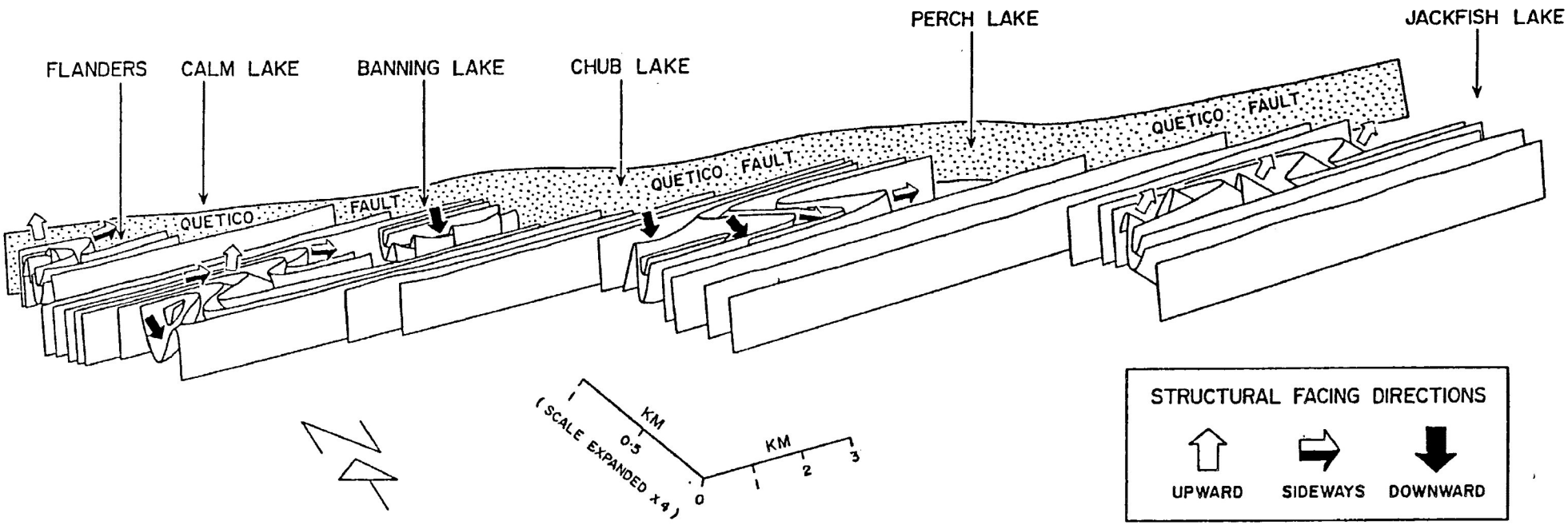

Figure 17.

THREE - DIMENSIONAL REPRESENTATION OF STRONGLY CURVILINEAR FOLDS IN THE QUETICO METASEDIMENTARY ROCKS OF THE CALM LAKE - PERCH LAKE AREA, WITH RELATIVE POSITION OF THE QUETICO FAULT (NOTE THAT WIDTHS OF STRUCTURES ARE EXAGGERATED RELATIVE TO LENGTHS).

4-2. Metamorphism.

The Quetico metasedimentary-gneissic belt (Fig. 1) everywhere displays a similar pattern of metamorphism: a progressive increase in regional metamorphism from both south and north margins toward a central axis comprised of paragneiss, migmatites and diatexite (Pirie and Mackasey, 1978). This progressive metamorphism is observed in the present study area. Metamorphism in the northern parts of the area, adjacent to the Quetico-Wabigoon belt boundary, is characterized by anchimetamorphism, typified by chlorite-sericite metapelites and phyllites. In the south parts of the study area, biotite schists are predominant.

Stable metamorphic mineral assemblages within the Quetico metasedimentary rocks, in order of increasing metamorphism (or from north to south), are as follows:

1. Chlorite-muscovite.
2. Chlorite-muscovite-epidote(-sphene).
3. Chlorite-muscovite-biotite-epidote(-sphene).
4. Biotite-chlorite-muscovite-epidote(-sphene).

(Metamorphic quartz and plagioclase are included in all assemblages).

Metamorphic isograds are approximately east-west, subparallel to regional structural trends.

Chlorite, muscovite, epidote and sphene are very fine-grained minerals which, with quartz and plagioclase, comprise most of the matrix of the metasedimentary rocks. Within metamorphosed mudstones and mica-rich laminations, fine-grained chlorite and muscovite assemblages form greater than 50 percent of the rock,

undoubtedly derived from the breakdown of detrital or diagenetic clay minerals such as illite and smectite. Sub-parallel orientation of the phyllosilicates defines the continuous cleavage of the rocks.

Epidote is first observed in the metasedimentary rocks approximately one kilometer south of the Quetico-Wabigoon boundary. In thin section, epidote is present in minor amounts as very fine-grained, sub-rounded, randomly dispersed crystals. It is also present as inclusions in poikioblastic plagioclase blasts and as an alteration product, along with muscovite and carbonate, in saussuritized plagioclase.

Sphene crystals are observed only rarely in thin section as a very fine-grained, sub-rounded grains scattered in trace amounts throughout the rock. Coincident with epidote, sphene is first observed in rocks approximately one kilometer south of the Quetico-Wabigoon boundary. Also like epidote, sphene persists southward and both minerals are in some cases present in the coarse biotite schists of the extreme south parts of the study area.

Biotite first appears in outcrops one to two kilometers south of the Quetico-Wabigoon interface. Less than 0.5 kilometer south of its first appearance, biotite is the predominant metamorphic mineral, comprising up to 30 percent of the volume of the biotite schists of the south study area. From thin section examination, it appears that there are two forms of biotite(Plate 1): Fine, elongate grains and more equidimensional grains. The fine-grained assemblage consists of elongate biotite less than 0.2 millimeters long, with sharp, regular grain boundaries. The laths have a strong preferred crystallographic orientation(p.c.o.) defining a continuous cleavage. The coarser-grained biotite assemblage consists of individual crystals and aggregates up to two millimeters in diameter, with elongate to stubby crystal forms and irregular (and in some cases ragged) grain

boundaries. The coarse assemblage has a moderately developed preferred dimensional orientation(p.d.o.), but a rather poorly developed p.c.o.

The amount of biotite increases southward. Concomitantly, the amounts of chlorite and muscovite decrease. Pirie and Mackasey(1978) observed a similar relationship in the eastern extension of the same Quetico sequence at Crooked Pine Lake. They propose that at least some biotite formed at the expense of both chlorite and muscovite.

Carbonate is present in the metasedimentary rocks in variable amounts. Textural relationships suggest three generations of carbonate are present: pre-, syn- and post-metamorphic in origin.

Pre-metamorphic carbonate is observed as patchy lenses and a pervasive carbonate cement binding the matrix. The amount of pre-metamorphic carbonate is probably very variable. The presence of sphene and epidote in many rocks might suggest there was relatively little carbonate in those rocks because calcium-bearing silicates generally do not survive when syn-metamorphic fluids contain moderate concentrations of CO_2(Turner, 1981, p.313).

Metamorphic carbonate is observed as an alteration product of saussuritized plagioclase. It is also intimately intergrown with mica and quartz in pressure shadows of quartz and feldspar fragments.

Post-metamorphic, or secondary carbonate, is observed replacing quartz and feldspar fragments, and as a vug-, fracture- and vein-filling mineral.

4-3. Deformational and metamorphic microfabrics

Microfabrics of the Quetico metasedimentary rocks are observed to be dominated by the preferred crystallographic orientation (p.c.o.)

of metamorphic chlorite, sericite and biotite, and by a number of deformational microstructures which impart a preferred dimensional orientation(p.d.o.) on quartz and feldspar crystals. Both p.c.o. and p.d.o. are penetrative fabric elements, and, combined, define the pervasive continuous cleavage of the rocks.

Quartz and feldspar grains are generally sub-rounded and elliptical. Feldspar grains are generally more deformed than quartz grains. Most grains display undulose extinction, indicating distortion of the mineral by the deformation mechanism of dislocation glide. Subgrain development in many grains indicates incipient recovery and dynamic recrystallization. In some places, development of ribbon quartz attests to more advanced recrystallization.

Most feldspar grains display some saussuritic alterations; many are highly saussuritized. Many feldspar grains also display mechanical twinning, as indicated by the irregular distribution and abrupt termination of twin planes.

Strain shadows are observed symmetrically distributed about some grains. The strain shadow regions are infilled with a fine-grained assemblage of carbonate, quartz, chlorite and mica. Asymmetric distribution of some strain shadows about weakly sigmoidal-shaped quartz grains suggests some component of mechanical rotation accompanying the other deformation mechanisms in development of the p.d.o. of the quartz and feldspar grains.

In the more weakly metamorphosed rocks, stylolitic surfaces are rather rarely observed. The stylolites are identified as dark, anastomosing bands less than 0.5 millimeter wide and rich in opaque minerals and phyllosilicates. Quartz and feldspar minerals within the bands are very fine-grained and coarse clasts of quartz, carbonate and feldspar in contact with the bands are abruptly terminated. The presence of stylolitic surfaces indicates that pressure solution

operated as a deformation mechanism.

There is no evidence in the microfabrics for a pre-existing tectonic fabric. Such evidence is generally in the form of overprinting criteria, such as crenulation cleavage development, or refolding of folds. Pre-existing fabrics can be completely destroyed by subsequent deformation, but such deformations are generally accompanied by high strains and extensive recrystallization at high metamorphic grades. Within the Quetico metasedimentary rocks, some evidence for pressure solution has been found. This mechanism is usually associated with relatively weak deformation, low strain rates and incipient cleavage development. It is difficult to envision the complete eradication of a previous fabric in anchimetamorphosed and weakly deformed rocks; and yet even within these rocks, no evidence for a pre-existing tectonic fabric is found.

It is concluded, then that the continuous cleavage of the Quetico metasedimentary rocks, as defined by the preferred orientation of quartz, feldspar and phyllosilicates is the first cleavage that these rocks have developed.

As noted previously, biotite schists commonly contain two forms of biotite: a fine-grained assemblage of elongate laths with a strong p.c.o.; and a coarse-grained assemblage consistiong of individual crystals and aggregates with elongate to stubby crystal forms and ragged grain boundaries and a very weak p.c.o.

Biotite, like all phyllosilicates, tends to grow fastest in a preferred crystallographic direction: parallel to the basal mineral cleavage planes. In the biotite schists of the Quetico rocks, the growth of the coarse biotite assemblage appears to be strongly influenced by the rock's tectonic fabric. Biotite crystals which grew perpendicular to the lithologic cleavage trace are short and stubby, while those which grew parallel to the cleavage trace are coarse and

elongate. As well, the coarse biotite crystals are observed to overgrow or replace quartz, feldspar and finer-grained phyllosilicates in some places. Such textural relationships imply that the coarse biotite assemblage is post-tectonic in origin. It is possible that metamorphism was longer-lived than tectonism, at least within the biotite schists of the southern part of the present study area.

CHAPTER FIVE
MAGNETIC FABRIC

5-1. Introduction: Terms and definitions.

Magnetic fabric, in the context of this study, refers to the physical arrangement of the magnetic components of the Quetico metasedimentary rocks. The magnetic components of the rocks are represented by certain discrete minerals, and, hence, the lithological magnetic fabric is controlled by the physical and spatial alignment of these *magnetic minerals*.

The magnetic properties of minerals are determined on an atomic scale, and are dependent on the arrangement and interaction of electrons around atomic nuclei. The movement of any electrical charge creates a magnetic field. Electrons are fundamental electrical charges, and movement of electrons create simple magnetic dipoles. Electrons, of course, move in complex orbitals around the nucleus, but they also spin about their own axes. The magnetic dipole associated with electron spin is much smaller than the dipole associated with orbital movement.

When an atom is placed in an external magnetic field, the force of the external field affects both types of electron motion:

Firstly, the orbital movement is modified slightly; electrons slow down and the magnetic dipole is weakened. Since the modification of the electron orbital opposes the external magnetic force, magnetization has a negative value and is termed *diamagnetism*.

Secondly, the axes of the spinning electrons, originally randomly oriented, are reoriented parallel to the direction of the external magnetic field. The electron spin, however, is not slowed and the strength of the spin dipole is unaffected.

It is energetically advantageous to group electrons into pairs in each electron orbital shell. However, when an atom has an uneven number of electrons, the outer shells will contain unpaired electrons. Paired electrons spin in opposite directions to each other. When all electrons of the outer shells are paired, the opposing spins of the electron pairs tend to cancel the directional magnetization caused by the alignment of the spin axis in the presence of an external magnetic field. However, when the outer electron shell contains unpaired electrons, realignment of the spin axes has the effect of adding the spin magnetic dipoles to the external magnetic field to increase the total magnetism. This magnetism has a positive value and is termed *paramagnetism*.

In the transitional series of elements, the atomic configuration allows a number of overlapping electron shells, and it is possible to have as many as five unpaired electrons. With such configurations, magnetism of these elements, and certain minerals containing these elements, is not related to single-atom electron motion, but to the interaction of the outer unpaired electrons of adjacent atoms. The crystal lattice arrangement of these elements and minerals is such that the outer electron shells overlap. Unpaired electrons of adjacent atoms interact and mutually re-align their respective spin axes.

The energy associated with the mutual alignment of spin axes is referred to as *exchange energy*. To reduce the exchange energy to a minimum, spin axes tend, in some cases to align into couples of opposite(or antiparallel) spin directions, effectively cancelling the magnetization(Fig. 19B). Such magnetism is termed *antiferromagnetism*. In some cases, however, electron spin axes are aligned such that the spins are in the same(parallel) direction(Fig. 19A). This leads to the creation of a strong internal magnetization which is often sustained even in the absence of an external magnetic

field (spontaneous magnetization). Such magnetization is termed *ferromagnetism*. Crystal lattices and electron shells are complex, however, and in most cases spin axes align with most in parallel spin direction and some in antiparallel spin direction (Fig. 19C). Thus, an internal magnetization is created which is not as strong as ferromagnetism. This type of magnetization is termed *ferrimagnetism*.

The strength of internal magnetization (at a given temperature) is a function of the strength of the external magnetic field for most substances (Fig. 18). For weak external fields, this relationship is defined by a simple equation:

$$J = kH$$

where J is the magnitude of internal magnetization, H is the magnitude of the external magnetic field and the proportionality constant, k, is the *magnetic susceptibility**.

In many crystals, it has been observed that the strength of internal magnetization varies according to how the crystal is oriented relative to an external magnetic field of constant strength and direction. That is, the crystal's magnetic susceptibility (k) is directionally variable. This property is generally refered to as *magnetic susceptibility anisotropy* (MSA). There are a number of causes of MSA:

*k as defined by the above equation, is dimensionless but may be measured in terms of unit mass, unit volume or unit gram molecular weight. In the present study, unless otherwise stated, k is measured on a per unit cubic centimeter basis, with J and H measured in c.g.s. units.

1. Magnetocrystalline anisotropy.
2. Shape anisotropy.
3. Stringing together of magnetic grains.
4. Alignment of magnetic domains.
5. Magnetostrictive (stress-induced) anisotropy.
6. Exchange anisotropy.

Each is reviewed by Bhatal(1971) and by Banerjee and Stacey(1967). For our purposes, 1. and 2. are by far the most common causes of MSA in rocks and minerals. 3. is a special case of 2.

Minerals, like all crystals, are an ordered arrangement of atoms. The structure of a crystal lattice generally tends to create one or more directions in which it is energetically easier to align electron spin axes (or exchange forces) and, hence, to create "easy" directions of magnetization. Alternately, directions in the crystallographic structure which require considerabe energy to align spin axes are "hard" directions of magnetization. These "easy" and "hard" crystallographic directions of magnetization define the *magnetocrystalline anisotropy.* When placed in an external magnetic field, the tendency of spin axes to align parallel to the direction of external magnetization is balanced by the tendency to seek the lowest magnetocrystalline energy state, as dictated by the "easy" direction of magnetization.

MSA may also depend on grain shape. Consider a crystal which is magnetocrystallographically isotropic(Fig. 20). The internal magnetic field of the crystal attempts to create two free magnetic poles on opposite ends of the crystal surface(Fig. 20A). A certain amount of energy, the *magnetostatic energy,* is required to maintain free magnetic poles. This energy is at a minimum when the poles are furthest apart. In a perfectly spherical grain(Fig. 20B), no strong

Figure 18. Relationship between applied external magnetic field (H) and internal magnetization (J) for a typical rock. In low magnetic fields, the relationship is approximately linear:

$$J = k \cdot H$$

where k is the magnetic susceptibility.

(from Strangway, 1970).

Figure 19. Schematic illustration of electron spin orientation.

A. Ferromagnetism - all spins are parallel, leading to a strong external magnetism is absence of applied field.

B. Antiferromagnetism - spins are in antiparallel orientation, so that there is no external magnetization in absence of an applied field.

C. Ferrimagnetism - an unequal number of spins are antiparallel, so that external magnetism is present in the absence of a applied field, but is much weaker than ferromagnetism.

(from Tarling, 1983).

Figure 20. Magnetic susceptibility anisotropy (MSA) and grain shape. In order to keep magnetostatic energy to a minimum, magnetostatic poles are placed furthest apart on the surface of an elongate grain (A). In a perfectly spherical grain, surface - to - surface distance is equal in all directions, and poles are established parallel to the direction of the applied field. In an elongate rod-shaped grain, poles generally establish at the ends of the grain regardless of the direction of the applied field.

(from Tarling, 1983).

Figure 18

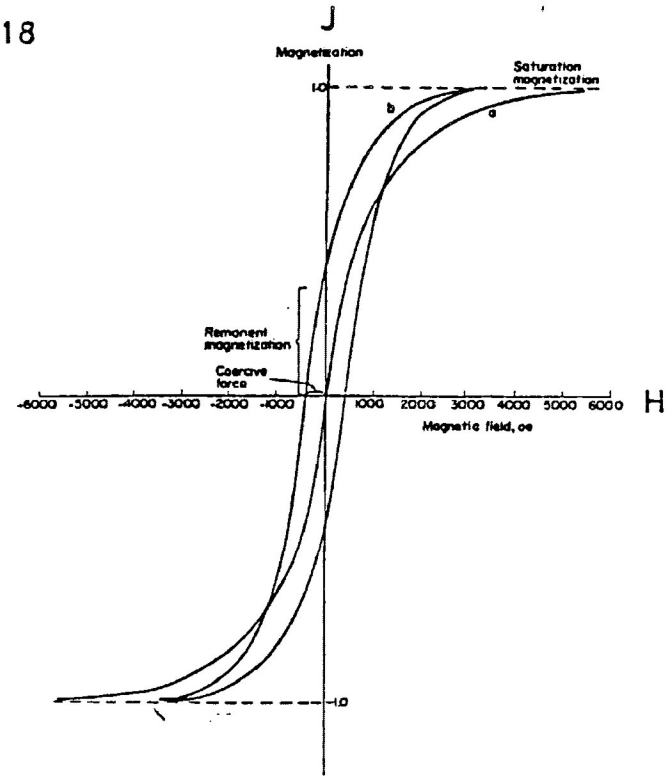

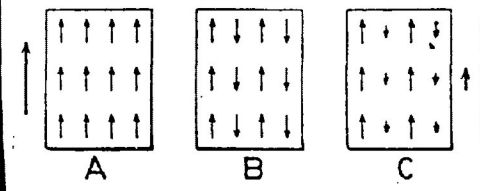

Figure 19

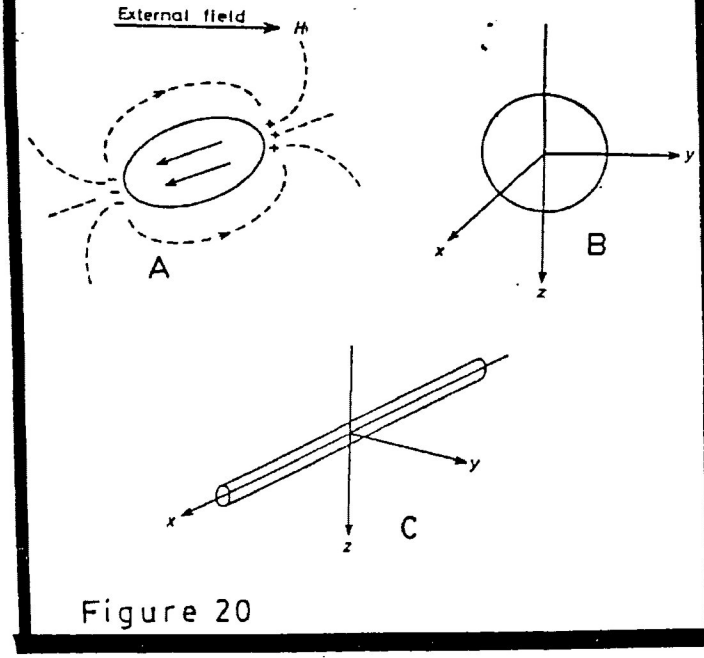

Figure 20

poles develop because distances from surface to surface through the center of the grain are equal in all directions. However, in an elongate, cylindrical-shaped grain(Fig. 20C), strong free magnetic poles develop at either end of the long axis of the grain, and the magnetization direction of the internal magnetic field is parallel to the long axis. When this cylindrical-shaped grain is placed in an external magnetic field, the direction of easiest magnetization is parallel to the grain's long axis because this direction encounters the least opposition from the forces of the internal magnetic field(Fig. 20A). For an ellipsoid-shaped grain, a measure of anisotropy is given by:

$$\Delta k = k_i^2(N_a - N_b)/(1 + N_a k_i)(1 + N_b k_i)$$

where Δk is the difference in susceptibility, k_i is the intrinsic susceptibility, and N_a and N_b are the maximum and minimum demagnetizing factors along the respective axes, caused by the presence of the internal magnetic field(Stacey, 1963). The term k_i^2 in the equation indicates that shape anisotropy is most important in minerals(and rocks) of high magnetic susceptibility. In minerals of high susceptibility, MSA is often defined by shape anisotropy even when the mineral has a pronounced magnetocrystalline anisotropy.

The three most important factors which control the MSA of a rock are:

1. Magnetocrystalline anisotropy of magnetic grains
2. Shape anisotropy of magnetic grains
3. Preferred orientation of magnetic grains

3. may be a preferred crystallographic and/or preferred dimensional orientation. Using mathematical modelling, Hrouda(1982) has graphically represented the relationships between rock MSA, grain MSA, grain dimensional ratio, degree of preferred orientation of grains, and bulk magnetic susceptibility (Fig. 21).

Figure 21B indicates that, for grains with low magnetic susceptibility, shape anisotropy (as represented by dimension ratio a/c) will have little effect on the grain MSA. Hence, in most paramagnetic and diamagnetic minerals (and many ferrimagnetic minerals), MSA is controlled solely by magnetocrystalline anisotropy. The MSA of rocks containing these minerals is dependent on the degree of magnetocrystalline anisotropy and on the preferred crystallographic orientation of the minerals.

Figure 21B also indicates that the grain MSA of minerals with high magnetic susceptibilities is significantly increased with increasing grain anisotropy. Magnetite is an example of a mineral which is magnetocrystallographically isotropic but has a high bulk susceptibility. The MSA of a rock containing magnetite is controlled by the grain anisotropy and the preferred dimensional orientation of the magnetite grains(Fig. 21A).

The MSA of a mineral or rock can be described by a tensor of the second order, the *magnetic susceptibility tensor*:

$$k_{11}\ k_{12}\ k_{13}$$

$$k_{21}\ k_{22}\ k_{23}$$

$$k_{31}\ k_{32}\ k_{33}$$

Completely defined, the magnetic susceptibility tensor describes the *magnitude ellipsoid of magnetic susceptibility*(Fig. 22), with principal orthogonal axes k_{11}, k_{22} and k_{33}. These three principal

Figure 21. The relationship between grain MSA, grain shape and rock MSA.

A. Relationship between degree of MSA of a rock (P_S) and degree of MSA of its grains (P_g). The parameter, C, characterizes the degree of preferred orientation of the uniaxial elongate grains in the rocks.

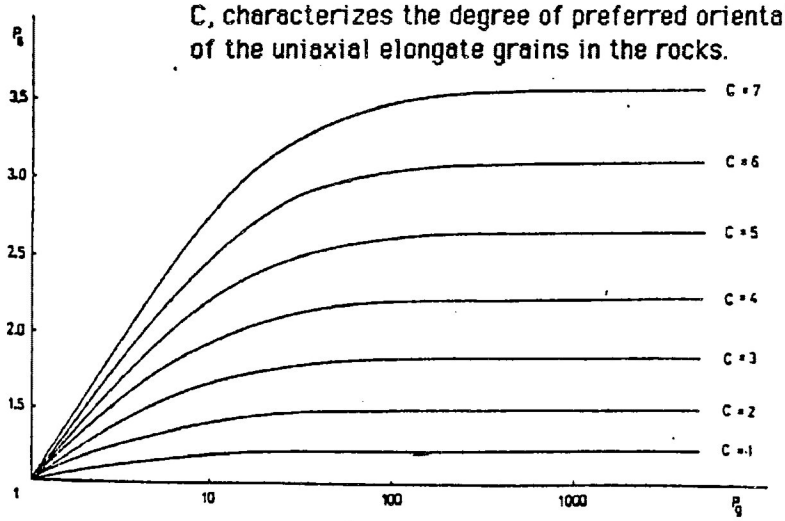

A

B. Relationship between degree of MSA (P_g) and dimensional ratio (a/c) for oblate spheroids. The parameter H characterizes the bulk magnetic susceptibility of the grains. (from Hrouda, 1982).

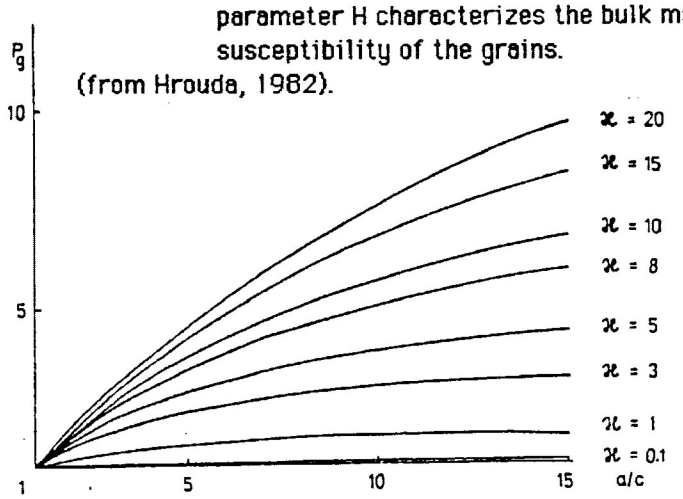

B

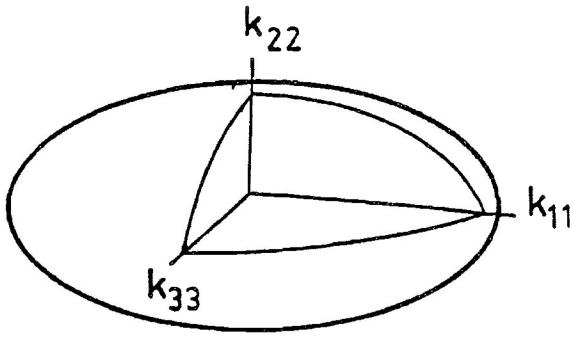

Figure 22. Magnitude ellipsoid of susceptibility with orthogonal principal magnetic susceptibility axes: $k_{11}(=k_{max})$, $k_{22}(=k_{int})$, $k_{33}(=k_{min})$.

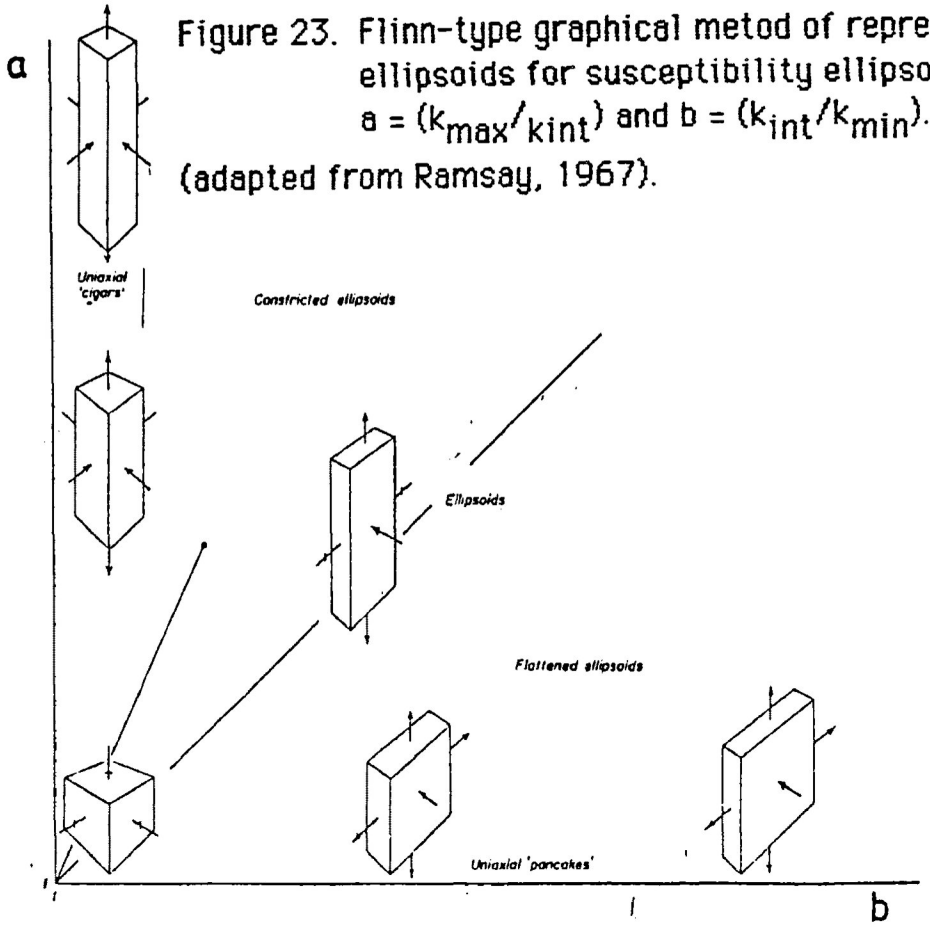

Figure 23. Flinn-type graphical metod of representing ellipsoids for susceptibility ellipsoids: $a = (k_{max}/k_{int})$ and $b = (k_{int}/k_{min})$. (adapted from Ramsay, 1967).

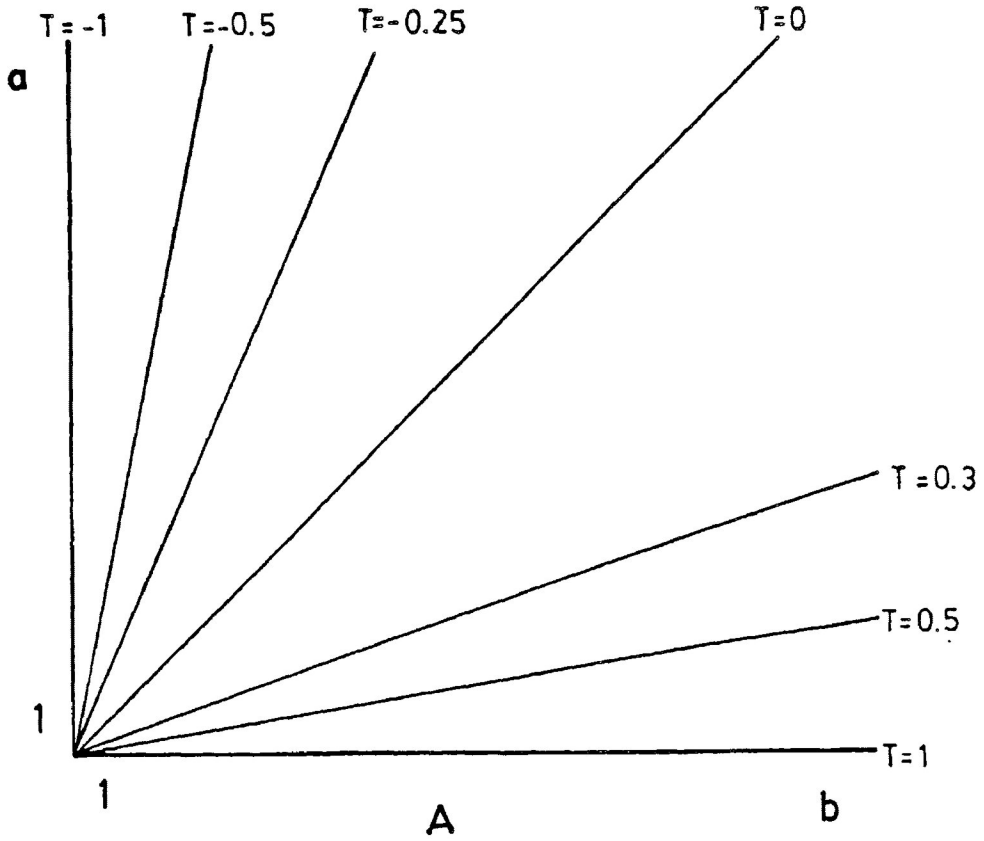

Figure 24. Flinn-type digram with MSA parameter contours.
A. T (ellipsoid shape parameter) contours.
B. P' (corrected degree of MSA parameter) contours.

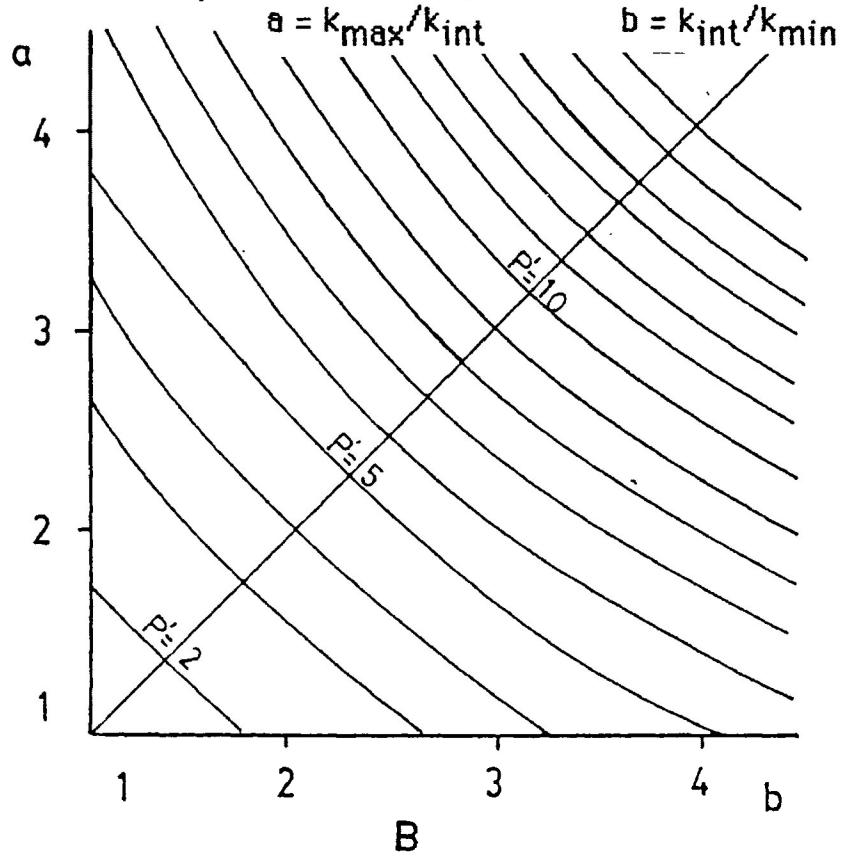

magnetic susceptibilities are the maximum, intermediate and minimum magnetic susceptibilities, respectively($k_{11} = k_{max}$; $k_{22} = k_{int}$; $k_{33} = k_{min}$).

The MSA of a rock or mineral is most commonly described by the shape and magnitude of its magnitude ellipsoid of magnetic susceptibility and by the orientation of the three principal magnetic susceptibilities. There are many parameters available to describe ellipsoids in general and susceptibility ellipsoids specifically(see, e.g., Hrouda, 1982, p.42). Most studies of the MSA of deformed rocks have utilized two parameters:

$$a = k_{max}/k_{int} \text{("magnetic lineation")}$$

$$b = k_{int}/k_{min} \text{("magnetic folation")}$$

The values of the two parameters can be used to construct an MSA version of a Flinn graph(Fig. 23). The Flinn graph is commonly employed to graphically describe strain ellipsoids. Each point on the graph represents an ellipsoid of a certain degree of anisotropy and a certain shape. The slope, m, of a line connecting a point with the graph's origin(1,1) is:

$$m = (a-1)/(b-1)$$

The value of m describes the ellipsoid shape:

$m = 0$	uniaxial oblate ellipsoid
$1 > m > 0$	flat-shaped ellipsoid
$m = 1$	intermediate ellipsoid
$\infty > m > 1$	elongate ellipsoid
$m = \infty$	uniaxial prolate ellipsoid

The distance of the point from the graph's origin indicates the

degree of anisotropy. Generally, the higher the value of a and/or b, the greater the degree of anisotropy.

One of the main disadvantages of the Flinn graph is that ellipsoids of low degree of anisotropy tend to plot very close together, making it difficult to distinguish ellipsoid shape. Also, the m-values have a pronounced numerical asymmetry. Elongate ellipsoids may have an endless range of m-values, from 1 to infinity. However, flat-shaped ellipsoids have a very restricted set of m-values, ranging from 0 to 1. These problems are avoided when two different parameters are used:

$$P' = \exp([2((n_1-n)^2+(n_2-n)^2+(n_3-n)^2)]$$

$$T = 2(n_2-n_3)/[(n_1-n_3)-1]$$

where n_1, n_2 and n_3 are the natural logarithms of k_{max}, k_{int} and k_{min}, respectively, and n is the arithmetic mean of n_1, n_2 and n_3.

P' is the corrected degree of anisotropy and T is an ellipsoid shape parameter. Both parameters were defined by Jelinek(1981) to characterize the magnetic fabric of rocks. Figure 24A is a contoured Flinn graph with lines of equal T-values. T-values, unlike m-values, are symmetrically distributed about the graph:

$T = 1$	uniaxial oblate ellipsoid
$1 > T > 0$	flat-shaped ellipsoid
$T = 0$	intermediate ellipsoid
$0 > T > -1$	elongate ellipsoid
$T = -1$	uniaxial prolate ellipsoid

Figure 24B is a contoured Flinn graph with lines of equal P'-values. The lines show an arithmetic progression of P'-values with distance

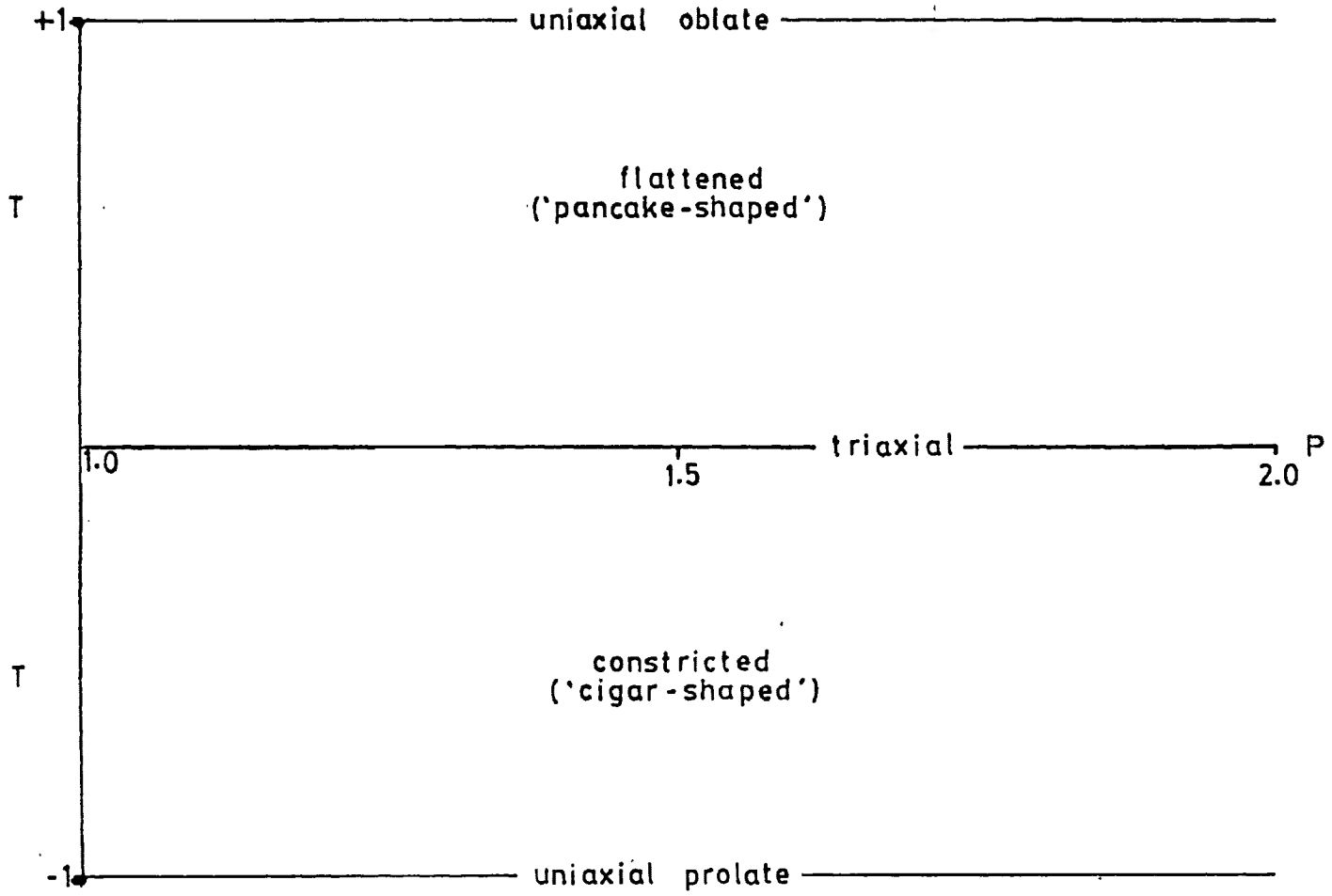

Figure 25. P' -T graph, showing fields of ellipsoid shape. Each point on the graph represents an ellipsoid of a certain shape (T) and degree of MSA (P').

from the origin; P' increases approximately arithmetically with increasing degree of anisotropy.

Hence, a P'-T graph(Fig. 25) is a better method of displaying susceptibility ellipsoids because it provides a field of equal distribution for all ellipsoids regardless of ellipsoid shape or degree of anisotropy.

There are a number of instruments capable of measuring susceptibility and MSA. The most common currently-used instruments are the spinner magnetometer, the torque magnetometer, the inductive bridge, the cryogenic magnetometer and the anisotropy delineator. Collinson(1983) and Tarling(1983) describe the operating principles behind each instrument.

In the present study, I used a Sapphire Instruments SI-1 standard induction coil unit(Plate 12). The instrument measures inductances parallel to the coil axis with and without a sample present, and compares the inductance difference with that of a standard of known susceptibility. The standard is MnO_2, which has a susceptibility of 3.29×10^{-4} SI units/gram (Weast and Astle, 1978). MSA is determined by measuring susceptibility of a sample in twelve different orientations. From the twelve measurements, a computer generates a best-fit magnitude ellipsoid of susceptibility and presents the magnitudes and orientations of the ellipsoid's three orthogonal axes relative to a sample reference mark.

A more detailed description of operating principles and sensitivity of the Sapphire Instruments SI-1 unit is presented in Appendix 1.

5-2. Uses of MSA

There are many applications and implications of MSA in geological and geophysical studies. Hrouda(1982) summarizes many of these in an excellent review paper. A brief outline is presented below.

MSA and palaeomagnetism

The realization that MSA could affect the orientation of the palaeomagnetic vector in rocks sparked the first serious studies into the MSA of rocks and minerals (e.g. Uyeda et. al., 1967). It has been found that the remanent magnetization (RM), or palaeomagnetic, vector is deflected from the external magnetic field direction and toward the long axis of the magnitude ellipsoid of susceptibility in rocks with a significant MSA (Fig. 26). The angle of deflection is dependent on the obliquity between the external field direction and the maximum susceptibility direction. Initially, workers believed that analysis of the rock's susceptibility tensor and removal of this component from the RM vector would resolve the "true" palaeomagnetic direction. Experimental results, however, have shown the relationship to be much more complex. More recent studies have focused on demagnetization of samples and determination of RM ellipsoids(e.g., Stephenson et. al., 1986).

MSA and applied geophysics

Because MSA is capable of deflecting magnetization vectors, it can have important implications in airborne, ground or down-hole geomagnetic surveys. MSA can significantly alter both the location and configuration of the magnetic anomaly associated with a magnetic body (Fig. 27). The influence will depend on the degree of MSA of the magnetic body and the orientation of its susceptibility

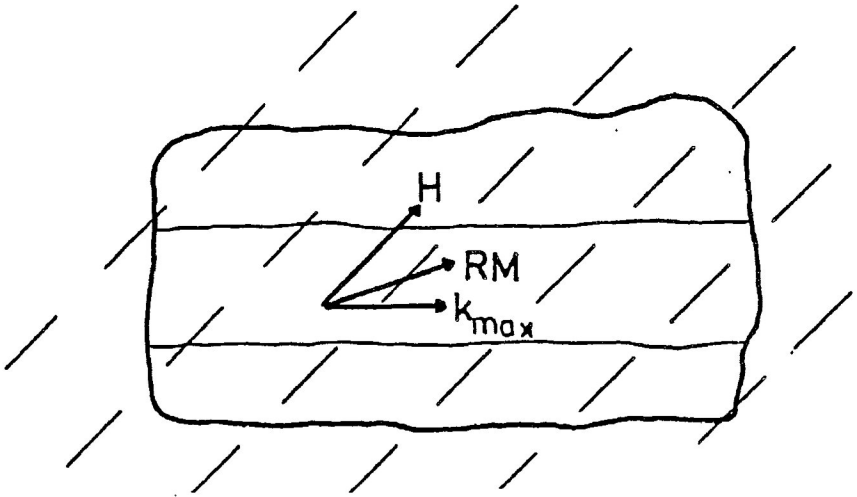

Figure 26. Schematic representation of the deflection of remanent magnetization vector. The applied directional magnetic field (H) is oblique to the maximum magnetic susceptibility direction (k_{max}), causing the specimen's internal remanent magnetization (RM) direction to be deflected from the H direction toward the k_{max} direction.

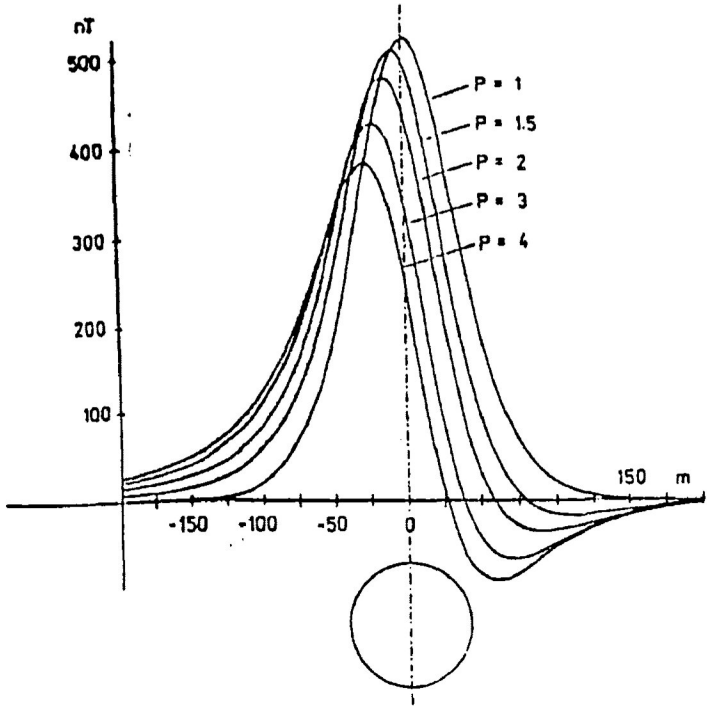

Figure 27. Schematic representation of the deflection of the magnetic anomaly peak over a spherical magnetic body for differing degrees of MSA (P).

(from Hrouda, 1982).

MSA of the magnetic body and the orientation of its susceptibility ellipsoid relative to field magnetic vectors. This effect could have serious implications when the location of magnetic anomalies from exploration geophysical surveys are important precursors to further exploration.

Besides the implications associated with the deflection of magnetization directions, MSA has considerable application in general geological studies. MSA studies evolved from the realization that, in most geological environments, the magnitude ellipsoid of susceptibility is generally consistently and systematically oriented parallel to one or another geologic fabric and, hence can be related to a given geologic process. This is understandable since a rock's magnetic fabric is defined by the spatial arrangement of its magnetic minerals.

One of the main advantages of an MSA study is the relatively rapid return of reliable results. As well, most equipment is inexpensive and many of the instruments are portable, so MSA studies can be conducted directly in the field or within the laboratory. Some of the geological applications of MSA studies include.

MSA and massive ores

The limited studies of MSA of massive ores have been found to be useful in detecting fabric that were otherwise unnoticed. Comparison of the magnetic fabrics with footwall and hanging wall fabrics have provided some workers(e.g. Schwarz, 1974; Porath, 1968b) with insight into the genetic and post-genetic evolution of the ores.

MSA of sedimentary rocks

The MSA of clastic sedimentary rocks are weak (P' values rarely

exceed 1.1) but correlative with sedimentary fabrics. Maximum susceptibility directions are usually parallel to sedimentary current directions, though there are two exceptions. When the current is strong, rolling of magnetic grains may cause maximum susceptibility direction to be perpendicular to current direction, especially when the MSA is dominated by shape anisotropy of magnetic grains. Secondly, when the principal magnetic mineral is hematite, the intermediate susceptibility direction is parallel to current direction (e.g. van den Ende, 1975).

MSA has been used to indicate, or support, palaeocurrent directions where traditional palaeocurrent indicators (cross-stratification, sole marks, groove-casts, etc.) are rare (e.g. Hamilton and Rees, 1971).

MSA of igneous rocks

Like sedimentary rocks, the MSA of igneous rocks are rather weak, but indicates flow direction - lava flow direction of volcanic rocks, or magma flow direction of plutonic rocks. Minimum susceptibility directions are perpendicular to the flow direction and both maximum and intermediate susceptibility directions have been observed to be parallel to the flow direction.

MSA has been utilized to elucidate the genesis of igneous rocks in geologically complex areas. One example involves the diabase rocks on Ronnbeck and Bastian Islands at Spitsbergen (Halvorsen, 1974). The rocks define a roughly circular pattern on a map sheet. Two hypotheses have been suggested to explain the evolution of these rocks. firstly, that they represent the remains of an irregularly sunken sill, and secondly, that they are parts of a ring dyke. Study of the MSA of the diabase revealed that minimum susceptibility

directions are oriented near-vertically and the principal susceptibility planes(also called the magnetic foliation) are near-horizontal. This observation lends support to the sill hypothesis, for, if the rocks represent the remains of a ring dyke, the principiipal susceptibility plane would be expected to be near-vertically oriented.

MSA of metamorphic and deformed rocks

As noted previously, sedimentary and igneous rocks have very weak MSA. When, however, the rocks are subjected to even a weak deformation and/or weak metamorphism, they very quickly develop a strong MSA. Interestingly, after this initial profound transition, the degree of MSA appears only slightly affected by additional progressive deformation and/or metamorphism.

All metamorphic and deformed rocks have relatively strong, but variable, MSA. P' values are generally greater than 1.1 and can exceed 2.0. Susceptibility ellipsoids are generally oblate (Fig. 28).

The rapid transition from weak to strong MSA is, at least partially, due to the ability of deformation mechanisms to quickly and efficiently re-orient magnetic minerals into preferred alignment. Borradaile and Alford(1987) deformed artificial cement-sand mixtures with magnetite grains in the laboratory and observed that the magnitude ellipsoid of magnetic susceptibility of these artificial rocks re-oriented relative to principal strain directions more rapidly than would be predicted for active rotation of a material line.

The strong MSA of metamorphic rocks may also, in part, be related to the preferred crystallographic growth of metamorphic minerals. The common metamorphic minerals - biotite, muscovite, chlorite, amphibole - are weakly to moderately paramagnetic, but have strong

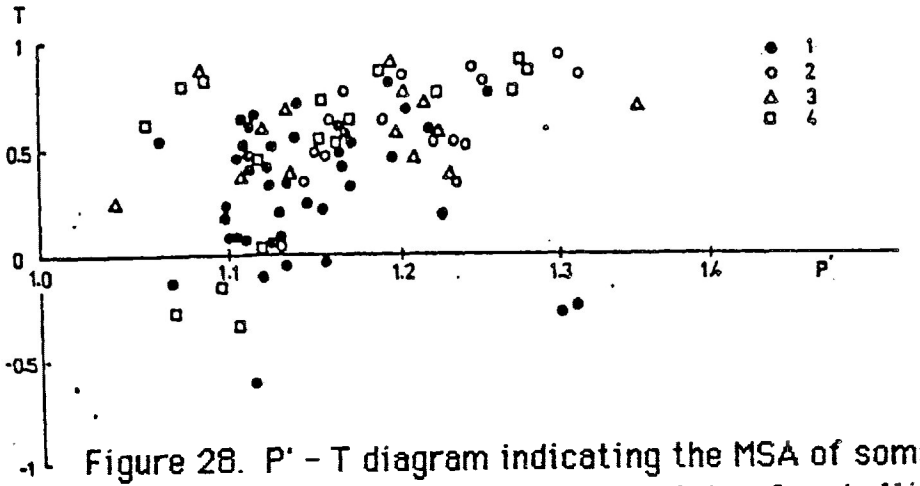

Figure 28. P' - T diagram indicating the MSA of some metamorphic rocks. 1 = slate. 2 = phyllite. 3 = mica schist. 4 = gneiss.
(from Hrouda, 1982).

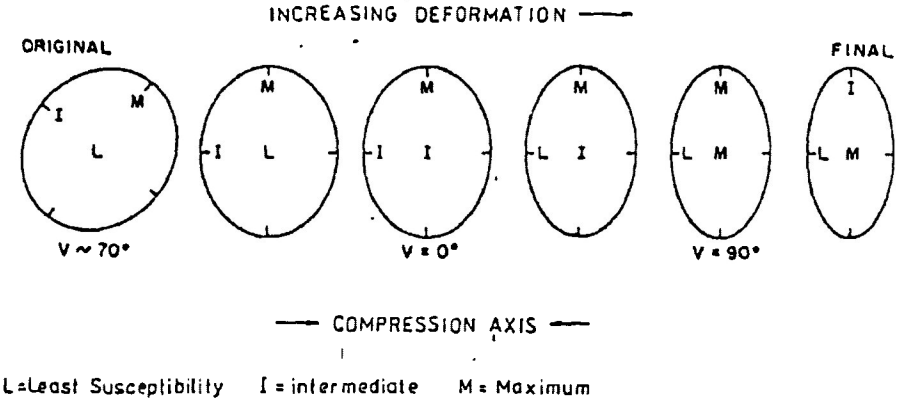

Figure 29. Schematic illustration of the change in direction of principal magnetic susceptibility axes of a sedimentary rock with progressive deformation, as viewed in the plane of the sedimentary bedding. Axes in the center of the ellipses are normal to bedding planes, and the other axes are parallel to bedding planes. See text for discussion.
(from Graham, 1966).

magnetocrystalline anisotropies(Table 2). These minerals commonly comprise a significant proportion of phyllites, schists and gneisses so, even though the bulk magnetic susceptibilities are weak, the minerals have been found to contribute significantly, or even entirely, to the bulk magnetic susceptibility of rocks(see, e.g., Owens and Bamford, 1976; Borradaile et. al.,1986). More importantly, the high degrees of mognetocrystalline anisotropy of these minerals, combined with the strong preferred crystallographic orientation, can produce a strong MSA for the rock.

Graham(1954) was first to recognize the important correlations between MSA and strain of deformed rocks. Graham(1966) studied the magnetic fabric of deformed sedimentary rocks at a tectonic front in the Appalachians. Here, the sedimentary sequence displays a progressive change from relatively undeformed to highly deformed tectonites. Deformation is dominantly horizontal bedding-parallel shortening, with the plane of principal strain vertical and perpendicular to bedding. Graham observed that k_{min} is perpendicular to bedding in the least deformed rocks. With progressive deformation, the principal magnetic susceptibilities orientations are gradually realigned in a systematic pattern (Fig. 29). In the first step, k_{min} remains perpendicular to bedding while k_{max} is reoriented to a direction within the bedding plane perpendicular to the shortening direction. As deformation continues, k_{min} is gradually reoriented to lie within the bedding planes and parallel to the direction of shortening. k_{int}, at the same time, is gradually re-oriented to become perpendicular to bedding. In the final phase of deformation, involving the initiation of buckling and folding, k_{int} and

k_{max} directions are switched, k_{max} becomes perpendicular to bedding and parallel to the direction of maximum extension (Fig. 29).

In areas of syn-deformational metamorphism, principal magnetic susceptibility directions correlate with metamorphic fabrics. In low-grade metamorphic terranes, k_{min} is perpendicular to cleavage or schistosity planes, while k_{max} is commonly observed to be parallel to bedding-cleavage intersection lineations(e.g. Hrouda, 1978; Stott and Schwerdtner, 1981; Borradaile and Tarling, 1981).

Other studies have compared magnetic susceptibility ellipsoids and strain ellipsoids determined from various strain markers. The studies have invariably shown a definite correlation between principal magnetic susceptibility directions(k_{max}, k_{int}, k_{min}) and principal strain directions (X, Y, Z): k_{min} is parallel to maximum shortening direction(Z), k_{max} is parallel to maximum extension direction(X), and k_{int} is parallel to intermediate strain direction(Y)(see, e.g., Kligfield et. al., 1982; Borradaile and Mothersill, 1984; Wood et. al., 1976; Rathore, 1980).

There have been some attempts to quantitatively correlate magnitudes of principal magnetic susceptibilities and principal strains (Wood et. al., 1976; Rathore, 1979, 1980). It was hoped that determination of the magnitude ellipsoid of susceptibility could directly provide, not only the directions of principal strains, but an estimate of the amount of strain experienced by the rock. It should be remembered, however, that the magnetic fabric represents only one component, and usually a very specific component, of the rock, and generally could not be considered a <u>representative</u> lithological strain recorder.

More recent studies of magnetic fabric and strain have indicated that a quantitative correlation is unwarrantable. Henry(1983) discusses the complexities introduced by a polyphase magnetic mineralogy. The case of significant contributions to the bulk magnetic susceptibility of the rock from both a trace amount of a ferrimagnetic fraction and an abundance of a paramagnetic matrix fraction is concievable, and may be very common. Ferrimagnetic minerals, such as magnetite, are usually present in only trace amounts. Nevertheless, because magnetic susceptibility of magnetite is so high, even only a few grains will contribute significantly to the bulk susceptibility to the rock. But the MSA of magnetite is dependent upon the shape anisotropy of the grain, and the contribution of magnetite grains to the MSA of the rock is controlled by the preferred dimensional orientation of these grains. The preferred crystallographic orientation of matrix minerals, such as micas and chlorites, is generally much stronger than the preferred dimensional orientation of accessory and trace minerals, such as magnetite. Hence, even though ferrimagnetic minerals may contribute significantly to the bulk magnetic susceptibility of the rock, the magnetic susceptibility <u>anisotropy</u> of that rock can be dominated by paramagnetic matrix minerals on the basis of high magnetocrystalline anisotropy and strong preferred crystallographic orientation (Borradaile et. al., in press).

This observation has important implications for the relationship between MSA and strain in syn-metamorphic tectonites. Firstly, if the MSA of the rock is dominantly controlled by the paramagnetic matrix fraction and these minerals originated from metamorphic growth, the MSA may be only indirectly related to bulk strain of the rock, and more a result of metamorphic processes. Secondly, as

Henry(1983) notes, the interaction of MSA of the ferrimagnetic and matrix fractions is generally complex, and principal susceptibility directions of each fraction may not coincide. So, even if the magnitude ellipsoid of susceptibility of the ferrimagnetic fraction, for instance, is representative of the strain ellipsoid, it is overshadowed, or masked, by the magnitude ellipsoid of susceptibility of the matrix fraction.

Borradaile and Alford(1987), from their experimental pure shear deformations of sand - cement - magnetite mixtures, have observed no correlation between the magnitudes of final susceptibility and strain ellipsoids, but a power law correlation between the strain ratio(X/Z) and the change in degree of magnetic susceptibility anisotropy($\Delta P'$):

$$\Delta P' \propto \ln(X/Z)$$

This relationship, obviously, is of limited practicality in field strain analyses. Firstly, the pre-strain degree of MSA would be required. Secondly, the conditions are somewhat limiting. The relationship is probably much more complex for a more realisitic situation of inhomogeneous strain, polyminerallic magnetic mineralogy and the influence of such factors as metamorphic processes.

In summary, studies of magnetic fabrics in metamorphic and deformed rocks have identified the following correlations.

1. MSA of metamorphic rocks and tectonites is generally strong. P' and T values are variable and show no simple correlation to degree of metamorphism or deformation(Fig. 28).
2. Directions of principal magnetic susceptibilities are

TABLE 2. Susceptibility data for common minerals of different metamorphic rocks and for magnetite.

Mineral	k_{min}	k_{int}	k_{max}	SG	mean susceptibility $SI/cm^3 \times 10^{-6}$	mass of sample used (g)
	(±95% limits)				(±s.d.)	
Actinolite (1)	0.947 (0.005)	0.982 (0.007)	1.076 (0.01)	2.90	3560.4 (8.9)	8.10
Actinolite (2)	0.899 (0.002)	1.027 (0.002)	1.083 (0.003)	3.42	6506.0 (19.1)	12.79
Hornblende (1)	0.809 (0.002)	0.917 (0.001)	1.347 (0.001)	3.28	8919.0 (11.0)	21.00
Crocidolite	0.958 (0.03)	0.992 (0.03)	1.052 (0.03)	*3.44	332.5 (8.2)	9.60
Glaucophane	0.908 (0.013)	1.006 (0.016)	1.094 (0.01)	3.17	787.1 (43.8)	5.76
Chlorite (1) (diabantite-ripidolite)	0.864 (0.028)	1.060 (0.035)	1.093 (0.035)	2.76	358.4 (53.7)	11.01
Chlorite (2) (leuchtenbergite)	0.734 (0.2)	1.058 (0.25)	1.287 (0.24)	*2.80	68.8 (23.0)	3.11
Chlorite (3) solid**	0.866 (0.01)	1.023 (0.01)	1.128 (0.01)	2.99	1553.6 (184.0)	12.94
Chlorite (4) (Thuringite)	0.921 (0.02)	1.020 (0.02)	1.063 (0.02)	2.76	371.9 (8.0)	6.44
Biotite (1) (large sheets)	0.812 (0.01)	1.106 (0.02)	1.114 (0.03)	2.94	1234.6 (6.5)	6.08
Biotite (2) (large sheets)	0.832 (0.01)	1.095 (0.01)	1.098 (0.01)	3.03	1183.4 (170.0)	9.62
Phlogopite (large sheets)	0.838 (0.01)	1.091 (0.01)	1.098 (0.01)	2.80	1178.2 (6.5)	10.21
Muscovite (large sheets)	0.820 (0.07)	1.052 (0.004)	1.159 (0.09)	2.82	165.0 (17.3)	5.21
Magnetite	0.951 (0.001)	0.989 (0.001)	1.063 (0.001)	5.17	5,841,000 (40,000)	25.0

*These densities were taken from published values.
**This was an unseparated, polygranular, solid sample of highly oriented schist.

from Borradaile, G., Keeler, W., Alford, C. and Sarvas, P., 1987:
Anisotropy of magnetic susceptibility of some metamorphic minerals,
Phys. Earth Planet. Int., vol. 48, p. 161-166.

generally related to the dominant metamorphic and/or deformational fabric. k_{min} is consistently found to be perpendicular to this fabric(cleavage, schistosity, gneissosity).

3. Principal magnetic susceptibility directions correlate well with principal strain directions: $k_{max} \parallel X$; $k_{int} \parallel Y$; $k_{min} \parallel Z$.

4. Despite the directional correlation, there is no simple relationship between magnitudes of principal magnetic susceptibilities and magnitudes of principal strains.

5-3. Magnetic mineralogy of the Quetico rocks - Introduction.

In order to interpret meaningfully the magnetic susceptibility and magnetic susceptibility anisotropy (MSA) of a rock, it is essential that the magnetic mineralogy be determined. Every mineral has not only a particular susceptibility, but a characterisitic MSA (Borradaile et. al., in press). If more than one magnetic mineral is present, the MSA of each will combine to produce a resultant lithological MSA. Thus, the bulk magnetic susceptibility and the MSA of a rock can be attributed to the following factors:

1. The magnetic minerals present in the rock.
2. The relative contributions of each magnetic mineral to the bulk magnetic susceptibility of the rock.
3. The MSA of each of the magnetic minerals.
4. The preferred orientations of each of the magnetic minerals.

The presence of more than one magnetic mineral in a rock should not be a rarity. Many authors (e.g. Rathore, 1979; Kligfield et. al.,

1982; Goldstein, 1980) tend to attribute a rock's magnetic susceptibility to single ferrimagnetic minerals such as magnetite or hematite. Such phases, however, are usually present only in very small amounts, commonly comprising less than one weight percent of the rock. Certain micas, pyroxenes and amphiboles have lower susceptibilities, but these paramagnetic minerals are often major phases in rocks. It would hardly be surprising, then, if rocks with weak to moderate susceptibilities (10^{-5} c.g.s. units/cm^3) have significant contrbutions from both a small amount of a ferrimagnetic component and a much greater amount of a paramagnetic phase.

Henry(1983) has described a method of graphically determining whether a rock has significant contribution from both a ferrimagnetic component and a paramagnetic (or matrix) component. The author shows that the principal magnetic susceptibilities of a rock can be defined as:

$$k_i = k[(k_f - k_m + \Delta_i - \partial_i) / (k_f - k_m)] \quad (2)$$

k_i is the principal magnetic susceptibility of the rock (i=1,2,3), k is the mean magnetic susceptibility of the rock, k_f is the mean magnetic susceptibility of the ferrimagnetic component of the rock, k_m is the mean magnetic susceptibility of the matrix component of the rock, and Δ_i and ∂_i are the fractions added to k_f and k_m, respectively, to define the anisotropy:

$$k_{f(max)} = k_f + \Delta_1$$

$$k_{f(int)} = k_f + \Delta_2$$

$$k_{f(min)} = k_f + \Delta_3$$

$$\Delta_1 + \Delta_2 + \Delta_3 = 0$$

$$k_{m(max)} = k_m + \partial_1$$

$$k_{m(int)} = k_m + \partial_2$$

$$k_{m(min)} = k_m + \partial_3$$

$$\partial_1 + \partial_2 + \partial_3 = 0$$

When the bulk magnetic susceptibility of a rock is due solely to a ferrimagnetic component, equation(1) simplifies to:

$$k_i = k[(k_f + \Delta_i)/(k_f)] \quad (2)$$

Conversely, when the matrix component is solely responsible for a rock's magnetic susceptibility, equation(1) simplifies to:

$$k_i = k[(k_m + \partial_i)/(k_m)] \quad (3)$$

Rocks are, of course, not mineralogically homogeneous. Specimens from the same sample will display slightly variable mineralogies, and so variable bulk magnetic susceptibilities. Equations (1) through (3), though, show that there is a predictable relationship between bulk magnetic susceptibility and principal magnetic susceptibilities of specimens from the same sample. Figures 30A and 30B illustrate this relationship.

In Figure 30A, the three lines representing k_{max}, k_{int} and k_{min} intersect at a common point, where $k_i = k$ and $\Delta_1 = \Delta_2 = \Delta_3 = 0$. The lines of Figure 30B, however, do not have a common intersection point.

Figure 30. Relationship between bulk magnetic susceptibility (k) and principal magnetic susceptibilities (k_i) in rocks with mono- or polyminerallic magnetic mineralogy (see text for explanation of symbols and discussion).

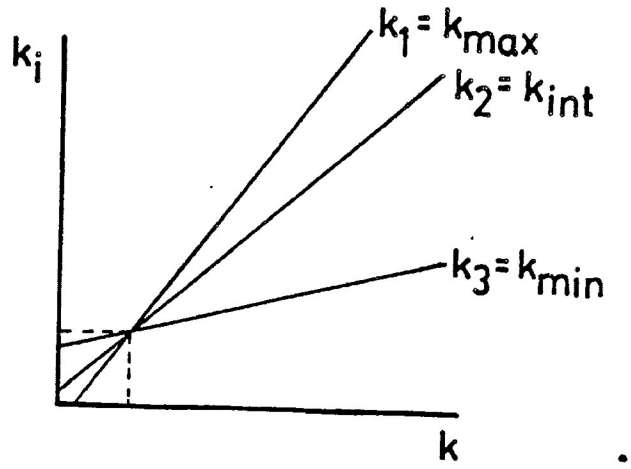

A. Rock with a ferrimagnetic or paramagnetic component, but not both. Slope of each line is $[(k + \Delta_i) / k]$, where i = 1, 2 or 3. The three lines intersect at a common point where $\Delta_1 = \Delta_2 = \Delta_3 = 0$.

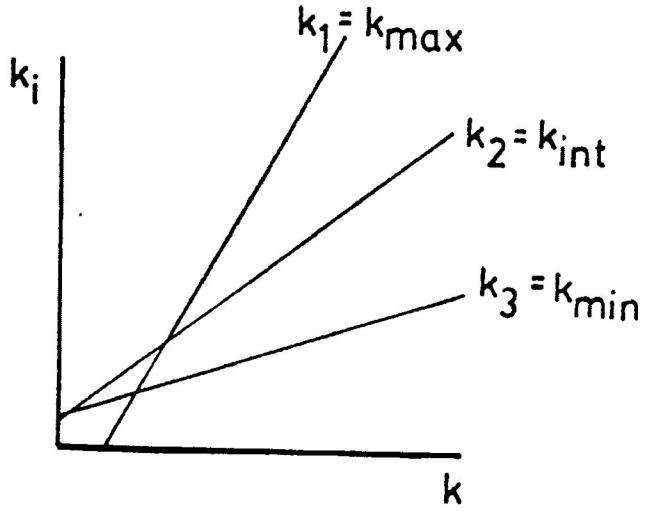

B. Rock with contribution from both a ferrimagnetic and paramagnetic component (polyminerallic magnetic mineralogy). Since $(\Delta_1/\partial_1) \neq (\Delta_2/\partial_2) \neq (\Delta_3/\partial_3)$, the three lines will not intersect at a common point.

As stated previously, different minerals rarely have a similar MSA. The MSA of magnetite, for instance, is very different from the MSA of a paramagnetic mineral such as biotite. Usually, then.

$$(\partial_1/\Delta_1) \neq (\partial_2/\Delta_2) \neq (\partial_3/\Delta_3)$$

When this relationship exists, and when both k_f and k_m contribute significantly to the bulk susceptibility of a rock, it follows, from equation (1), that there would not be a common point of intersection for lines representing k_{max}, k_{int} and k_{min} of the rock specimens from the same sample (Fig. 30B).

If we consider k_m to be relatively constant from one specimen to another, it can be seen that, for low k values, k_f will be near zero and the lines will be best described by equation (3). High k values will have k_f overshadowing k_m and the lines would closely resemble those defined by equation (2).

Figure 31 illustrates the mean magnetic susceptibilities against principal magnetic susceptibilities for 45 samples of Quetico metasedimentary rocks. The lines for k_{max}, k_{int} and k_{min} do not quite intersect at a common point, suggesting the Quetico metasedimentary rocks owe their magnetic susceptibilities to significant contributions from both a ferrimagnetic component and a paramagnetic component, though one or the other may be dominant.

In order to verify or refute this observation, steps were taken to determine the magnetic mineralogy of three Quetico rock samples by physically separating their component minerals.

Magnetic mineralogy - Experimental procedures

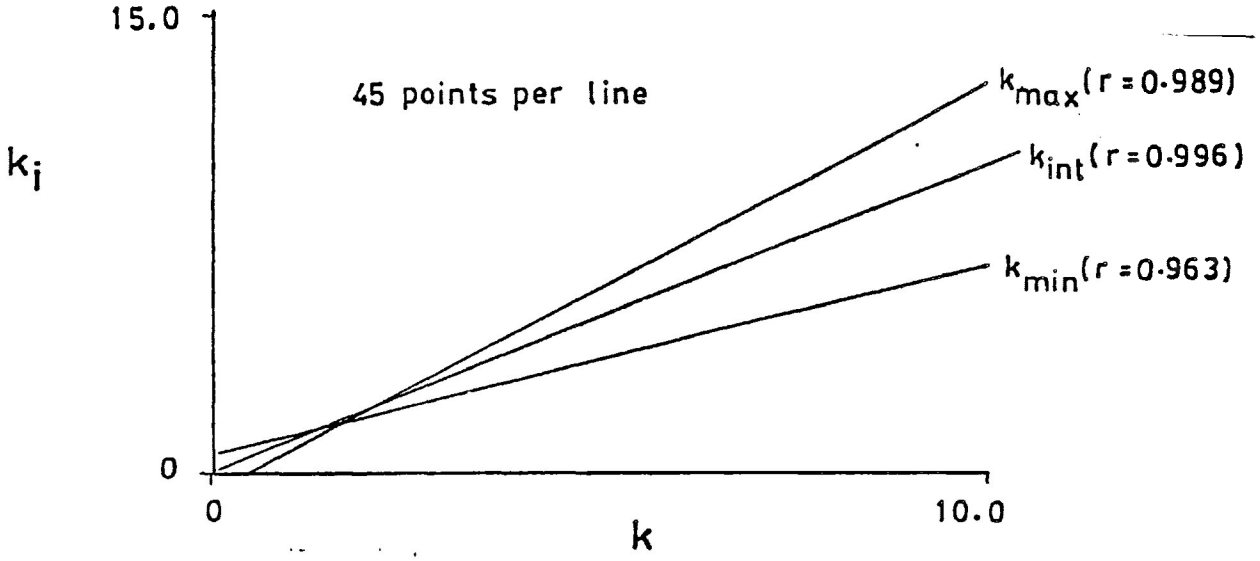

Figure 31. Magnitudes of mean magnetic susceptibility against principal magnetic susceptibility for 45 rock samples from the study area. Correlation coefficients (r) for each line are shown. The three lines do not quite intersect at a common point, suggesting more than one type of magnetic mineral is contributing to the MSA of the rock, though one type may dominate (see text for discussion). Units $\times 10^{-5}$ c.g.s./cm^3.

The three samples are:

PS4 - laminated argillite/matrix-rich sandstone interbeds.

S18 - medium-grained matrix-rich sandstone.

R22 - medium- to coarse-grained matrix-rich sandstone.

The rocks were first crushed, then sieved. The grain size fraction from 2ø to 3ø (0.25mm to 0.125mm) was retained. The above steps were repeated a number of times in order to collect a 2ø to 3ø sample size of at least 50 grams. (In fact, this sample size proved to be too small).

The grains were then washed repeatedly in distilled water to remove the rock dust, then dried.

Next, the grains were passed through a Frantz Isodynamic model L-1 magnetic separator, with the track tilted at 12.5 degrees from the horizontal along its length and 6 degrees from the horizontal perpendicular to its length.

Each sample was separated into five fractions: a very highly magnetic (VHM) fraction, a highly magnetic (HM) fraction, a moderately magnetic (MM) fraction, a weakly magnetic (WM) fraction and a very weakly magnetic (VWM) fraction. The VHM fraction was composed of grains attracted with a hand-held magnet. The other fractions consisted of grains separated at different current settings on the Franz magnetic separator:

Fraction	Separated at (amperes)
HM	0.15
MM	0.25
WM	0.50
VHM	(the remainder)

The strengths of the magnetic fields were chosen based on the

amount of grains being separated, and on the composition of the separated grains when viewed under a microscope.

The specific magnetic susceptibility (in c.g.s. units/ gram) of each fraction was then measured on the Sapphire Instruments SI-1 AMS instrument. Each fraction was measured ten times, from which the mean magnetic susceptibility and the standard deviation were calculated.

Each fraction was then analysed by a powder x-ray diffraction (XRD) technique. The equipment consisted of Phillips model PW1010 high voltage generator and model 1050/25 goniometer and diffractometer.

Finally, polished grain mounts of each of the VHM fraction of samples PS4 and S18 were made and observed under the reflected light microscope. These grain mounts were made to assist identification of minerals in this fraction, since results from the XRD process were inconclusive.

Magnetic mineralogy - Results

Results of the magnetic separation are presented in Table 3. The weights, weight percentages, mean magnetic susceptibility and standard deviation, and relative contributions to bulk magnetic susceptibility of each of the five fractions are shown.

XRD diffractometer graphs for each fraction can be found in Appendix B.

The following minerals, in order of abundance, are present in the polished grain mounts of the VHM fraction. pyrite, pyrrhotite and magnetite. Other minerals observed include quartz, mica, chlorite and feldspar. These minerals are often observed to be attached to, or to have small inclusions of, pyrite, pyrrhotite or magnetite grains.

Table 3. Contributions of the magnetically-separated fractions of three samples of Quetico metasedimentary rocks to the bulk magnetic susceptibility of the samples (see text for explanation of symbols).

Fraction	W_n	$\%W_n$	K_n(±s.d.)	k_n	$\%k_n$
R22					
VHM	0.03	0.04	73,320(±13,400)	85.90	71.01
HM	0.53	0.76	764.20(±51.94)	15.70	12.98
MM	7.65	11.00	16.82(± 0.77)	5.03	4.16
WM	48.03	69.05	6.98(± 0.03)	13.10	10.83
VWM	13.32	19.15	2.39(± 0.23)	1.24	1.03
S18					
VHM	0.07	0.23	54,810(±5,034)	350	82.11
HM	0.48	1.60	1,215(± 17)	53.10	12.46
MM	5.69	18.97	25.85(± 0.39)	13.40	3.14
WM	16.73	55.79	6.34(± 0.23)	9.66	2.27
VWM	7.02	23.41	0.19(± 0.38	0.12	0.03
PS4					
VHM	0.19	0.13	6,271(± 67)	22.10	35.58
HM	0.31	0.21	308.30(± 7.15)	1.77	2.85
MM	3.15	2.16	44.18(± 0.59)	2.58	4.15
WM	62.38	42.71	24.04(± 0.56)	27.80	44.77
VWM	80.02	54.79	5.30(± 0.26)	7.86	12.65

K_n in c.g.s. units/gram, k_n in c.g.s. units/cm^3.

Grain counts of the two specimens gave the following figures.

	Pyrite	Pyrrhotite	Magnetite	Others
PS4	79	36	11	647
S18	301	15	14	422

There were not sufficient grains in the VHM fraction of sample R22 for a grain mount.

Magnetic mineralogy - Discussion

The grain sizes of the matrix minerals comprising the Quetico metasedimentary rocks are, generally, less than 0.125mm. Thus, most of the grains of the separated fractions are polyminerallic. This is reflected in most of the XRD diffractometer graphs, which show strong peaks for quartz and, usually, feldspar in almost every fraction. Quartz and feldspar are very weakly diamagnetic and they contribute very little to the bulk magnetic susceptibility of the rocks. They are, however, the two most common minerals in the Quetico rocks and are frequently separated when attached to more strongly magnetic minerals. This has two detrimental effects. Firstly, the quartz and feldspar increase the weight of each fraction, causing the susceptibility on a mass basis to be inaccurate. Secondly, the strong quartz and feldspar peaks on diffractometer graphs often distort and overshadow peaks of other minerals.

The second effect is particularily troublesome. Certain peaks (especially those at 2ø angles of 12.5 degrees and 9 degrees) suggest the magnetic minerals in the moderately magnetic and weakly magnetic fractions are a chloritic phase and/or a micaceous phase. Unfortunately, interference of quartz and feldspar peaks prevents the reliable determination of the exact chloritic and micaceous phase.

Microscopic examination of polished grain mounts of PS4 and S18

indicate that pyrite, pyrrhotite and magnetite, in that order, represent the most abundant minerals of the VHM fraction. Both fractions also have a high percentage of other minerals, mainly quartz, feldspar and phyllosilicates. Apparently, these minerals separated out because they were attached to the metallic minerals. Small inclusions of pyrite, pyrrhotite and magnetite are commonly observed in these grains. In the grain mount of PS4, most magnetite crystals are observed intimately intergrown along lamellae with pyrrhotite.

Pyrite is considered a paramagnetic mineral(Strangway, 1970, p.38) with a reported average suscepibility of 130×10^{-6} c.g.s./cm^3 (Weast and Astle, 1978). This is several orders of magnitude lower than the average susceptibility of $500{,}000 \times 10^{-6}$ c.g.s./cm^3 for magnetite (Weast and Astle, 1978). Thus, though pyrite is more abundant than magnetite, it contributes very weakly to the magnetic susceptibility of the VHM fraction and insignificantly to the bulk magnetic susceptibility of the rock. Pyrrhotite has a very variable susceptibility, depending on chemical composition. Weast and Astle (1978) report a range from 100 to $500{,}000 \times 10^{-6}$ c.g.s./cm^3, with an average susceptibility of $150{,}000 \times 10^{-6}$ c.g.s/cm^3. It is possible, then, that both magnetite and pyrrhotite contribute significantly to the magnetic susceptibility of the VHM fraction.

The magnetic mineralogy of the highly magnetic (HM) fraction is more difficult to identify. Diffractometer graphs for these fractions are inconclusive. Observation under the microscope, however, indicates that the magnetic mineral is metallic and is probably, like the VHM fraction, pyrite, pyrrhotite and magnetite. In the HM fraction, however, these minerals are much finer grained and attached to larger grains of quartz, feldspar and mica.

The magnetic minerals of the moderately magnetic (MM) and weakly magnetic (WM) fractions are, based on analysis of diffractometer graphs, probably chloritic and micaceous. As noted previously,however, interference by quartz and feldspar peaks make positive identification difficult. On the diffractometer graph for the MM fraction of PS4, strong peaks for the chlorites daphnite, thuringite and ophrosiderite are defined. All graphs for the MM and WM fractions also indicate the presence of muscovite and biotite. All these chlorites and micas are weakly to moderately paramagnetic and could account for the bulk magnetic susceptibility of the MM and WM fractions.

Based on the microscopic and XRD observations of mineralogy, the following densities are attributed to each magnetic fraction.

Fraction	Density(grams/cm^3)
VHM	5.0
HM	3.8
MM	2.7
WM	2.7
VWM	2.7

The contribution of each magnetic fraction to the bulk magnetic susceptibility of the sample can be calculated from the following.

$$k_n = K_n\, p_n/(\Sigma W_n/p_n)$$

$$k = (\Sigma K_n\, p_n)/(\Sigma W_n/p_n)$$

k_n is the magnetic susceptibility of the n fraction (n = 1,2,3,4,5). k is the total magnetic susceptibility (c.g.s./cm^3) of the sample, K_n is the specific magnetic susceptibility (c.g.s./gram) of the n fraction, p_n is the density (grams/cm^3) of the n fraction, W_n is the weight (grams)

of the n fraction. The percentage contribution of each fraction to the magnetic susceptibility of the sample is:

$$\%k_n = (k_n / k) \times 100$$

Results are shown in Table 3.

When the magnetic susceptibility contributions of the five magnetic fractions of samples S18 and R22 are added, the totals are of the order 10^{-4} c.g.s./cm^3. This is high when compared to the bulk magnetic susceptibility of the unseparated samples, and when compared to the bulk magnetic susceptibility of the Quetico metasedimentary rocks in general. The VHM fraction of both these samples is very small. It is, in fact, difficult to obtain a precise measurement of the weights of these fractions. Since the measured weight is used to calculate magnetic susceptibility contributions, it is possibly that imprecise weights may have led to calculation of magnetic susceptibility contributions for these two VHM fractions that is higher than the true values. It is apparent that larger samples are required than those collected for the two samples to give a reliable weight measurement of the VHM fractions.

In any case, the data for sample PS4 show that there are significant (in fact, almost equal) contributions to the magnetic susceptibility of the sample from a ferrimagnetic component (magnetite and, possibly, pyrrhotite) and from a paramagnetic component (chlorite and mica). It is interesting to note, also, that in sample R22, although the calculated contribution by the VHM fraction is probably exaggerated due to an imprecise weight measurement, there is still a significant contribution (over 11 percent) from the weakly magnetic fraction. Results from R22 and S18, however, indicate that the highly magnetic fraction comprises the dominant magnetic minerals of the Quetico rocks.

It is not sufficient to conclude, on the basis of XRD graph analyses and microscopic examinations, that the magnetic minerals of the moderately and weakly magnetic fractions are chlorite and mica. It is entirely possible that the magnetic susceptibility is imparted by tiny (submicroscopic) exsolved or included ferrimagnetic phases with these minerals. Such textures, in fact, are commonly observed microscopically in the polished grain mounts of the VHM fractions of samples PS4 and S18.

There are techniques to resolve the source of magnetic susceptibility in these fractions. The best techniques involve measuring the change in magnetic properties of the specimen as temperature or applied magnetic field strength are varied (see, e.g., Tarling, 1983 and Collinson, 1983). Unfortunately, the facilities for such tests were not available for this study.

Having left this problem unresolved, it should, nevertheless, be remembered that the principal concern of magnetic mineralogy in the present study is how it contributes to the MSA of the Quetico rocks. Even though the paramagnetic component may not be the sole source of magnetic susceptibility, it may still control the MSA. The magnetic susceptibility of a mica grain may be from tiny included magnetite particles, but the shape and orientation of the magnetite particles, and hence the MSA of the grain, may be controlled by the crystallographic structure of the mica.

Magnetic mineralogy - Conclusions

1. Ferrimagnetic minerals identified in the Quetico metasedimentary rocks are magnetite and pyrrhotite.
2. The ferrimagnetic minerals comprise less than one weight percent of the rocks, but still contribute significantly to its bulk magnetic

susceptibility.

3. Paramagnetic minerals in the Quetico rocks include chlorites, biotite and muscovite.
4. The paramagnetic minerals may also contribute significantly to the magnetic susceptibility of the rocks and probably especially to its MSA.
5. The ferrimagnetic minerals contribute most significantly to the bulk magnetic susceptibility of the rocks, and yet may not control the MSA of the rocks.

5-4. MSA of the Quetico metasedimentary rocks.

MSA - Introduction

Studies of the magnetic susceptibility anisotropy of the Quetico metasedimentary rocks involved collection of oriented samples from the study area and a number of laboratory experimental procedures. MSA results are recorded by parameters of magnetic susceptibility ellipsoids and by the magnitudes and orientations of principal magnetic susceptibilities of the ellipsoids.

MSA results, of samples from the entire study area and from specific locations within the study area, are compared to each other. As well, the principal susceptibilities directions are correlated with structural elements.

MSA - Sample collection

A systematic collection of oriented rock samples, both on a regional and on a more detailed scale, initiated the study of the MSA

of the Quetico rocks.

On a regional scale, hand specimen samples were collected along Highway 11, the C.N.R. railroad, the Seine River system, and the hydro-electric power lines which crossed the study area (Fig. 6). Samples were taken at approximately 300 meter intervals. Two methods were utilized to orient the samples:

1. A mark was made on a well-exposed S_1 cleavage surface, and the orientation of this surface was recorded before the sample was taken.
2. Using a circular bubble level, a surface as close to horizontal as possible was found on an outcrop surface. On this surface, an arrow pointing in the north direction was marked before the sample was taken.

In addition to the regional sampling procedure, a selective, more detailed sampling, on an outcrop scale, was conducted. The detailed sampling was initiated to allow a more direct comparison of MSA and structural elements: a major and a minor fold closure, and a sequence of well-developed refracted cleavage were all sampled.

A "G.S.C."-style of portable backpack drill was utilized for the detailed sampling. An arrow pointing in the north direction was marked at the spot to be drilled. Using a 2.54 cm diameter drill bit, each sample location was drilled to a depth of at least 10 centimeters. The core from each hole was then carefully removed and labelled.

MSA - Laboratory procedures

In the laboratory, each of the hand specimens sampled were cored with a drill press to obtain a core of 2.54 centimeters in diameter. The samples were cored in such a manner that the core axis was

perpendicular to the surface containing the orientation mark (Fig. 32).

Taking care to retain the orientation mark, each core was cut and ground as closely as possible to a length of 2.13 centimeters. This produced a core length/diameter ratio of 0.84. In terms of MSA measurements, cores with this ratio behave most closely to a perfectly spherical sample (Porath et. al., 1966). Cores obtained from the detailed sampling using the backpack drill were also cut and ground to a length/diameter ratio of 0.84.

The MSA of each core was then measured in the Sapphire Instruments SI-1 AMS unit. This involved measurement of each core in twelve different orientations corresponding to nine axes. With the twelve-orientation measurement procedure, three of the nine axes (A1, A2, and A3; see Fig. 33) have repeat measurements.

From these measurements, the AMS unit calculated a susceptibility tensor for each sample and output the magnitudes and directions of k_{min}, k_{int} and k_{max}. The instrument requires only six measurements along six axes to calculate a susceptibility tensor. When twelve measurements were taken, the AMS unit calculated and compared two (initial) susceptibility tensors and gave an averaged (final) susceptibility tensor for these two sets of measurements. (A more detailed description of the operation principles and sensivity of the AMS unit can be found in Appendix A).

To determine directions of the principal magnetic susceptibilities, the AMS unit assumed the ends of the cores (containing the orientation mark) to be horizontal surfaces. This gave the true directions for the cores obtained from the backpack drill sampling and for the samples collected using the second of the two orientation techniques. However, for samples collected using the first of the

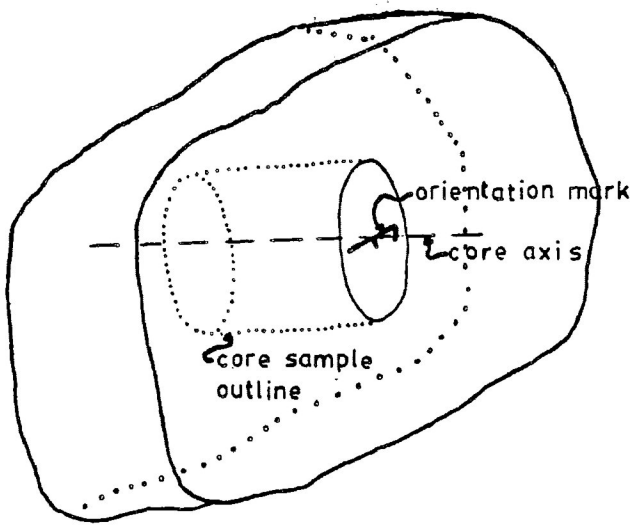

Figure 32. Illustration of a hand specimen with an orientation mark indicating strike and dip of an oriented S_1 surface. The axis of the drill core is perpendicular to the oriented surface.

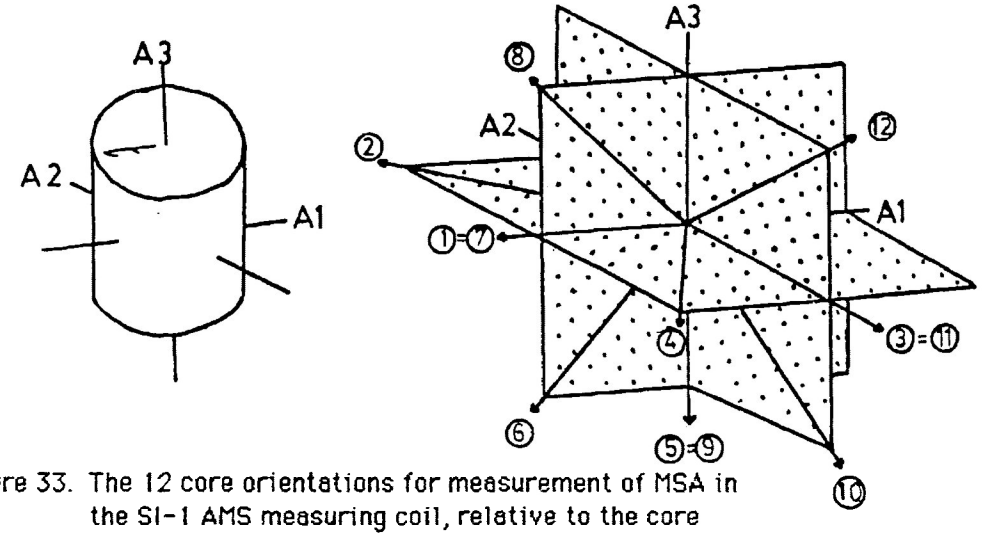

Figure 33. The 12 core orientations for measurement of MSA in the SI-1 AMS measuring coil, relative to the core coordinate axes. (A1 ∥ orientation arrow; A2 ⊥ orientation arrow; A3 ∥ core axis). The 12 orientations correspond to 9 axes. Note that A1, A2 and A3 axes are each measured twice. The circled numbers indicate the sequence of oriented measurement. During measurement, the relevant axis is parallel to the coil axis of the AMS unit.

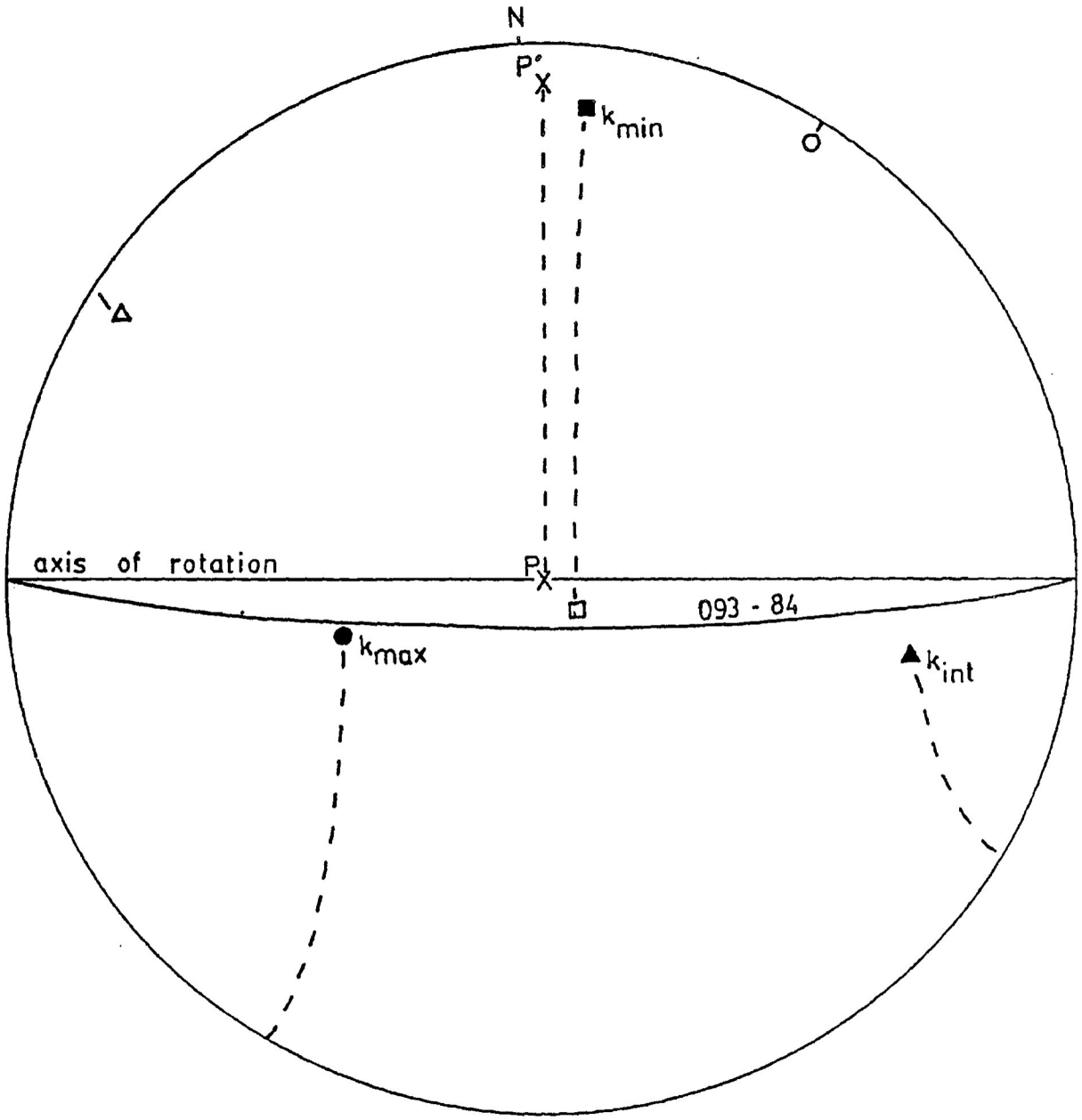

Figure 34. Example of rotating the principal magnetic susceptibility axes to the corrected orientations. The AMS unit gives the principal susceptibility directions (open symbols) relative to a horizontal reference surface with a vertical pole (P). The surface, however, has a true orientation of 093-84. The pole to the reference surface is rotated about an axis of rotation through an angle to its true orientation (P'), and the principal susceptibility axes are rotated about the same axis of rotation, and through the same angle, to the correct orientation (closed symbols).

orientation techniques (orientation mark on S_1 surface), the directions of principal magnetic susceptibilities had to be corrected. This was done on an equal-area stereographic net (Fig. 34). The pole to the reference surface was rotated from a vertical plunge to its true orientation, and the axes of k_{max}, k_{int} and k_{min} were rotated in the same direction and over the same angle along the same axis of rotation.

The AMS unit also output what it labeled R95 and E95 values for each of the three principal magnetic susceptibilities. R95 is a measure of the angular deviation of directions of k_{max}, k_{int} and k_{min}. It is arrived at by comparing the principal susceptibility directions calculated for the final susceptibility tensor with those calculated for the initial two susceptibility tensors. Similarly, E95 is a measure of the deviation of magnitudes of k_{max}, k_{int} and k_{min}, calculated in a similar manner.

MSA - Results

A. General

Many of the collected samples have a very well-developed slaty cleavage. The fissility, as well as cracks and fractures, made retrieval of intact core difficult. Many cores came out in two or three pieces and were glued back together with araldite. Of the 213 hand specimens drilled, however, 21 cores were insufficiently intact for MSA measurement, and were rejected.

Similarly, of the 54 cores obtained from drilling with the G.S.C. backpack drill, 12 were considered unsuitable for MSA measurement.

Figures 35A through 35C present the shapes (T) and degrees of anisotropy (P') of the susceptibility ellipsoids for the measured

Quetico metasedimentary rock samples. P' and T ranges are typical of metamorphosed rocks (compare Fig. 28). For 153 data points, the arithmetic mean of P' and T are 1.35 and +0.53, respectively. The susceptibility ellipsoids have an asymmetric distribution, with most plotting within a narrow range of P' and T values (P' = 1.2 to 1.5 and T = +0.3 to +0.8). Generally, susceptibility ellipsoids of the Quetico metasedimentary rocks are flat-shaped ellipsoids with moderate to strong degrees of anisotropy.

An interesting observation is the correlation between degree of anisotropy (P') and mean magnetic susceptibility ($k = k_{max} + k_{int} + k_{min}/ 3$) (Fig. 36). For 153 data points, the two parameters have a correlation coefficient of 0.84. The correlation is perhaps not strong enough to define a mathematical relationship, but it can be safely stated that increase in the bulk susceptibility of the rocks is accompanied by a corresponding increase in degree of anisotropy of MSA.

B. Principal magnetic susceptibility directions

For a sample volume of approximately 11 cubic centimeters, and a measurement time of 4 seconds per orientation, the SI-1 AMS unit has a sensitivity in the range of 5×10^{-7} c.g.s./cm^3 (see Appendix A). Bulk susceptibility of the Quetico rocks is in the order of 10^{-5} c.g.s./cm^3, but susceptibility ellipsoids are generally oblate, meaning there is commonly little difference between magnitudes of k_{max} and k_{int}. This difference is often within the range of 10^{-7} c.g.s./cm^3. For these samples, the ability of the AMS units to resolve the two susceptibility directions depends, for the most part,

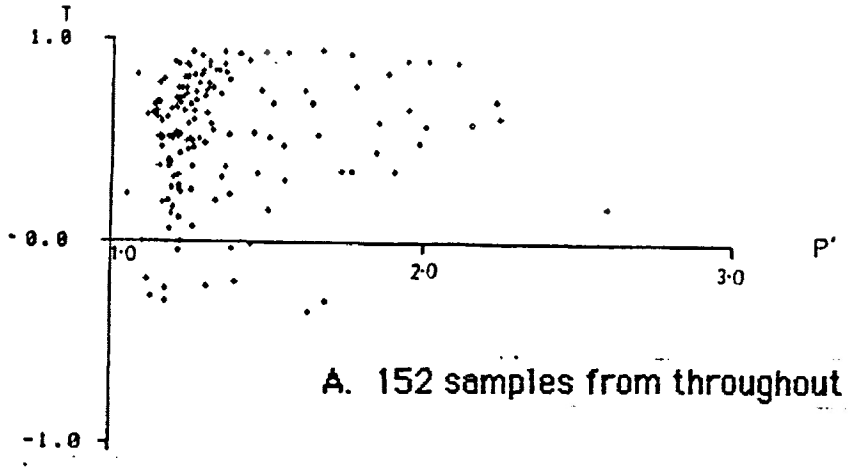

A. 152 samples from throughout the study area.

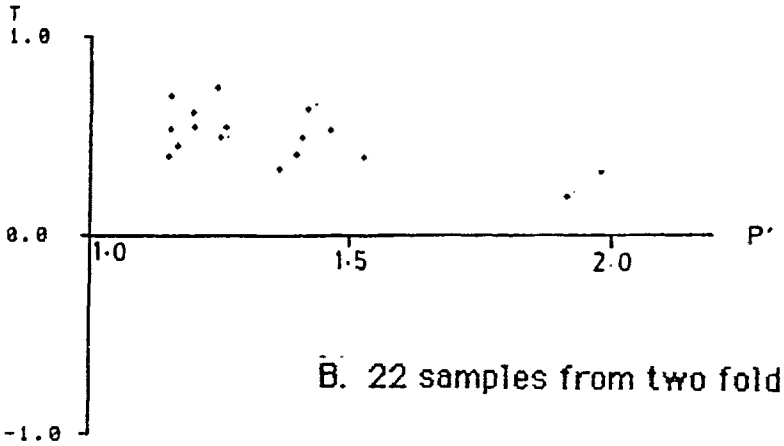

B. 22 samples from two fold closures.

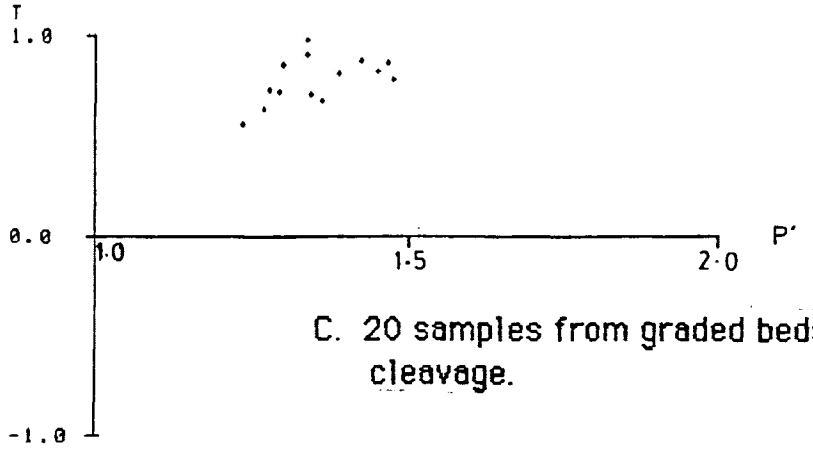

C. 20 samples from graded beds with refracted cleavage.

Figure 35. P' - T graphs for the magnetic susceptibility ellipsoids of the Quetico metasedimentary rocks.

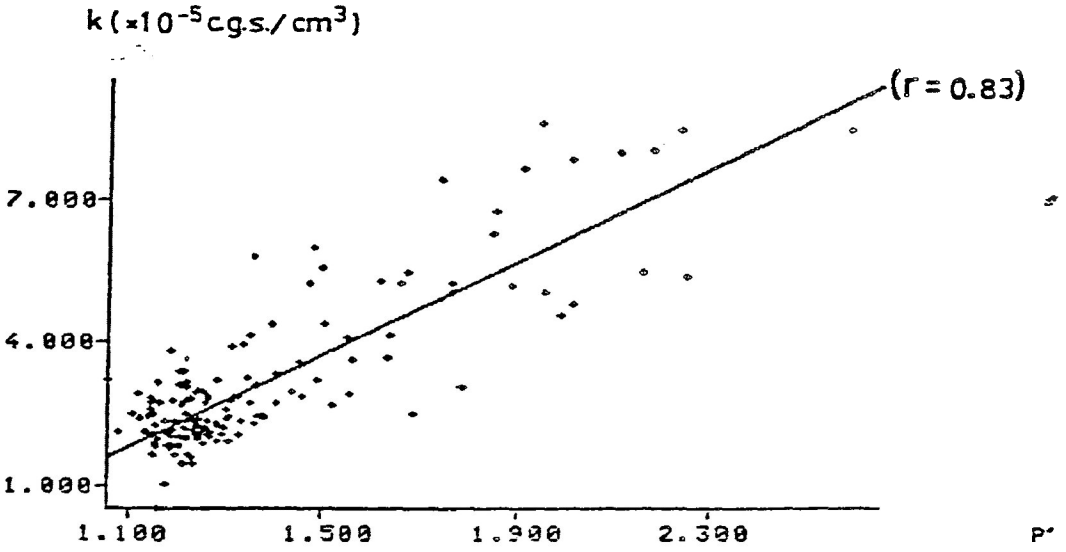

Figure 36. Mean magnetic susceptibility (k) against degree of anisotropy (P') of magnitude ellipsoid of susceptibility for 153 samples of Quetico rocks from the present study area. The best-fit line has a correlation coefficient of 0.83.

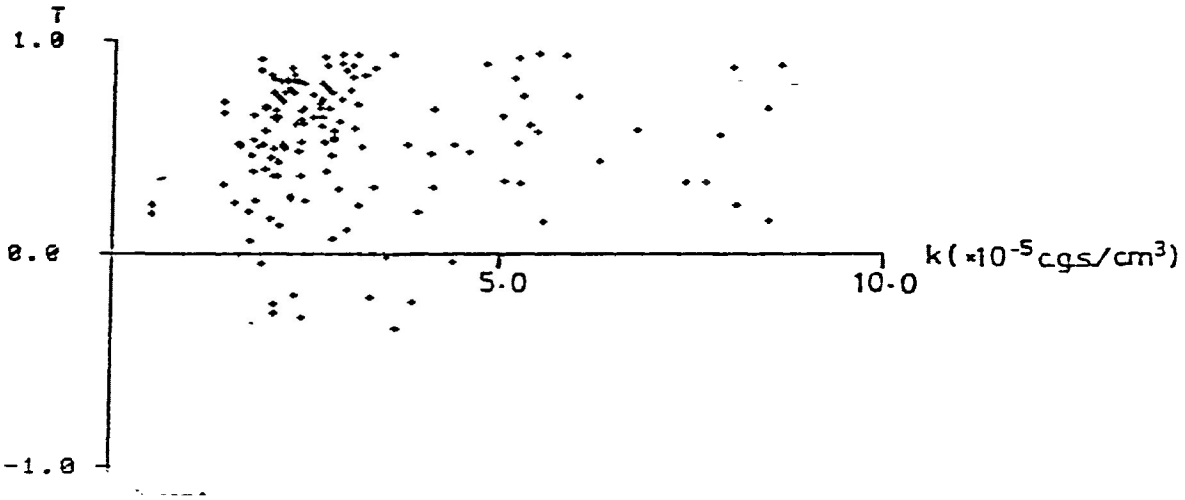

Figure 37. Mean magnetic susceptibility (k) against shape of magnitude ellipsoid of susceptibility (T) for 153 samples of Quetico rock samples from the present study area. Most ellipsoids are flat-shaped.

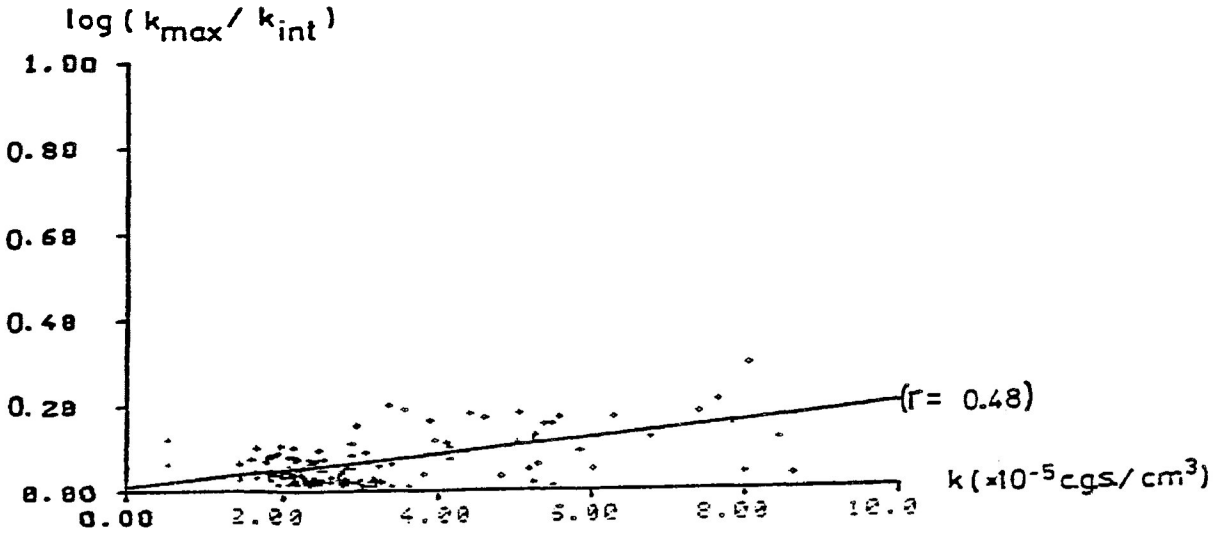

Figure 38. Mean magnetic susceptibility (k) against the logarithmic "magnetic lineation" (log [k_{max}/k_{int}]) for 153 samples of Quetico rocks from the present study area. The best-fit line has a correlation coefficient of 0.48.

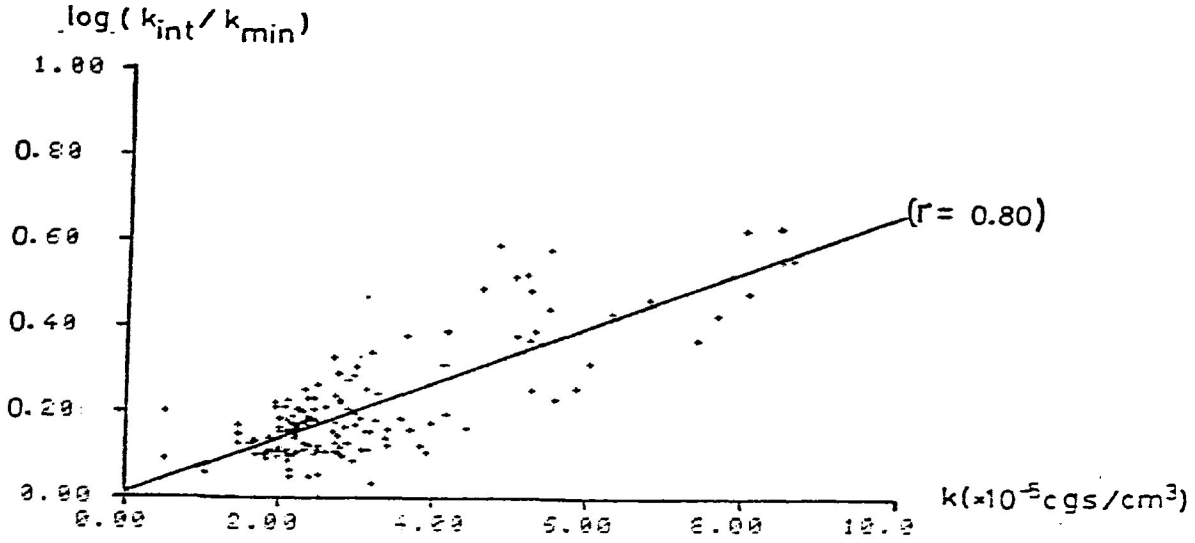

Figure 39. Mean magnetic susceptibility (k) against the logarithmic "magnetic foliation" (log [k_{int}/k_{min}]) for 153 samples of Quetico rocks from the present study area. The best-fit line has a correlation coefficient of 0.80.

on the levels of background magnetic "noise" during measurement and on how well the core has been oriented within the coil for each of the 12 oriented measurements. For some samples, the difference is simply too small for the instrument to reliably resolve, even after repeated measurements.

High R95 and E95 values are generally indicators of unreliable results. E95 values are a measure of principal susceptibility deviation, and so indicate a range of magnetic susceptibilities of the principal susceptibilities. When the E95 values of k_{max} and k_{int} of a sample indicate a zone of overlap, the k_{max} and k_{int} directions of this sample are rejected as unreliable. As an example, sample B05 has the following MSA measurements:

k_{int}		k_{max}	
magnitude	E95	magnitude	E95
3.1464×10^{-5}	$\pm 0.0550 \times 10^{-5}$	3.1654×10^{-5}	$\pm 0.0698 \times 10^{-5}$

In this example, k_{int} has a measured range from 3.0915 to 3.2015 $\times 10^{-5}$ c.g.s./cm^3, and k_{max} has a measured range from 3.0956 to 3.2353 $\times 10^{-5}$c.g.s./cm^3. Thus, both k_{max} and k_{int} may have a magnitude in the range of 3.0956 to 3.2015 $\times 10^{-5}$ c.g.s./cm^3, and it is possible for k_{int} to have a higher magnitude than k_{max}. It is concluded that the AMS unit could not resolve magnitudes and directions of the two principal susceptibilities for the magnitude ellipsoid of susceptibility of this sample, and the directions of k_{int} and k_{max} are rejected as unreliable.

The MSA of 192 samples from throughout the study area were

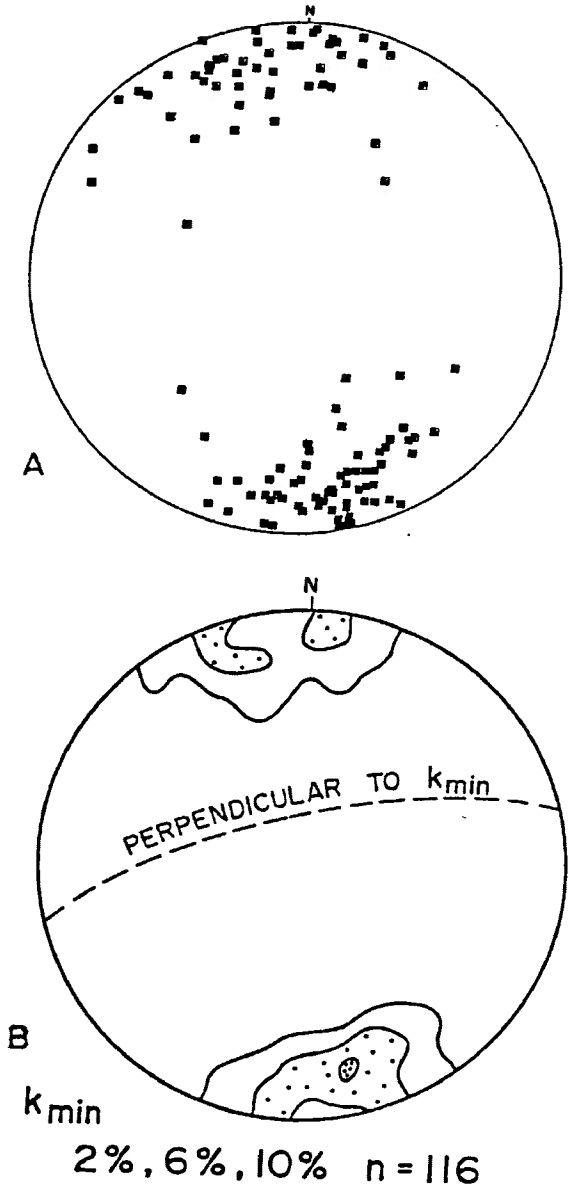

Figure 40. Stereographic projection of minimum magnetic susceptibility orientations in 116 samples of Quetico metasedimentary rocks from the present study area. The contoured stereograph (40B) indicates a strong maxima of k_{min} axes perpendicular to a plane with orientation (256-74).

Figure 41. MSA data at fold closures in the present study area.

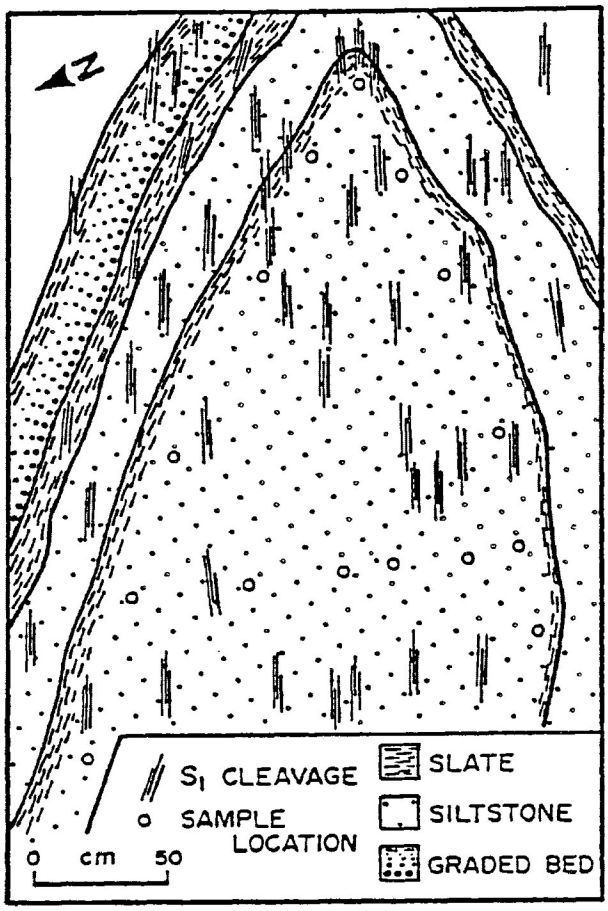

A. Illustration of the major fold profile, showing folded S_0 planes and axial planar S_1-cleavage traces, and sample locations. The fold axis plunges near-vertically.

B. Stereographic projection of principal magnetic susceptibility orientations in 15 samples from the major fold closure. The k_{min} axes have a narrow range of orintations perpendicular to S_1 planes. The k_{max} axes are closely subparallel to S_0/S_1 intersection lineations and to the fold axis.

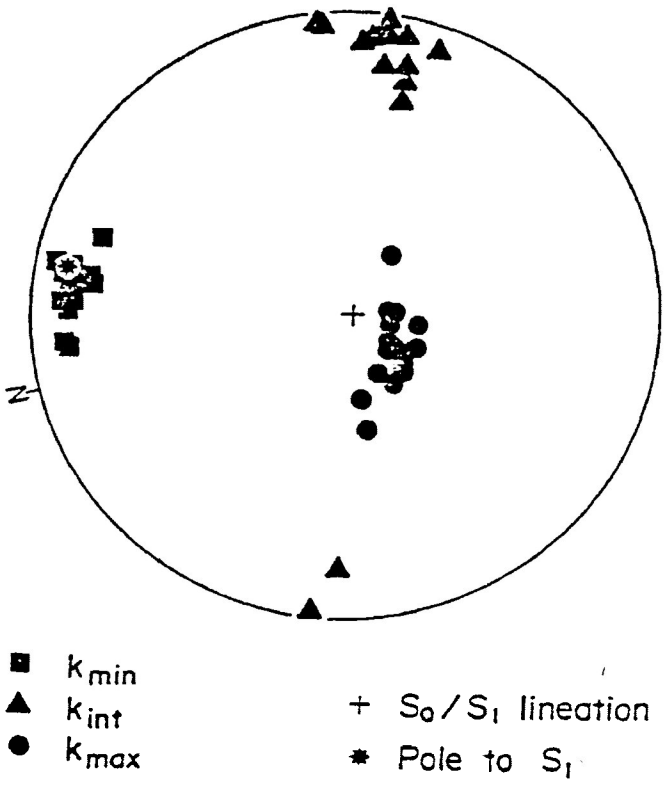

Figure 41 (cont'd).

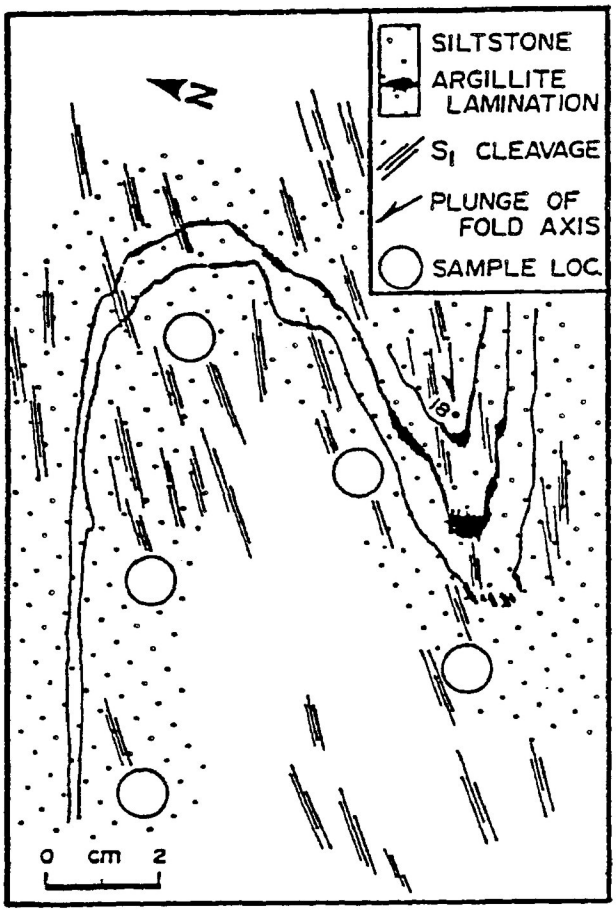

C. Illustration of the minor fold profile, showing folded S_0 planes and axial planar S_1-cleavage traces, and sample locations. The fold axis plunges toward the west at an angle of approximately 20 degrees.

D. Stereographic projection of principal magnetic susceptibility orientations in 5 samples from the minor fold. Again, the k_{min} axes have a narrow range of orientations perpendicular to S_1 planes. The k_{max} axes are closely subparallel to S_0/S_1 intersection lineations, and to the fold axis.

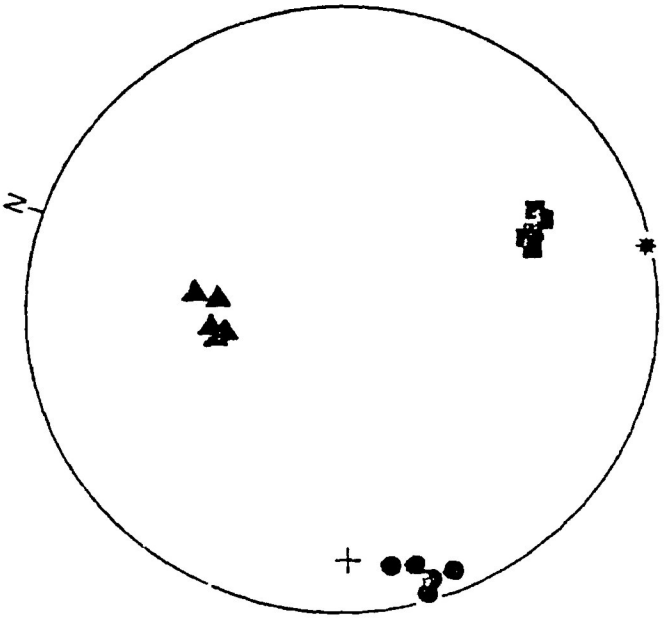

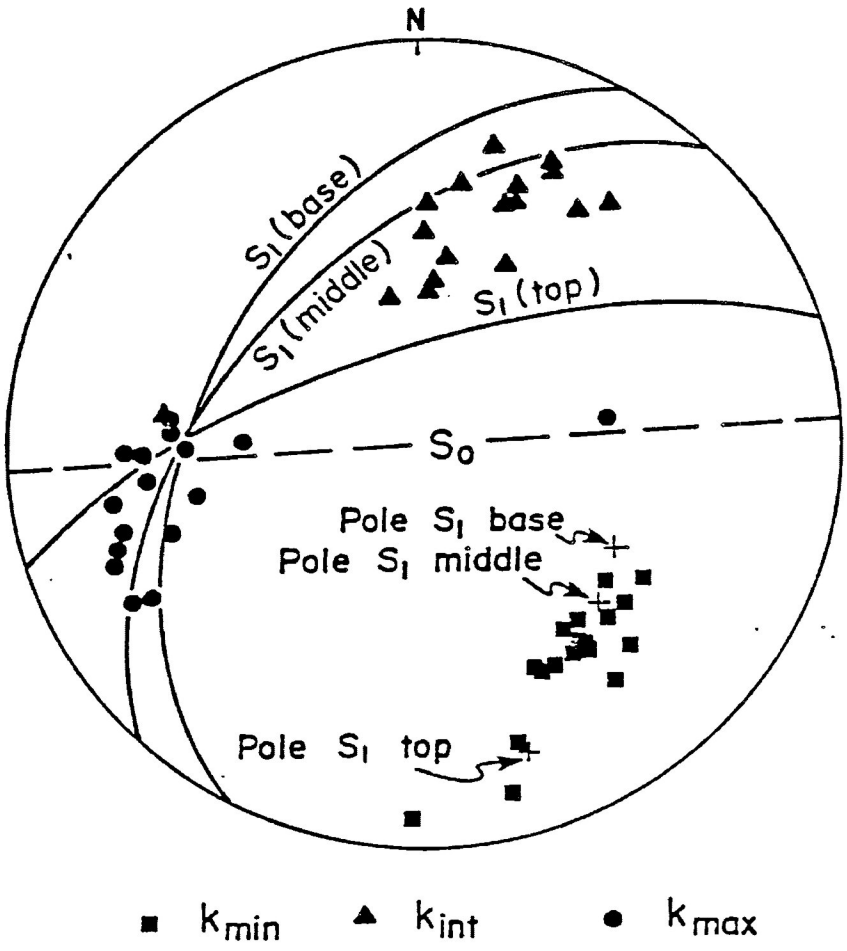

Figure 42. Stereographic projection of principal magnetic susceptibility orientations in 20 samples from graded beds with refracted S_1 cleavage planes. The range of k_{max} axis orientations corresponds with the range of orientations of poles to S_1 planes. k_{max} axes are closely subparallel to the S_0/S_1 intersection lineation direction.

measured. Of these, the principal susceptibility directions of 65 samples were rejected as unreliable.

Principal magnetic susceptibility directions of the remaining samples are recorded stereographically for the regional samples as well as for the samples collected from the fold closures and the refracted cleavage.

C. Directional distribution of k_{min} axes

k_{min} axes display a strong orientation throughout the study area, plunging near-horizontally along a NNW/SSE axis (Fig. 40A). This is approximately perpendicular to both bedding (S_0) and cleavage (S_1) planes. A contoured stereograph of point density distribution indicates a strong maxima of k_{min} axes at an orientation of 165-16, or perpendicular to a plane with orientation 256-74 (Fig. 40B).

The same, consistent direction of k_{min} axes is observed in samples from the major and minor fold closures, even though orientations of S_0 planes vary considerably (Fig. 41).

Most k_{min} axes of the refracted cleavage samples are within the range of orientations of the poles to the refracted S_1 planes (Fig. 42).

D. Directional distribution of k_{max} and k_{int} axes

Within the study area, both k_{max} and k_{int} axes display a wide variation in orientation (Fig. 43 and 44). In both cases, however, the orientations coelesce in modal density distributions approximating a great circle distribution pattern, as best seen in a contoured point density stereograph (Fig. 43B and 44B). This is to be expected, since

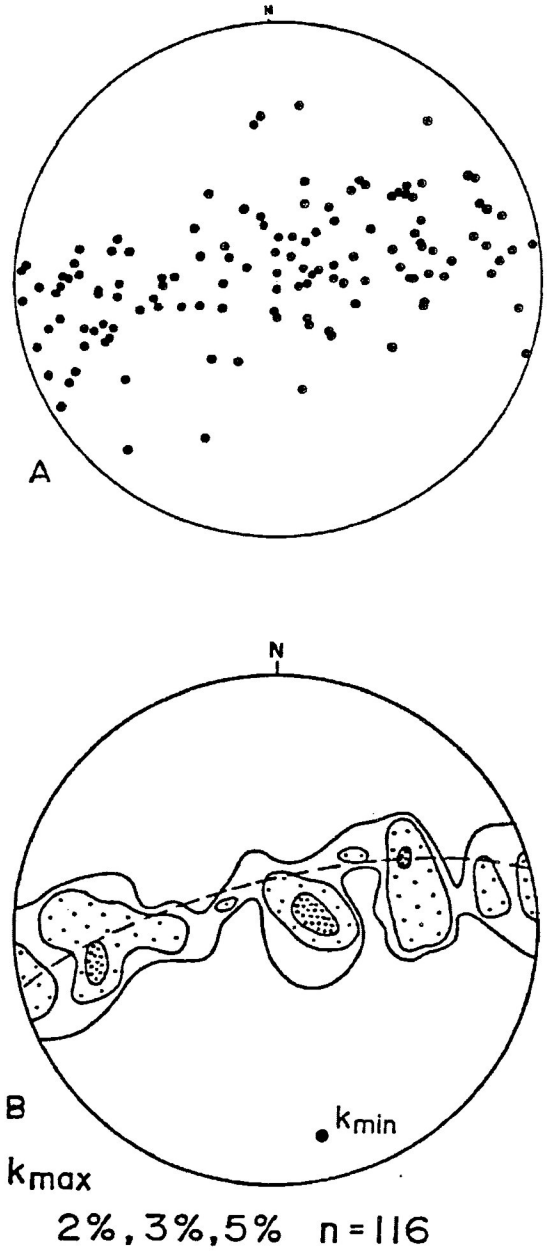

Figure 43. Stereographic projections of maximum magnetic susceptibility orientations in 116 samples of Quetico metasedimentary rocks from the present study area. The contoured stereograph indicates a modal distribution of k_{max} axes which approximate a great circle pattern. The plane perpendicular to the k_{min} axes maxima (see Fig. 40) is contained in the pattern.

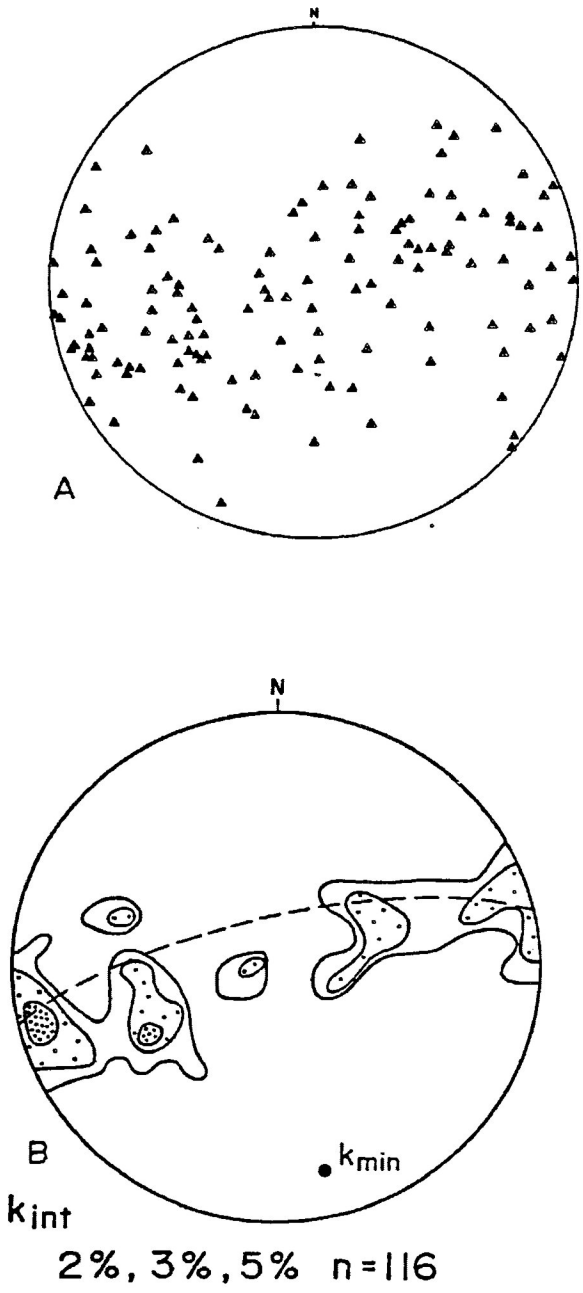

Figure 44. Stereographic projections of intermediate magnetic susceptibility orientations in 116 samples of Quetico rocks from the present study area. The contoured stereograph indicates a modal distribution of k_{int} axes which approximates a great circle pattern. The plane perpendicular to the k_{min} axes maxima (see Fig. 40) is contained in the pattern.

k_{min} axes have such a strong preferred orientation. The plane 256-74 (perpendicular to the greatest concentration of k_{min} axes) is contained in both k_{max} and k_{int} density distribution girdles (Fig. 43B and 44B).

The contoured stereographs also indicate that, for the most part, k_{max} axes plunge more steeply than k_{int} axes, but there is no strong preferred direction for either axes on a regional scale.

E. Relationship between k_{max} and k_{int} axes and S_0/S_1 intersection lineations

Many magnetic fabric studies of deformed rocks have revealed a correlation between the k_{max} direction and direction of the dominant structural lineation within the area (e.g. Hrouda, 1978, Kligfield et. al., 1982; Goldstein, 1980; Stott and Schwerdtner, 1981). The dominant lineation of the Quetico metasedimentary rocks is the bedding-cleavage (S_0/S_1) intersection lineation. As S_1 cleavage planes are axial planar, S_0/S_1 lineations also indicate the direction of plunge of major fold axes.

Like k_{max} and k_{int} axes, S_0/S_1 lineations are generally variably oriented within a plane which strikes approximately east-west and dips steeply toward the north. That is, S_0/S_1 intersection lineations are generally contained within a plane which is perpendicular to k_{min} axes (Fig. 16). There are three sets of preferred orientations of S_0/S_1 lineations in the study area: 253-28, 270-68 and 081-30 (Fig. 16B). These three directions correspond with four sections in the

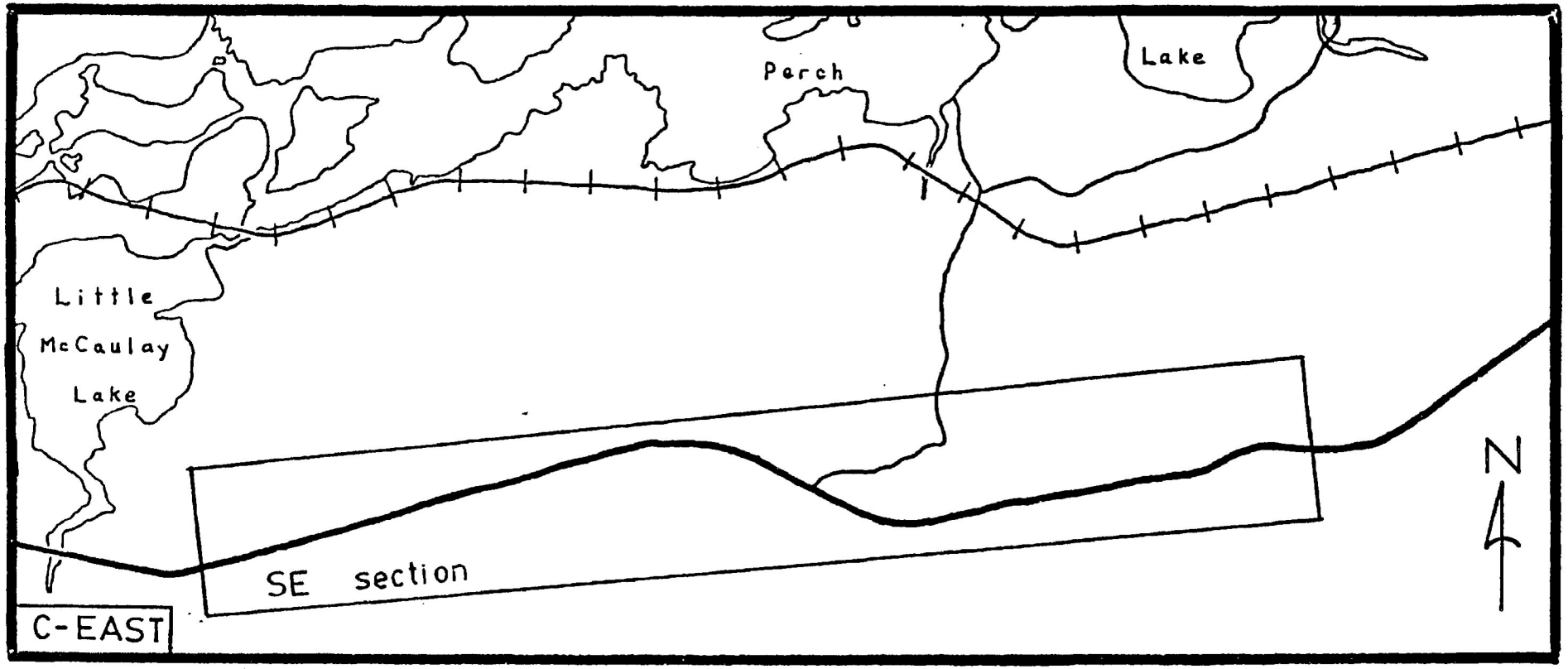

Figure 45.

Sections of detailed study in the present study area. Each section has relatively consistent S_0/S_1 intersection lineation directions.

Scale 0 1 2 km

Canadian National Railroad

Provincial highway. 11

Other road

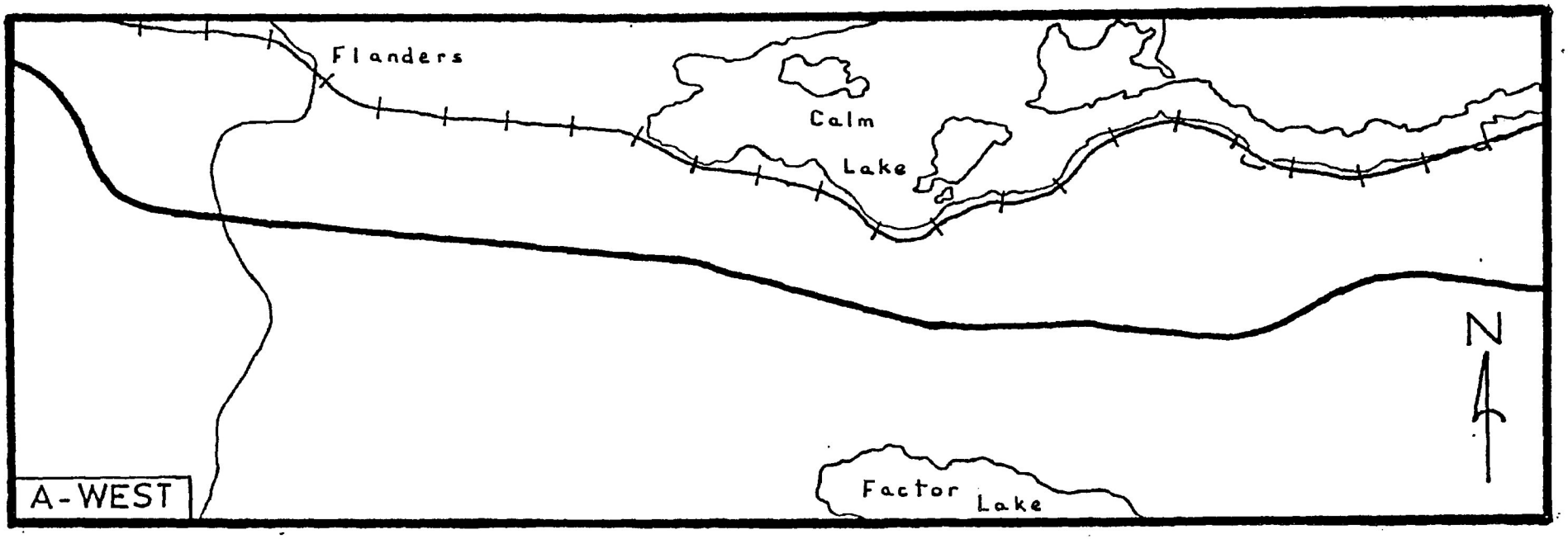
Flanders
Calm
Lake
Factor Lake
N
A-WEST

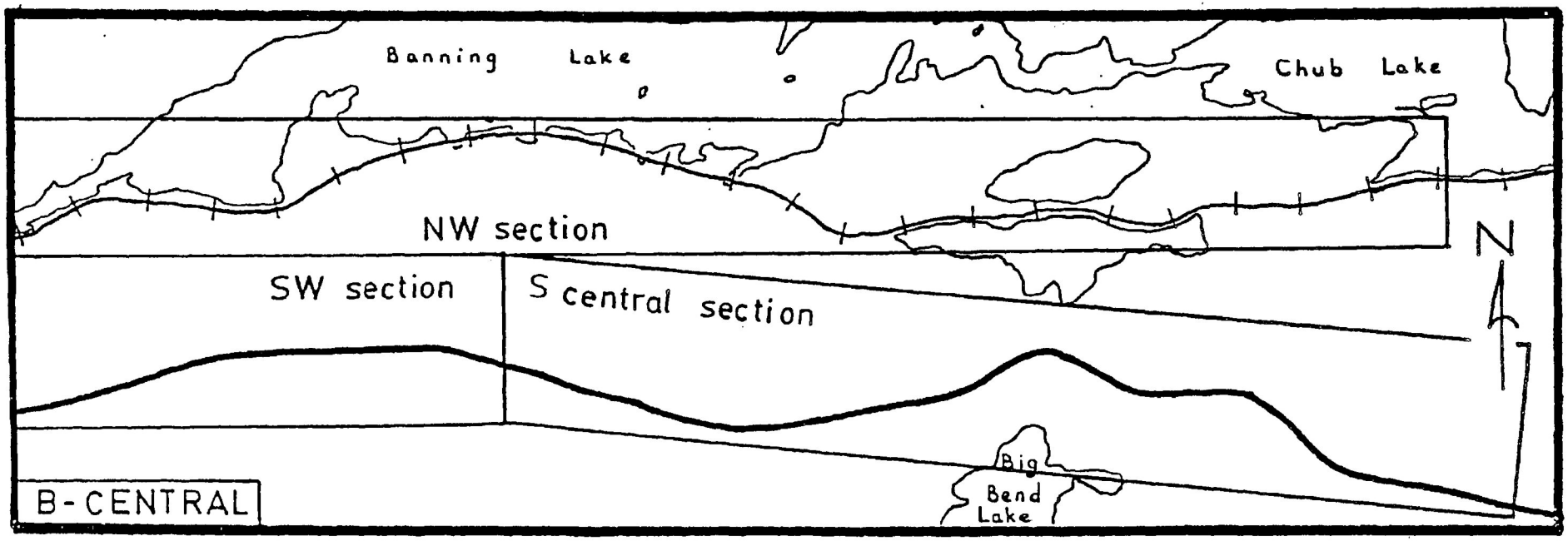
Banning Lake
Chub Lake
NW section
SW section
S central section
N
Big
Bend
Lake
B-CENTRAL

study area in which S_0/S_1 lineations are rather consistently oriented (Fig. 45):

253-28	Southwest section
270-68	Northwest and southcentral sections
081-30	Southeast section

Despite a strong preferred orientation of S_0/S_1 lineations in the southwest section, samples from this area display a rather wide dispersion of k_{max} and k_{int} axes (Fig. 46A). Neither of the two principal magnetic axes have a preferred orientation.

In each of the other three sections, however (Fig. 46B, 46C and 46D), k_{max} and k_{int} axes align in groupings of relatively consistent orientations. Interestingly, S_0/S_1 lineations correlate neither with k_{max} nor k_{int}, but appear to actually bisect the angle between the two principal magnetic axes. This is best observed in the stereograph of the southeast section (Fig. 46D).

Conversely, S_0/S_1 lineations, and fold axes, appear to correlate quite strongly with the k_{max} axis sets of the fold closure samples (Fig. 41). As well, the set of k_{max} axes of samples from the refracted S_1 beds correlate strongly with the S_0/S_1 lineation of this area (Fig. 42).

Most samples from both the fold closures and from the refracted cleavage beds are observed to have higher mean magnetic susceptibilities (k) and higher degrees of anisotropy for susceptibility ellipsoids (P') than the average values for samples from the entire study area:

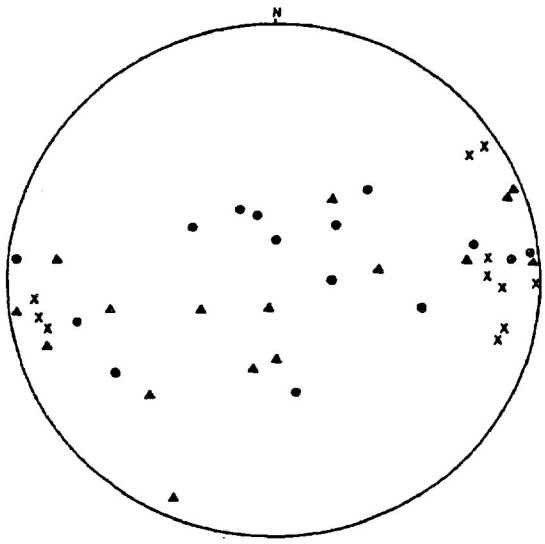

A. Southwest (SW) section.

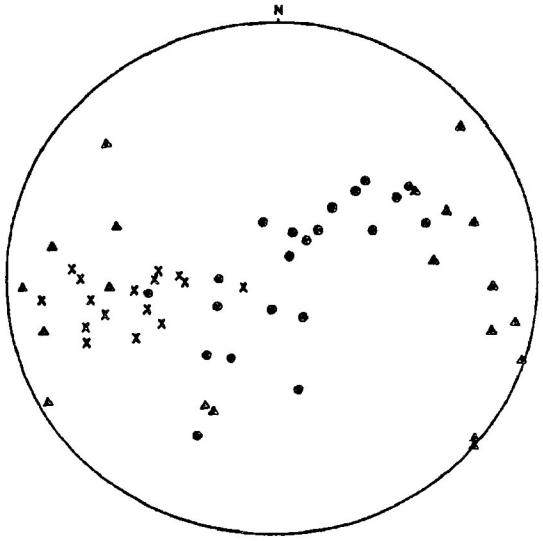

B. Southcentral (Scentral) section.

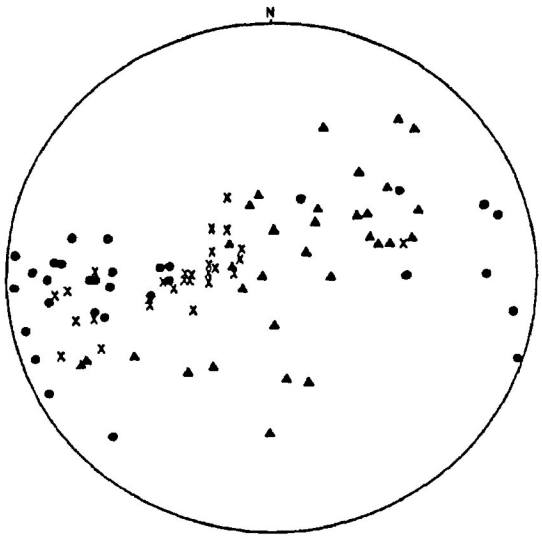

C. Northwest (NW) section.

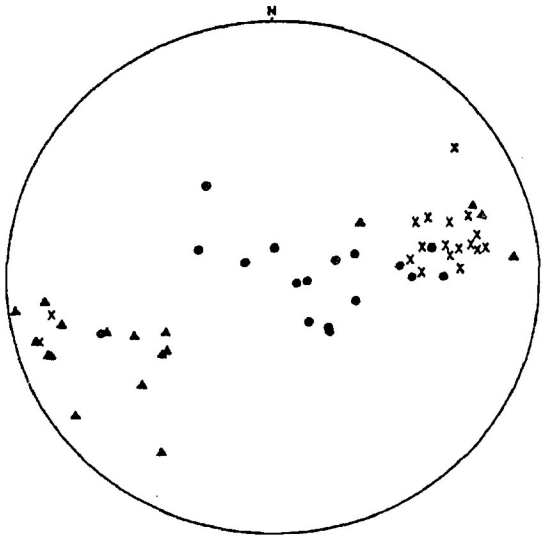

D. Southeast (SE) section.

Figure 46. Stereographic projections of maximum (O) and intermediate (Δ) magnetic susceptibility orientations and S_0/S_1 intersection lineation directions (X) in samples from specific sections of the present study area (see Fig. 45). Each secton has a relatively consistent S_0/S_1 intersection direction.
See text for discussion of the directional relationships.

	Arithmetic means	
	P'	k ($x10^{-5}$ c.g.s./cm^3)
153 Quetico rock samples	1.37	3.12
22 samples from fold closures	1.47	4.88
15 samples from refracted S1 beds	1.52	4.28

F. MSA and refracted cleavage

The well-developed cleavage refraction in parts of the study area (e.g. sample location P51, see Fig. 6) is always associated with graded bedding. South of Perch Lake, refracted cleavage (S_1) surfaces vary from 210-45 at the coarse-grained base of beds to 253-70 at the fine-grained tops. Bedding (S_0) surfaces strike at 087 degrees and dip vertically.

Refracted cleavage is a common feature of deformed rock sequences with graded beds or alternating lithologies. As previously noted, it represents variations in the state of finite strain of the rocks. However, it is not yet certain how cleavage refraction develops. The refraction is obviously related to lithological variation and, hence, to contrasting rheological properties. In the case of the Quetico rocks, this must be controlled by two properties: grain size and quartz- phyllosilicate content.

A number of mechanisms for development of refracted cleavage have been suggested, and it is probable that more than one mechanism may, separately or in combinations, develop refracted cleavage for a given deformation history. A summary of some of these mechanisms is given in Figure 55.

Besides its strain-state implications, refracted cleavage provides

Figure 47. Relationships of MSA parameters to bed location in samples from graded beds with refracted cleavage.

A. T (shape parameter of magnitude ellipsoid of susceptibility). The magnitude ellipsoids of susceptibility become progressively more flat-shaped in samples from the base to top of the graded beds.

B. P' (degree of anisotropy of the susceptibility magnitude ellipsoid). The degree of anisotropy of the susceptibility magnitude ellipsoids progressively increases in samples from the base to the middle of the graded beds, but decreases sharply in samples from the argillaceous tops of the beds.

C. k (mean magnetic susceptibility $\times 10^{-6}$ c.g.s./cm^3). The mean magnetic susceptibility (like P') increases progressively in samples from the base to middle of the graded beds, but decreases sharply in samples from the argillaceaus tops of the beds.

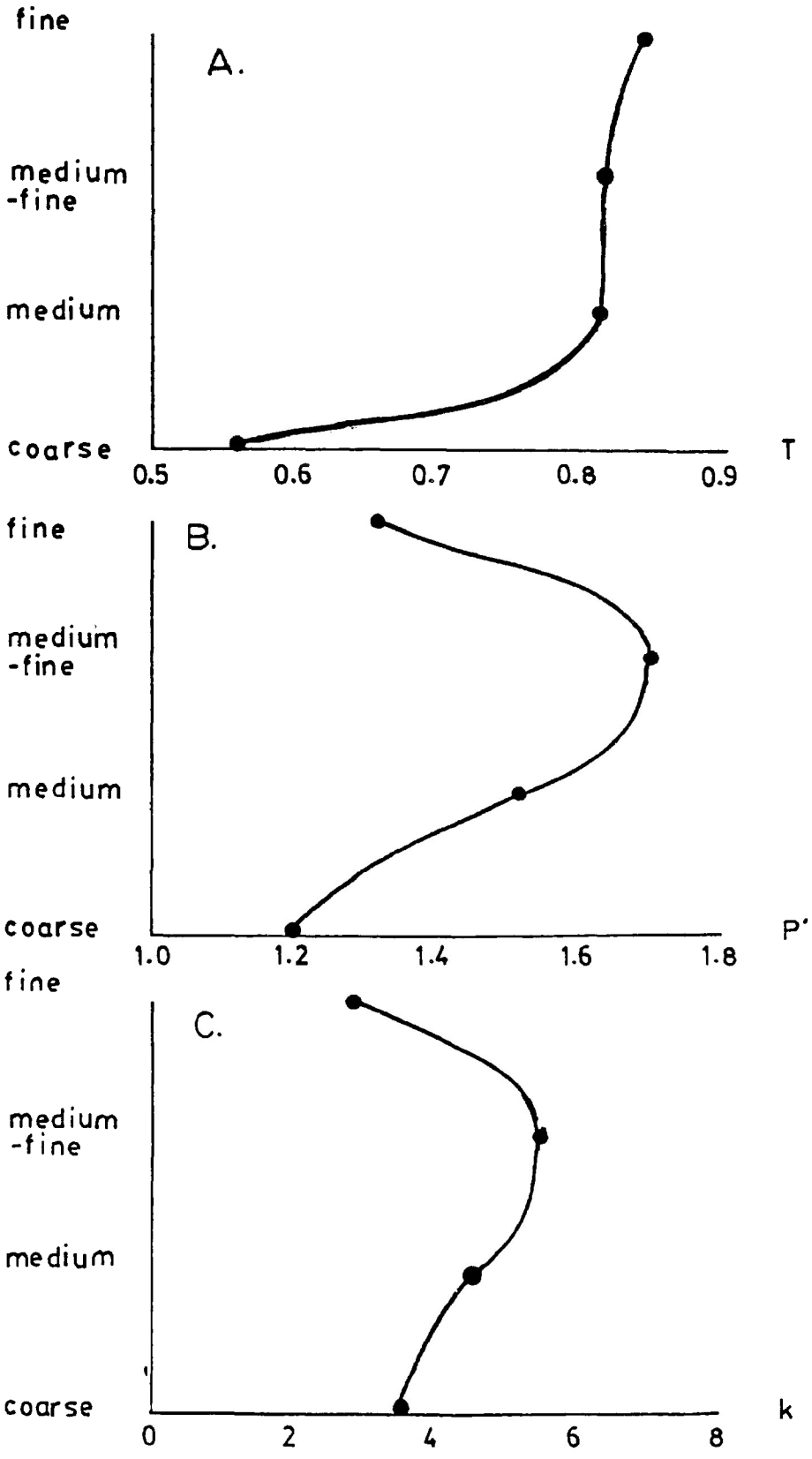
fine
A.
medium
-fine
medium
coarse
0.5
0.6
0.7
0.8
0.9
T
fine
B.
medium
-fine
medium
coarse
1.0
1.2
1.4
1.6
1.8
P'
fine
C.
medium
-fine
medium
coarse
0
2
4
6
8
k

an opportunity to study variations in MSA of the rocks while S_1 vary systematically in both orientation and intensity, and while both S_0 surfaces and S_0/S_1 lineations remain consistently oriented (Fig. 42).

The T parameter gradually increases from base to top of beds (Fig. 47A); The magnitude ellipsoid of susceptibility becomes more flat-shaped as cleavage spacing becomes more intense. The relationship of P' and bulk magnetic susceptibility with S_1 surface orientation and position in the graded bed is more complex (Fig. 47B and 47C). Both parameters increase gradually, then sharply from the base to the middle of the beds, followed by an abrupt decrease at the top of the bed.

The set of k_{min} axes are parallel to the range of orientations of the poles to the S_1 planes (Fig. 42). An interesting relationship of k_{min} directions to S_1 and S_0 surfaces is observed: at the base of the graded beds, k_{min} axes are aligned in a direction intermediate between the poles to S_0 and S_1 surfaces, but closer to the S_1 surface (Fig. 48A). In the middle of the graded beds, k_{min} axes are more closely parallel to S_1-surface poles (Fig. 48B). At the tops of the graded beds, k_{min} axes are again subparallel to S_1-surface poles (Fig. 48C), but are also subparallel to S_0-surface poles because at the argillaceous tops of the graded beds, S_0 and S_1 surfaces are nearly parallel.

k_{int} axes display a similar relationship. At the base of beds, k_{int} axes are aligned between the S_0 and S_1 planes (Fig. 49A). In the

Figure 48. Stereographic projections of k_{min} axis orientations in samples from the graded beds with refracted cleavage.

A. Base of beds. k_{min} axes are oriented in a direction intermediate between S_0 bedding poles and S_1 cleavage poles.

B. Middle of beds. k_{min} axes are closely subparallel to the S_1 cleavage poles.

C. Tops of beds. k_{min} axes are again oriented in a direction closely parallel to S_1 cleavage poles, which is also very close to the S_0 bedding pole direction.

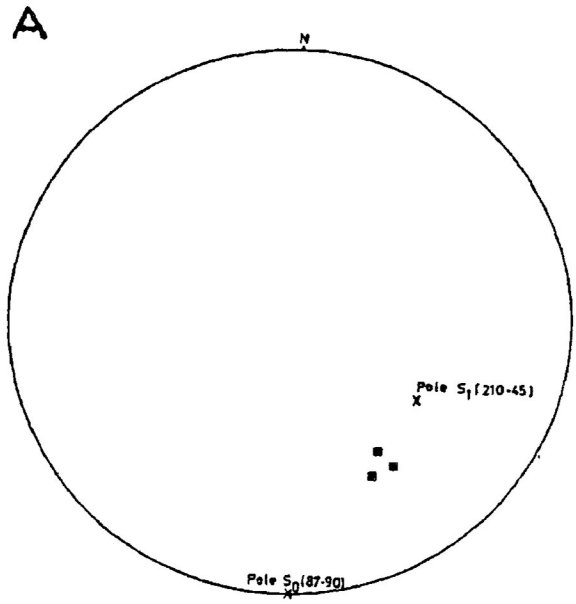
A
N
Pole S_1 (210-45)
Pole S_0 (87-90)

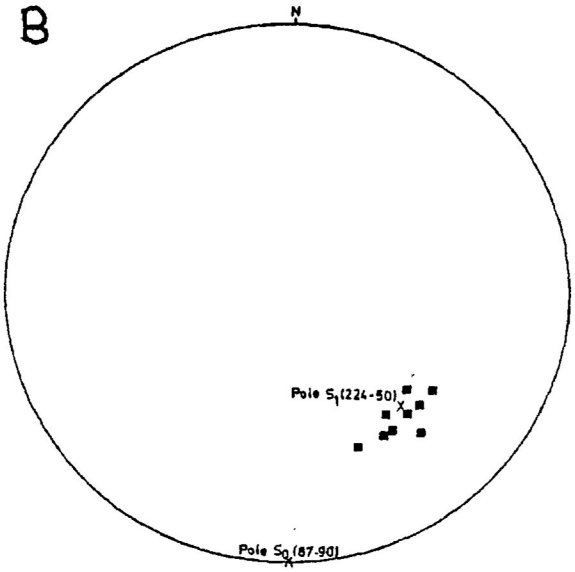
B
N
Pole S_1 (224-50)
Pole S_0 (87-90)

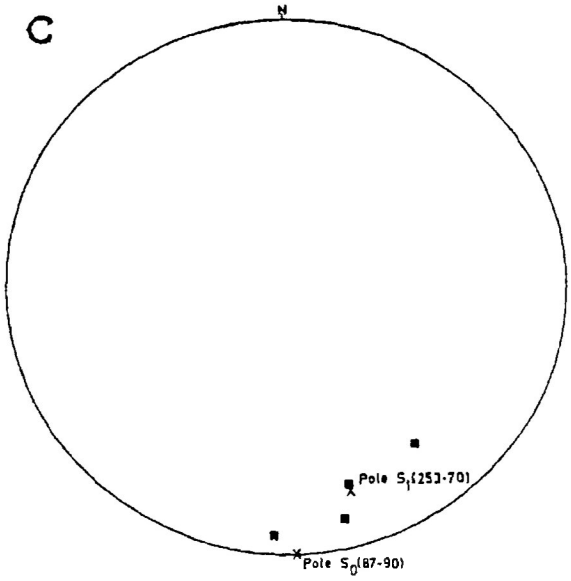
C
N
Pole S_1 (253-70)
Pole S_0 (87-90)

Figure 49. Stereographic projections of k_{int} axis orientations in samples from the graded beds with refracted cleavage.

A. Base of beds. k_{int} axes are contained within planes which are intermediate in orientation between S_0 and S_1 planes.

B. Middle of beds. k_{int} axes are contained within planes which are closely subparallel to S_1 planes.

C. Top of beds. k_{int} axes are again contained within planes which are subparallel to S_1 planes.

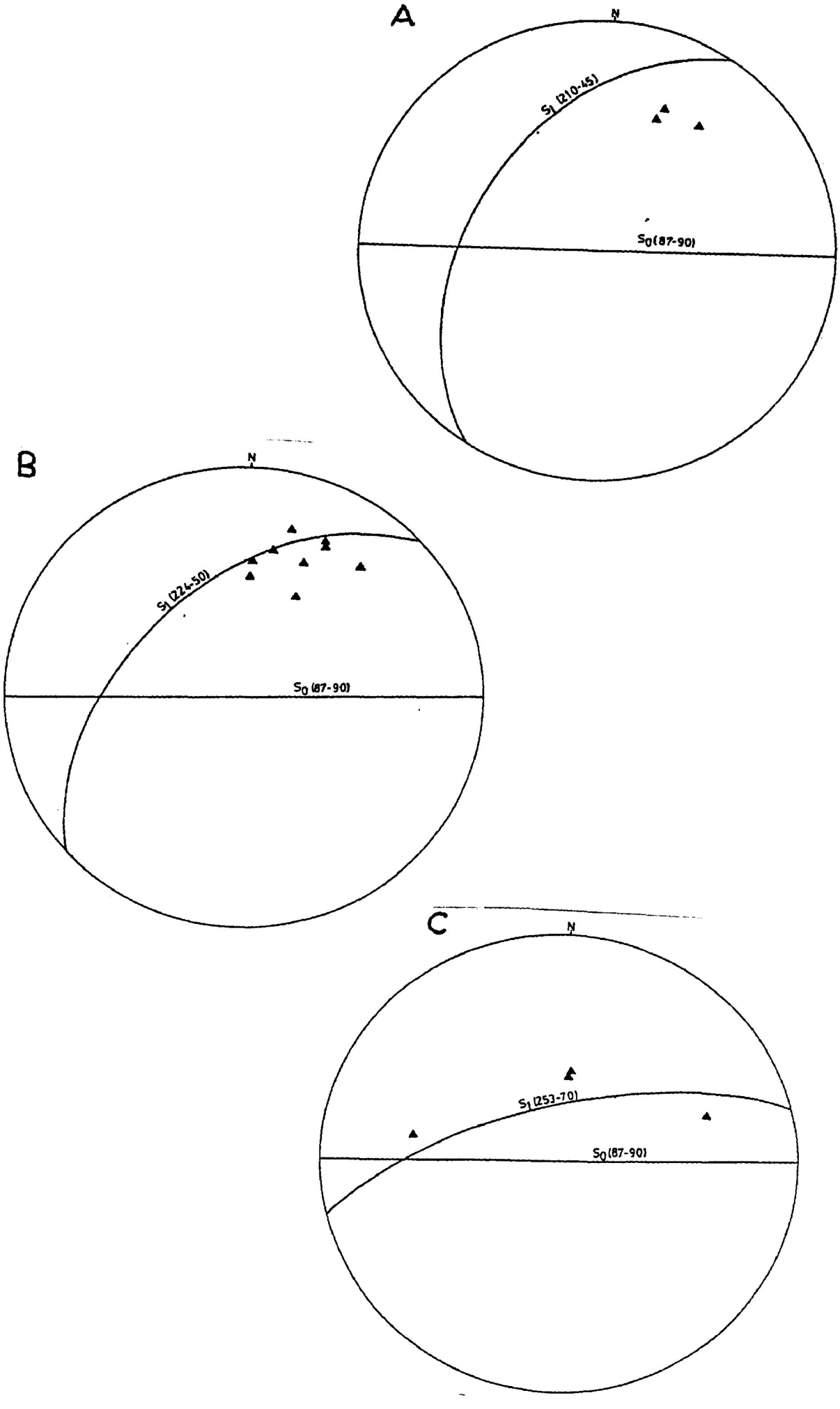
A
N
S1 (210-45)
S0 (87-90)
B
N
S1 (224-50)
S0 (87-90)
C
N
S1 (253-70)
S0 (87-90)

Figure 50. Orientations of k_{max} axes in samples from graded beds with refracted cleavage.

A. Base of beds. k_{max} axes are closely subparallel to the S_0/S_1 intersection lineation direction.

B. Middle of beds. In samples near the base of the beds, k_{max} axes are again subparallel to the S_0/S_1 intersection direction, but the axes deviate steadily from this direction in samples in the middle of the beds. The greatest deviation of k_{max} axes from the S_0/S_1 intersection direction is found in samples near the top of the beds.

C. Top of beds. k_{max} axes deviate markedly from the S_0/S_1 intersection direction.

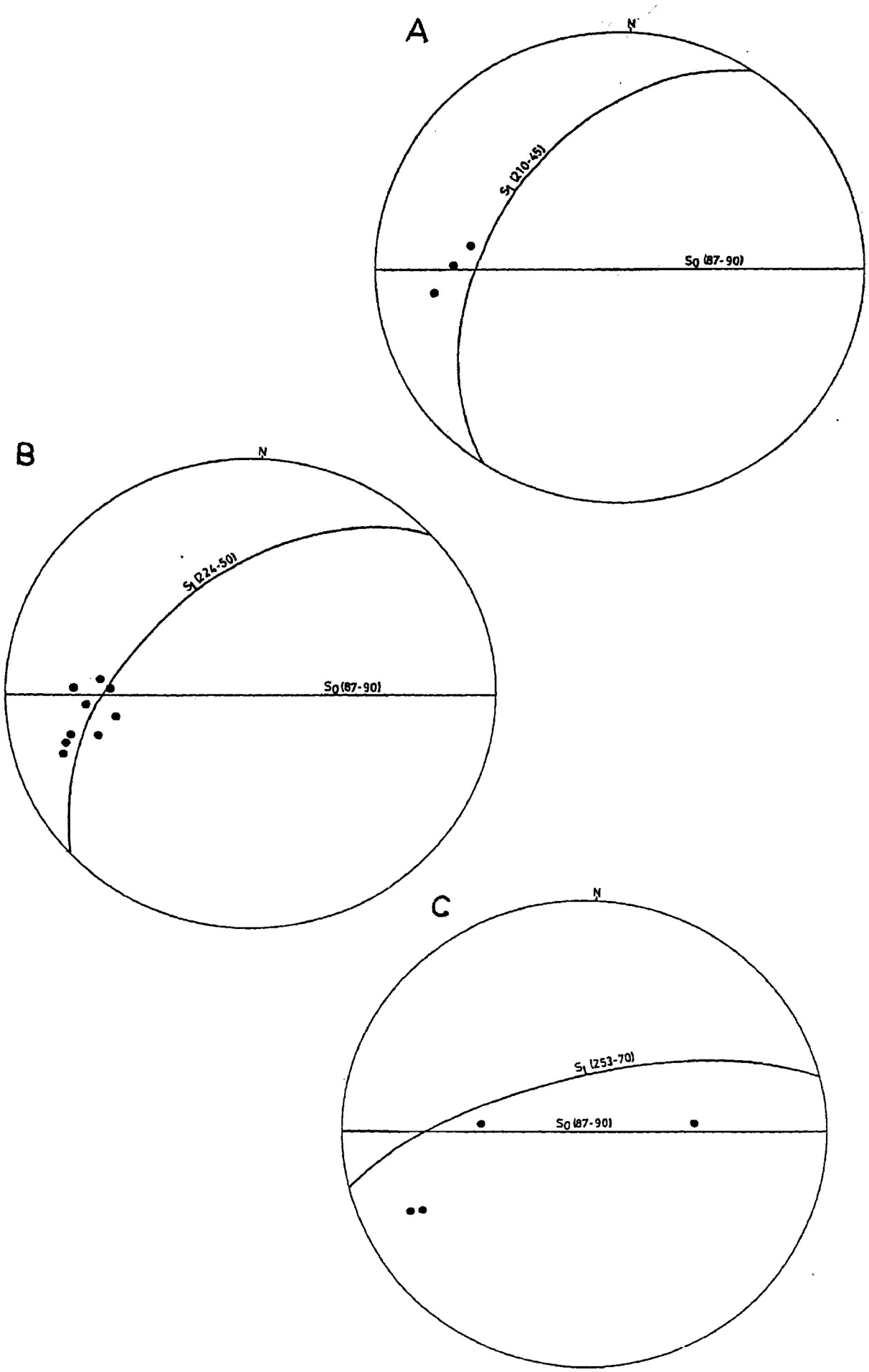
A
N
S1 (210-45)
S0 (87-90)
B
N
S1 (224-50)
S0 (87-90)
C
N
S1 (253-70)
S0 (87-90)

middle and top of the beds. k_{int} axes are generally contained within the S_1 planes (Fig. 49B and 49C).

k_{max} axes are aligned parallel or closely subparallel to S_0/S_1 lineations (Fig. 50). However, k_{max} axes from the base of graded beds are most closely parallel to S_0/S_1 lineations, and the angle between k_{max} axes and S_0/S_1 lineation consistently increases from the base to the top of the graded beds (Fig. 50).

5-5. Discussion of magnetic fabric results.

To summarize and collate the results and observations of the magnetic fabric studies:

1. Magnetite and pyrrhotite are the two ferrimagnetic minerals identified in the rocks. The ferrimagnetic minerals comprise less than two percent, by weight, of the rock but still contribute significantly to the bulk magnetic susceptibility.
2. Paramagnetic minerals identified include chlorite, biotite and muscovite. The paramagnetic minerals can also contribute significantly to the rock's bulk magnetic susceptibility.
3. Most susceptibility ellipsoids of the Quetico rocks are flat-shaped with fairly high degrees of anisotropy(averages: T = +0.53, P' = 1.35). The variations of P' and T parameters are typical of that of metamorphic and deformed rocks (compare Figs. 35 and 28).
4. Throughout the entire study area, k_{min} axes have a strong preferred orientations perpendicular to the regional trend of both S_0 bedding and S_1 cleavage surfaces (Fig. 40). In areas where there is a significant variation in S_0 and S_1 surfaces

(e.g. fold closures, cleavage refraction), k_{min} axes are generally found to be perpendicular to S_1 surfaces (Figs. 41 and 42).

5. Both k_{max} and k_{int} axes have a wide directional distribution throughout the study area, within a range of planes perpendicular to k_{min} axes (Fig. 43 and 44). In areas of consistent S_0/S_1 intersection lineation directions, generally (though not always - e.g. Fig. 46A), k_{max} and k_{int} axes also have rather consistent orientations. In these areas, the orthogonal k_{max} and k_{int} axes are bisected by the S_0/S_1 lineations. Conversely, at fold closures and in the graded beds with refracted cleavage, k_{max} axes are found to be closely subparallel to fold axes and S_0/S_1 lineations (Fig. 41 and 42).

6. Related to the above observation, the average mean magnetic susceptibility and degree of anisotropy of samples from the fold closures and the beds with refracted cleavage are higher than those of the entire study area:

	P'	k (x 10-5c.g.s./cm3)
Entire study area(153 samples)	1.37	3.12
Fold closures(22 samples)	1.47	4.88
Refracted cleavage(15 samples)	1.52	4.28

7. From the MSA studies of the graded beds with refracted cleavage, there are a number of important observations:

Susceptibility ellipsoids become progressively flatter from base to top of the graded beds. The most flat-shaped ellipsoids are always associated with phyllosilicate-rich, argillaceous

rocks (Fig. 47A).

Both bulk magnetic susceptibility and magnitude ellipsoid of susceptibility degree of anisotropy progressively increase from base to middle of the graded beds, then decrease sharply at the argillaceous tops (Fig. 47B and 47C).

k_{min} axes of the susceptibility ellipsoids are perpendicular to S_1 cleavage planes at the middle and top of the graded beds. At the base of the beds, though, k_{min} axes deviate slightly from the pole to S_1 toward the pole to S_0 planes (Fig. 48).

Similarly, k_{int} axes are generally contained within the S_1 cleavage planes at the middle and top of the graded beds. At the base of the beds, however, the k_{int} axes are contained within a plane intermediate between S_1 and S_0 planes (Fig. 49).

At the base of the graded beds, k_{max} axes are very closely subparallel to the S_0/S_1 intersections lineation direction. From the base to the top of the beds, though, the k_{max} direction deviates slightly but progressively from the S_0/S_1 lineation direction (Fig. 50).

The consistent correlation of k_{min} axes with S_1 cleavage planes suggests the magnetic fabric of the Quetico metasedimentary rocks is predominantly a tectonic magnetic fabric. This is supported by both the relatively high degree of anisotropy and the range of P' and T values of susceptibility ellipsoids. P' values of depositional magnetic fabrics rarely exceed 1.1.

In the Quetico metasedimentary rocks, a tectonic magnetic fabric includes components of both a metamorphic and a deformational magnetic fabric.

Although the magnetic fabric is clearly predominantly tectonic, there is still evidence of a preserved depositional component in some rocks. These rocks are the coarse-grained sandstones with relatively wide-spaced cleavage surfaces at the base of the graded beds with refracted cleavage. Here, the k_{min} axis is oriented at a direction intermediate between the poles to the S_0 and S_1 surfaces (Fig. 48A). If the magnetic fabric were completely deformational, one would expect the k_{min} axis to align parallel to the S_1 cleavage pole. The angular deviation toward the S_0 pole may reflect the influence and interference of a depositional component.

Borradaile and Tarling (1981) have detected a component depositional magnetic fabric in weakly deformed sedimentary rocks at up to 30 percent shortening. The spaced S_1 cleavage surfaces at the base of the Quetico graded beds may represent a similar situation: undeformed microlithons between cleavage surfaces contain a predominantly depositional magnetic fabric, with k_{min} axes perpendicular to S_0 surfaces. Within the S_1 cleavage planes, magnetic fabric is strongly tectonic and k_{min} axes are perpendicular to S_1 surfaces. The resultant k_{min} direction is intermediate between the depositional and tectonic k_{min} directions (Fig. 51B) and may also explain k_{max} being parallel to the bedding-cleavage intersection.

The magnetic susceptibility and MSA of a rock are both controlled by the magnetic mineralogy. This study has shown that the magnetic

susceptibilities of the Quetico metasedimentary rocks have significant contributions from ferrimagnetic minerals (magnetite and pyrrhotite) and can have significant contributions from paramagnetic minerals (chlorite, biotite and muscovite). The paramagnetic minerals are all metamorphic in origin. This component, then, characterizes the metamorphic magnetic fabric of the Quetico rocks. Chlorite, biotite and muscovite have relatively low magnetic susceptibilities (Table 2) but their susceptibility ellipsoids have generally flat shapes and high degrees of anisotropy (Fig. 52). Within the Quetico rocks, the metamorphic minerals also have a well-developed preferred crystallographic orientation (p.c.o). With this combination, the metamorphic magnetic fabric of the Quetico rocks should have a flat-shaped ellipsoid (the *paramagnetic ellipsoid* with a strong magnetocrystalline anisotropy.

During deformation, detrital grains of sedimentary rocks are variably influenced by a number of deformation mechanisms and aligned into preferred orientations relative to principal strain directions. The ferrimagnetic minerals in the Quetico rocks may be mainly detrital in origin. Given the significant contribution of the ferrimagnetic minerals to the bulk magnetic susceptibility of the Quetico rocks, and the strong correlation of the rock's susceptibility ellipsoids with tectonic fabrics, the ferrimagnetic component may represent the deformational magnetic fabric.

Because both are highly ferrimagnetic, the MSA of individual magnetite and pyrrhotite grains depend on their shape anisotropies (Fig. 21B). The shape and degree of anisotropy of the rock's *ferrimagnetic ellipsoid* would be dependent on the grain shapes and on the preferred dimensional orientation (p.d.o.) of the ferrimagnetic

Figure 51. Model for the development of magnetic fabric associated with stylolitic cleavage (from Borradaile and Tarling, 1981).

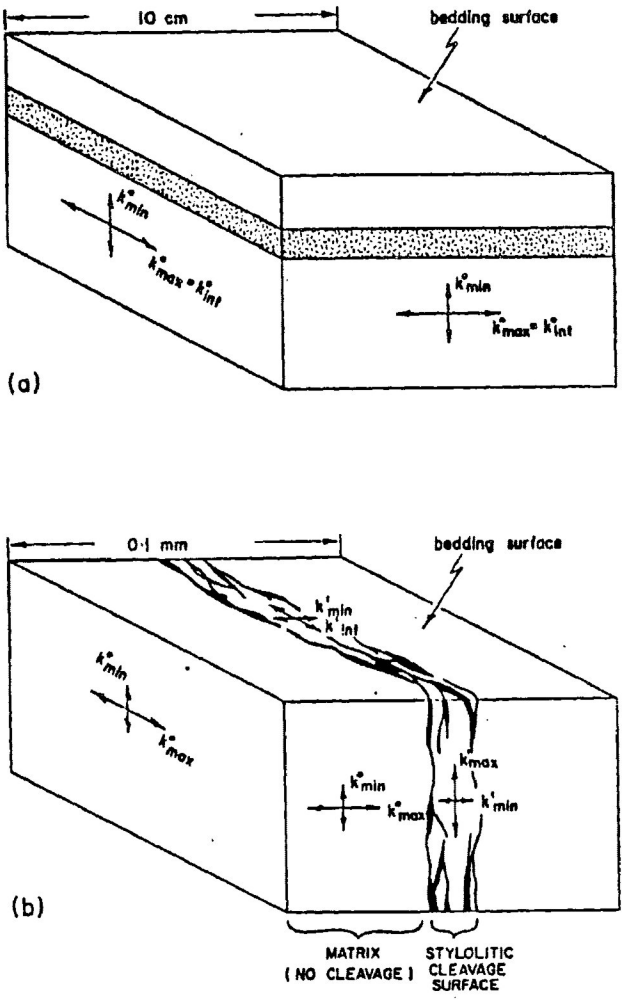

a. Undeformed rock shows primary magnetic fabric with k°_{min} perpendicular to bedding.

b. Deformed rock shows localized development of a tectonic magnetic fabric in stylolitic cleavage zones, where k_{max} is parallel to cleavage. Interference of the localized tectonic fabric (susceptibilities k') with the original fabric (susceptibilities k°) can produce the magnetic fabrics with overall maximum susceptibility (k_{max}) parallel to cleavage-bedding intersection.

Figure 52. Degree of anisotropy (P') and shape (T) of susceptibility ellipsoids for certain rock-forming minerals. The field outlined indicates the main range for metamorphic rocks presented in Hrouda(1982). The triangle represents metamorphic magnetite from a large number of different rocks and the triangle inside a circle represents detrital magnetite from a very immature sediment (from Borradaile et. al., in press).

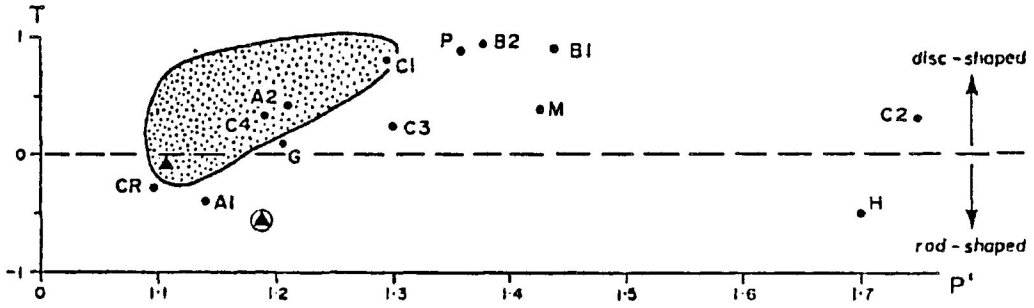

A1 A2	Actinolite
H	Hornblende
CR	Crocidolite
G	Glaucophane
C1 C2 C3 C4	Chlorite
B1 B2	Biotite
P	Phlogopite
M	Muscovite

Figure 53. Hypothetical curves indicating the number of grains in a given orientation in specimens with a preferred orientation of grains (dashed line at 0°). Each of the three specimens has the same degree of preferred orientation of grains, but the frequency of grains in the preferred orientation increases with the number of grains in the specimen. When the grains are considered magnetic grains, it can be seen that the specimen with the greatest number of grains will have the strongest degree of magnetic susceptibility anisotropy (MSA).

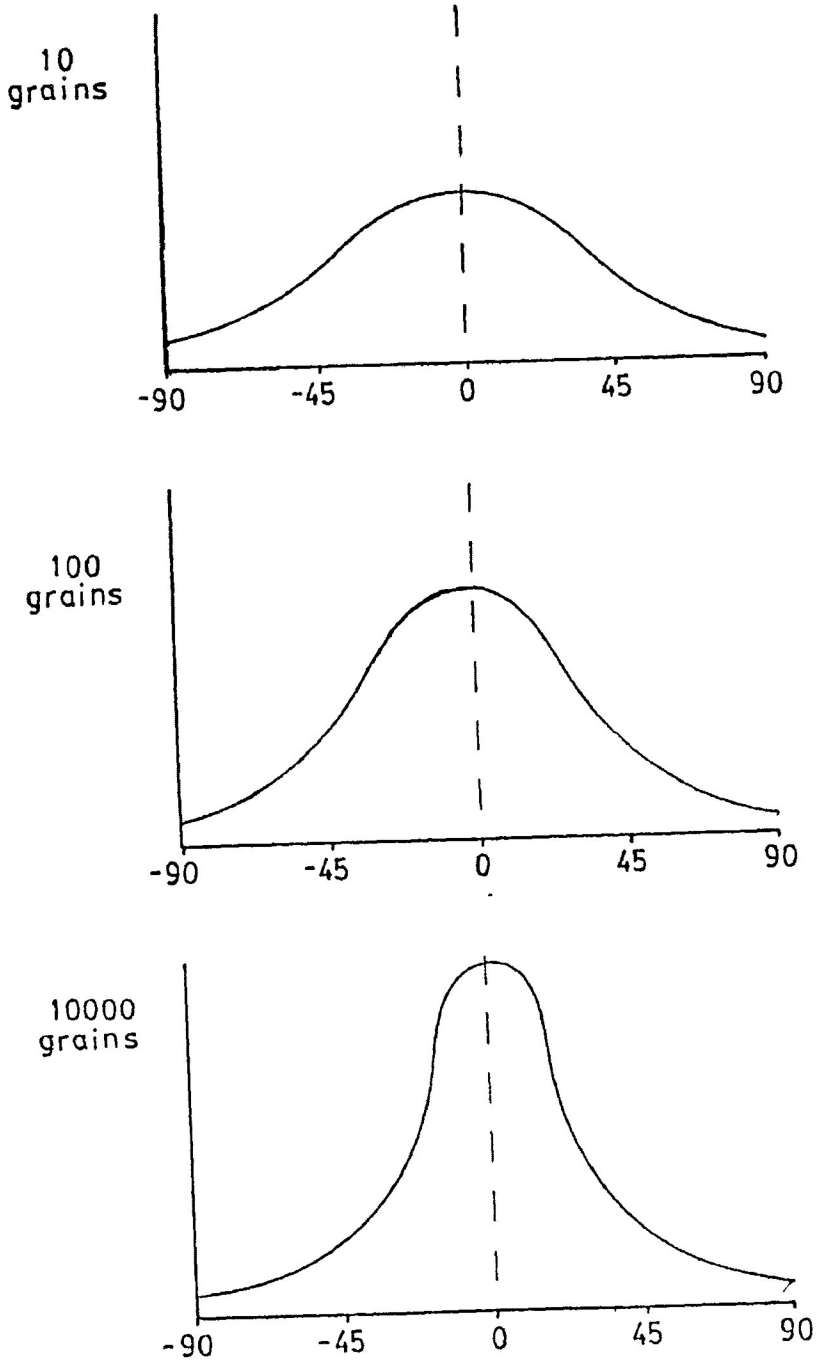

minerals. The p.d.o. fabric of a metamorphosed tectonite need not be very strong and is not in the present study area, especially when compared to the p.c.o. of a metamorphic fabric. The strength of a p.d.o. fabric is dependent on the amount of deformation, but also on the number of grains which define the fabric. The p.d.o defined by two grains would be relatively poor, but by 20 grains significantly better (Fig. 53). In the Quetico rocks, ferrimagnetic minerals comprise less than two percent, by weight, of the rock. The relatively few grains of this component of the rock fabric, then, would not defined a strong p.d.o. fabric.

Compared to the paramagnetic ellipsoid, then, the ferrimagnetic ellipsoid of the Quetico rocks should have a moderate to weak shape anisotropy. The degree of anisotropy (and the mean magnetic susceptibility) of the deformational magnitude ellipsoid of susceptibility should increase with increased amounts of ferrimagnetic grains, because more grains define a better frequency distribution in the preferred orientation (Fig. 53). The shape and degree of anisotropy of the ferrimagnetic ellipsoid are both dependent on the strength and character of the p.d.o. fabric (and, hence, on the magnitudes of the principal finite strains), and on the shapes of the ferrimagnetic grains.

The ferrimagnetic minerals can also represent the depositional magnetic fabric. This fabric is apparently preserved in undeformed microlithons in rocks with wide-spaced cleavage surfaces. Even in these rocks, though, the magnetic fabric is predominantly tectonic. k_{min} axes are much closer to S_1 cleavage poles than to S_0 bedding poles (Fig. 55).

The relationship between bulk magnetic susceptibility (k) and the degree of anisotropy (P') of the rocks (Fig. 36) is also related to

magnetic mineralogy. An increase in bulk magnetic susceptibility of the rock may reflect an increased concentration of magnetic minerals. Thus, a correlative increase of k with P' may somehow be related to an increase in the preportion of higher susceptibility minerals. There are three possible explanations for this relationship.

1. An increase in the content of paramagnetic phyllosilicates creates an increase in bulk magnetic susceptibility of the rock. The phyllosilicates define the paramagnetic ellipsoid, with a strong magnetocrystalline anisotropy. The increased phyllosilicate content causes the paramagnetic ellipsoid to have a greater influence on the MSA of the rock, which, in turn, increases the P' of the rock.
2. An increase in the content of ferrimagnetic minerals causes an increase in the bulk magnetic susceptibility of the rock. With increased number of ferrimagnetic grains, the frequency of grains at or close to the preferred orientation increases, which has the effect of defining a better shape anisotropy (and a higher P') for the ferrimagnetic ellipsoid. With increased ferrimagnetic mineral content, the ferrimagnetic ellipsoid has a greater influence on the MSA of the rock. The P' of both the ferrimagnetic ellipsoid and the magnitude ellipsoid of susceptibility of the rock increase with increased ferrimagnetic mineral content. The new ferrimagnetic grains may also have a higher degree of MSA.
3. A combined increase in paramagnetic and ferrimagnetic mineral content.

While a simultaneous increase in phyllosilicate content and P' of the rock is theoretically quite possible, there is little evidence to support this hypothesis in the Quetico rocks. The magnetic

susceptibilities of phyllosilicates are not high (Table 2), so a significant increase in bulk magnetic susceptibility would require a significant increase in phyllosilicate content. Most of the samples of Quetico rocks collected for MSA studies are sandstones. The phyllosilicate contents of these sandstones are not observed to flucuate greatly.

As well, individual phyllosilicate minerals generally describe flat-shaped susceptibility ellipsoids (Fig. 52), so the paramagnetic ellipsoid described by this component of the rock should also be flat. An increased influence of the paramagnetic ellipsoid, then, should also lead to a positive increase in the T shape parameter (a flatter ellipsoid) for the rock's magnitude ellipsoid of susceptibility. There is, however, no such sympathetic relationship between P' and T, or between bulk magnetic susceptibility and T in the Quetico rocks (Fig. 35 and 37).

Conversely, the ferrimagnetic minerals have very high magnetic susceptibilities. So, though magnetite and pyrrhotite comprise only a small fraction (less than 2 weight percent) of the physical constituents of the rocks, they represent a significant proportion of the rock's bulk magnetic susceptibility. Because of their high magnetic susceptibilities, only a small increase in the ferrimagnetic content can substantially increase the bulk magnetic susceptibility of the rock. Addition of a few more ferrimagnetic grains would also increase the frequency of grains in a preferred orientation (Fig. 53), and so increase the degree of anisotropy of both the ferrimagnetic and the lithological magnitude ellipsoid of susceptibility.

It would appear, then, that variations of ferrimagnetic content in the Quetico rocks is the better explanation for the correlative relationship between mean magnetic susceptibility and degree of

anisotropy of the susceptibility ellipsoids. A combined variation in ferrimagnetic and paramagnetic content, however, cannot be ruled out.

Perhaps the best supporting evidence for the controlling influence of the ferrimagnetic fraction on both bulk magnetic susceptibility and degree of anisotropy is found in the MSA variations observed within the graded beds with refracted cleavage. The beds have a progressive increase in phyllosilicate content from base to top. Susceptibility ellipsoids show a progressive increase in k and P', and become progressively flatter, from the base to the middle of the beds. At the top of the beds, magnitude ellipsoids of susceptibility are the most flat-shaped(T = +0.85), but both the magnitude and degree of anisotropy decrease sharply.

The progressively flatter shape of susceptibility ellipsoids from base to top of the beds indicates the increasing influence of the paramagnetic ellipsoid as phyllosilicate content increases (Fig. 54). However, the sudden decrease in P' and k at the tops of the beds, where phyllosilicate content is greatest, indicate that the paramagnetic ellipsoid does not control either the bulk magnetic susceptibility of the rock or the degree of anisotropy of its magnitude ellipsoid of susceptibility. These must be controlled by the ferrimagnetic mineral content. It is apparent that, with phyllosilicate content, ferrimagnetic mineral content increases from top to middle of the graded beds, causing an increase in P' and k. At the argillaceous tops of the beds, the decrease in k may indicate a decrease in the amount of magnetite and pyrrhotite. The decrease in P' may be the result of a weaker degree of anisotropy of the ferrimagnetic ellipsoid because of fewer ferrimagnetic grains (Fig. 54).

Figure 54. Relationship between magnetic mineralogy, MSA and orientation of S-surfaces in graded beds with refracted cleavage. The magnetic mineralogy consists of a ferrimagnetic component (dark grains) and a paramagnetic component (grains with cleavage trace). See the text for a more detailed discussion.

A. Base of bed. S_1 surfaces are widely spaced and there are microlithons with preserved depositional magnetic fabric. The rocks have relatively few ferrimagnetic and paramagnetic minerals, so both bulk magnetic susceptibility and MSA of the rocks are weak. The ferrimagnetic minerals have a weak preferred orientation, and long axes of these grains are subparallel to S_0 planes in the undeformed microlithons.

B. Middle of bed. S_1 surfaces are more pervasive, so microlithons are very small and depositional magnetic fabric is no longer detectable. An increase in both ferrimagnetic and paramagnetic mineral content causes an increase in both bulk magnetic susceptibility and degree of MSA of the rocks. The ferrimagnetic grains here need not be more strongly aligned in a preferred direction than grains at the base of the beds, but because there are more grains there would be a greater frequency of grains parallel or subparallel to the S_1 planes.

C. Top of bed. S_1 surfaces are now so closely spaced that they can be considered pervasive and continuous. The increase in paramagnetic phyllosilicates causes the rocks' MSA ellipsoid to become flatter. The decrease in the number of highly magnetic ferrimagnetic grains, however, causes a decrease in bulk magnetic susceptibility of the rocks. It also causes a decrease in the frequency of ferrimagnetic grains subparallel to the S_1 planes, so the degree of MSA of the rocks is also weaker.

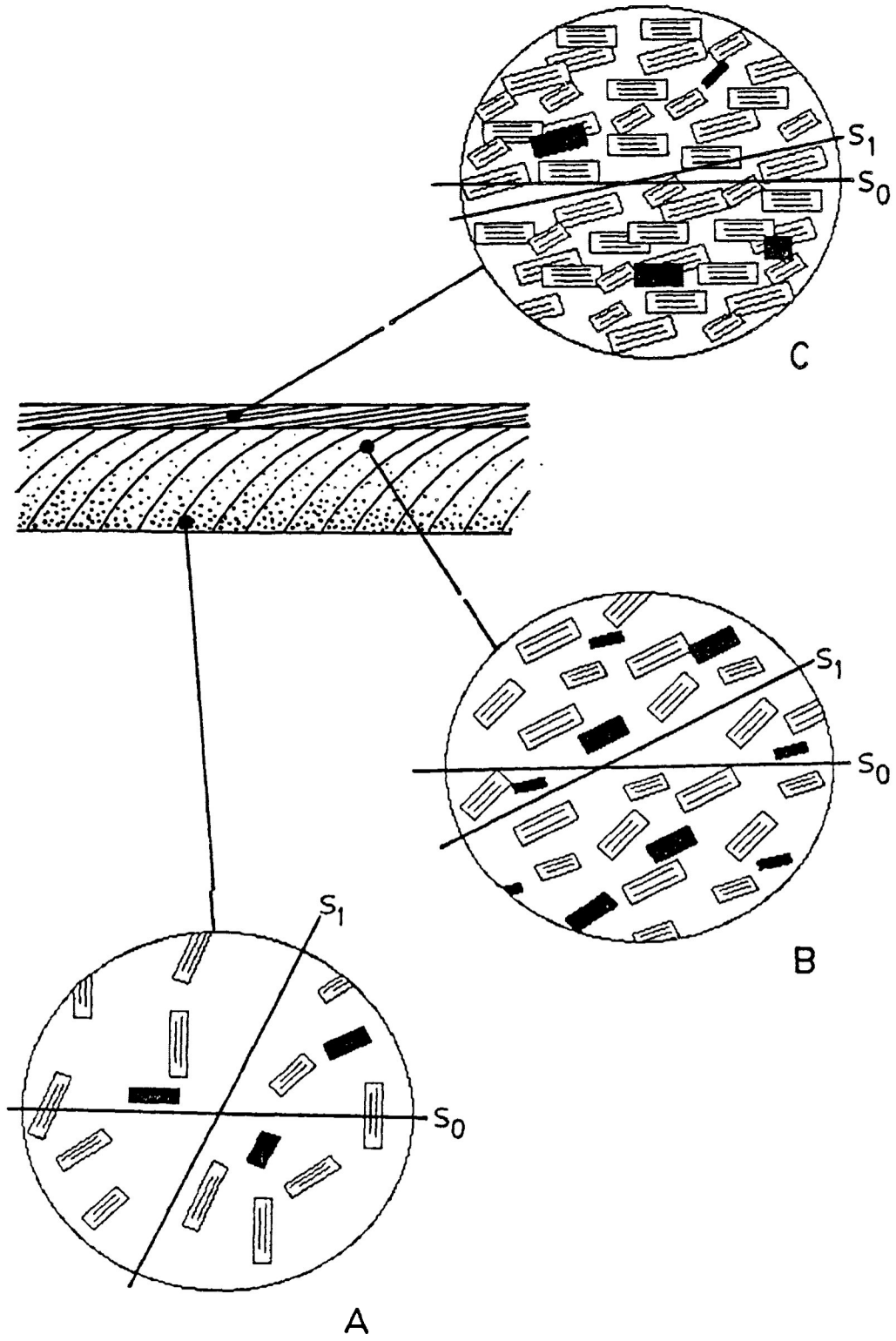
S1
S0
C
S1
S0
B
S1
S0
A

The decrease in P' at the tops of graded beds has important implications, for it indicates that the ferrimagnetic ellipsoid not only controls, but can have a disruptive influence on the MSA of the rock. Because it is defined by phyllosilicates with a highly-developed p.c.o., we know that the paramagnetic ellipsoid can have a high degree of anisotropy. At the phyllosilicate-rich top of the bed, this paramagnetic ellipsoid should have not only a high P', but its greatest influence on the MSA of the rock. The low bulk magnetic susceptibility of these rocks indicates a low ferrimagnetic mineral content, which, in turn, should define a rather weak ferrimagnetic ellipsoid. The paramagnetic and ferrimagnetic ellipsoids combine to describe the resultant magnitude ellipsoid of susceptibility of the rock. The low degree of anisotropy of the graded bed tops indicates that the ferrimagnetic ellipsoid, even with a weak magnitude, still has a strong influence on the lithological magnitude ellipsoid.

The ferrimagnetic ellipsoid may represent the deformational magnetic fabric of the Quetico metasedimentary rocks, while the paramagnetic ellipsoid may represent the metamorphic fabric. Since the ferrimagnetic content has greatest influence over the bulk magnetic suscetibilities, rocks with very high bulk magnetic susceptibilities could have predominantly deformational magnetic fabrics. Rocks with significant phyllosilicate content and very low bulk magnetic susceptibilities could have predominantly metamorphic magnetic fabrics which, nevertheless, could be overshadowed by the presence of only a few ferrimagnetic grains. Most Quetico rocks would have a tectonic magnetic fabric defined by a combination of deformational and metamorphic magnetic fabrics.

An alternative explanation, however, is presented by Rochette (1987) and Rochette and Vialon(1984) in their study of the magnetic

fabric of black shales in the Alps. The authors show a correlation between an increase in bulk magnetic susceptibility and in metamorphically-derived pyrrhotite across an area of progressive regional metamorphism. Rochette(1987) contends, also, that pyrrhotite has a stronger intrinsic MSA than both magnetite and the phyllosilicates. Hence, an increase in lithological MS and MSA may be achieved by an increase in pyrrhotite content(from the metamorphic breakdown of pyrite).

k_{min} axes are strongly perpendicular to tectonic planar fabrics (S_1 cleavage planes, fold axial surfaces). The S_1 cleavage planes are, in fact, defined by the preferred orientation of both metamorphic and deformational fabric elements (p.c.o. of metamorphic phyllosilicates, p.d.o. of quartz, feldspar and other, including ferrimagnetic, minerals), so both metamorphic and deformational magnetic fabrics have combined to define a strong regional k_{min} direction.

The tectonic relationship of k_{max} and k_{int}, however, is more complex. Both k_{max} and k_{int} directions are variable regionally within a plane broadly perpendicular to k_{min} axes (Fig. 43 and 44). In some sections of the study area, k_{max} and k_{int} axes have fairly consistent orientations (Fig. 46). Here, both axes deviate from the S_0/S_1 intersection lineation direction. At the locations of special structural features studied in the area (fold closures, refracted cleavage), however, k_{max} axes are generally parallel to the S_0/S_1 lineation direction (Fig. 41, Fig. 50).

In samples from the fold closures and the graded beds with refracted cleavage, both the mean magnetic susceptibility (k) and P'

are higher than the average k and P' of samples from the entire study area. This would imply that the magnetic fabric of samples from the minor structures have a greater influence from the ferrimagnetic ellipsoid than the typical sample of Quetico rock. It would appear, then, that the maximum susceptibility direction of the ferrimagnetic ellipsoid, at least at these locations, is parallel to the S_0/S_1 lineation direction.

In the graded beds with refracted cleavage, the sandstone beds display a gradational and significant increase in phyllosilicate content from base to top. In samples from the base of the beds, k_{max} axes are very closely subparallel to the S_0/S_1 lineation directions (Fig. 50A). From the base to the top of the bed, the k_{max} axis deviates, at an increasing angle from the lineation direction (Fig. 50 B and 50C).

At the phyllosilicate-poor base of these beds, the paramagnetic ellipsoid would have little influence, and the MSA of the rock would be dominated by the ferrimagnetic ellipsoid. From base to top, the influence of the paramagnetic ellipsoid increases with increasing phyllosilicate content. The deviation of k_{max} from the S_0/S_1 lineation direction may reflect the increasing influence of a non-coaxial paramagnetic ellipsoid on the dominant ferrimagnetic ellipsoid, causing the k_{max} and k_{int} directions of the resultant lithological magnitude ellipsoid of susceptibility to change slightly.

On the other hand, refracted cleavage indicated variation in the state of strain within the bed, and the deviation of k_{max} direction may record non-coaxial strain increments. Refracted cleavage is cited by some workers as an indication that the top of the graded bed

is more deformed than the base (see Fig. 55). If the principal magnetic susceptibility directions are parallel to the principal finite strain directions, the k_{max} axes may record a change in extension direction as the rock becomes more deformed.

It should be noted that, by definition, ferrimagnetic minerals (such as magnetite and pyrrhotite) can maintain an internal magnetic field even in the absence of an external magnetic field - a remanent magnetization (RM). Paramagnetic minerals, on the other hand, have no measurable RM. RM in a rock or mineral, like magnetic susceptibility, can be directionally variable. That is, a specimen can possess a remanent magnetization anisotropy (RMA).

If the RMA of the Quetico rocks were determined, the RM ellipsoid may give a better indication of finite strain directions than the MS ellipsoid because the principal RM directions would be related to the fabric of the ferrimagnetic minerals with no contribution from paramagnetic minerals(whose intrinsic MS ellipsoids have negligible differences between k_{max} and k_{int} magnitudes).

5-6. Conclusions

The results from the magnetic mineralogy and MSA studies of the Quetico metasedimentary rocks support the following conclusions:

1. The rocks have a polymineralllic magnetic mineralogy, comprising a ferrimagnetic component and a paramagnetic component. The ferrimagnetic component consists predominantly of magnetite and pyrrhotite. The paramagnetic component consists of chlorite, biotite and muscovite. Though less than two weight percent of the rock, the ferrimagnetic component appears to nevertheless dominate the bulk magnetic

Figure 55. Three possible mechanisms for refracted cleavage development. All three mechanisms are based on the observation that cleavage planes coincide with the principal plane of finite strain.

A. LPS vs. TLS. Layers undergoing buckling experience varying contributions from two internal deformation mechanisms: layer-parallel shear (LPS) and tangential-longitudinal strain (TLS). LPS is dominant in incompetant material (such as mudstones), while TLS is dominant in competent material (such as sandstones). The principal finite strain plane of TLS is oriented at a higher angle to the layer boundary than the principal finite strain plane of LPS; hence the cleavage refraction may record the gradational change from LPS-controlled to TLS-controlled internal deformation in a graded bed (from Ramsay, 1967).

B. Layer-parallel shortening vs. plane rotation. Initially, layer-parallel shortening causes development of spaced cleavage in all layers perpendicular to longitudinal compression. At the on-set of buckling, the "more deformable" incompetent layers are still affected by layer-parallel shortening, and cleavage planes are constantly re-oriented to remain perpendicular to longitudinal compression. Competent layers, however, are more resistant to layer-parallel shortening, and cleavage planes simply rotate as planes perpendicular to the layer boundary (from Lebedeva, 1982).

C. Progressive finite strain in a shear zone. Cleavage planes appear to converge, becoming more closely-spaced, in the incompetent layers. This suggests a possible convergence of principal strain trajectories, which, in turn, suggests the incompetent layers may have experienced a greater amount of finite strain. A shear zone may be an analogy: deformation fabrics at the center of shear zones are better-developed, closer-spaced, and more closely parallel to zone boundaries than defomation fabrics adjacent to the zone boundaries (from Ramsay and Huber, 1983, p. 181).

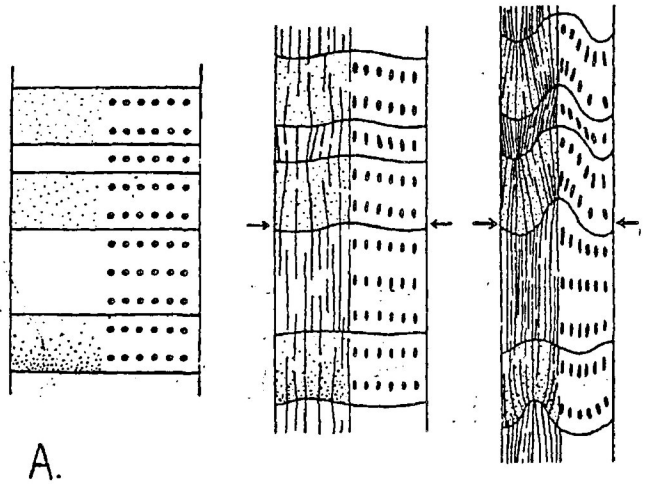

A.

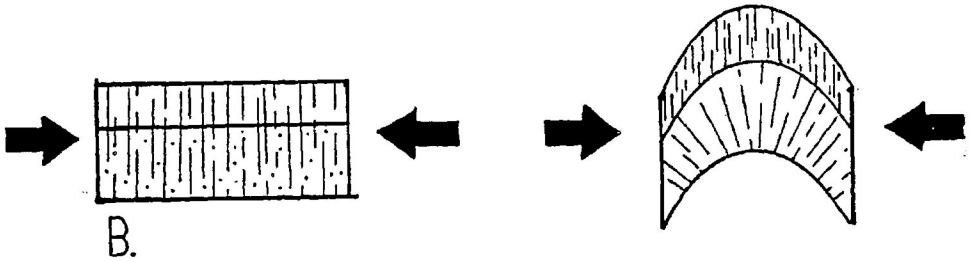

B.

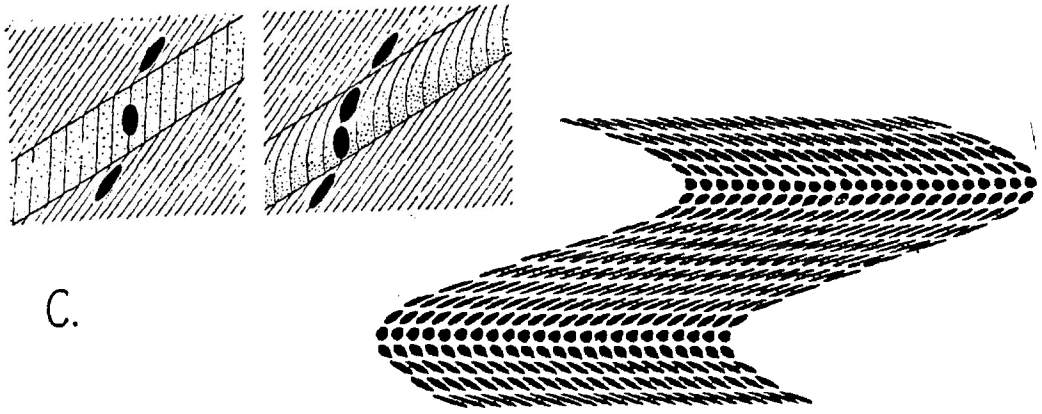

C.

susceptibility of most rocks. The paramagnetic component, however, can also contribute significantly to the bulk magnetic susceptibility of some rocks, and, because individual phyllosilicates generally have a high degree of MSA, may contribute very significantly to the MSA of most rocks.

2. The rocks possess a predominantly tectonic magnetic fabric. The minimum magnetic susceptibility direction is consistently perpendicular to the dominant regional planar tectonic fabric (the S_1 cleavage planes) and intermediate and maximum magnetic susceptibility directions are contained within this planar fabric. The tectonic magnetic fabric may have two components: The deformational magnetic fabric is described by ferrimagnetic minerals realigned by deformation mechanisms into preferred directions relative to finite strain directions. The metamorphic magnetic fabric evolved from the syntectonic preferred crystallographic growth of the metamorphic phyllosilicates (and pyrrhotite?).
3. In some rocks, a depositional magnetic fabric is partially preserved. These rocks are coarse-grained sandstones with wide-spaced cleavage planes at the base of graded beds with refracted cleavage. It is probable that the depositional magnetic fabric is preserved in relatively undeformed microlithons between the spaced cleavage planes. Hence, massive sandstones and rocks with wide-spaced cleavage planes may also preserve a component depositional magnetic fabric.

4. The magnetic fabric of the Quetico metasedimentary rocks is a

combination of deformational, metamorphic and depositional magnetic fabrics. The depositional magnetic fabric is always subordinate and, in most cases, so weak as to have no detectable influence on the rock's MSA.

5. The principal magnetic directions of the metamorphic magnetic fabric need not coincide with principal finite strain directions. Since the magnetic fabric of most rocks has a significant metamorphic component, it follows that the principal magnetic susceptibility directions of the rock's MSA cannot be considered reliable indicators of principal finite strain directions. This is apparently supported by the wide variation in maximum and intermediate susceptibility directions, and the general lack of correlation of these principal susceptibilities with the dominant linear structural feature (S_0/S_1 intersection lineations) on a regional scale(although the variation may indicate regional inhomogeneous finite strain). Nevertheless,the minimum susceptibility direction is so consistently perpendicular to schistosity that it would appear that this susceptibility direction correponds either to the minimum finite strain or to some combination of that and the pole to the metamorphic phyllosilicate fabric.

   In some smaller-scale structural features, such as minor folds and refracted cleavage, maximum and intermediate susceptibility directions are not only consistent in all samples, but the maximum susceptibility direction is consistently parallel to the S_0/S_1 intersection lineation direction. In these features, it could be argued that the principal magnetic

susceptibilities are coincident with principal finite strain directions.

In any case, it is apparent that great care must be taken in interpreting the significance of principal magnetic susceptibility directions.

6. A better indication of finite strain directions may be attained from study of the Quetico rocks' remanent magnetization anisotropy (RMA). The principal directions of the RM ellipsoid may be controlled solely by the fabric of the ferrimagnetic minerals with no contribution from paramagnetic minerals.

CHAPTER SIX

INTERPRETATION OF REGIONAL STRUCTURAL GEOLOGY

The Quetico metasedimentary rocks are deformed into a number of major F_1 folds. The major folds are characterized by the following features:

1. Folds are tight to isoclinal with hinge zones of relatively small volume in narrow zones.
2. Folds are asymmetric, with long north-facing limbs and relatively short south-facing limbs.
3. Folds are non-cylindrical, with strongly curvilinear fold axes.
4. The folds crop out roughly in en echelon arrangement subparallel to the dominant east-west structural trend, with the asymmetric folds separated by approximately three to four kilometers along strike.

Folds with such strongly curvilinear fold axes have been documented, but their geneses are not easily deciphered. Three general models can be evoked to explain the genesis of such fold geometries:

1. Polyphase deformation.
2. Amplification of original topographical asperities.
3. Passive folding, imposed upon (2) above.

Polyphase deformation will almost invariably produce a complex fold geometry. Ramsay(1967, pp. 539-45) describes in detail how variations in orientations of F2 fold axes are related to F1 fold geometry and to the angular relationship of the F1 and F2 axial planes (Fig. 56).

Figure 56. Stereographic projections showing variations in second-fold (F_2) axes orientations from geometry and orientation of the first-fold structures and orientation of second-fold axial surfaces ($AXPL_2$) (from Ramsay, 1967, Fig. 10-23).

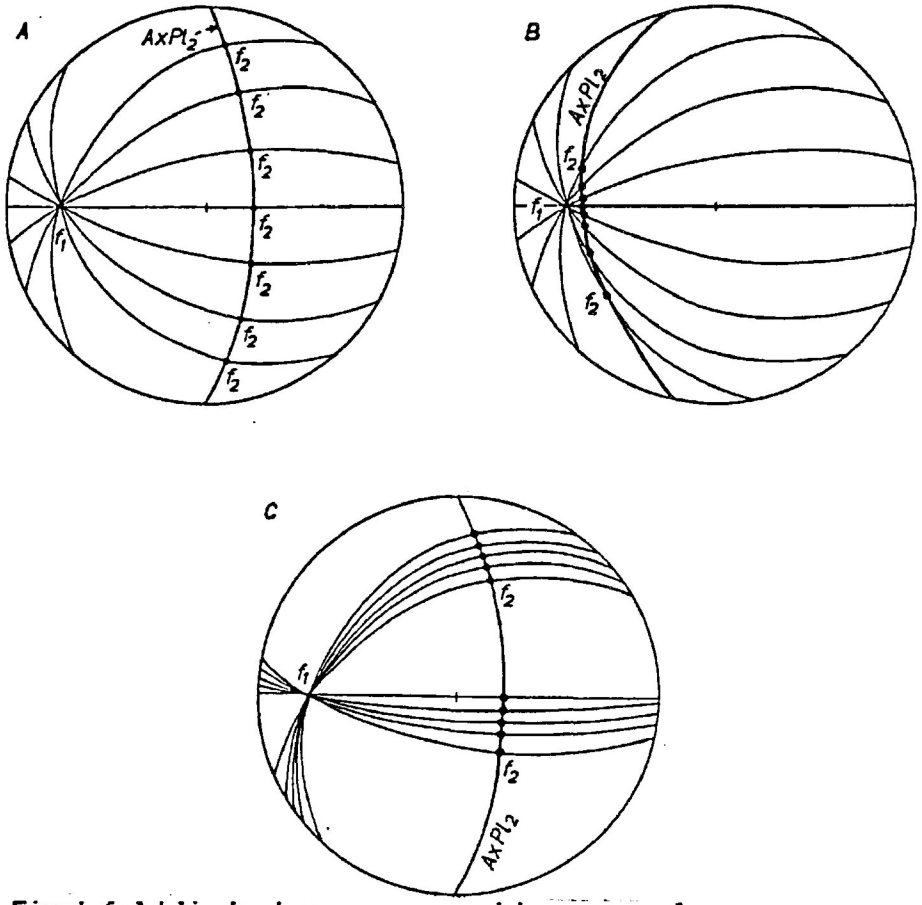

A. First fold limbs have a very wide range of orientations, and second-fold axial surfaces ($AXPL_2$) makes a large angle with first-fold axis (f_1). There is a very wide range of second-fold (f_2) axis orientations.

B. First fold limbs have a very wide range of orientations, but $AXPL_2$ makes a small angle with f_1. There is a relatively narrow range of f_2 orientations, which are close to the f_1 orientation.

C. First folds have narrow hinge zones and two narrow ranges of fold limb orientations. $AXPL_2$ makes a large angle with f_1. Within narrow ranges, there are two dominant f_2 orientations.

The problem with polyphase deformation as applied to the Quetico metasedimentary belt is that the present study, and previous studies, have invariably identified only a single regional penetrative cleavage with very little variation in orientation. As well, there is no evidence for a previous tectonic fabric, even though the grade and degree of recrystallization of the rocks is low.

Amplification of original topographical asperities may also lead to significant variation in fold axis orientation. Ramsay (1967, chapter 9) approaches this problem by considering two separate planes inclined to each other by a certain dihedral angle (Fig. 57). One plane is folded cylindrically about an axis, while the other is obliquely folded. Where this argument is applied to an infinite number of obliquely inclined surfaces which, combined, describe a curved surface, Ramsay shows folding of curved surfaces can lead to significant variation in measured fold axis orientation, with fold axis distribution depending on mechanism of folding and the degree of curvature of the surface.

Passive folding describes development of a fold shape in layering during which the layering itself takes no active part. Hence, during the layer-parallel shortening, no buckling of the layers is initiated. The layering simply passively changes from an initial shape to a final shape resembling a fold. Passive folds have a characteristic geometry (Fig. 58), classifying as a Class 2, or similar, fold (see Ramsay, 1967, section 7-5). Passive folding can only occur in material in which layering has little or no competency contrast.

Many authors (e.g. Ramsay, 1967, Hudleston, 1977) describe the evolution of passive (or similar) folds in terms of flow lines. Flow lines are vector components that describe the direction and magnitude of displacement of particles in a layer being deformed

Figure 57. Illustration of the effect of pre-fold curved surfaces on the orientation of the folded surfaces and the fold axis (from Ramsay, 1967, pp. 492-96).

A. Two planes A and B intersecting in the direction l_0 and with dihedral angle ∂_0.

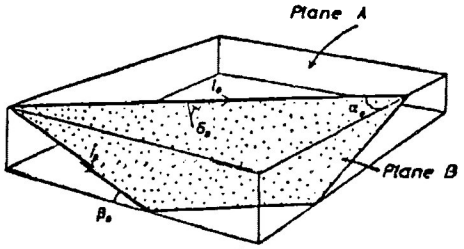

B. The two planes are deformed by flexural slip into fold forms. Plane A is cylindrically folded about an axis f_A. Plane B is folded into a curved surface with a range of intersection directions (l') and dihedral angles (∂') with plane A.

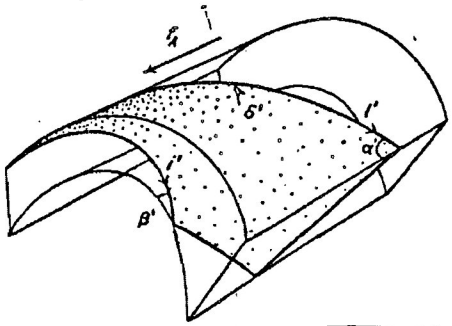

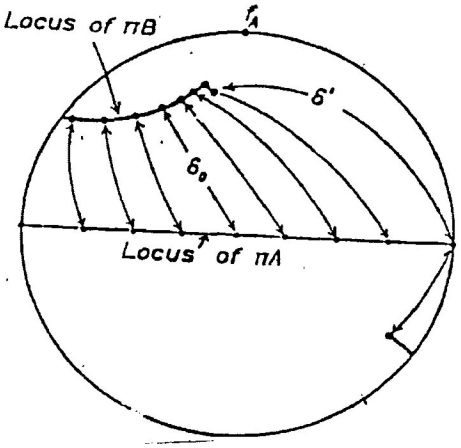

C. Stereographic projection showing the locus of directions of poles to plane A (πA) and poles to plane B (πB). πA directions define a great circle distribution perpendicular to f_A, but the locus of πB define a complex relationship.

When an infinite set of planes, defining a curved surface, is considered, a very complex range of π-pole directions will result. The range and distribution are dependent on mechanism of folding, and on the degree of original curvature of the curved surface.

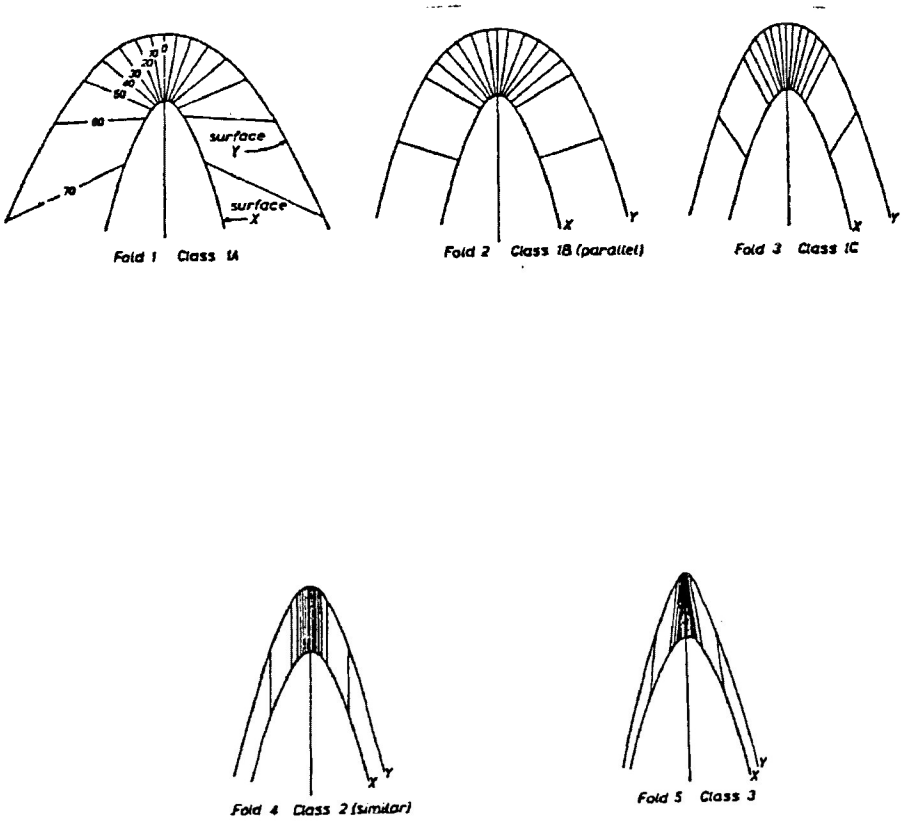

Figure 58. Fundamental classification of folds from inter-relationship of dip isogons. Dip isogons are lines that join points of equal slope on the upper and lower curved surfaces. Class 2 (similar) folds have parallel dip isogons. The upper and lower surfaces have the same change of curvature throughout the fold. The distance from lower to upper curved surface in the direction parallel to the axial trace is equal throughout the fold.
(from Ramsay, 1967, section 7-5).

Hudleston(1977) describes the development of sub-similar folds at the base of a glacier as the result of the deflection of flow lines from a steady-state condition. At the base of the glaciers, conditions of quasi-simple shear prevail, with flow lines parallel to the shear direction. Banding within the glaciers develops parallel to flow lines. As long as homogeneous strain and steady state conditions prevail, the banding will develop no folds. When the glaciers over-ride an obstacle, such as a rock ridge, an instability is initiated, causing a departure from steady state conditions and a deviation of flow lines from parallelism with the banding. In turn, the bands deform into recumbent sub-similar folds. The folds also have strongly curved fold axes, with the axes displaying a tendency to orient subparallel to the glacier transport direction.

Another theoretical mechanism for developing similar folds, involving the tranmission of differential shear into passive layers from an underlying formation, is described by Ramsay(1967, pp.309-27).

The initiation of instability in layering, causing buckling, is the crucial phase which distinguishes a passive fold from a buckle fold, but buckling is only one phase in the development of a buckle fold. In fact, the deformation processes of the phases before and after buckling can be very simialr to the processes which can develop a passive fold. Many buckle folds modified by subsequent homogeneous deformation, can very closely approach the passive fold shape(see, e.g., Dieterich, 1970). Such folds can also be non-cylindrical.

Sheath fold has recently come into relatively common usage to describe non-cylindrical folds with strongly curvilinear fold axes, formed during a single phase of deformation(Carreras et. al, 1977, Minnigh, 1979; Quinquis et. al., 1978, Henderson, 1981, Lacassin and

Mattauer, 1985). Observations of sheath folds in natural and experimental settings have indicated that, with progressive development of a sheath fold (Fig. 59A), the nose region becomes progressively smaller while the sheath limbs become correspondingly larger, by transposition. As such, most fold axes will be oriented in a direction parallel to the regional elongation. However, during a single deformation phase, several generations of sheaths may be present (Fig. 59A, folds 1, 2, 3 and 4) in various stages of development. Areas of sheath fold development tend to have a wide variation of fold axis orientation. Where the nose of a sheath fold is exposed, it may possess a distinctive "eye fold" structure in outcrop (see, e.g., Lacassin and Mattauer, 1985, Fig. 2). However, nose regions, because of their areal extent, are only rarely exposed, and the eye fold structure is only readily recognized where the exposed surface is approximately perpendicular to the central axis of the nose (Fig. 59B). Henderson(1981) notes that, generally, isoclinal sheath folds will resemble cylindrical folds in most sections.

Most sheath folds described to date are associated with environments of extensive, progressive shear, such as in thrust and fold nappes (Quinquis et. al., 1978; Henderson, 1981,, Lacassin and Mattauer, 1985) and in mylonite zones (Carreras et. al., 1977). Cobbold and Quinquis (1980) produced sheath folds in simple shear experiments. Three experimental models all developed strongly non-cylindrical sheath folds. The mechanisms proposed by the authors for development of these sheath folds are very similar to those described by Hudleston(1977) for development of the non-cylindrical, sub-similar folds at the base of glaciers.

The major F_1 folds of the Quetico metasedimentary rocks can be

Figure 59. Form and development of sheath folds.

A. A model for the development and growth of sheath and non-cylindrical folds in an environment of progressive simple shear (from Quinquis et. al., 1978).

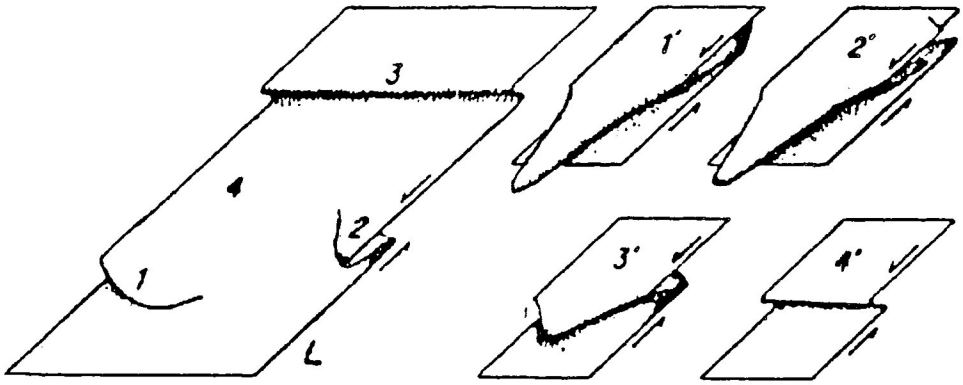

In the early stages of development, a simple shear environment produces cylindrical (3), non-cylindrical (1) and sheath (2) folds in one stage. With progressive shear, new folds develop (4'), cylindrical folds become non-cylindrical (3 to 3'), non-cylindrical folds become sheath folds (1 to 1') and sheath folds become modified to a more highly non-cylindrical form (2 to 2').

The model shows how folds of differing degrees of non-cylindricity can form both from one stage of deformation and from the progressive propagation and modification of different generations of folds.

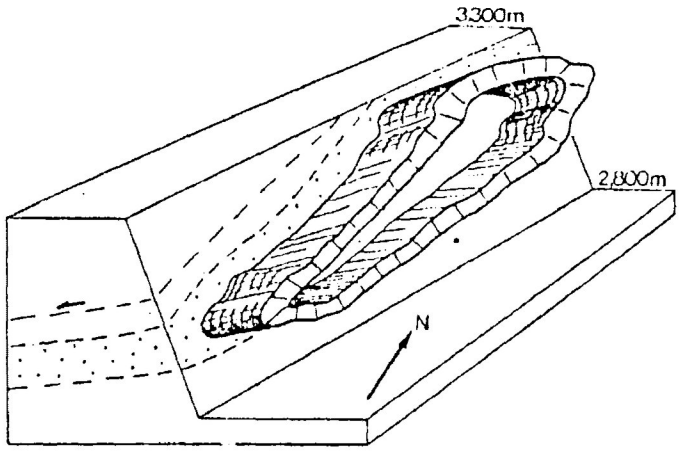

B. Schematic illustration of an "eye fold" structure in metasedimentary rocks in the Monte Rosa nappe, near Mattmark, Swiss Alps (from Lacassin and Mattauer, 1985).

described as sheath-like. The wide variation in S_0/S_1 intersection lineation directions, and in structural facing direction, indicate that the folds are strongly non-cylindrical. Also, the folds have narrow hinge zones with small volumes relative to the fold limbs. The asymmetric nature of the F_1 folds is also a characteristic of sheath folds.

Does the presence of these sheath-like major F_1 folds indicate that an environment of progressive simple shear existed during deformation of the Quetico metasedimentary rocks? Certainly, the existence of the Quetico fault zone at the interface of the Quetico and Wabigoon subprovinces is evidence that the area was subjected to shear displacement, albeit much later. The Quetico fault is a major transcurrent fault with predominantly dextral displacement(see, e.g., Kennedy, 1984).En echelon folds are relatively common features in wrench fault environments (see, e.g., Hobbs et. al., 1976, section 9.4). The structural association of wrench faults and en echelon folds, in fact, has been cited as evidence of compressional strike-slip movement, or "transpression" (Harland, 1971; Lowell, 1972).

However, the Quetico fault is a discrete, and in places a very narrow, zone. It is also a much later tectonic structure, certainly much younger than the major F_1 folds of the Quetico metasedimentary rocks, perhaps initiated during the late Archean (Schwerdtner et. al., 1979). Nevertheless, one cannot rule out the possible presence of precursor motions to the Quetico fault. A proto-Quetico progressive shear environment at the Quetico-Wabigoon interface could not only have affected a wider area, but could have been of a more ductile character than the subsequent Quetico fault zone. Indeed, within the Quetico fault zone itself, Kennedy(1984) observed a transition from

predominantly ductile deformation to brittle deformation occurred during the time the fault was active, though this possibly indicates exhumation of the fault rocks. Harris(1974) observed an abrupt change from migmatites to fault rocks with decreasing distance from the fault zone. In the present study area, the brecciated fragments of sandstone with well-developed S_1 cleavage surfaces (at sample location P26, see Fig. 6) is evidence of a late-stage, brittle deformation phase in the Quetico metasedimentary rocks.

It is proposed, then, that during deformation of the Quetico metasedimentary rocks, the (present) Quetico subprovince was in motion relative to the adjacent (present) Wabigoon subprovince. The motion created a wide progressive ductile shear environment within the rocks which comprised the present study area, leading to development of a series of en echelon, asymmetric sheath folds. The orientation of the en echelon folds relative to the Quetico-Wabigoon interface suggests displacement was dextral. However, the high grade of metamorphism of rocks in the central axis of the Quetico subprovince(paragneisses, migmatites), as compared to the typical lower greenschist assemblages of the Wabigoon subprovince,also suggests a vertical component of displacement. It is proposed that the Quetico subprovince moved up and right-laterally relative to the Wabigoon subprovince during this deformational episode, based of the geometry of the folds examined.

Evidence for regional "transpression" at Archean belt boundaries of the Canadian Shield has recently grown. Hudleston et. al.(1987) have proposed dextral transpression at the Quetico-Shebandowan belt boundary west of Lake Superior (see Fig. 1). The authors have identified "eye fold" structures" and delineated sheath folds in this area.

The structure of the present study area may also represent a period of transpressional tectonics and synchronous vertical displacement (Fig. 60). The relative motion of the north and south subprovinces, with both vertical and horizontal displacement, is indicated by the en echelon arrangement of asymmetric folds, and by the disparity of metamorphic grades between the two subprovinces.(Perhaps the wide variation of k_{max} and k_{int} directions in the Quetico rocks is symptomatic of a contemporaneous vertical- and horizontal-motion tectonic environment) A NNW-directed crustal shortening is indicated by the pervasive planar tectonic fabric, the tight to isoclinal folding and the flat-shaped MS ellipsoids of the Quetico metasedimentary rocks.

The deformation may then have culminated in a fairly rapid transition to brittle-ductile and brittle, horizontal-motion deformation. The deformation is confined to discrete zones at a location of inherent structural weakness (the subprovince interface), evolving into the Quetico fault zone with prodominantly dextral horizontal displacement.

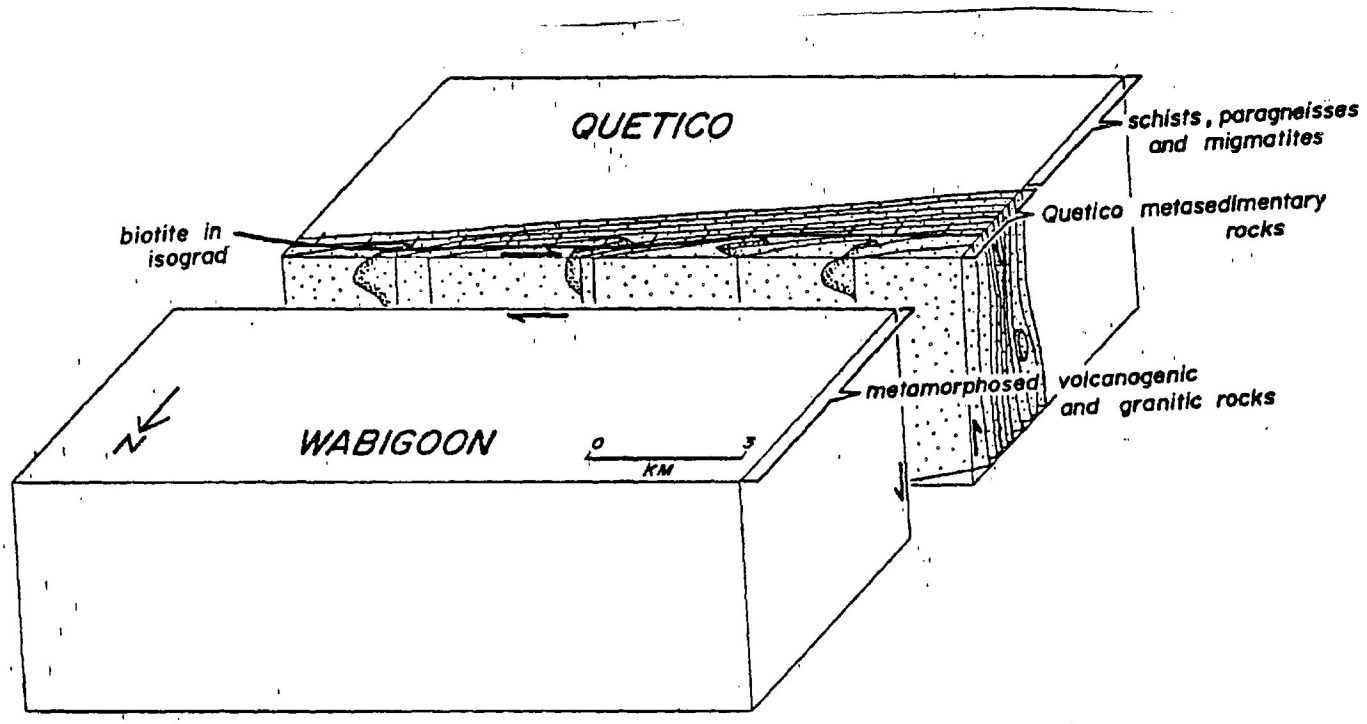

Figure 60. Three-dimensional sketch illustrating the proposed transpressional tectonic evolution of the Quetico-Wabigoon interface. North-south regional compression together with east-west dextral shear, led to the development of en echelon, tight to isoclinal; asymmetric sheath folds in the Quetico metasedimentary rocks. At the same time, vertical displacement at the interface (south side up) led to the exhumation of higher grade metamorphic rocks in the Quetico belt than in the Wabigoon belt.

CHAPTER SEVEN
SUMMARY

The present study of the Quetico metasedimentary rocks in the Calm Lake - Perch Lake area has yielded the following observations and conclusions:

General

1. The Quetico metasedimentary rocks are comprised of a repetative interstratification of the metamorphosed equivalents of sandstones and mudstones. Sandstones are predominantly matrix - rich lithic subarkoses and subarkoses.

2. The sedimentary association of repetatively interlayered, laterally continuous sandstone - mudstone beds, along with deeper water primary sedimentary structures, suggests the Quetico metasedimentary rocks comprise a turbidite sequence.

3. The east and west parts of the study area are characterized by ABE, ABDE and BDE turbidites, interpreted as part of the lower submarine fan depositional environment. The central part of the study area is characterized by ABE, BCE and AE turbidites, with an increase in both proportion and thickness of the A horizon. These are interpreted as representing the mid fan region of a submarine fan.

4. Metamorphic grade increases progressively from north to south in the present study area. Stable metamorphic mineral assemblages in order of increasing metamorphism are:

Chlorite - muscovite

Chlorite - muscovite - epidote (- sphene)

Chlorite - muscovite - biotite - epidote (- sphene)

Biotite - chlorite - muscovite - epidote (- sphene)

Metamorphic isograds are approximately east - west, subparallel to regional structural trend. All rocks in the present study area are within lower greenschist facies metamorphism.

Magnetic Fabric

5. The Quetico metasedimentary rocks have a polymineralllic magnetic mineralogy, comprising a ferrimagnetic component and a paramagnetic component. The ferrimagnetic component consists predominantly of magnetite and pyrrhotite. The paramagnetic component consists of chlorite, biotite and muscovite. Though less than two weight percent of the rock, the ferrimagnetic component appears to nevertheless dominate the bulk magnetic susceptibility of most rocks. The paramagnetic component, however, can also contribute significantly to the bulk magnetic susceptibility of some rocks, and, because individual phyllosilicates generally have a high degree of MSA, may contribute very significantly of the MSA of most rocks.

6. The rocks possess a predominantly tectonic magnetic fabric. The minimum magnetic susceptibility direction is consistently perpendicular to the dominant regional planar tectonic fabric (the S_1 cleavage planes) and intermediate and maximum magnetic susceptibility directions are contained within this planar fabric. The tectonic magnetic fabric has two components: The deformational magnetic fabric is described by ferrimagnetic minerals realigned by deformation mechanisms into preferred directions relative to finite strain directions. The metamorphic magnetic fabric evolved from the syntectonic preferred crystallographic growth of the metamorphic

phyllosilocates.

7. In some rocks, a depositional magnetic fabric is partially preserved. These rocks are coarse-grained sandstones with wide-spaced cleavage planes at the base of graded beds with refracted cleavage. It is probable that the depositional magnetic fabric is preserved in relatively undeformed microlithons between the spaced cleavage planes. Hence, massive sandstones and rocks with wide-spaced cleavage planes may also preserve a component depositional magnetic fabric.

8. The magnetic fabric of the Quetico metasedimentary rocks is a combination of deformational, metamorphic and depositional magnetic fabrics. The depositional magnetic fabric is always subordinate and, in most cases, so weak as to have no detectable influence on the rock's MSA.

9. Orientations of ferrimagnetic minerals are generally controlled by deformational processes, but the orientations of paramagnetic minerals are controlled principally by metamorphic processes, so the principal magnetic directions of the metamorphic paramagnetic fabric need not coincide with principal finite strain directions. Since the magnetic fabric of most rocks has a significant metamorphic component, it follows that the principal magnetic susceptibility directions of the rock's MSA cannot be considered reliable indicators of principal finite strain directions, although minimum susceptibility directions probably correspond to minimum finite strain directions. Great care must be taken in interpreting the significance of principal magnetic susceptibility directions.

Structural Geology

10. The Quetico rocks of the present study area possess a single,

pervasive penetrative cleavage. Observation of this cleavage on an outcrop scale and in thin section fail to show any evidence of a pre-existing deformational fabric even though the rocks are at a low degree of recrystallization; hence the cleavage is designated S_1.

11. The S_1 cleavage surfaces are axial planar to major F_1 folds.

12. The major F_1 folds are tight to isoclinal, asymmetric *sheath* folds. The strongly non-cylindrical (i.e. sheath) folds are arranged en echelon, slightly oblique to the dominant east-west structural trend. The asymmetric folds are separated from each other by approximately three to four kilometers along strike of the dominant structural trend.

13. Both the S_0 bedding and S_1 cleavage planes are displaced along conjugate sets of kink bands and brittle-ductile shear zones, oriented at approximately 035 - 90 and 120 - 90, displaying right-lateral and left-lateral displacements, respectively. These S_2 surfaces are local, discontinuous structural features with an insignifacant effect on the S_1 and F_1 structures. Displacement along S_2 surfaces rarely exceeds 10 centimeters.

14. Two deformational episodes are defined within the present study area:

The D_1 episode is characterized by the development of the pervasive penetrative S_1 cleavage and the major F_1 folds with a dominant east-west structural trend. Very local late-stage brittle deformation, forming dicrete, discontinuous brecciation zones, ended this episode.

The D2 episode is characterized by the development of the

conjugate set of minor, irregularily-spaced, discontinuous kink bands and brittle-ductile shear zones.

15. From the nature of the F_1 sheath folds, it is proposed that the Quetico metasedimentary rocks of the present study area experienced a regional dextral transpressional tectonic evolution. North-south regional shortening together with east-west regional dextral shear may have led to the development of the en echelon, tight to isoclinal, asymmetric F_1 sheath folds. This may have been accompanied by vertical displacement (south side up) at the Quetico - Wabigoon subprovince interface, causing the exhumation of higher grade metamorphic rocks in the Quetico belt than in the Wabigoon belt.

APPENDIX A

OPERATING PRINCIPLE AND SENSITIVITY OF THE SAPPHIRE INSTRUMENTS SI-1 AMS UNIT.

A1-1. Introduction.

The Sapphire Instruments SI-1 AMS unit (Plate 12) is an instrument which is capable of measuring both the bulk magnetic susceptibility and anisotropy of magnetic susceptibility of rocks, minerals and other materials. It is designed to be used both in the laboratory and in the field. Basic components include:

1. A sensing coil of inner volume of 160 cm^3.
2. Digital circuitry capable of measuring inductance to seven significant digits.
3. Interface circuitry which enters the measured inductance into a Hewlett-Packard HP-41CV calculator.
4. The Hewlett-Packard HP-41CV calculator. This calculator serves as a microcomputer and functions as.

- a program operator, controlling such functions as inductance measuring time.
- a display for input and output data.
- a data storer.
- a data processor.
- a control for the measuring procedure, through PROMPTs to the operator.

A1-2. Operating Principle.

To measure the bulk magnetic susceptibility of a sample, the sample is first placed in the coil. A timed electrical current is passed through the coil, and the inductance within the coil is

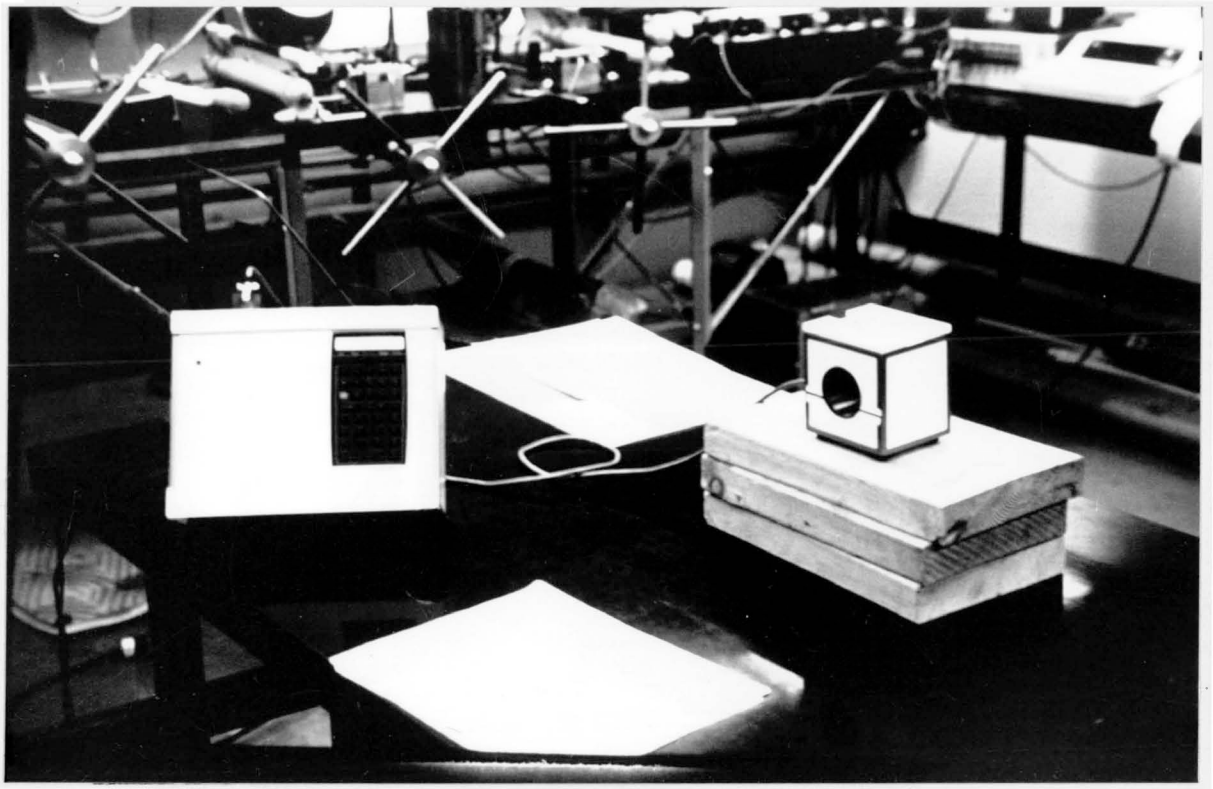

Plate Twelve. Sapphire Instruments SI-1 AMS unit. The instrument is capable of measuring both bulk magnetic susceptibility and anisotropy of magnetic susceptibility. Components include:

A. Sensing coil (160 cm3).
B. Hewlett-Packard HP-41CV calculator.
C. Interface circuitry.

measured and recorded. (The elapsed time of a generated electrical current in the coil is termed the measurement time. The SI-1 unit allows a choice of measurement times - two, four, six and eight seconds.)

Next, an air inductance reading is taken (that is, another timed electric current is passed through the coil with the coil empty), and the inductance within the coil is measured and recorded.

If the sample completely fills the sensing coil, the measured inductances can be related to magnetic susceptibility by the equation.

$$L_S/L_A = (\mu_0 + k_S) / (\mu_0 + k_A) \quad (1)$$

L_S and L_A are the inductances of the sample and air, respectively, μ_0 is the magnetic permeability of free space (12.57×10^{-7} henry/meter); k_S and k_A are the magnetic susceptibilities of the sample and air, respectively.

When the sample does not completely fill the coil, two factors relate the actual inductance due to the presence of the sample (L_S) to the measured inductance of the sample and air within the coil:

1. The fraction of volume of the coil occupied by the sample (C)
2. The position of the sample within the coil

While C can be easily calculated, the effect of the second factor is determined by comparing inductance of the sample to that of a standard of known susceptibility of similar volume and placed in the same position within the coil. A sample of MnO_2 of similar volume (magnetic susceptibility of 26.21×10^{-6} c.g.s./gram) is the standard

used. The comparison gives a calibration factor (CF). Incorporating the CF into equation (1) and reorganizing the equation:

$$k_S = \mu_0 CF((L_S/L_A) - 1) + k_A CF((L_S/L_A) - 1) + k_A$$

When the susceptibility is expressed in units of c.g.s., $\mu_0 = 1$, so:

$$k_S = CF((L_S/L_A) - 1) + CFk_A((L_S/L_A) - 1) + k_A \quad (2)$$

The term $CFk_A((L_S/L_A) - 1)$ is very small and can be considered zero. Air is considered weakly paramagnetic. The vessel holding the sample, on the other hand, is weakly diamagnetic, so k_A is also very small, and can also be considered zero. This reduces equation (2) to:

$$k_S = CF((L_S/L_A) - 1) \quad (3)$$

Because a coil calibration factor is necessary, each MS and AMS program requires inputting the volume of the sample before susceptibility values are calculated from inductance measurements.

A1-3. Sensitivity.

The sensitivity of the SI-1 AMS unit is, for the most part, dependent on three inter-related factors:

1. Electrical interference or "Noise".
2. Volume of the sample.
3. Measurement time.

Because the method of magnetic susceptibility measurement of the SI-1 unit involves comparison of a sample and an air reading, the sensitivity of the instrument will largely involve changes in external

conditions between the two readings, and between consecutive measurements. That is, the air reading is considered a "null" reading. Any two consecutive air readings should measure the same value of inductance in the coil. If the readings are not the same, the deviation is due to factors which change conditions within the sensing range of the coil. These external factors are collectively termed "noise".

In order to determine the sensitivity of the SI-1 unit at Lakehead University, an experiment was conducted involving different samples. The samples were:

1. PSR-10. Quetico metasandstone (volumes 10.55cm^3 and 4.45cm^3).
2. Carrara marble (volumes 10.55cm^3 and 4.45cm^3).
3. Manganese dioxide (volume 11cm^3).
4. DF-2. Artificially deformed cement-magnetite (volume 5cm^3).
5. Test Specimen No. 1 (volume 11cm^3). This is a cubical test sample supplied by the manufacturer.

Each of the samples were measured 20 separate times at measurement times of two, four and eight seconds. From the results, the mean susceptibility and standard deviation of each was determined.

In addition, "noise" measurements were determined by taking two consecutive air readings (rather than alternating sample and air readings). This, again, was repeated 20 times to determine a mean susceptibility and standard deviation. Three mean susceptibilities for "noise" are calculated for "mock" input volumes of 160cm^3, 10.55cm^3 and 4.45cm^3.

Table A1. The mean magnetic susceptibilities (k) and standard deviations (s.d.) of 20 measurements of bulk magnetic susceptibility for the selected samples of different volume (V) and for varying measurement times (T).

Sample	V (cm^3)	T (seconds)	k ($\times 10^{-6}$ c.g.s./cm^3)	±s.d. ($\times 10^{-6}$ c.g.s./cm^3)
"Noise"	160	2	0.020	0.030
	10.55	2	-0.016	0.386
	4.45	2	-0.223	0.903
	160	4	0.019	0.012
	10.55	4	0.196	0.208
	4.55	4	-0.055	0.581
	160	8	0.041	0.022
	10.55	8	0.205	0.098
	4.45	8	0.468	0.302
Carrara marble	10.55	2	-2.127	0.360
	4.45	2	-3.077	0.733
	10.55	4	-2.064	0.236
	4.45	4	-3.782	0.430
	10.55	8	-2.107	0.236
	4.45	8	-3.782	0.430
Quetico meta-sandstone	10.55	2	62.10	0.424
	4.45	2	67.55	0.756
	10.55	4	62.47	0.315
	4.45	4	67.20	0.524
	10.55	8	62.13	0.296
	4.45	8	67.03	0.756
MnO_2	10.55	2	53.44	1.237
	10.55	4	52.91	0.228
	10.55	8	52.30	0.480
Cement-magnetite mixture	5.00	2	2413	0.703
	5.00	4	2413	0.818
	5.00	8	2412	0.459
Test specimen	10.55	2	79270	19.19
	10.55	4	79160	39.80

Results of the experiment are presented in Table A1.

A measure of sensitivity is represented by the standard deviation of each set of measurements for each sample. Standard deviation, from sample to sample, displays a very wide range (from 4×10^{-5} c.g.s./cm^3 to 1×10^{-8} c.g.s./cm^3). It is apparent that the effects of noise, sample volume and measurement time must all be considered to understand better the anticipated sensitivity of the instrument for a given sample.

Figure A1-1 presents the mean susceptibility and standard deviation of selected samples against volume. Filling the coil volume completely with a large ($160cm^3$) sample will allow a more accurate measurement of susceptibility because it reduces the effect of external noise from that fraction of coil sensing range not displaced by the sample.

It is apparent, however, from Figure A1-1(a), that the magnitude of noise is affected by factors other than sample volume. Data in Figure A1-1(a) are measurements purely of noise (no sample in the coil). The only difference in parameters between the three measurements is the "mock" volumes input into the program to determine magnetic susceptibility. And yet, standard deviation increases from 1×10^{-8}c.g.s./cm^3 for a volume of $160cm^3$ to 6×10^{-6} c.g.s./cm^3 for a volume of $4.45cm^3$.

The same trend is displayed in the Carrara marble samples (Fig. A1-1(b)). For a four second measurement time, standard deviation is 2.4×10^{-7}c.g.s./cm^3 for a $10.55cm^3$ sample, and nearly doubles to 4.3×10^{-7} c.g.s./cm^3 for a $4.45cm^3$ sample.

Again, standard deviation for the Quetico metasandstone increases

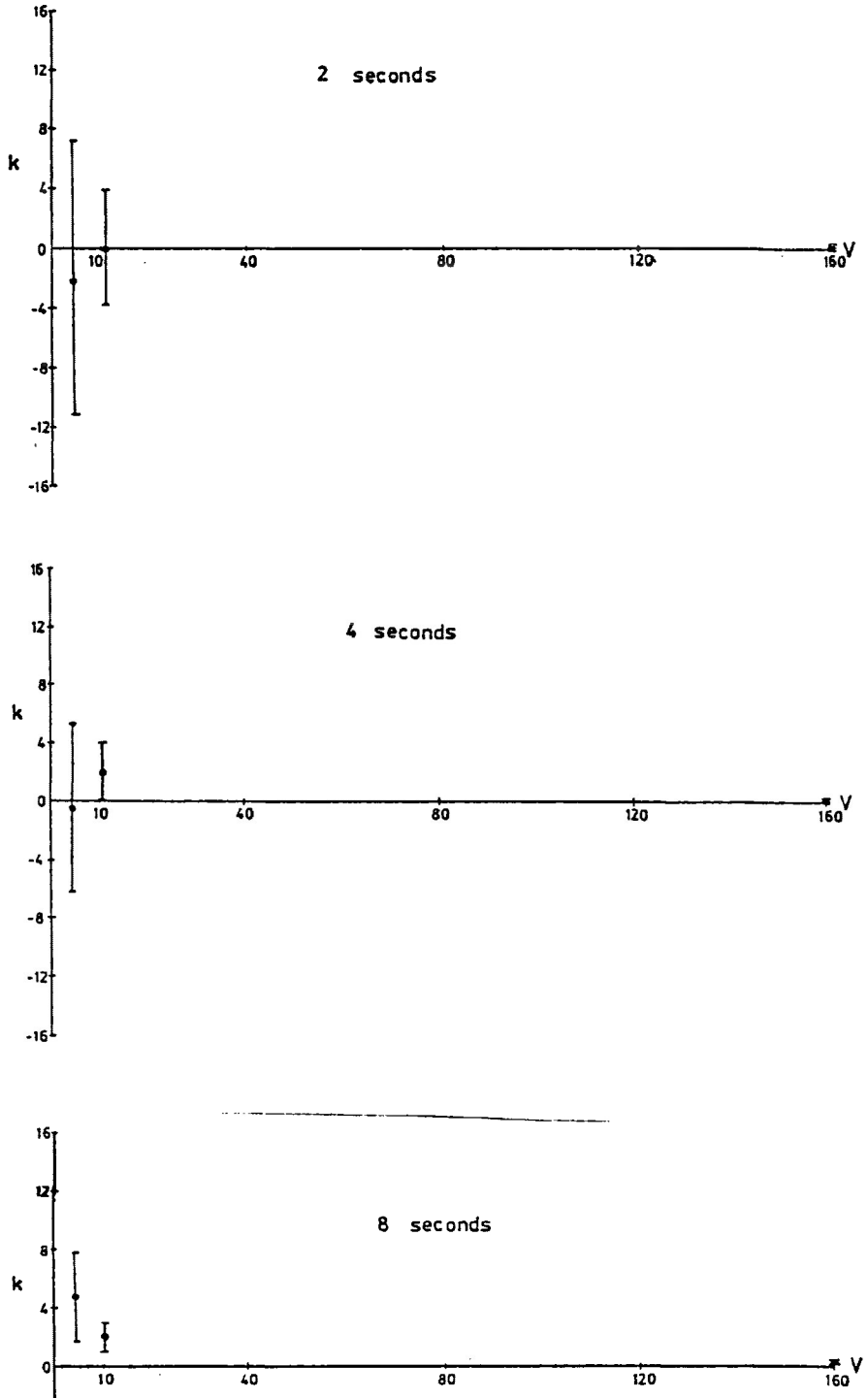

Figure A1-1(a). Mean magnetic susceptilility of 20 measurements (k) (with standard deviation bars) against "sample volume"(see text) for background "noise" measurements of the SI-1 unit. K is in $((c.g.s./cm^3)x10^{-7})$ units. V in cubic centimeters. The standard deviation of the magnetic susceptibility measurement is much less for the larger "sample volume" than for the smaller "sample volumes" even though no actual sample has been measured. See text for further discussion.

2, 4, and 8 seconds refer to the measurement times.

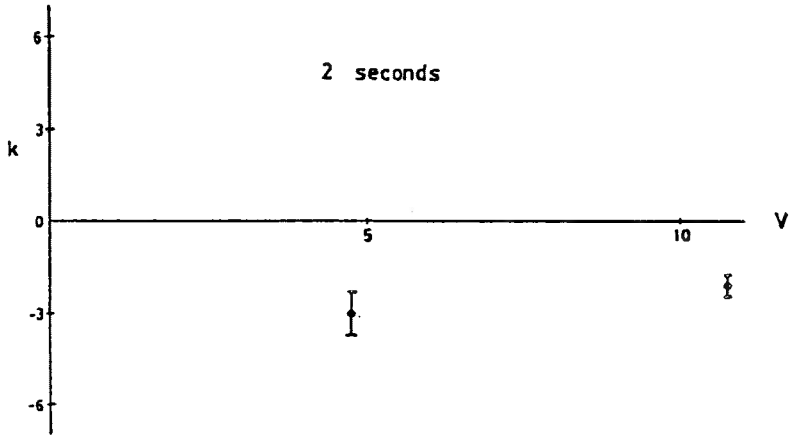

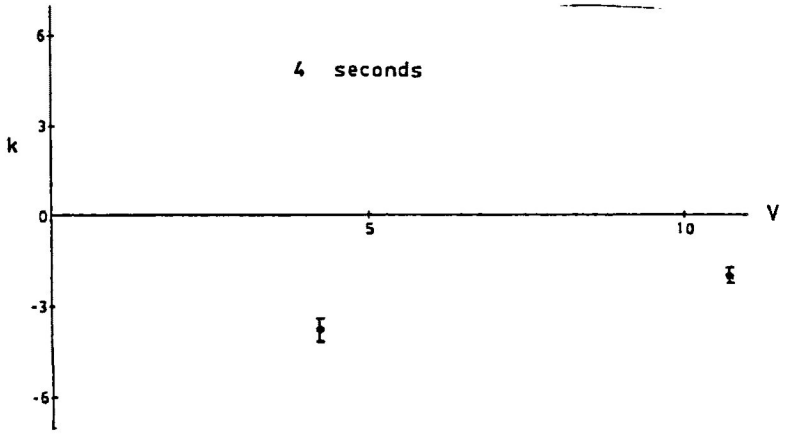

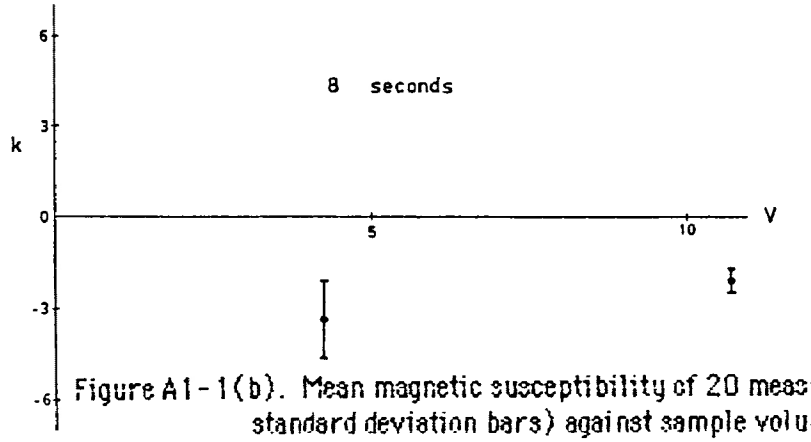

Figure A1-1(b). Mean magnetic susceptibility of 20 measurements (k) (with standard deviation bars) against sample volume (V) for Carrara marble specimens. Again, the standard deviation of the measured magnetic susceptibility in the larger samples is less than that in the smaller samples. See text for further discussion.

k in $((c.g.s./cm^3)\times10^{-6})$ units. V in cubic centimeters.

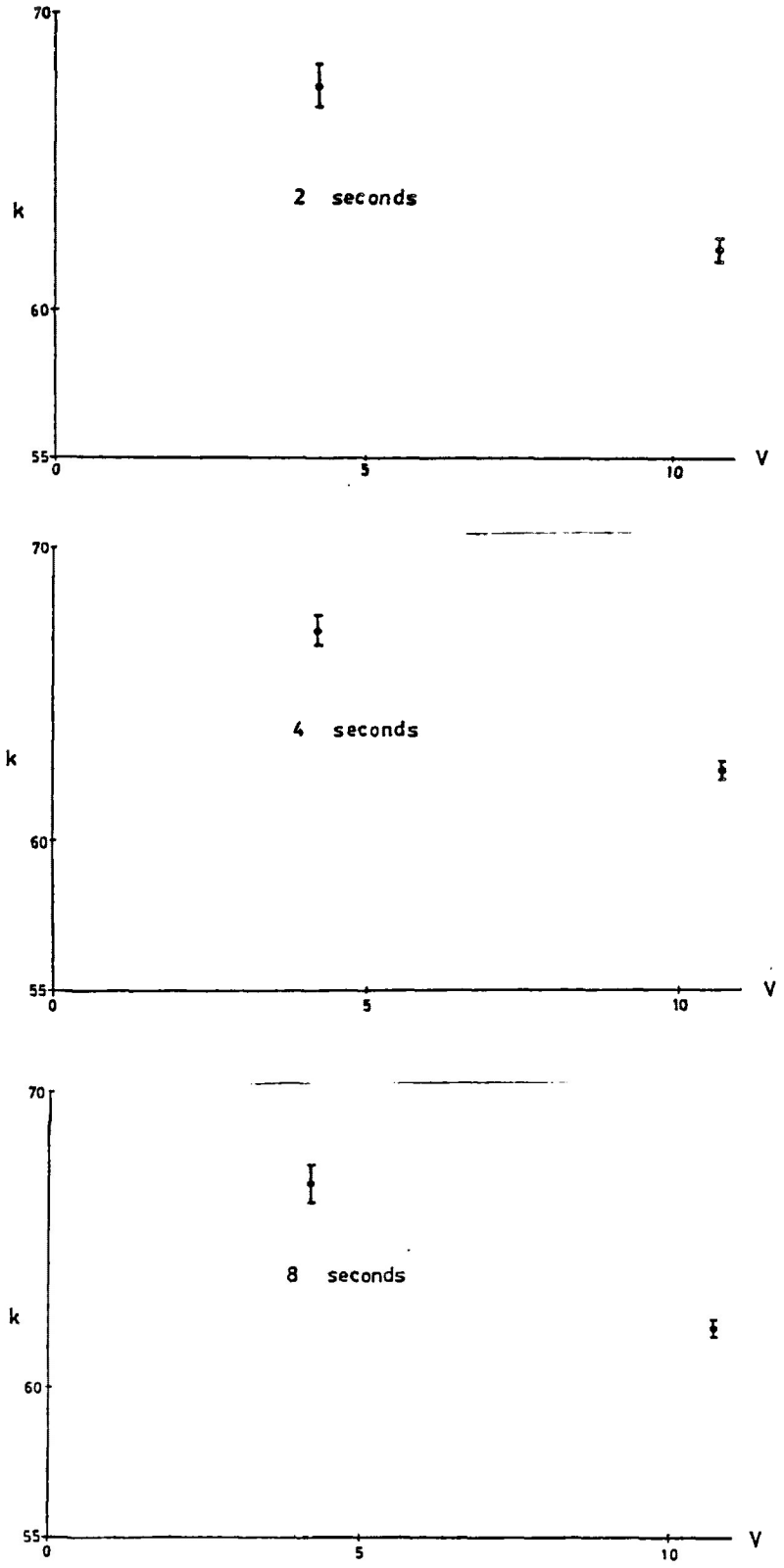

Figure A1-1(c). Mean magnetic susceptibility (k) of 20 measurements (with standard deviation bars) against sample volume (V) for Quetico metasandstone specimens. Once again, the standard deviation of the measured magnetic susceptibility is less in the larger sample. See text for further discussion.

k in $((c.g.s./cm^3)\times 10^{-6})$ units. V in cubic centimeters.

from 3×10^{-7}c.g.s./cm^3 for a 10.55cm^3 sample to 5×10^{-7}c.g.s./cm^3 for a 4.45cm^3 sample (Fig. A1-1(c)).

The difference relates back to equation (3):

$$k_S = CF((L_S/L_A) - 1)$$

As explained previously, the coil calibration factor, CF, is required to determine the actual contribution of the sample to change in inductance when the sample does not completely fill the coil. It is apparent from Figure A1-1(a) that the coil calibration factor also has the effect of geometrically increasing the magnitude of the noise contribution to susceptibility, when inductance measurements are converted into susceptibility.

Thus, sample volume can affect instrument sensitivity in two ways:

1. A larger sample volume may displace potential sources of noise in the sensing range of the coil.
2. A larger sample volume will equate to a smaller calculated coil calibration factor, and the contribution of noise to calculated susceptibility will not be as exaggerated.

For a sample volume of 160cm^3 (the internal volume of the entire sensing coil) the standard deviation of a magnetic susceptibility measurement is in the range of 5×10^{-8}c.g.s./cm^3 for the SI-1 unit. For sample volumes near 11cm^3, standard deviation of a magnetic susceptibility measurement is in the range of 5×10^{-7}c.g.s./cm^3, while for volumes around 4cm^3, the standard deviation range is near 1×10^{-6}c.g.s./cm^3.

Figure A1-2 presents mean susceptibility and standard deviation

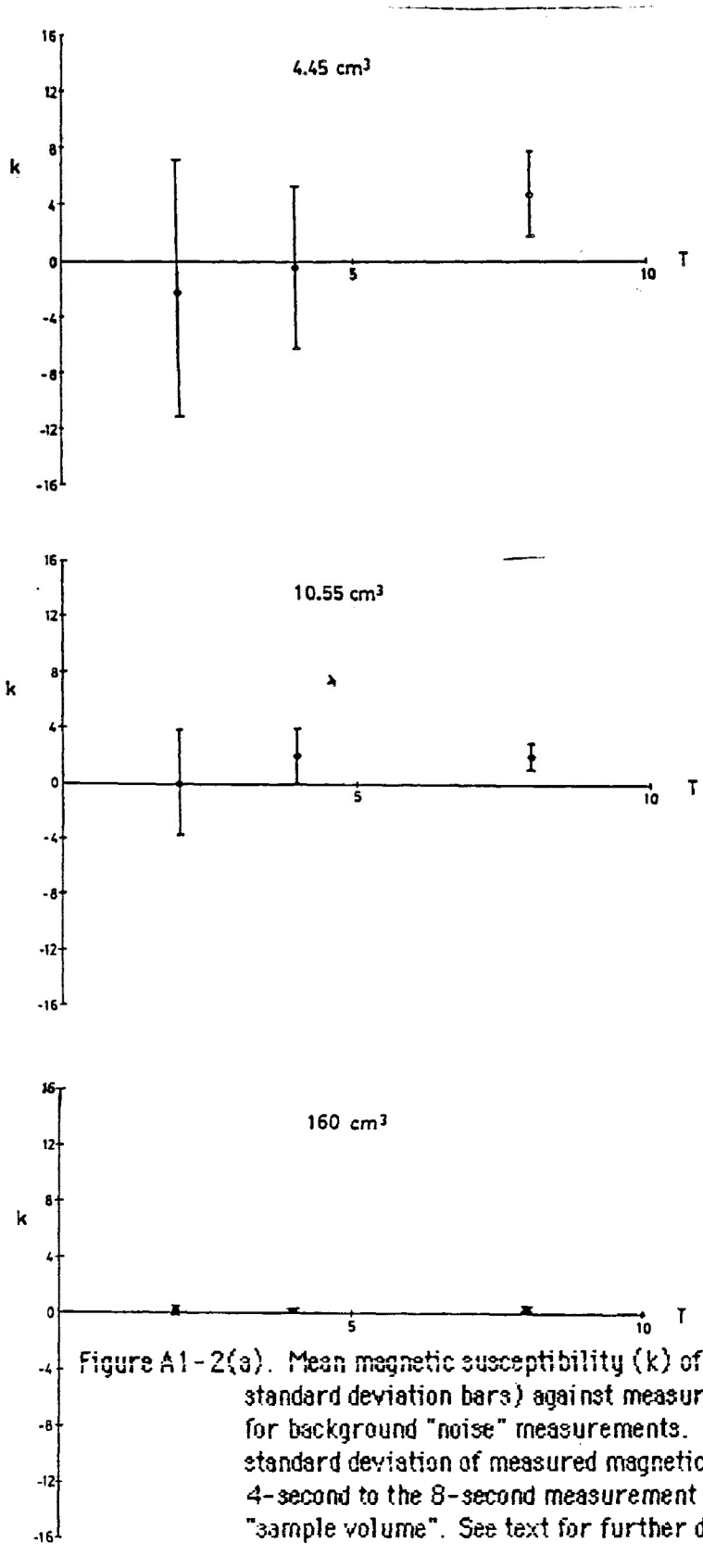

Figure A1-2(a). Mean magnetic susceptibility (k) of 20 measurements (with standard deviation bars) against measurement time (T - see text) for background "noise" measurements. Note the increase in standard deviation of measured magnetic susceptibility from the 4-second to the 8-second measurement time for the 160 cm^3 "sample volume". See text for further discussion.

k in ((c.g.s./cm^3($x10^{-7}$) units. T in seconds.

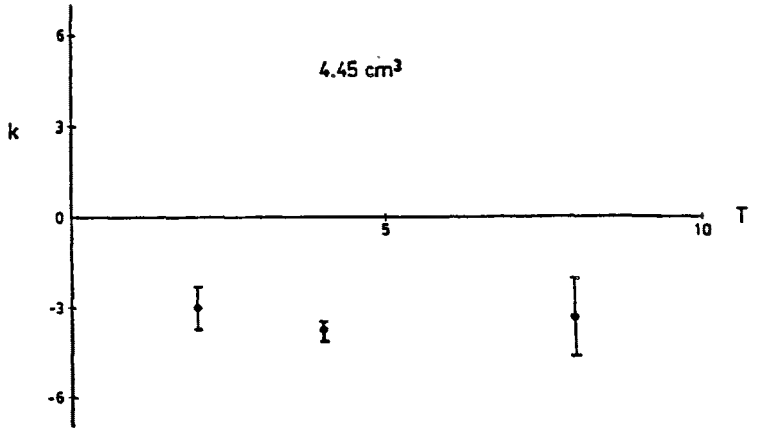

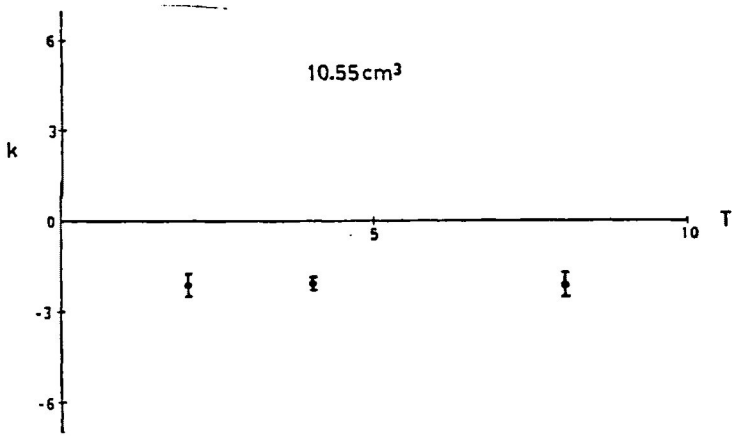

Figure A1-2(b). Mean magnetic susceptibility (k) of 20 measurements (with standard deviation bars) against measurement time (T) for Carrara marble specimens. For both sample volumes (4.45 cm^3 and 10.55 cm^3), the standard deviation of measured magnetic susceptibility is greater for the 8-second measurement time than for the 4-second measurement time. See text for further discussion.

k in $((c.g.s./cm^3)\times 10^{-6})$ units. T in seconds.

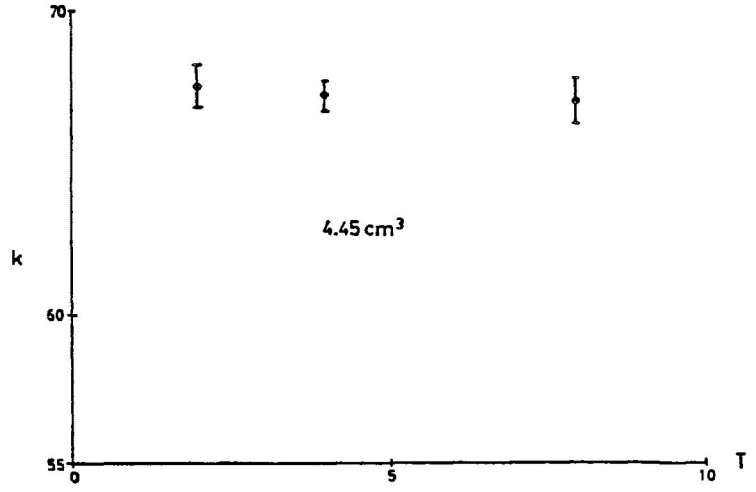

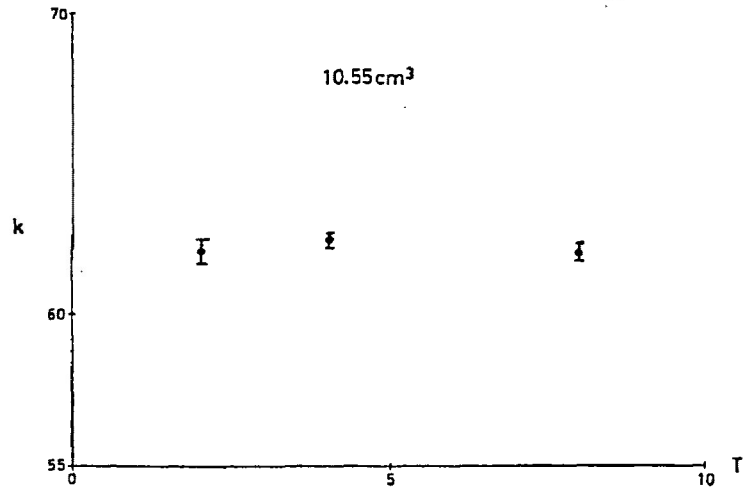

Figure A1-2(c). Mean magnetic susceptibility (k) of 20 measurements (with standard deviation bars) against measurement time (T) for Quetico metasandstone specimens. For both sample volumes, the standard deviation of measured magnetic susceptibility is greater for the 8-second measurement time than for the 4-second measurement time. See text for further discussion.

k in $((c.g.s./cm^3) \times 10^{-6})$ units. T in seconds.

against measurement time for the Carrara marble, Quetico metasandstone, MnO_2 and air readings. Differences in standard deviation define an interesting trend. For all samples, regardless of volume, a decrease in standard deviation is recorded when measurement time is changed from two seconds to four seconds. However, only the noise (air) readings for "mock" volumes of $4.45cm^3$ and $10.55cm^3$ show a decrease in standard deviation for an eight second measurement time when compared to four seconds. All other samples actually display an increase in standard deviation.

This increase may reflect short-term flucuations in noise levels. Figure A1-3 displays these flucuations as a series of pulses of varying amplitude. If these pulses have periods of eight seconds or greater, then higher noise levels may be expected for eight second measurement times than for four second measurement times.

It should be noted, however, that while the sensitivity range may be best for a four second measurement time, precision of measured susceptibility may still be improved by using an eight second interval (depending upon magnitude of bulk susceptibility).

A1-4. Precision of SI-1 unit.

The SI-1 AMS unit measures inductance as a seven-digit number. Precision is related to the significance of these seven digits. As such, precision is affected by four factors:

1. Measurement time.

A larger measurement time allows a larger inductance to be measured in the coil. It would be expected that a more precise measurement of inductance is obtained from an eight second than

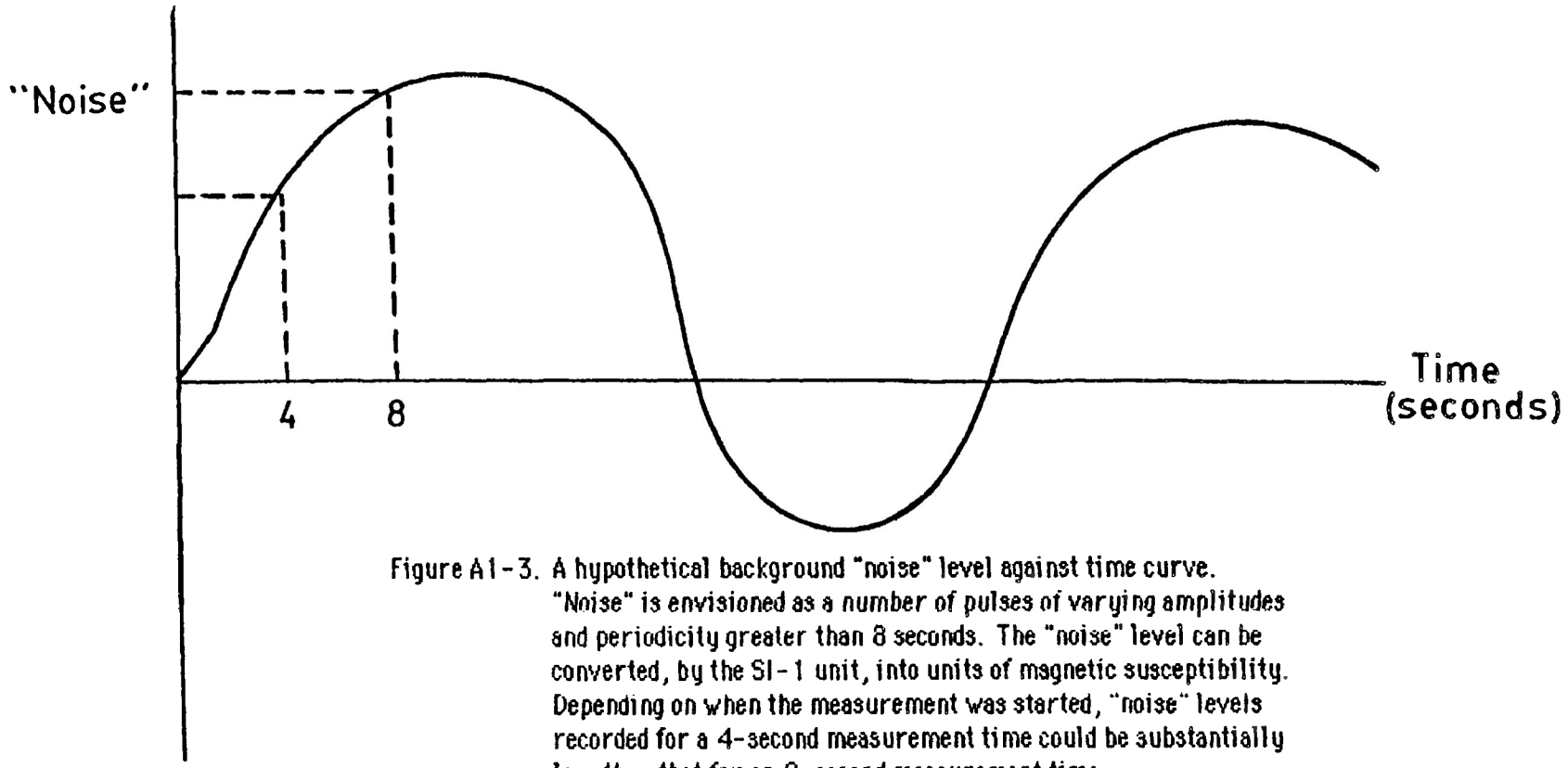

Figure A1-3. A hypothetical background "noise" level against time curve. "Noise" is envisioned as a number of pulses of varying amplitudes and periodicity greater than 8 seconds. The "noise" level can be converted, by the SI-1 unit, into units of magnetic susceptibility. Depending on when the measurement was started, "noise" levels recorded for a 4-second measurement time could be substantially less than that for an 8-second measurement time.

from a two second measurement time. This must be tempered, however, especially for materials with weak susceptibilities, with the possibility of greater contribution of noise and drift over longer measurement times (Fig. A1-3). Thus, the measurement may be more precise, but less accurate.

2. Volume of sample.

As discussed previously, the inductance measured in the coil will have a larger component attributable to the sample for a large sample than for a small sample of the same material. It follows that the magnitude of the measured inductance itself will be larger (inductance of air is near zero). Thus, a more precise inductance is measured when a sample fills most of the sensing coil.

3. Magnitude of susceptibility

Magnitude of bulk susceptibility is probably the most important factor in determining instrument precision. The maker, Sapphire Instruments (operating manual, 1983), states that susceptibility measurement precision exceeds five significant figures for samples with susceptibility in the range of 10^{-1} c.g.s./cm^3. The precision decreases to one significant figure for weakly paramagnetic or diamagnetic susceptibilies in the range of 10^{-6} c.g.s./cm^3.

4. Repeated measurements.

Precision of susceptibility can also be improved by taking replicate measurements. In this case, improvement of standard deviation is approximately proportional to the square root of the number of repeat measurements.

APPENDIX B

MSA AND MAGNETIC MINERALOGY DATA

Part One - magnitudes and orientations of the magnitude ellipsoids of susceptibility for each Quetico rock sample.

Explanation:

Sample No./orientation: Rock sample number (see Fig. 6, Fig. A2-1 and Fig. A2-2 for locations) / Strike and dip of the oriented surface of the sample (H = horizontal surface).

Minimum, Intermediate, Maximum: Minimum magnetic susceptibility, intermediate magnetic susceptibility, maximum magnetic susceptibility.

Dec: Declination of the principal magnetic susceptibility (in degrees Azimuth).

Inc: Inclination of the principal magnetic susceptibility (in degrees from horizontal). (Note. most principal magnetic susceptibility directions recorded on the data sheets are uncorrected. To correct principal susceptibility directions to the true orientations, see section 5-4).

EV: Magnitude of principal magnetic susceptibilities ($x10^{-6}$c.g.s./cm^3).

R95: Angular deviation of the principal magnetic susceptibility from an averaged direction (see Appendix A).

E95: Deviation of the magnitude of the principal magnetic susceptibility from an averaged magnitude ($x10^{-6}$c.g.s./cm^3) (see Appendix A).

T: Shape factor of the magnitude ellipsoid of susceptibility.

$$T = 2(n_2-n_1)/[(n_1-n_3)-1]$$ (see section 5-1)

P': Corrected degree of anisotropy of the magnitude ellipsoid of susceptibility

$$P' = \exp([2((n_1-n)^2+(n_2-n)^2+(n_3-n)^2)]$$ (see section 5-1)

Part Two - X-ray diffractographs for each of the separated magnetic fractions of Quetico rock samples PS4, S18 and R22.

VHM - very highly magnetic fraction
HM - highly magnetic fraction
MM - moderately magnetic fraction
WM - weakly magnetic fraction
VWM - very weakly magnetic fraction

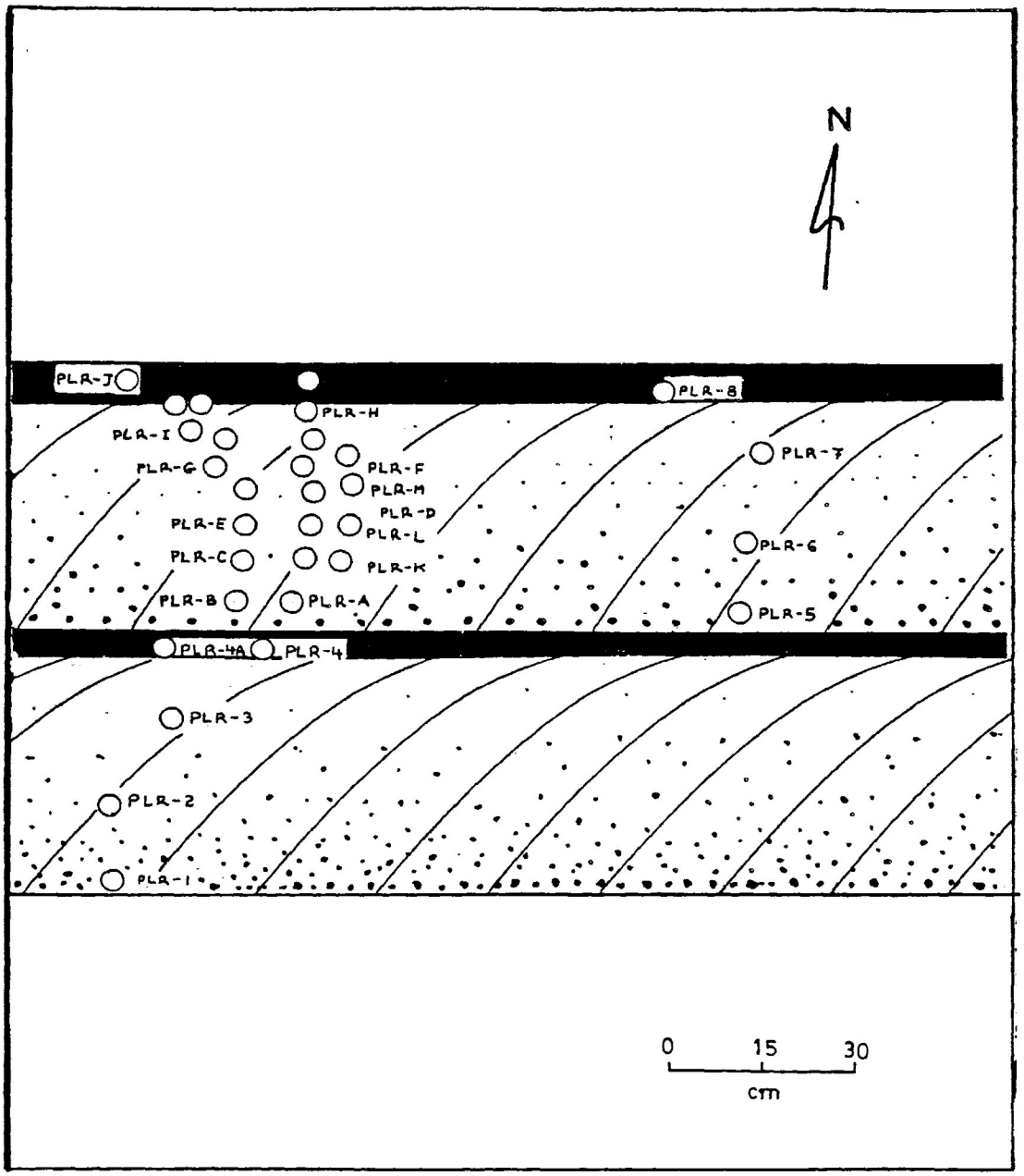

Figure A2-1. Sample locations of PLR samples from the graded arenite beds with refracted cleavage next to the Perch Lake cottage road(see Fig. 6 for the location of the PLR samples relative to the entire study area).

Figure A2-2. Sample locations of F1 samples from a major fold closure in interbedded arenite-argillite beds next to Highway 11 near Flanders (see Fig. 6 for location of F1 samples relative to the entire study area).

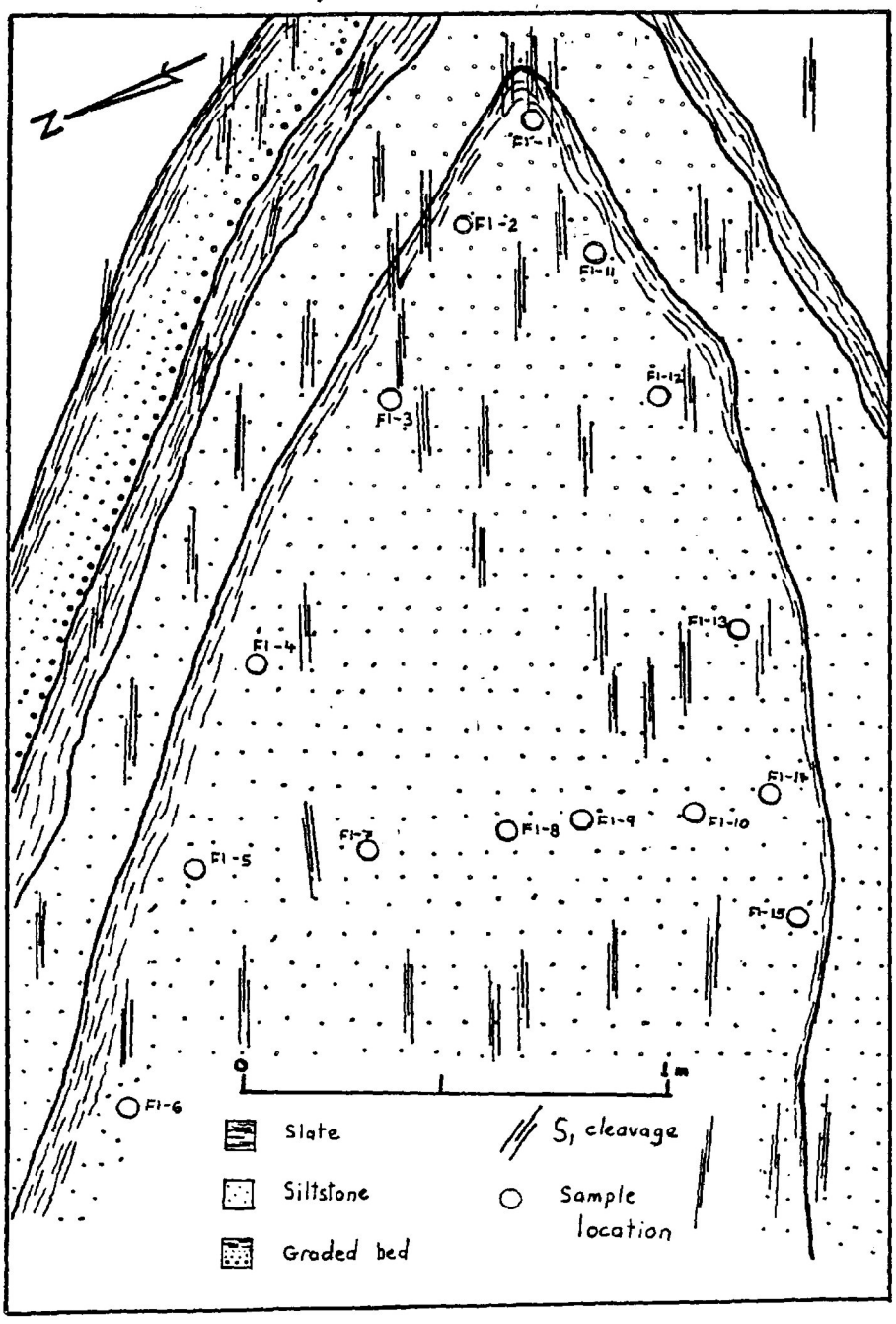

Figure A2-3. Sample locations of F2 samples from a minor asymmetric fold in interbedded arenite-argillite next to Highway 11 near Big Bend Lake(see Fig. 6 for location of F2 samples relative to the entire study area).

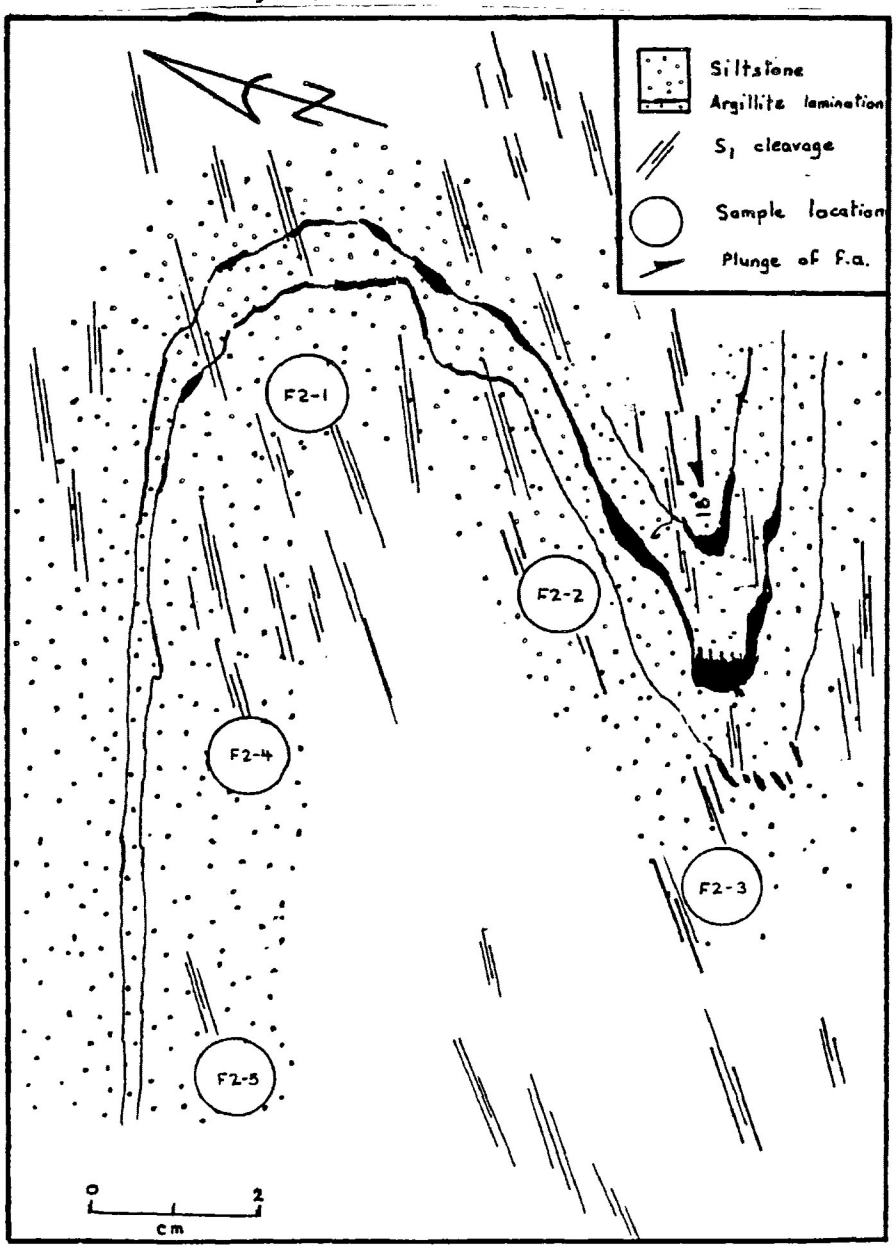

Sample No./	MINIMUM			INTERMEDIATE			MAXIMUM			FABRIC PARAMETERS	
Orientation	DEC	INC	EV	DEC	INC	EV	DEC	INC	EV	T	P'
B01/085-90	35.51	-76.30	28.78	305.70	0.05	33.56	35.71	13.70	34.96	+0.509	1.28
	R95	0.46	E95	0.14	R95	4.41	E95	0.73	R95	4.41	E95	0.78		
B02/280-64	53.36	-38.38	19.33	344.80	24.80	21.25	278.92	41.50	22.20	+0.37	1.15
	R95	4.40	E95	0.74	R95	4.19	E95	0.45	R95	4.44	E95	0.73		
B03/095-70	334.32	-58.06	19.70	30.95	18.93	21.66	291.88	24.71	22.13	+0.63	1.13
	R95	2.63	E95	0.305	R95	8.03	E95	0.23	R95	7.68	E95	0.66		
B04/136-60	301.36	-68.28	27.62	346.54	15.68	30.06	72.35	-14.65	30.67	+0.62	1.12
	R95	2.38	E95	0.49	R95	7.87	E95	0.45	R95	7.57	E95	0.83		
B05/074-88	22.62	-77.65	25.93	310.95	3.94	31.47	41.78	11.68	31.65	+0.94	1.25
	R95	1.40	E95	0.41	R95	2.83	E95	0.55	R95	3.08	E95	0.70		
B06/085-82	7.20	-63.93	20.14	286.48	4.59	21.42	25.83	18.87	21.54	+0.82	1.08
	R95	1.80	E95	0.22	R95	1.78	E95	0.08	R95	2.50	E95	0.23		
B07/088-88	344.96	-75.62	24.15	340.42	14.32	26.82	70.70	1.09	27.44	+0.64	1.15
	R95	4.27	E95	0.77	R95	8.48	E95	0.66	R95	7.33	E95	0.95		
B08/064-88	51.73	-78.64	34.47	358.29	6.83	38.29	89.38	9.04	45.10	-0.22	1.31
	R95	0.09	E95	0.10	R95	0.03	E95	0.11	R95	0.10	E95	0.05		
B09/081-83	35.25	61.28	54.74	358.80	-23.78	78.92	275.65	15.14	94.26	+0.35	1.74
	R95	0.58	E95	0.36	R95	0.61	E95	0.61	R95	0.32	E95	0.43		
B10/075-80	25.90	80.11	53.10	5.02	-9.25	85.79	275.59	3.46	114.76	+0.24	2.18
	R95	0.07	E95	0.34	R95	0.15	E95	0.54	R95	0.15	E95	0.31		

Sample No./ Orientation	MINIMUM			INTERMEDIATE			MAXIMUM			FABRIC PARAMETERS	
	DEC	INC	EV	DEC	INC	EV	DEC	INC	EV	T	P'
B11/080-90	22.52	65.38	24.69	60.34	-19.90	28.28	325.21	13.90	28.66	+0.71	1.21
	R95	2.34	E95	0.49	R95	24.31	E95	1.93	R95	24.35	E95	2.12		
B12/078-90	358.80	78.26	53.37	270.86	-0.43	100.39	0.95	-11.75	112.62	+0.69	2.24
	R95	0.02	E95	0.44	R95	0.04	E95	0.22	R95	0.06	E95	0.34		
B13/070-79	7.91	69.23	53.88	25.90	-19.84	82.67	293.76	-5.92	101.68	+0.35	1.23
	R95	0.19	E95	0.44	R95	1.35	E95	1.18	R95	1.34	E95	1.48		
B16/080-86	340.79	-79.45	26.41	58.61	2.26	31.21	329.19	10.31	31.51	+0.72	1.24
	R95	0.87	E95	0.25	R95	33.69	E95	0.27	R95	33.69	E95	0.27		
B17/092-85	33.19	-83.94	20.53	31.64	6.05	23.22	301.65	-0.17	23.77	+0.75	1.21
	R95	1.98	E95	0.42	R95	8.76	E95	0.70	R95	8.53	E95	0.86		
B18/068-78	331.08	-65.48	19.87	318.73	24.02	22.89	50.81	4.65	23.94	+0.52	1.22
	R95	2.45	E95	0.44	R95	2.50	E95	0.49	R95	0.72	E95	0.16		
B19/100-78	38.04	-74.75	15.01	62.15	14.00	16.62	330.65	6.00	18.04	0.0	1.23
	R95	1.52	E95	0.25	R95	7.62	E95	0.99	R95	7.64	E95	1.17		
B20/120-85	354.98	-80.77	17.65	67.62	2.78	21.20	337.19	8.81	21.67	+0.68	1.22
	R95	0.03	E95	0.33	R95	4.72	E95	0.27	R95	4.72	E95	0.49		
B21/100-88	31.26	-73.70	19.39	291.52	-2.83	23.02	20.70	16.04	23.43	+0.81	1.23
	R95	2.57	E95	0.40	R95	1.24	E95	0.23	R95	3.76	E95	0.63		
B22/116-82	18.86	-77.64	35.16	66.73	8.36	39.35	335.34	9.04	41.33	+0.39	1.18
	R95	0.20	E95	0.84	R95	2.46	E95	0.47	R95	2.45	E95	1.02		

Sample No./	MINIMUM			INTERMEDIATE			MAXIMUM			FABRIC PARAMETERS	
Orientation	DEC	INC	EV	DEC	INC	EV	DEC	INC	EV	T	P'
B23/092-90	48.12	87.06	21.36	270.72	2.16	25.49	0.70	-2.14	25.97	+0.81	1.24
	R95	0.12	E95 0.03	R95	0.38	E95 0.22	R95	0.39	E95 0.31		
B24/090-90	315.54	-88.52	24.15	338.03	1.36	32.59	68.02	-0.57	32.81	+0.90	1.44
	R95	0.04	E95 0.11	R95	47.51	E95 2.96	R95	47.51	E95 2.98		
B25/104-78	294.39	-83.51	19.98	317.30	5.98	23.81	47.04	-2.51	24.26	+0.81	1.24
	R95	0.18	E95 0.34	R95	13.96	E95 1.11	R95	13.96	E95 1.22		
B26/090-78	24.43	83.59	14.57	279.10	2.76	17.02	8.69	-5.70	17.11	+0.25	1.23
	R95	0.68	E95 0.20	R95	78.62	E95 3.14	R95	78.73	E95 3.18		
B27/089-89	279.63	-87.65	30.64	340.46	1.14	34.54	70.42	-2.05	36.55	+0.32	1.20
	R95	0.05	E95 0.03	R95	0.03	E95 0.12	R95	0.04	E95 0.11		
B28/092-87	55.70	86.77	52.06	288.96	1.94	97.31	18.87	-2.59	101.24	+0.88	2.11
	R95	0.02	E95 0.03	R95	2.57	E95 1.19	R95	2.57	E95 1.26		
B29/093-84	322.00	-84.41	22.12	310.08	5.29	35.32	40.25	1.80	37.54	+0.77	1.78
	R95	0.16	E95 0.20	R95	2.71	E95 0.58	R95	2.71	E95 0.63		
B30/093-86	291.66	-86.54	20.86	338.52	2.36	24.73	68.42	-2.52	25.17	+0.81	1.23
	R95	0.38	E95 0.07	R95	0.30	E95 0.34	R95	0.28	E95 0.34		
B32/085-82	32.32	82.01	20.56	8.31	-7.29	24.60	278.70	3.22	24.89	+0.88	1.24
	R95	0.43	E95 0.10	R95	0.49	E95 0.24	R95	0.35	E95 0.22		
B33/072-82	293.30	-79.21	49.81	322.15	8.11	61.23	55.50	-5.80	64.68	+0.58	1.32
	R95	1.00	E95 0.53	R95	7.34	E95 0.72	R95	3.09	E95 1.41		

Sample No. /	MINIMUM			INTERMEDIATE			MAXIMUM			FABRIC PARAMETERS	
Orientation	DEC	INC	EV	DEC	INC	EV	DEC	INC	EV	T	P'
B34/060-90	63.32	83.78	52.97	50.52	-6.07	88.98	320.67	1.37	102.84	+0.56	2.01
	R95	0.03	E95 0.33	R95	0.90	E95 0.76	R95	0.90	E95 0.84		
B35/095-84	24.70	83.37	32.57	331.77	-4.01	44.14	62.14	-5.28	48.86	+0.47	1.55
	R95	0.16	E95 0.06	R95	0.60	E95 0.14	R95	0.60	E95 0.39		
B37/068-62	16.15	-85.84	16.63	78.19	1.95	20.78	348.07	3.67	21.15	+0.86	1.31
	R95	0.34	E95 0.32	R95	9.04	E95 0.48	R95	9.04	E95 0.54		
B38/080-90	283.14	85.01	25.33	309.07	-4.60	35.55	38.91	1.94	35.99	+0.93	1.49
	R95	0.05	E95 0.11	R95	0.06	E95 0.04	R95	0.04	E95 0.04		
PS02/094-90	81.85	71.34	18.08	230.79	17.71	20.13	8.97	-5.68	20.82	+0.51	1.16
	R95	0.91	E95 0.19	R95	2.06	E95 0.31	R95	1.90	E95 0.47		
PS03/278-80	341.34	-55.94	34.06	346.19	33.98	40.48	74.67	-2.25	45.44	+0.20	1.34
	R95	0.88	E95 0.30	R95	1.35	E95 0.16	R95	1.14	E95 0.46		
PS04/262-85	234.92	-74.59	34.85	317.52	14.77	39.42	48.69	4.41	40.99	+0.52	1.18
	R95	0.46	E95 0.45	R95	2.21	E95 0.48	R95	2.16	E95 0.77		
PS05/080-78	11.96	56.09	28.97	350.38	-32.00	32.37	86.72	-10.02	33.31	+0.59	1.16
	R95	8.77	E95 2.10	R95	8.82	E95 2.42	R95	2.12	E95 8.16		
PS06/245-84	354.37	67.95	26.79	330.22	-20.27	32.00	63.31	-8.28	32.44	+0.87	1.24
	R95	3.24	E95 0.89	R95	24.99	E95 2.48	R95	24.87	E95 2.82		
PS01/264-85	327.66	-78.27	44.85	7.72	9.03	68.88	276.54	7.42	81.34	+0.44	1.85
	R95	2.07	E95 0.08	R95	0.15	E95 0.10	R95	0.15	E95 0.25		

Sample No./	MINIMUM			INTERMEDIATE			MAXIMUM			FABRIC PARAMETERS	
Orientation	DEC	INC	EV	DEC	INC	EV	DEC	INC	EV	T	P'
S01/265-77	334.12	87.44	21.31	87.27	1.01	29.52	357.31	-2.35	31.41	+0.68	1.52
	R95	0.05	E95 0.11	R95	0.50	E95 0.21	R95	0.50	E95 0.15		
S02/268-76	311.06	83.69	19.06	62.17	2.28	22.37	332.41	-5.88	23.19	+0.64	1.23
	R95	0.69	E95 0.15	R95	0.33	E95 0.23	R95	0.63	E95 0.26		
S03/260-40	59.73	76.48	51.36	81.45	-12.59	89.14	350.37	-4.84	132.57	+0.16	2.59
	R95	0.54	E95 0.33	R95	0.65	E95 1.24	R95	0.37	E95 0.80		
S04/088-85	72.09	-27.21	9.49	62.69	62.48	10.04	340.10	-3.85	11.12	-0.30	1.17
	R95	3.65	E95 0.30	R95	4.13	E95 0.25	R95	4.75	E95 0.47		
S05/257-72	32.24	77.14	31.35	75.21	-9.49	46.18	343.76	-8.61	49.70	+0.68	1.64
	R95	0.27	E95 0.13	R95	1.26	E95 0.39	R95	1.28	E95 0.54		
S07/262-65	352.11	-77.98	35.69	78.88	0.69	43.39	348.73	12.00	47.99	+0.32	1.35
	R95	0.11	E95 0.33	R95	0.26	E95 0.07	R95	0.28	E95 0.25		
S08/074-55	63.79	-76.98	18.32	54.21	12.84	21.88	324.69	-2.09	22.75	+0.64	1.26
	R95	0.71	E95 0.10	R95	3.36	E95 0.32	R95	3.30	E95 0.37		
S09/258-85	272.75	69.11	4.42	276.53	-20.85	5.39	6.05	1.26	6.10	+0.23	1.38
	R95	2.28	E95 0.12	R95	3.04	E95 0.13	R95	2.03	E95 0.15		
S10/238-87	10.24	-78.35	25.02	304.36	4.82	28.37	35.26	10.58	28.78	+0.80	1.17
	R95	0.69	E95 0.11	R95	14.05	E95 1.17	R95	14.05	E95 1.23		
S11/088-86	26.94	-59.36	61.24	44.22	29.50	78.03	309.91	7.57	90.25	+0.28	1.49
	R95	0.72	E95 0.41	R95	0.76	E95 0.61	R95	0.37	E95 0.39		

Sample No./	MINIMUM			INTERMEDIATE			MAXIMUM			FABRIC PARAMETERS	
Orientation	DEC	INC	EV	DEC	INC	EV	DEC	INC	EV	T	P'
S12/234-74	68.80	-78.60	21.23	274.97	-10.26	23.77	4.07	4.92	25.36	+0.27	1.20
	R95 0.56	E95	0.05	R95 1.83	E95	0.24	R95 1.91	E95	0.72		
S13/274-70	13.01	-72.03	22.96	21.90	17.79	25.66	291.07	2.61	26.20	+0.68	1.15
	R95 0.84	E95	0.52	R95 8.59	E95	0.60	R95 8.54	E95	0.80		
S15/080-85	354.21	-66.91	37.45	0.01	23.38	44.00	89.10	-2.08	52.49	-0.04	1.39
	R95 0.69	E95	0.19	R95 0.77	E95	0.29	R95 0.05	E95	0.12		
S16/085-82	325.68	-66.40	40.27	330.76	23.52	57.85	59.92	-1.85	67.31	+0.61	2.25
	R95 0.34	E95	0.33	R95 1.09	E95	0.50	R95 1.07	E95	0.69		
S17/095-84	358.46	-71.37	28.66	1.65	18.60	32.79	271.32	0.97	40.04	-0.20	1.40
	R95 0.95	E95	0.15	R95 0.97	E95	0.27	R95 0.06	E95	0.23		
S18/088-84	339.58	-74.93	25.63	356.96	14.42	29.03	85.85	-4.31	32.35	+0.07	1.26
	R95 2.69	E95	0.59	R95 2.82	E95	0.96	R95 0.83	E95	0.24		
S19/075-77	287.15	-75.03	25.88	14.87	0.62	28.65	284.69	14.96	29.23	+0.78	1.15
	R95 0.35	E95	0.22	R95 5.85	E95	0.33	R95 5.80	E95	0.61		
S20/241-72	77.67	-82.67	24.66	359.21	1.51	30.34	89.41	7.18	32.25	+0.54	1.32
	R95 0.03	E95	0.33	R95 0.06	E95	0.44	R95 0.03	E95	0.33		
S21/285-84	21.41	76.60	25.27	319.77	-6.45	29.78	51.11	-11.69	30.46	+0.76	1.23
	R95 0.57	E95	0.18	R95 8.76	E95	0.91	R95 8.75	E95	1.04		
S22/070-90	2.98	-78.26	22.72	307.96	6.80	25.14	39.11	9.53	25.64	+0.67	1.14
	R95 0.93	E95	0.14	R95 0.79	E95	0.46	R95 0.87	E95	0.46		

Sample No./ Orientation	MINIMUM			INTERMEDIATE			MAXIMUM			FABRIC PARAMETERS	
	DEC	INC	EV	DEC	INC	EV	DEC	INC	EV	T	P'
S23/078-70	295.09	74.41	27.96	273.04	-14.50	32.64	4.47	-5.61	32.98	+0.88	1.20
	R95 0.14	E95	0.22	R95 1.00	E95	0.21	R95 1.01	E95	0.34		
S24/270-85	21.34	71.05	27.65	24.69	-18.92	30.85	294.34	-1.03	33.67	+0.12	1.22
	R95 0.95	E95	0.23	R95 2.59	E95	0.49	R95 2.45	E95	0.71		
S26/252-68	359.05	79.69	20.75	48.42	-6.72	23.01	317.51	-7.73	23.82	+0.50	1.15
	R95 2.50	E95	0.30	R95 14.69	E95	1.58	R95 14.67	E95	1.65		
S27/060-90	26.85	89.26	28.07	279.15	0.20	41.03	9.18	-0.88	41.53	+0.94	1.56
	R95 0.02	E95	0.11	R95 13.85	E95	1.10	R95 13.86	E95	1.23		
S28/244-84	64.01	-71.14	68.24	32.63	16.26	73.85	305.37	-9.30	75.22	+0.61	1.11
	R95 0.91	E95	0.91	R95 1.71	E95	0.11	R95 1.60	E95	0.49		
S29/ ?	314.33	-83.37	82.47	353.80	5.13	95.07	83.43	-4.19	110.58	-0.02	1.35
	R95 0.34	E95	0.25	R95 0.45	E95	0.78	R95 0.29	E95	0.32		
	R95	E95		R95	E95		R95	E95			
	R95	E95		R95	E95		R95	E95			
	R95	E95		R95	E95		R95	E95			
	R95	E95		R95	E95		R95	E95			

Sample No./ Orientation	MINIMUM				INTERMEDIATE				MAXIMUM				FABRIC PARAMETERS	
	DEC	INC	EV		DEC	INC	EV		DEC	INC	EV		T	P'
R01/063-80	318.33	78.50	25.30		333.65	-11.11	28.08		63.07	2.96	28.72		+0.64	1.15
	R95	0.56	E95	0.31	R95	11.89	E95	1.16	R95	11.91	E95	1.25		
R02/261-88	323.98	-80.21	16.80		287.44	7.89	18.59		18.24	5.75	19.29		+0.46	1.16
	R95	1.55	E95	0.22	R95	8.17	E95	0.64	R95	8.21	E95	0.73		
R03/?	325.08	-82.22	26.14		335.98	7.63	29.08		65.79	-1.46	29.65		+0.69	1.15
	R95	0.99	E95	0.25	R95	4.23	E95	0.35	R95	4.13	E95	0.43		
R04/072-86	0.33	-77.97	28.40		32.09	10.33	33.16		300.95	6.23	34.06		+0.71	1.22
	R95	0.49	E95	0.15	R95	12.37	E95	1.66	R95	12.37	E95	1.69		
R05/074-90	287.24	-72.74	45.03		272.79	16.74	56.92		4.02	4.06	67.45		+0.16	1.50
	R95	0.15	E95	0.06	R95	0.15	E95	0.10	R95	0.02	E95	0.03		
R06/084-84	27.28	-84.84	21.73		338.59	3.36	24.53		68.82	3.80	25.27		+0.61	1.17
	R95	1.08	E95	0.21	R95	9.32	E95	0.67	R95	9.28	E95	1.03		
R07/090-81	290.60	-70.48	30.27		343.46	12.08	35.53		70.15	-15.09	35.92		+0.87	1.21
	R95	0.36	E95	0.33	R95	1.01	E95	0.43	R95	1.01	E95	0.46		
R08/250-88	355.35	78.59	37.81		31.61	-9.25	61.29		300.53	-6.63	62.38		+0.93	1.77
	R95	0.10	E95	0.22	R95	0.30	E95	0.45	R95	0.29	E95	0.45		
R09/056-50	298.42	83.33	18.71		282.03	-6.40	22.61		12.24	-1.86	23.26		+0.74	1.27
	R95	0.17	E95	0.22	R95	4.20	E95	0.21	R95	4.19	E95	0.41		
R10/074-60	309.18	68.80	39.46		278.69	-18.48	57.16		12.08	-10.02	64.05		+0.53	1.66
	R95	0.63	E95	0.56	R95	0.83	E95	0.43	R95	0.58	E95	0.46		

Sample No./ Orientation	MINIMUM			INTERMEDIATE			MAXIMUM			FABRIC PARAMETERS	
	DEC	INC	EV	DEC	INC	EV	DEC	INC	EV	T	P'
R11/264-68	286.82	82.50	14.78	283.01	-7.48	16.81	13.07	-0.50	17.52	+0.51	1.19
	R95 0.87	E95	0.12	R95 0.88	E95	0.26	R95 0.80	E95	0.24		
R12/064-90	85.80	-86.31	13.05	21.97	1.63	15.11	292.06	-3.31	15.55	+0.67	1.20
	R95 0.52	E95	0.08	R95 10.56	E95	0.60	R95 10.56	E95	0.78		
R13/256-87	293.39	43.76	15.09	284.33	-45.88	17.18	19.03	-4.54	17.93	+0.51	1.19
	R95 2.87	E95	0.34	R95 3.70	E95	0.43	R95 2.38	E95	0.32		
R14/262-89	327.60	81.84	22.98	86.53	3.97	29.13	357.02	-7.13	30.23	+0.73	1.35
	R95 0.75	E95	0.11	R95 2.21	E95	0.27	R95 2.33	E95	0.67		
R15/260-77	89.29	-62.96	29.74	85.71	26.99	35.73	356.45	-1.45	43.12	-0.01	1.45
	R95 0.42	E95	0.14	R95 0.45	E95	0.16	R95 0.16	E95	0.23		
R16/250-88	301.67	-59.11	23.98	299.59	30.87	25.25	30.14	0.92	26.51	0.0	1.11
	R95 2.20	E95	0.27	R95 2.20	E95	0.36	R95 0.05	E95	0.22		
R17/258-80	82.58	86.65	48.13	270.17	3.32	65.95	0.16	-0.48	69.07	+0.75	1.48
	R95 0.02	E95	0.11	R95 0.02	E95	0.03	R95 0.12	E95	0.22		
R18/244-87	303.57	56.45	20.58	292.41	-33.05	25.32	25.77	-5.15	27.83	+0.37	1.36
	R95 4.43	E95	0.88	R95 4.38	E95	1.23	R95 0.73	E95	0.25		
R19/240-85	284.36	72.28	16.66	282.18	-17.72	19.14	12.19	-0.05	20.80	+0.25	1.25
	R95 7.07	E95	1.02	R95 7.23	E95	1.22	R95 1.55	E95	0.41		
R20/083-72	279.13	53.87	35.61	79.96	34.59	63.39	356.35	-9.17	73.75	+0.58	2.16
	R95 1.20	E95	0.93	R95 1.23	E95	1.28	R95 0.27	E95	0.40		

Sample No./ Orientation	MINIMUM			INTERMEDIATE			MAXIMUM			FABRIC PARAMETERS	
	DEC	INC	EV	DEC	INC	EV	DEC	INC	EV	T	P'
R21/248-75	77.52	-57.22	35.14	68.25	32.44	47.29	340.92	-4.23	52.02	+0.51	1.51
	R95	1.35	E95	0.66	R95	3.16	E95	0.75	R95	2.94	E95	1.30		
R22/074-82	37.77	-76.25	16.70	70.48	11.64	18.29	338.98	7.23	19.81	+0.06	1.19
	R95	1.59	E95	0.03	R95	2.76	E95	0.22	R95	2.63	E95	0.64		
R23/082-73	71.72	-73.73	22.64	281.11	-14.37	23.73	9.16	7.66	25.42	-0.19	1.12
	R95	2.96	E95	0.27	R95	2.97	E95	0.56	R95	0.59	E95	0.35		
R24/257-85	276.89	67.82	37.09	82.56	51.91	54.06	1.55	-6.98	64.81	+0.35	1.77
	R95	0.73	E95	0.45	R95	0.73	E95	0.55	R95	0.04	E95	0.23		
R25/249-77	276.54	-17.63	19.79	293.53	41.11	21.04	16.00	-8.53	23.21	-0.23	1.17
	R95	7.15	E95	0.89	R95	7.15	E95	0.90	R95	1.22	E95	0.24		
R26/267-85	313.26	38.40	20.01	272.33	-43.62	20.94	24.75	-21.81	22.68	-0.28	1.14
	R95	2.88	E95	0.28	R95	3.01	E95	0.32	R95	1.14	E95	0.23		
R27/257-85	74.47	65.30	21.83	277.69	22.91	28.61	3.97	-8.73	30.80	+0.57	1.44
	R95	1.03	E95	0.31	R95	1.04	E95	0.39	R95	0.24	E95	0.07		
	R95		E95		R95		E95		R95		E95			
	R95		E95		R95		E95		R95		E95			
	R95		E95		R95		E95		R95		E95			

Sample No./ Orientation	MINIMUM			INTERMEDIATE			MAXIMUM			FABRIC PARAMETERS	
	DEC	INC	EV	DEC	INC	EV	DEC	INC	EV	T	P'
T01/092-83	354.97	85.87	1957.3	271.98	-0.53	2245.1	2.01	-4.60	2340.1	+0.54	+1.21
	R95 0.11	E95	1.79	R95 0.05	E95	2.78	R95 0.98	E95	2.86		
T02/257-76	54.40	78.23	20.95	63.21	-11.64	24.85	332.83	-1.75	25.43	+0.76	1.24
	R95 1.20	E95	0.17	R95 4.63	E95	0.24	R95 4.47	E95	0.44		
T03/249-74	30.34	81.82	17.20	319.69	-2.73	20.56	50.06	-7.71	21.27		
	R95 1.22	E95	0.24	R95 33.90	E95	3.73	R95 33.89	E95	3.82		
T04/260-60	28.85	79.07	40.29	35.51	-10.86	59.32	305.28	-1.24	62.71	+0.75	1.62
	R95 0.16	E95	0.04	R95 4.36	E95	1.51	R95 4.36	E95	1.58		
T05/ 268-60	47.25	87.19	19.99	65.21	-2.67	24.45	335.17	-0.86	25.06	+0.78	1.28
	R95 0.13	E95	0.11	R95 12.58	E95	1.44	R95 12.58	E95	1.23		
T06/ 260-67	334.82	78.99	17.69	309.81	-10.00	22.17	40.61	-4.56	22.85	+0.76	1.32
	R95 0.80	E95	0.53	R95 0.84	E95	0.30	R95 0.49	E95	0.25		
T07/270-68	42.17	-88.14	20.50	341.32	0.91	26.64	71.35	1.63	27.43	+0.80	1.38
	R95 0.10	E95	0.44	R95 18.51	E95	1.70	R95 18.51	E95	1.82		
T08/277-55	21.13	75.10	58.84	32.50	-14.62	103.03	301.77	-2.81	106.09	+0.90	1.94
	R95 0.11	E95	0.63	R95 4.64	E95	2.00	R95 4.64	E95	2.06		
T09/ 240-78	344.11	83.48	31.29	80.75	0.76	51.15	350.83	-6.48	60.65	+0.49	1.99
	R95 0.09	E95	0.10	R95 0.95	E95	0.55	R95 0.94	E95	0.59		
T10/ 230-60	28.02	83.77	36.01	296.73	0.14	60.74	26.71	-6.23	63.79	+0.83	1.89
	R95 0.12	E95	0.42	R95 0.84	E95	0.28	R95 0.84	E95	0.32		

Sample No./	MINIMUM			INTERMEDIATE			MAXIMUM			FABRIC PARAMETERS	
Orientation	DEC	INC	EV	DEC	INC	EV	DEC	INC	EV	T	P'
T11/243-70	355.01	84.74	22.69	37.13	-3.91	30.28	306.89	-3.52	30.62	+0.93	1.40
	R95 0.07	E95	0.11	R95 17.19	E95	1.39	R95 17.18	E95	1.41		
T12/215-65	352.31	83.78	34.44	85.50	0.35	57.82	355.54	-6.22	64.42	+0.66	1.95
	R95 0.02	E95	0.11	R95 0.37	E95	0.40	R95 0.37	E95	0.22		
T13/260-82	348.48	-87.98	40.75	341.29	2.00	63.25	71.30	0.25	64.00	+0.95	1.67
	R95 0.02	E95	0.11	R95 11.63	E95	1.80	R95 11.63	E95	1.83		
T14/258-85	25.71	80.34	20.41	43.36	-9.21	25.74	312.99	-2.88	27.67	+0.53	1.37
	R95 0.30	E95	0.08	R95 4.83	E95	0.82	R95 4.83	E95	0.89		
T18/095-70	17.30	87.50	20.09	301.44	-0.61	25.40	31.46	-2.43	25.95	+0.84	1.33
	R95 0.14	E95	0.11	R95 15.82	E95	1.44	R95 15.82	E95	1.51		
T19/110-88	25.89	-85.11	16.86	312.02	1.37	20.80	42.14	4.70	20.98	+0.92	1.28
	R95 0.13	E95	0.03	R95 0.07	E95	0.11	R95 0.14	E95	0.11		
T20/253-70	319.74	87.42	16.73	343.38	-2.36	19.11	73.34	1.03	19.67	+0.65	1.19
	R95 0.10	E95	0.02	R95 6.65	E95	0.50	R95 6.65	E95	0.53		
T21/250-70	295.47	-87.84	20.73	40.05	-0.51	25.13	310.06	2.00	25.60	+0.82	1.26
	R95 0.11	E95	0.11	R95 27.67	E95	2.60	R95 27.67	E95	2.63		
T22/250-75	17.63	77.60	47.81	2.16	-11.97	75.95	272.84	3.21	85.70	+0.59	1.85
	R95 0.09	E95	0.08	R95 0.11	E95	0.23	R95 0.06	E95	0.05		
T23/259-70	81.74	74.65	19.01	337.58	3.84	23.32	66.56	-14.84	24.14	+0.71	1.29
	R95 2.00	E95	0.47	R95 21.38	E95	2.10	R95 21.42	E95	2.24		

Sample No./ Orientation	MINIMUM			INTERMEDIATE			MAXIMUM			FABRIC PARAMETERS	
	DEC	INC	EV	DEC	INC	EV	DEC	INC	EV	T	P'
T25/242-65	80.16	82.50	17.74	85.61	-7.47	20.85	355.52	-0.71	21.76	+0.58	1.24
	R95	1.09	E95 0.26	R95	1.52	E95 0.21	R95	1.08	E95 0.36		
T26/100-79	20.79	73.88	19.59	72.15	-10.23	22.98	339.89	-12.32	24.27	+0.50	1.25
	R95	0.77	E95 0.39	R95	1.32	E95 0.30	R95	1.38	E95 0.33		
T27/242-45	289.75	-83.57	19.62	303.24	6.25	24.07	33.07	-1.49	24.55	+0.82	1.28
	R95	0.50	E95 0.19	R95	6.13	E95 0.48	R95	6.11	E95 0.55		
T28/300-74	45.00	81.61	19.50	315.00	0.00	25.18	45.00	-8.39	25.62	+0.87	1.36
	R95	0.34	E95 0.32	R95	13.75	E95 1.02	R95	13.75	E95 1.30		
T29/273-74	72.13	78.02	17.87	32.56	-9.29	32.10	303.79	7.50	22.50	+0.85	1.29
	R95	1.42	E95 0.43	R95	12.84	E95 0.89	R95	12.84	E95 0.98		
T30/279-78	274.10	-84.90	23.12	313.77	3.93	30.70	43.55	-3.24	35.74	+0.30	1.56
	R95	0.18	E95 0.10	R95	2.50	E95 0.73	R95	2.50	E95 0.86		
T31/273-77	75.10	87.86	16.34	44.96	-1.85	18.06	315.00	1.08	19.31	+0.20	1.18
	R95	0.58	E95 0.32	R95	5.07	E95 0.55	R95	5.04	E95 0.65		
T32/250-80	73.50	74.84	12.95	315.12	7.34	15.29	43.39	-13.19	15.72	+0.72	1.23
	R95	0.02	E95 0.11	R95	0.17	E95 0.11	R95	0.17	E95 0.11		
T34/261-78	28.72	79.86	27.58	306.21	-1.34	35.20	36.45	-10.05	35.92	+0.84	1.34
	R95	0.12	E95 0.22	R95	4.14	E95 0.45	R95	4.14	E95 0.60		
T36/236-74	324.43	88.02	26.01	77.79	0.78	33.58	347.82	-1.84	34.37	+0.84	1.36
	R95	0.12	E95 0.33	R95	5.61	E95 0.58	R95	5.60	E95 0.67		

Sample No./ Orientation	MINIMUM			INTERMEDIATE			MAXIMUM			FABRIC PARAMETERS	
	DEC	INC	EV	DEC	INC	EV	DEC	INC	EV	T	P'
T37/246-88	325.55	50.64	4.74	299.20	-36.31	5.18	39.06	-13.11	5.50	+0.19	1.16
	R95 0.17	E95	0.11	R95 0.17	E95	0.11	R95 0.07	E95	0.11		
T38/060-80	38.46	82.85	49.09	80.80	-5.30	63.43	350.33	-4.78	63.73	+0.93	1.36
	R95 0.03	E95	0.11	R95 3.65	E95	0.33	R95 3.64	E95	0.41		
T39/237-70	22.07	85.06	19.29	30.31	-4.89	22.15	300.25	-0.71	23.38	+0.43	1.22
	R95 0.46	E95	0.07	R95 4.47	E95	0.54	R95 4.45	E95	0.65		
T40/238-68	289.62	-80.32	17.60	340.70	6.17	19.55	69.88	-7.54	20.24	+0.51	1.16
	R95 0.40	E95	0.21	R95 5.92	E95	0.50	R95 5.93	E95	0.61		
T41/246-78	22.84	-83.26	18.58	28.32	6.70	20.69	298.25	0.64	22.35	+0.16	1.20
	R95 1.84	E95	0.17	R95 1.83	E95	0.44	R95 0.10	E95	0.33		
T42/267-85	39.19	-66.76	18.29	34.48	23.17	20.52	305.21	-1.70	21.54	+0.41	1.18
	R95 1.70	E95	0.19	R95 3.36	E95	0.13	R95 2.93	E95	0.34		
T43/285-82	36.09	-82.43	25.34	14.18	7.03	28.49	284.53	-2.80	30.00	+0.39	1.19
	R95 0.96	E95	0.50	R95 5.30	E95	0.74	R95 5.29	E95	0.87		
T45/075-87	355.41	-77.16	19.05	35.86	9.84	22.13	304.43	8.17	23.72	+0.37	1.25
	R95 1.19	E95	0.21	R95 1.94	E95	0.09	R95 1.72	E95	0.30		
T46/251-79	19.48	72.02	21.00	340.52	-14.16	25.30	73.29	-10.85	27.00	+0.48	1.30
	R95 0.69	E95	0.16	R95 5.95	E95	0.88	R95 5.92	E95	0.98		
T47/253-83	17.93	84.59	22.36	15.32	-5.40	27.64	285.35	0.25	28.50	+0.75	1.30
	R95 0.15	E95	0.66	R95 3.82	E95	0.30	R95 3.82	E95	0.58		

Sample No./	MINIMUM			INTERMEDIATE			MAXIMUM			FABRIC PARAMETERS	
Orientation	DEC	INC	EV	DEC	INC	EV	DEC	INC	EV	T	P'
T48/252-78	40.55	-44.62	22.18	44.73	45.33	22.53	312.62	2.09	29.74	+0.62	1.15
	R95	46.59	E95 4.75	R95	46.59	E95 4.81	R95	0.89	E95 0.54		
T49/263-78	55.24	83.25	24.99	9.31	-4.71	28.61	279.71	4.83	29.89	+0.53	1.22
	R95	0.24	E95 0.21	R95	2.55	E95 0.23	R95	2.55	E95 0.40		
T51/260-74	287.16	-88.58	23.22	22.50	-0.13	30.58	292.51	1.41	33.24	+0.54	1.46
	R95	0.08	E95 0.55	R95	1.68	E95 0.32	R95	1.68	E95 0.39		
T52/263-84	309.32	72.60	18.65	31.06	-1.81	22.17	300.66	-12.26	22.92	+0.68	1.25
	R95	1.26	E95 0.15	R95	0.32	E95 0.12	R95	1.26	E95 0.31		
T53/264-76	354.00	78.32	17.61	355.17	-11.74	21.18	85.11	0.23	21.91	+0.69	1.27
	R95	0.70	E95 0.06	R95	1.02	E95 0.35	R95	0.75	E95 0.24		
T54/257-80	40.78	72.54	18.57	48.72	-17.30	21.66	318.02	-2.27	22.81	+0.50	1.24
	R95	0.76	E95 0.28	R95	7.72	E95 0.90	R95	7.74	E95 1.03		
T55/095-88	23.85	-52.45	13.01	348.13	31.97	14.76	89.52	17.57	15.73	+0.33	1.21
	R95	6.47	E95 0.79	R95	8.03	E95 0.54	R95	6.18	E95 0.70		
T56/063-90	48.89	74.26	23.98	11.11	-12.55	30.08	283.21	9.33	30.51	+0.88	1.31
	R95	0.27	E95 0.07	R95	6.90	E95 0.51	R95	6.91	E95 0.57		
T57/258-73	41.90	83.23	20.98	29.33	-6.60	25.69	299.49	1.46	26.91	+0.63	1.30
	R95	0.23	E95 0.22	R95	4.50	E95 0.61	R95	4.49	E95 0.66		
T58/234-69	63.12	82.30	15.37	26.28	-6.18	17.02	296.77	4.58	17.58	+0.52	1.15
	R95	0.96	E95 0.30	R95	0.86	E95 0.16	R95	0.50	E95 0.13		

Sample No./	MINIMUM			INTERMEDIATE			MAXIMUM			FABRIC PARAMETERS	
Orientation	DEC	INC	EV	DEC	INC	EV	DEC	INC	EV	T	P'
T59/275-73	11.02	-67.23	24.97	356.43	22.11	29.42	88.54	5.18	31.24	+0.46	1.26
	R95	2.01	E95 0.36	R95	2.02	E95 0.56	R95	0.38	E95 0.15		
T61/252-84	7.21	80.62	17.88	346.25	-8.77	19.67	76.76	-3.30	21.80	-0.04	1.22
	R95	1.71	E95 0.10	R95	2.60	E95 0.18	R95	1.99	E95 0.39		
T62/079-90	7.86	79.90	32.27	315.84	-6.25	58.13	46.71	-7.90	59.97	+0.90	2.01
	R95	0.04	E95 0.22	R95	1.77	E95 0.45	R95	1.77	E95 0.46		
T63/278-88	21.54	-49.51	29.75	32.13	40.00	34.85	297.71	5.25	48.26	-0.35	1.64
	R95	1.39	E95 0.41	R95	1.47	E95 0.35	R95	0.70	E95 0.58		
T64/282-80	18.69	-51.99	19.66	28.21	37.63	23.58	294.63	4.62	32.98	-0.30	1.69
	R95	0.14	E95 0.33	R95	0.25	E95 0.31	R95	0.24	E95 0.27		
T65/273-81	80.02	83.07	22.60	16.67	-3.12	25.54	287.10	6.18	27.49	+0.25	1.22
	R95	0.24	E95 0.09	R95	5.68	E95 0.87	R95	5.68	E95 1.01		
T66/080-85	353.47	-68.02	19.64	16.18	20.42	23.16	283.26	7.78	24.49	+0.50	1.26
	R95	5.58	E95 1.13	R95	5.47	E95 1.29	R95	1.73	E95 0.68		
T67/086-85	302.99	-84.85	25.04	5.09	2.40	33.02	274.93	4.54	33.37		
	R95	0.65	E95 0.50	R95	78.66	E95 4.31	R95	78.64	E95 4.37		
T69/242-82	20.07	84.22	33.08	281.23	0.84	35.12	11.18	-5.93	35.57	+0.61	1.08
	R95	0.51	E95 0.04	R95	30.78	E95 1.85	R95	30.77	E95 1.90		
T70/263-85	62.21	80.97	19.18	335.77	-0.57	21.42	65.86	-9.01	22.56	+0.36	1.18
	R95	0.40	E95 0.54	R95	2.08	E95 0.25	R95	2.10	E95 0.50		

Sample No./	MINIMUM				INTERMEDIATE				MAXIMUM				FABRIC PARAMETERS	
Orientation	DEC	INC	EV		DEC	INC	EV		DEC	INC	EV		T	P'
T71/256-87	318.78	-86.50	42.67		21.21	1.62	54.92		291.12	3.10	62.20		+0.34	1.47
	R95	0.09	E95	0.44	R95	0.88	E95	0.42	R95	0.87	E95	0.52		
T72/247-84	286.52	-74.15	31.10		29.01	-3.49	32.10		299.96	15.45	32.74		+0.23	1.05
	R95	4.53	E95	0.68	R95	4.14	E95	0.25	R95	5.29	E95	0.80		
T73/266-82	38.07	-80.63	19.96		14.86	8.63	22.04		285.44	-3.63	23.77		+0.14	1.19
	R95	0.38	E95	0.21	R95	1.02	E95	0.30	R95	0.94	E95	0.27		
T74/095-90	6.19	-72.92	21.03		6.88	17.12	23.83		276.82	0.20	25.60		+0.27	1.22
	R95	1.25	E95	0.13	R95	1.76	E95	0.16	R95	1.24	E95	0.38		
T75/267-85	45.29	78.18	24.08		342.54	-5.47	28.66		73.55	-10.45	29.93		+0.60	1.26
	R95	0.20	E95	0.33	R95	1.36	E95	0.13	R95	1.35	E95	0.39		
T76/060-82	57.11	-80.39	18.13		8.87	6.43	21.12		279.68	-7.11	22.37		+0.45	1.24
	R95	1.56	E95	0.60	R95	2.49	E95	0.08	R95	2.17	E95	0.39		
	R95		E95		R95		E95		R95		E95			
	R95		E95		R95		E95		R95		E95			
	R95		E95		R95		E95		R95		E95			
	R95		E95		R95		E95		R95		E95			

Sample No. /	MINIMUM			INTERMEDIATE			MAXIMUM			FABRIC PARAMETERS	
Orientation	DEC	INC	EV	DEC	INC	EV	DEC	INC	EV	T	P'
P01/H	347.49	-0.44	30.57	77.64	-18.52	33.31	76.19	71.48	35.19	+0.23	1.15
	R95 1.93	E95	0.39	R95 5.39	E95	0.84	R95 5.06	E95	1.06		
P02/H	346.64	16.48	19.34	74.75	-6.37	21.62	324.29	-72.29	21.70	+0.93	1.14
	R95 0.01	E95	0.22	R95 0.03	E95	0.24	R95 0.40	E95	0.20		
P05/H	333.70	12.48	19.55	51.78	-43.03	21.20	76.17	44.29	21.84		
	R95 4.98	E95	0.76	R95 18.93	E95	1.71	R95 18.98	E95	1.93		
P06/H	340.52	8.93	21.71	67.40	-19.08	23.76	274.41	-68.79	24.37		
	R95 0.97	E95	0.12	R95 6.75	E95	0.58	R95 6.74	E95	0.70		
P09/H	325.66	6.66	28.64	54.81	-7.24	34.24	277.83	-80.14	34.85	+0.82	1.24
	R95 1.04	E95	0.32	R95 1.86	E95	0.31	R95 1.54	E95	0.18		
P11/H	334.46	-5.94	20.33	71.85	-51.01	23.23	59.74	38.36	23.71		
	R95 2.29	E95	0.45	R95 9.38	E95	0.71	R95 9.42	E95	0.88		
P12/H	338.35	-6.95	22.06	56.88	58.48	24.90	72.48	-30.57	25.53	+0.66	1.17
	R95 0.88	E95	0.15	R95 5.08	E95	0.45	R95 5.03	E95	0.50		
P13A/H	348.29	12.20	23.72	67.25	-41.53	29.06	271.18	-45.90	29.96	+0.74	1.29
	R95 0.36	E95	0.20	R95 0.36	E95	0.17	R95 0.04	E95	0.11		
P13/H	333.34	17.93	21.46	50.78	-33.91	23.34	86.38	50.43	24.11	+0.44	1.13
	R95 1.48	E95	0.34	R95 1.49	E95	0.43	R95 0.19	E95	0.33		
P13B/H	330.11	8.14	24.18	56.07	-26.22	28.86	75.97	62.36	29.52		
	R95 8.25	E95	2.06	R95 9.94	E95	2.25	R95 6.21	E95	0.83		

Sample No./	MINIMUM			INTERMEDIATE			MAXIMUM			FABRIC PARAMETERS	
Orientation	DEC	INC	EV	DEC	INC	EV	DEC	INC	EV	T	P'
P14/H	338.00	11.23	19.73	56.26	-45.71	21.85	78.34	42.11	22.49	+0.55	1.15
	R95	3.29	E95 0.50	R95	3.66	E95 0.50	R95	2.07	E95 0.27		
P15/H	346.07	7.68	13.15	72.76	-23.71	15.53	273.20	-65.41	15.75		
	R95	0.60	E95 0.31	R95	10.98	E95 0.40	R95	10.97	E95 0.58		
P18B/H	337.59	19.05	17.21	55.38	-31.50	20.70	273.80	-51.97	21.07		
	R95	1.14	E95 0.24	R95	15.32	E95 0.99	R95	15.33	E95 1.09		
P22A/H	351.30	7.17	23.07	81.46	1.28	27.62	355.23	-83.06	27.85		
	R95	0.74	E95 0.16	R95	76.50	E95 1.19	R95	74.87	E95 1.26		
P22/H	333.66	1.06	17.74	63.35	-16.39	21.04	67.26	73.57	21.56		
	R95	1.52	E95 0.23	R95	8.83	E95 0.58	R95	8.70	E95 0.70		
P16/H	354.84	30.23	16.78	52.52	-42.53	19.59	286.86	-32.55	19.71		
	R95	1.08	E95 0.26	R95	28.24	E95 1.11	R95	28.23	E95 1.17		
P17/H	343.97	-3.13	19.87	80.77	-65.22	21.87	72.54	24.55	22.41		
	R95	0.80	E95 0.20	R95	9.52	E95 0.76	R95	9.51	E95 0.86		
P18N/H	345.10	20.48	20.73	71.14	-10.47	24.70	315.63	-66.78	25.04	+0.86	1.23
	R95	0.00	E95 0.01	R95	0.00	E95 0.06	R95	0.02	E95 0.05		
P18/H	356.10	-30.90	18.46	74.22	18.97	22.43	317.54	52.57	23.07	+0.74	1.28
	R95	2.65	E95 0.56	R95	1.68	E95 0.31	R95	2.45	E95 0.58		
P19/H	351.16	13.73	21.38	63.49	-51.17	23.06	271.19	-35.47	23.60	+0.54	1.11
	R95	2.79	E95 0.41	R95	5.93	E95 0.20	R95	5.28	E95 0.54		

Sample No./	MINIMUM			INTERMEDIATE			MAXIMUM			FABRIC PARAMETERS	
Orientation	DEC	INC	EV	DEC	INC	EV	DEC	INC	EV	T	P'
P20/H	340.57	12.85	23.25	56.02	-47.75	29.58	81.36	39.38	30.25	+0.83	1.34
	R95	0.29	E95 0.31	R95	4.07	E95 0.33	R95	4.07	E95 0.53		
P22/H	333.66	1.06	17.74	63.35	-16.39	21.04	67.26	73.57	21.56		
	R95	1.52	E95 0.23	R95	8.83	E95 0.58	R95	8.70	E95 0.70		
P22A/H	358.17	9.93	27.61	83.81	-23.51	33.10	289.44	-64.24	34.18	+0.70	1.26
	R95	0.05	E95 0.15	R95	3.05	E95 0.35	R95	3.05	E95 0.49		
P25/H	345.49	6.84	23.59	61.09	-64.24	30.58	78.66	24.70	30.87		
	R95	0.42	E95 0.05	R95	17.04	E95 1.14	R95	17.04	E95 1.20	+0.93	1.36
P23/H	355.50	22.74	20.61	69.01	-34.11	24.45	292.27	-47.07	25.07		
	R95	0.00	E95 0.00	R95	0.00	E95 0.02	R95	0.00	E95 0.02	+0.75	1.24
P24/H	347.55	17.67	21.76	276.56	-45.64	25.35	62.58	-39.04	26.05		
	R95	1.20	E95 0.13	R95	4.78	E95 0.06	R95	4.92	E95 0.75	+0.69	1.21
P26A/H	346.41	-14.87	37.68	70.71	20.52	54.97	289.81	64.25	57.70		
	R95	0.88	E95 0.31	R95	7.65	E95 2.16	R95	7.60	E95 2.35	+0.77	1.60
P26/H	345.21	22.04	15.53	71.01	-10.25	19.29	317.67	-65.46	19.51		
	R95	0.01	E95 0.11	R95	0.19	E95 0.11	R95	0.19	E95 0.11	+0.90	1.29
P27/H	347.81	8.81	18.81	72.25	-32.00	21.92	271.36	-56.52	22.56		
	R95	1.01	E95 0.07	R95	1.01	E95 0.21	R95	0.08	E95 0.19	+0.69	1.22
P28/H	352.26	-12.55	28.94	82.19	0.31	36.92	347.52	77.52	37.09		
	R95	0.53	E95 0.37	R95	2.63	E95 0.24	R95	0.28	E95 0.25		

Sample No./	MINIMUM			INTERMEDIATE			MAXIMUM			FABRIC PARAMETERS	
Orientation	DEC	INC	EV	DEC	INC	EV	DEC	INC	EV	T	P'
P29/H	356.70	-5.00	19.69	85.91	9.04	24.10	295.34	79.65	24.47	+0.86	1.27
	R95	0.16	E95	0.23	R95	0.15	E95	0.12	R95	0.15	E95	0.12		
P30/H	308.91	15.46	32.53	33.20	-19.79	36.08	74.31	64.47	36.82	+0.67	1.14
	R95	0.88	E95	0.15	R95	2.06	E95	0.29	R95	1.99	E95	0.44		
P32/H	345.31	3.80	24.32	74.91	-6.04	31.05	287.32	-82.86	32.08	+0.77	1.35
	R95	0.71	E95	0.22	R95	5.36	E95	0.49	R95	5.32	E95	0.71		
P33/H	352.54	-8.64	17.53	82.63	-0.55	21.26	356.48	81.31	21.76	+0.78	1.27
	R95	0.31	E95	0.32	R95	0.33	E95	0.23	R95	0.52	E95	0.23		
P34/H	354.40	-5.28	19.41	80.93	33.18	23.55	272.37	56.29	24.15	+0.81	1.28
	R95	0.65	E95	0.16	R95	23.20	E95	2.19	R95	23.20	E95	2.23		
P35/H	357.74	-7.40	19.79	85.78	14.75	24.21	293.61	73.42	24.75	+0.81	1.28
	R95	0.21	E95	0.33	R95	3.07	E95	0.24	R95	3.07	E95	0.35		
P36/H	338.30	-4.12	23.37	57.09	69.67	28.85	69.79	-19.87	29.19		
	R95	0.41	E95	0.22	R95	13.23	E95	0.92	R95	13.23	E95	0.99		
P37/H	329.28	-13.32	6.60	81.27	-57.71	8.32	51.79	28.82	8.66		
	R95	0.88	E95	0.22	R95	8.59	E95	0.31	R95	8.56	E95	4.18		
P38/H	356.98	4.63	31.20	88.09	14.46	48.61	69.57	-74.79	51.77	+0.75	1.74
	R95	0.14	E95	0.09	R95	3.18	E95	0.95	R95	3.18	E95	1.13		
P37B/H	347.83	-27.42	72.26	67.17	19.63	88.51	306.24	55.25	89.28		
	R95	5.05	E95	0.27	R95	4.59	E95	0.48	R95	5.15	E95	0.48		

Sample No./	MINIMUM			INTERMEDIATE			MAXIMUM			FABRIC PARAMETERS	
Orientation	DEC	INC	EV	DEC	INC	EV	DEC	INC	EV	T	P'
P38B/H	329.99	4.68	49.39	64.77	45.53	82.40	55.45	-44.08	85.46	+0.87	1.85
	R95 1.70	E95	1.67	R95 5.76	E95	1.53	R95 5.75	E95	2.82		
P39/H	350.01	-8.05	27.24	79.38	4.43	46.37	320.84	80.80	47.65	+0.90	1.88
	R95 0.13	E95	0.22	R95 0.65	E95	0.08	R95 0.64	E95	0.17		
P43/H	341.30	16.20	26.66	31.60	-65.54	30.69	76.66	17.82	31.21	+0.53	1.19
	R95 0.62	E95	0.12	R95 6.61	E95	0.61	R95 6.63	E95	0.68		
P52/H	350.59	-28.60	29.81	23.11	57.11	33.60	88.90	-14.85	34.86	+0.52	1.18
	R95 2.24	E95	0.57	R95 2.55	E95	0.59	R95 1.25	E95	0.21		
P60/H	330.21	-19.13	30.02	47.54	32.31	34.98	85.74	-51.17	40.01	+0.06	1.33
	R95 0.77	E95	0.12	R95 2.20	E95	0.64	R95 2.29	E95	0.86		
	R95	E95		R95	E95		R95	E95			
	R95	E95		R95	E95		R95	E95			
	R95	E95		R95	E95		R95	E95			
	R95	E95		R95	E95		R95	E95			
	R95	E95		R95	E95		R95	E95			

Sample No./	MINIMUM			INTERMEDIATE			MAXIMUM			FABRIC PARAMETERS	
Orientation	DEC	INC	EV	DEC	INC	EV	DEC	INC	EV	T	P
F1-1/H	88.79	-1.05	21.97	358.94	7.83	26.15	351.60	-81.71	26.79	+0.75	1.24
	R95 0.04	E95	0.38	R95 1.69	E95	0.19	R95 1.61	E95	0.41		
F1-2/H	272.16	2.15	35.28	1.56	-15.65	46.16	9.80	74.21	48.98	+0.64	1.42
	R95 0.07	E95	0.37	R95 0.68	E95	0.15	R95 0.68	E95	0.20		
F1-3/H	270.71	-1.70	49.46	0.71	-0.02	56.67	87.13	-88.30	58.46	+0.63	1.20
	R95 0.03	E95	0.00	R95 0.19	E95	0.12	R95 0.02	E95	0.13		
F1-4/H	88.43	-2.32	34.07	357.41	-23.70	37.80	3.69	66.17	38.99	+0.54	1.15
	R95 0.06	E95	0.13	R95 2.13	E95	0.35	R95 2.16	E95	0.37		
F1-5/H	84.07	-4.55	26.07	352.95	-13.81	30.64	11.87	75.42	32.34	+0.50	1.25
	R95 0.48	E95	0.48	R95 3.13	E95	0.50	R95 3.09	E95	0.74		
F1-6/H	86.67	-6.15	37.70	356.11	-4.29	47.42	51.38	82.49	52.16	+0.41	1.40
	R95 0.22	E95	0.21	R95 0.34	E95	0.05	R95 0.39	E95	0.31		
F1-7/H	86.57	-5.66	41.48	355.06	-14.94	50.90	16.75	73.98	56.28	+0.34	1.37
	R95 0.11	E95	0.24	R95 0.36	E95	0.13	R95 0.35	E95	0.19		
F1-8/H	87.70	-4.06	35.55	356.53	-16.01	40.63	11.53	73.46	42.24	+0.55	1.20
	R95 0.58	E95	0.21	R95 6.38	E95	1.17	R95 6.38	E95	1.50		
F1-9/H	76.59	-6.99	44.36	344.13	-19.27	56.63	5.64	69.41	61.55	+0.49	1.41
	R95 0.16	E95	0.11	R95 1.36	E95	0.56	R95 1.37	E95	0.68		
F1-10/H	271.29	7.76	27.95	0.71	-5.02	31.30	41.12	77.99	31.94	+0.70	1.15
	R95 0.28	E95	0.10	R95 8.13	E95	0.32	R95 3.95	E95	0.42		

Sample No./	MINIMUM			INTERMEDIATE			MAXIMUM			FABRIC PARAMETERS	
Orientation	DEC	INC	EV	DEC	INC	EV	DEC	INC	EV	T	P'
F1-11/H	280.70	5.79	27.88	9.48	-11.83	30.66	36.30	76.79	31.95	+0.40	1.15
	R95	1.40	E95 0.28	R95	2.34	E95 0.25	R95	1.93	E95 0.31		
F1-12/H	270.90	10.06	22.75	358.05	-15.67	25.37	32.40	71.25	26.43	+0.45	1.17
	R95	0.04	E95 0.12	R95	1.77	E95 0.23	R95	1.79	E95 0.26		
F1-13/H	272.83	8.85	28.20	359.42	-20.94	33.51	24.45	67.09	35.27	+0.55	1.26
	R95	0.28	E95 0.36	R95	8.11	E95 0.76	R95	4.12	E95 0.82		
F1-14/H	77.29	-8.40	47.78	343.85	-22.11	63.10	6.84	66.18	68.57	+0.54	1.46
	R95	0.42	E95 0.21	R95	1.06	E95 0.30	R95	0.97	E95 0.47		
F1-15/H	86.59	-1.98	38.27	355.02	-38.52	54.48	359.07	51.42	57.51	+0.73	1.56
	R95	0.00	E95 0.13	R95	0.03	E95 0.12	R95	0.05	E95 0.13		
F1-16/H	314.98	-80.74	49.09	305.65	9.14	81.42	35.88	1.48	83.68	+0.90	1.82
	R95	0.09	E95 0.21	R95	3.92	E95 1.23	R95	3.92	E95 1.44		
	R95		E95	R95		E95	R95		E95		
	R95		E95	R95		E95	R95		E95		
	R95		E95	R95		E95	R95		E95		
	R95		E95	R95		E95	R95		E95		

Sample No./	MINIMUM			INTERMEDIATE			MAXIMUM			FABRIC PARAMETERS	
Orientation	DEC	INC	EV	DEC	INC	EV	DEC	INC	EV	T	P'
F2-1/H	80.44	36.26	34.45	288.17	50.35	49.90	0.86	-13.85	59.19	+0.37	1.74
	R95 1.12	E95	0.62	R95 1.12	E95	0.77	R95 0.04	E95	0.25		
F2-2/H	79.79	34.19	38.22	272.95	55.10	51.03	354.01	-6.19	57.81	+0.40	1.53
	R95 0.53	E95	0.29	R95 0.54	E95	0.33	R95 0.14	E95	0.15		
F2-3/H	84.00	36.38	34.39	87.67	-53.57	60.12	355.29	-1.76	70.47	+0.56	2.12
	R95 0.68	E95	0.49	R95 0.67	E95	0.71	R95 0.09	E95	0.63		
F2-4/H	75.27	30.89	45.00	89.16	-58.36	66.60	349.00	-6.20	85.85	+0.21	1.92
	R95 0.93	E95	0.42	R95 0.90	E95	0.86	R95 0.40	E95	0.61		
F2-5/H	78.21	30.36	38.62	286.17	56.45	60.42	355.93	-12.92	75.63	+0.33	1.98
	R95 0.37	E95	0.08	R95 0.41	E95	0.30	R95 0.29	E95	0.46		
	R95	E95		R95	E95		R95	E95			
	R95	E95		R95	E95		R95	E95			
	R95	E95		R95	E95		R95	E95			
	R95	E95		R95	E95		R95	E95			
	R95	E95		R95	E95		R95	E95			

Sample No./	MINIMUM			INTERMEDIATE			MAXIMUM			FABRIC PARAMETERS	
Orientation	DEC	INC	EV	DEC	INC	EV	DEC	INC	EV	T	P'
PLR-2/H	319.72	-40.24	47.37	25.79	25.61	75.22	272.96	39.00	79.03	+0.81	1.76
	R95 1.34	E95	1.19	R95 8.10	E95	3.28	R95 8.18	E95	3.78		
PLR-3/H	301.62	-37.38	55.86	11.69	24.04	94.56	77.09	-43.02	101.04	+0.78	1.92
	R95 1.21	E95	1.49	R95 2.26	E95	0.99	R95 2.52	E95	0.24		
PLR-4A/H	346.37	-10.54	25.13	69.30	33.47	32.33	271.46	54.45	32.40	+0.98	1.34
	R95 0.53	E95	0.15	R95 0.59	E95	0.21	R95 0.25	E95	0.14		
PLR-5/H	323.62	-41.78	35.72	20.45	31.48	55.82	87.81	-32.16	59.99	+0.72	1.75
	R95 1.26	E95	0.83	R95 4.66	E95	1.60	R95 4.77	E95	2.11		
PLR-7/H	319.98	-41.52	29.42	1.67	40.10	39.60	71.36	-22.47	40.40	+0.88	1.43
	R95 1.45	E95	0.63	R95 0.72	E95	0.03	R95 2.11	E95	0.88		
PLR-8/H	321.69	-25.73	28.33	6.19	55.96	35.20	62.18	-20.70	35.82	+0.85	1.30
	R95 0.65	E95	0.23	R95 3.99	E95	0.42	R95 4.01	E95	0.51		
PLR-9/H	2.00	-7.14	28.48	277.42	37.01	36.43	82.75	52.07	36.88	+0.91	1.34
	R95 0.10	E95	0.35	R95 0.14	E95	0.24	R95 0.13	E95	0.24		
PLR-10/H	325.77	-22.02	23.59	334.08	67.77	28.94	56.94	-2.91	29.95	+0.71	1.30
	R95 2.21	E95	0.61	R95 2.74	E95	0.47	R95 2.62	E95	0.67		
PLR-12/H	323.41	-28.38	28.00	348.53	59.18	34.05	59.45	-11.03	35.11	+0.73	1.28
	R95 2.76	E95	0.93	R95 2.85	E95	0.38	R95 3.79	E95	1.10		
PLR-B/H	322.29	-35.77	28.30	18.88	37.39	36.05	79.68	-32.55	37.78	+0.68	1.36
	R95 1.93	E95	0.76	R95 6.91	E95	1.29	R95 7.17	E95	1.63		

Sample No./	MINIMUM			INTERMEDIATE			MAXIMUM			FABRIC PARAMETERS	
Orientation	DEC	INC	EV	DEC	INC	EV	DEC	INC	EV	T	P'
PLR-C/H	322.09	-37.99	32.02	8.53	41.43	43.58	73.81	-25.36	44.92	+0.82	1.46
	R95 0.83	E95	0.33	R95 4.38	E95	0.68	R95 4.34	E95	0.91		
PLR-D/H	324.43	-36.47	32.57	21.65	36.22	44.70	83.18	-33.06	46.51	+0.78	1.48
	R95 1.39	E95	0.71	R95 5.57	E95	1.11	R95 5.64	E95	1.50		
PLR-G/H	309.55	-36.93	30.92	9.35	33.79	44.87	71.36	-35.04	46.47	+0.83	1.57
	R95 1.28	E95	0.68	R95 2.85	E95	0.55	R95 3.11	E95	1.07		
PLR-H/H	314.49	-29.97	17.92	3.36	48.76	21.54	60.44	-25.47	22.46	+0.64	1.27
	R95 0.78	E95	0.29	R95 2.53	E95	0.19	R95 2.45	E95	0.44		
PLR-I/H	314.13	-38.23	44.66	23.08	24.51	75.53	88.98	-41.84	80.20	+0.80	1.90
	R95 1.22	E95	1.12	R95 4.73	E95	1.83	R95 4.77	E95	2.55		
PLR-K/H	334.79	38.03	31.44	25.02	39.26	41.21	89.29	-27.98	42.40	+0.81	1.39
	R95 1.49	E95	0.45	R95 2.14	E95	0.82	R95 1.57	E95	0.32		
PLR-L/H	322.79	-37.08	32.08	2.14	45.65	44.23	69.38	-20.70	45.28	+0.86	1.47
	R95 2.68	E95	1.36	R95 4.07	E95	0.31	R95 4.82	E95	1.78		
	R95	E95		R95	E95		R95	E95			
	R95	E95		R95	E95		R95	E95			
	R95	E95		R95	E95		R95	E95			

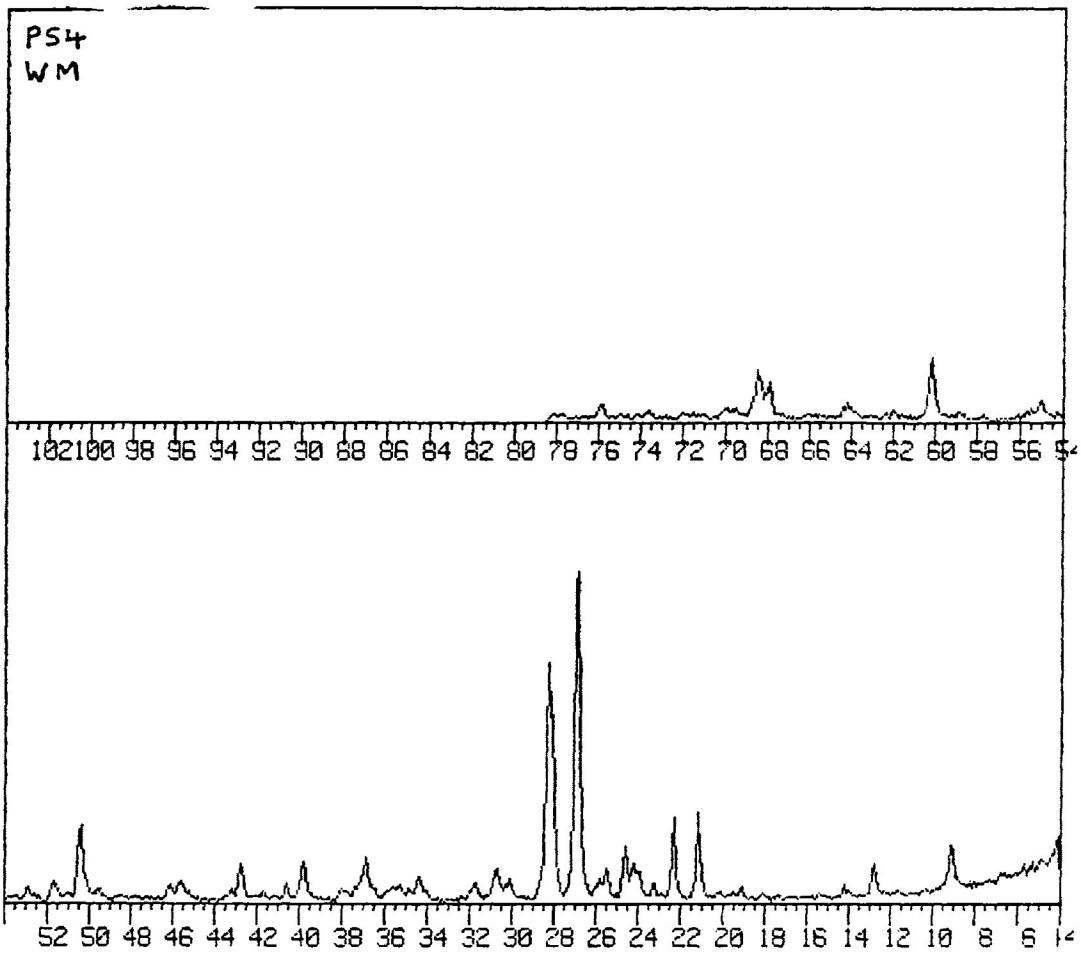
PS4
WM
102100 98 96 94 92 90 88 86 84 82 80 78 76 74 72 70 68 66 64 62 60 58 56
52 50 48 46 44 42 40 38 36 34 32 30 28 26 24 22 20 18 16 14 12 10 8 6

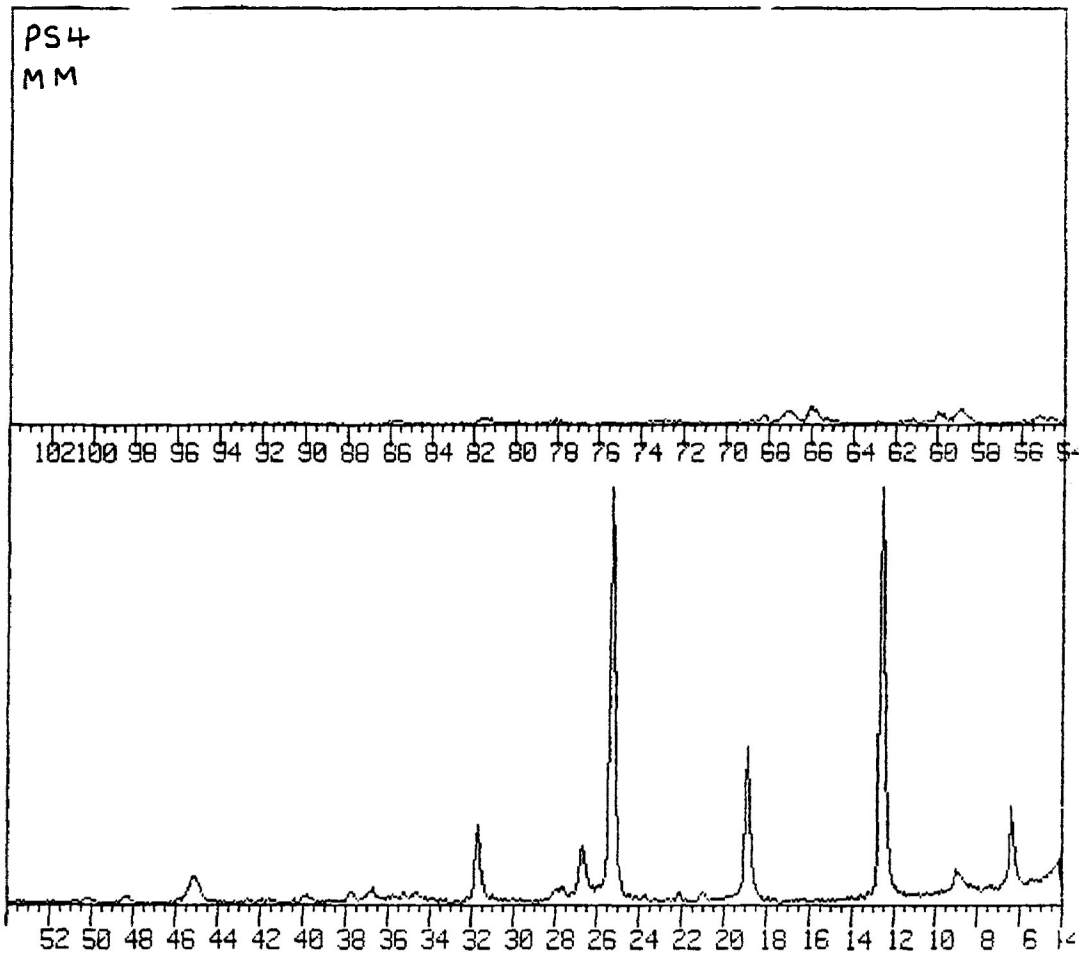
PS4
MM
102100 98 96 94 92 90 88 86 84 82 80 78 76 74 72 70 68 66 64 62 60 58 56
52 50 48 46 44 42 40 38 36 34 32 30 28 26 24 22 20 18 16 14 12 10 8 6

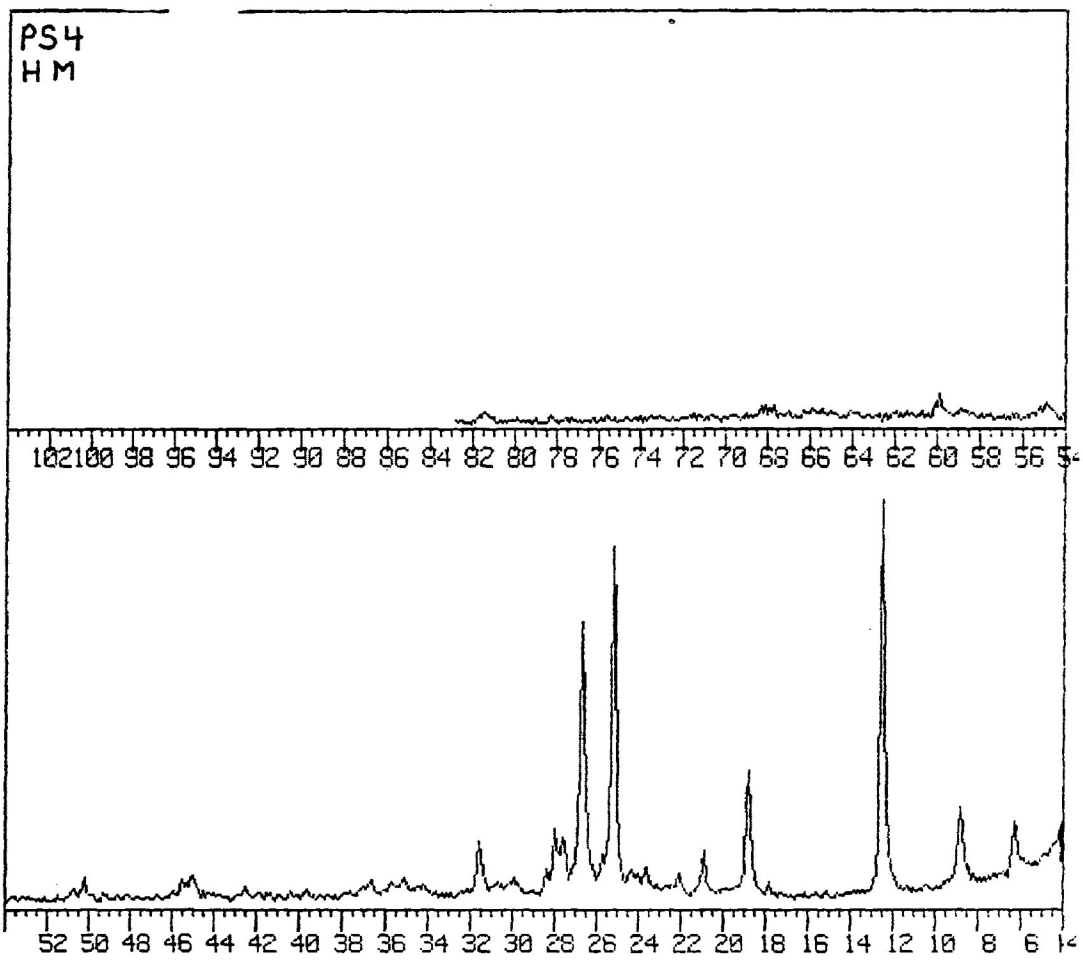
PS4
H M
102100 98 96 94 92 90 88 86 84 82 80 78 76 74 72 70 68 66 64 62 60 58 56
52 50 48 46 44 42 40 38 36 34 32 30 28 26 24 22 20 18 16 14 12 10 8 6

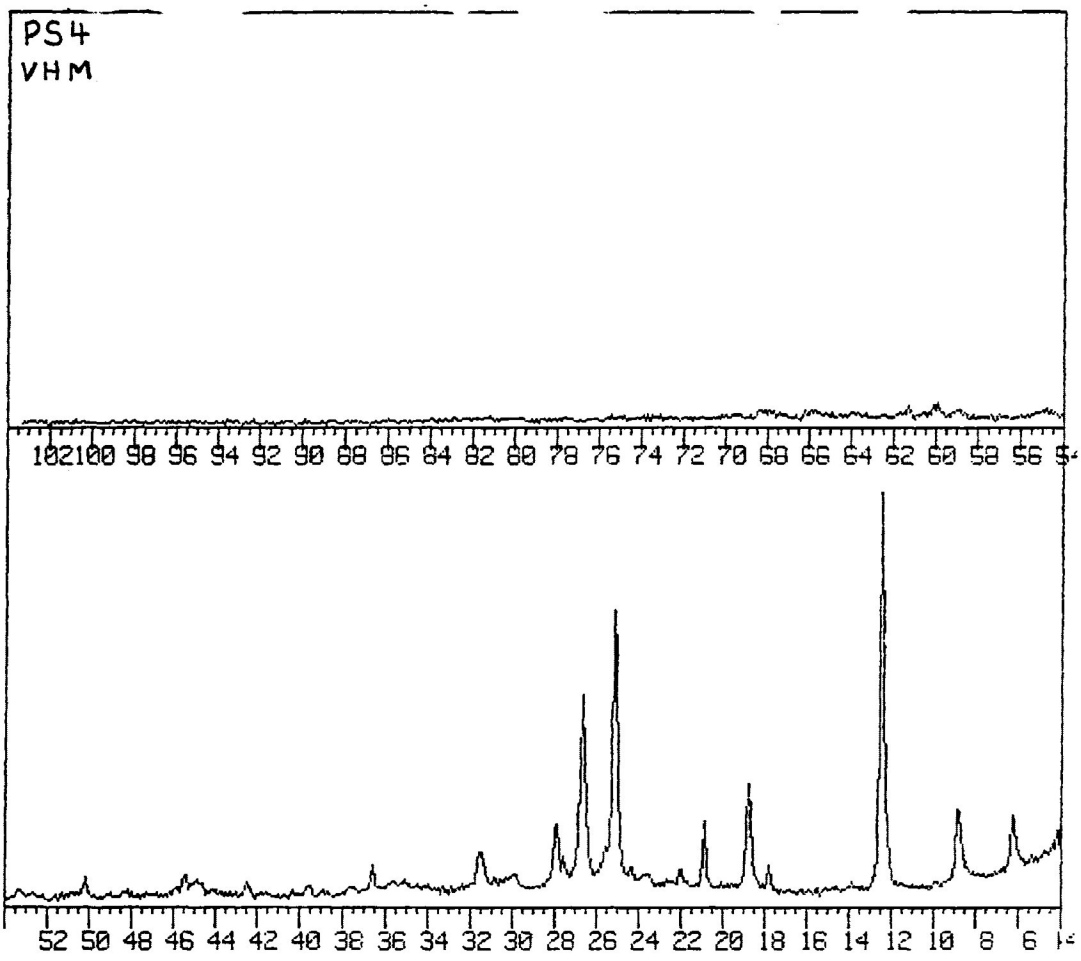
PS4
VHM
102100 98 96 94 92 90 88 86 84 82 80 78 76 74 72 70 68 66 64 62 60 58 56
52 50 48 46 44 42 40 38 36 34 32 30 28 26 24 22 20 18 16 14 12 10 8 6

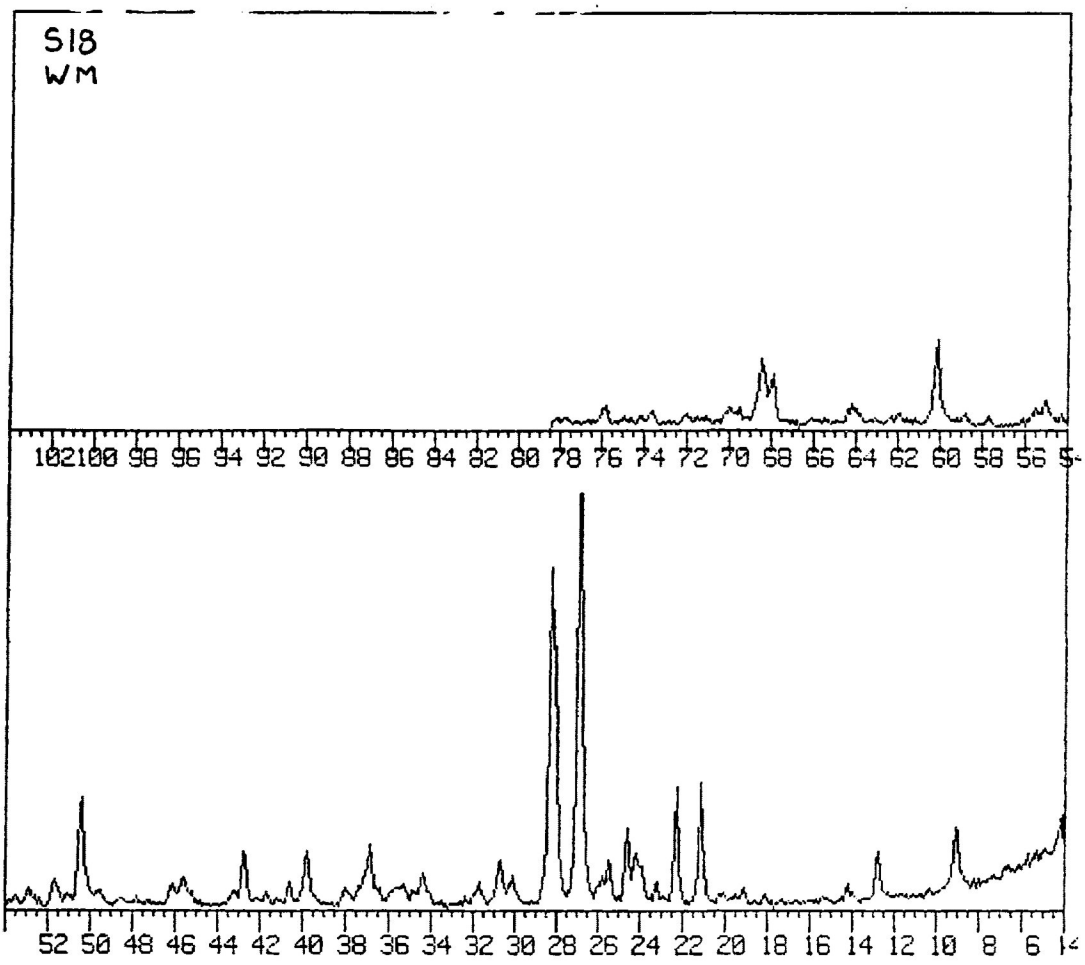
S18
WM
102100 98 96 94 92 90 88 86 84 82 80 78 76 74 72 70 68 66 64 62 60 58 56
52 50 48 46 44 42 40 38 36 34 32 30 28 26 24 22 20 18 16 14 12 10 8 6

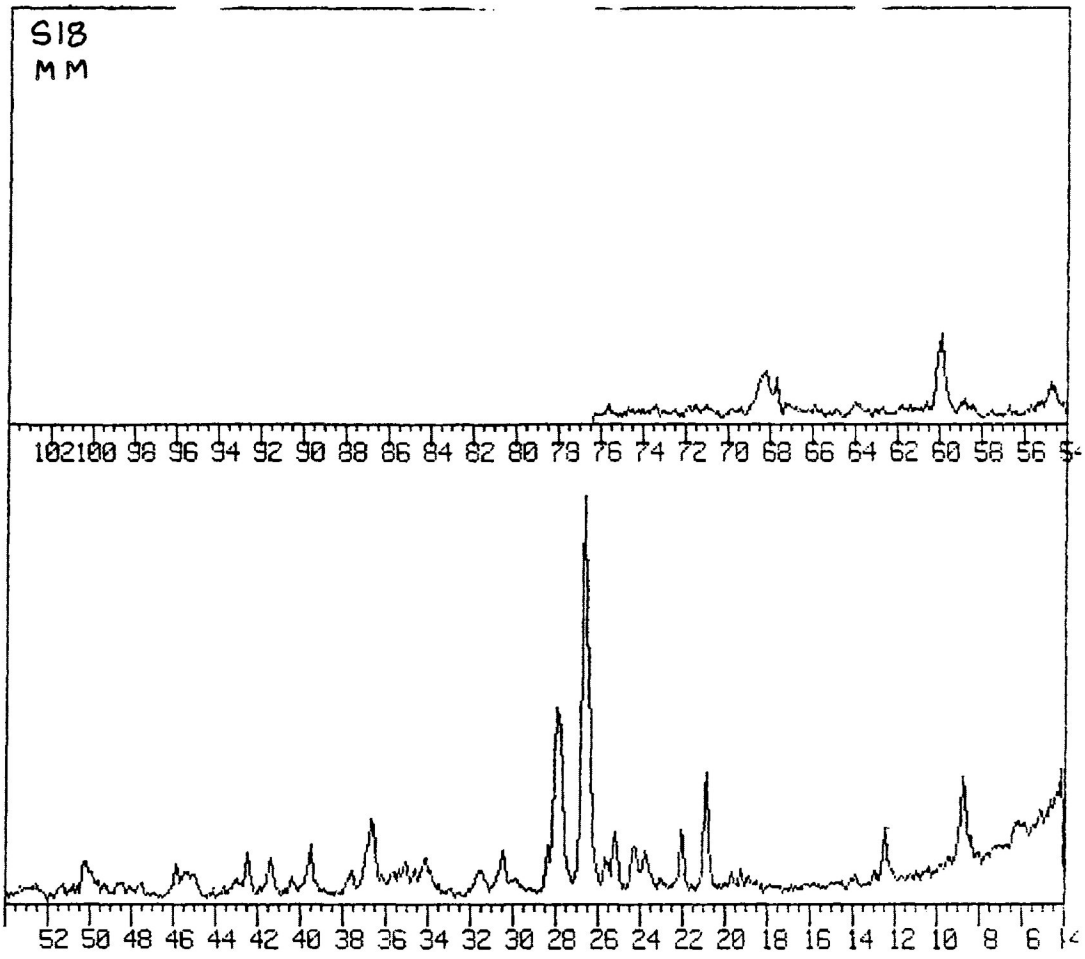
S18
MM
102100 98 96 94 92 90 88 86 84 82 80 78 76 74 72 70 68 66 64 62 60 58 56
52 50 48 46 44 42 40 38 36 34 32 30 28 26 24 22 20 18 16 14 12 10 8 6

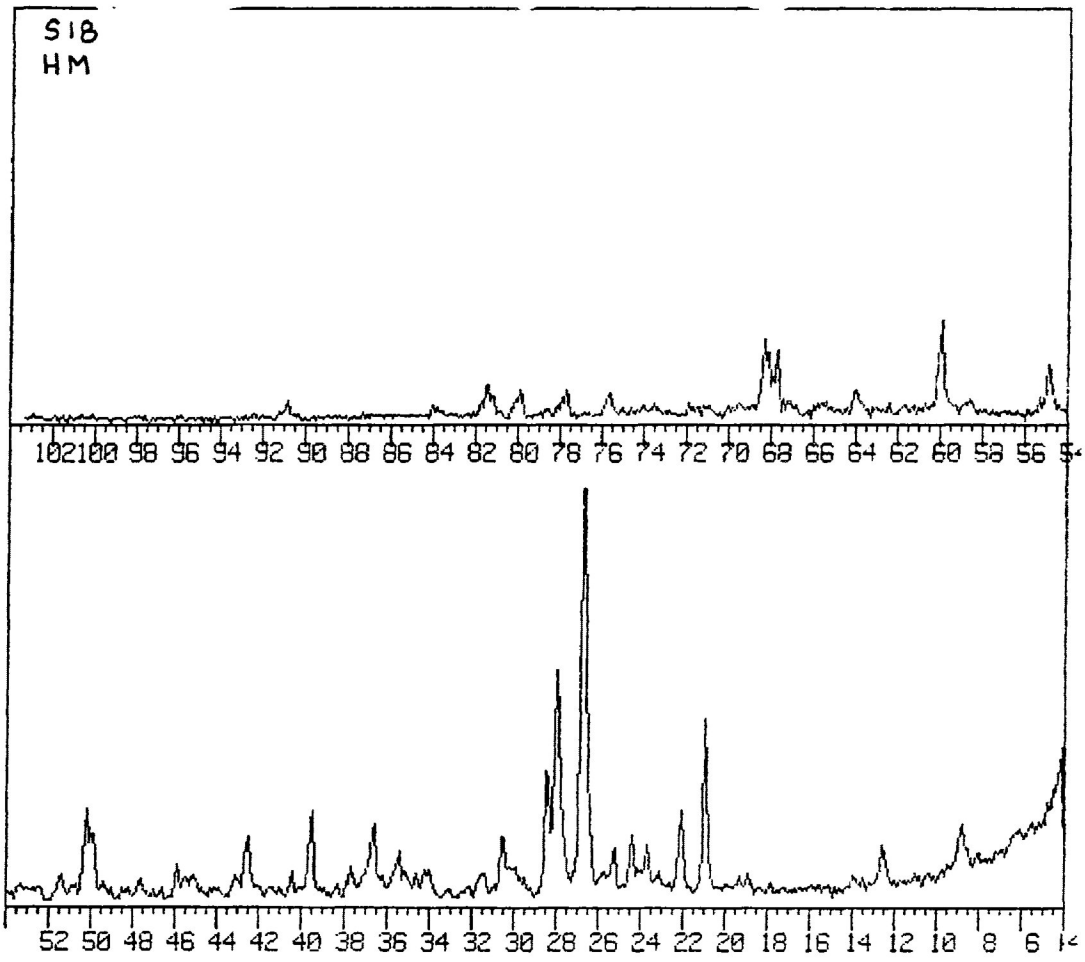
S18
HM
102100 98 96 94 92 90 88 86 84 82 80 78 76 74 72 70 68 66 64 62 60 58 56
52 50 48 46 44 42 40 38 36 34 32 30 28 26 24 22 20 18 16 14 12 10 8 6

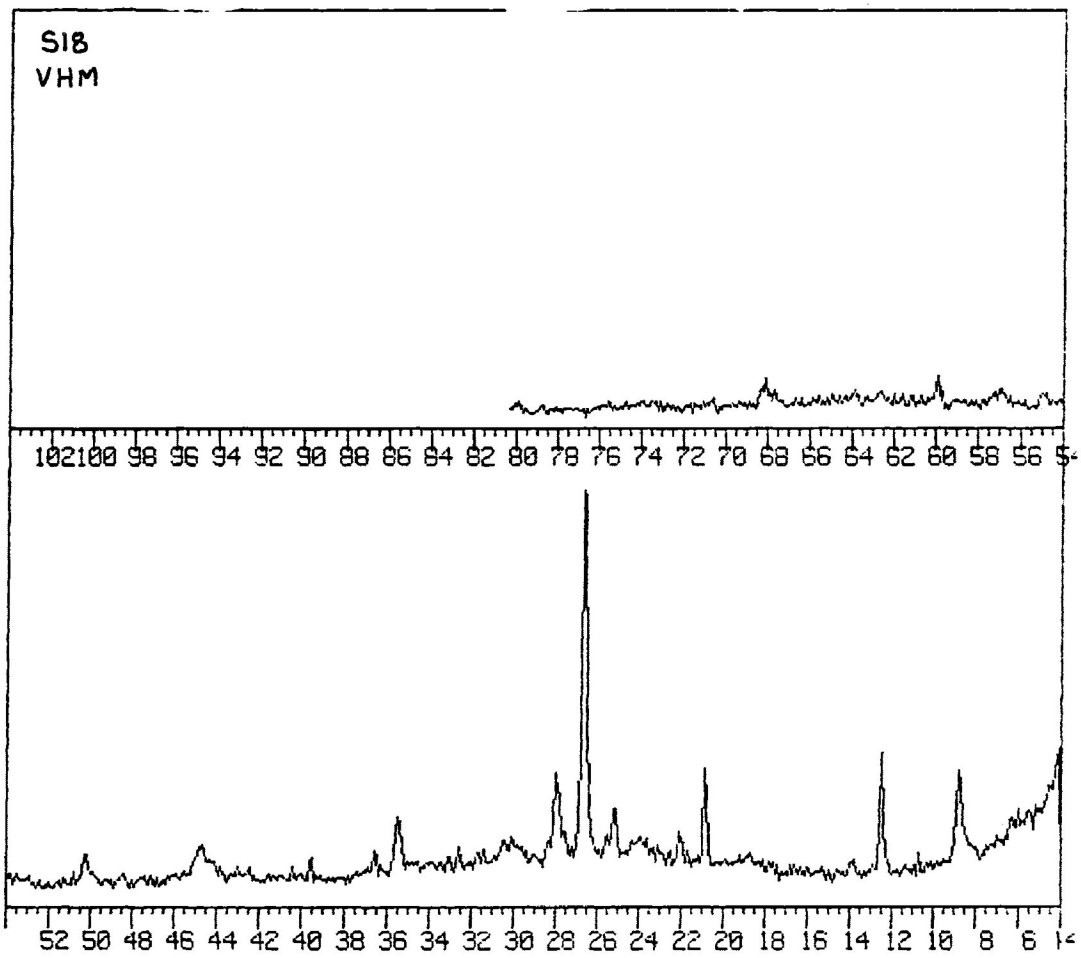
S18
VHM
102100 98 96 94 92 90 88 86 84 82 80 78 76 74 72 70 68 66 64 62 60 58 56
52 50 48 46 44 42 40 38 36 34 32 30 28 26 24 22 20 18 16 14 12 10 8 6

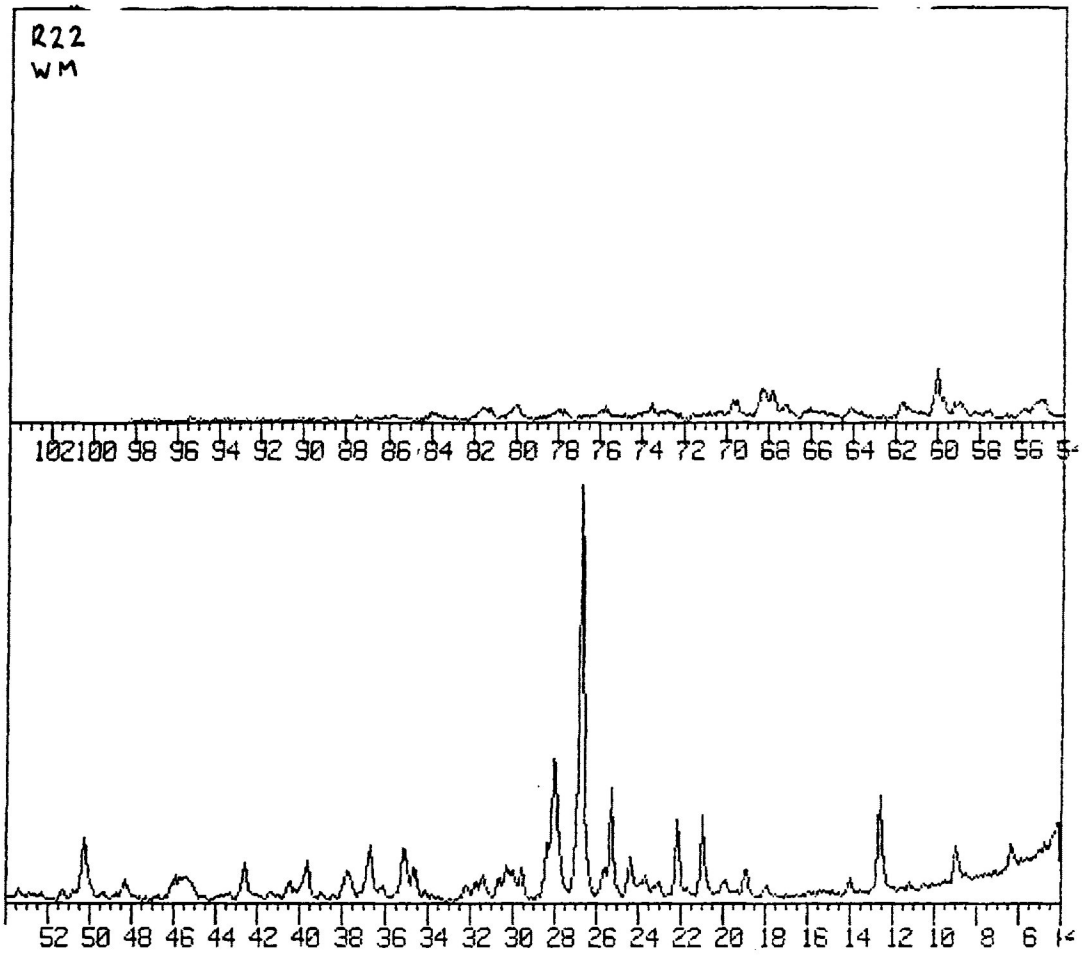
R22
WM
102100 98 96 94 92 90 88 86 84 82 80 78 76 74 72 70 68 66 64 62 60 58 56
52 50 48 46 44 42 40 38 36 34 32 30 28 26 24 22 20 18 16 14 12 10 8 6

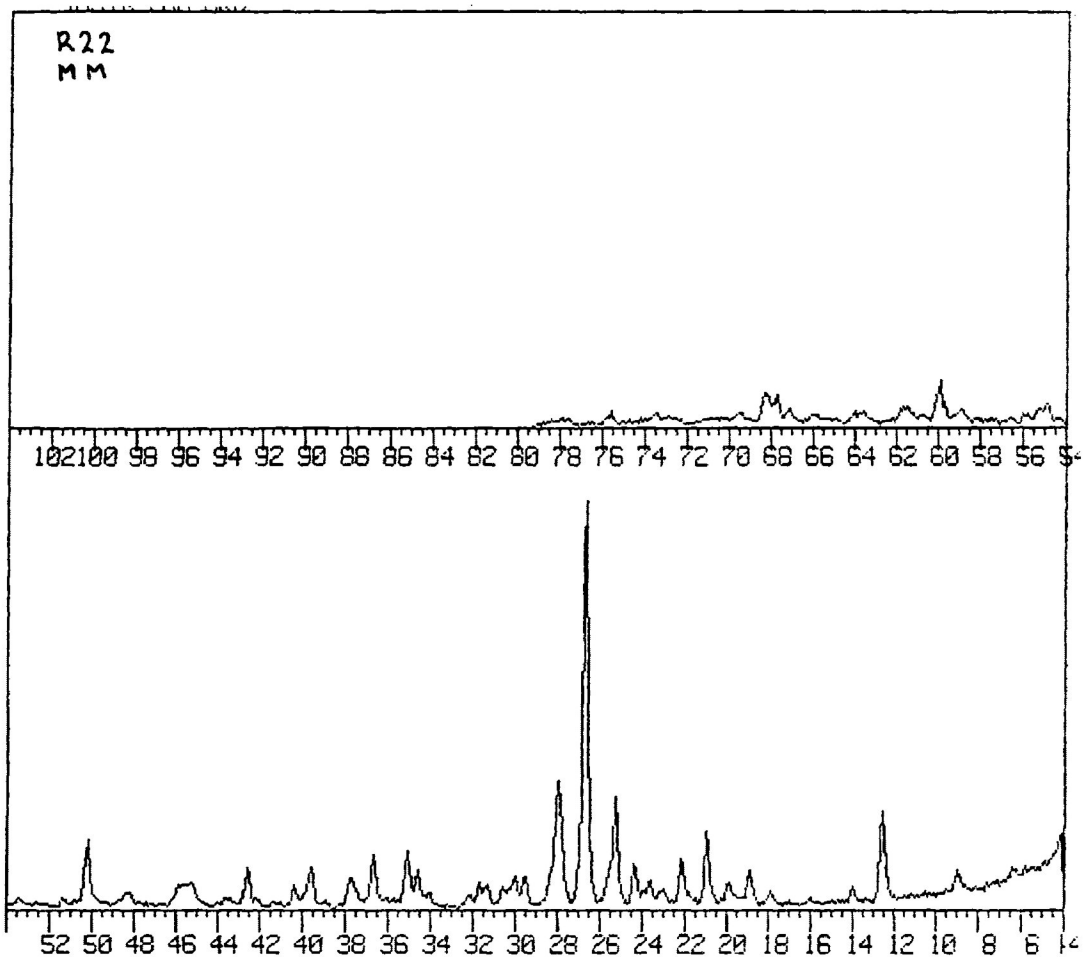
R22
M M
102100 98 96 94 92 90 88 86 84 82 80 78 76 74 72 70 68 66 64 62 60 58 56
52 50 48 46 44 42 40 38 36 34 32 30 28 26 24 22 20 18 16 14 12 10 8 6

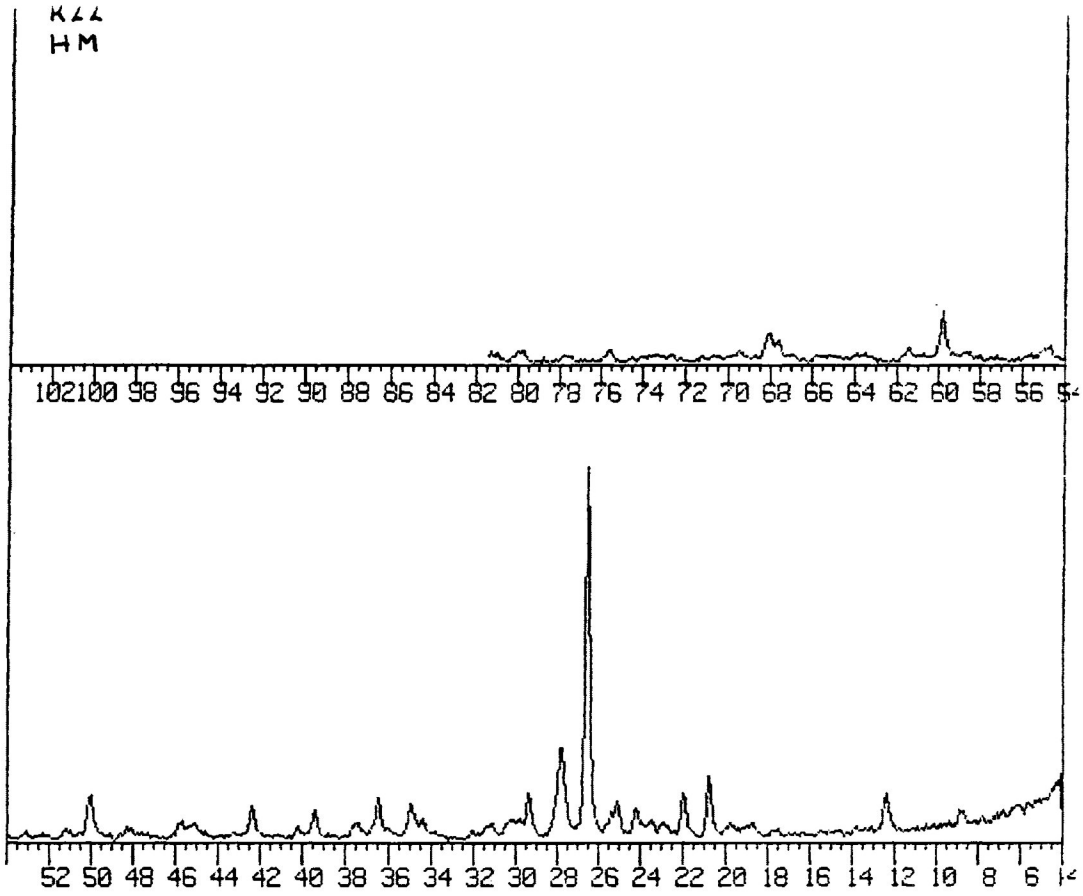
HM
102100 98 96 94 92 90 88 86 84 82 80 78 76 74 72 70 68 66 64 62 60 58 56
52 50 48 46 44 42 40 38 36 34 32 30 28 26 24 22 20 18 16 14 12 10 8 6

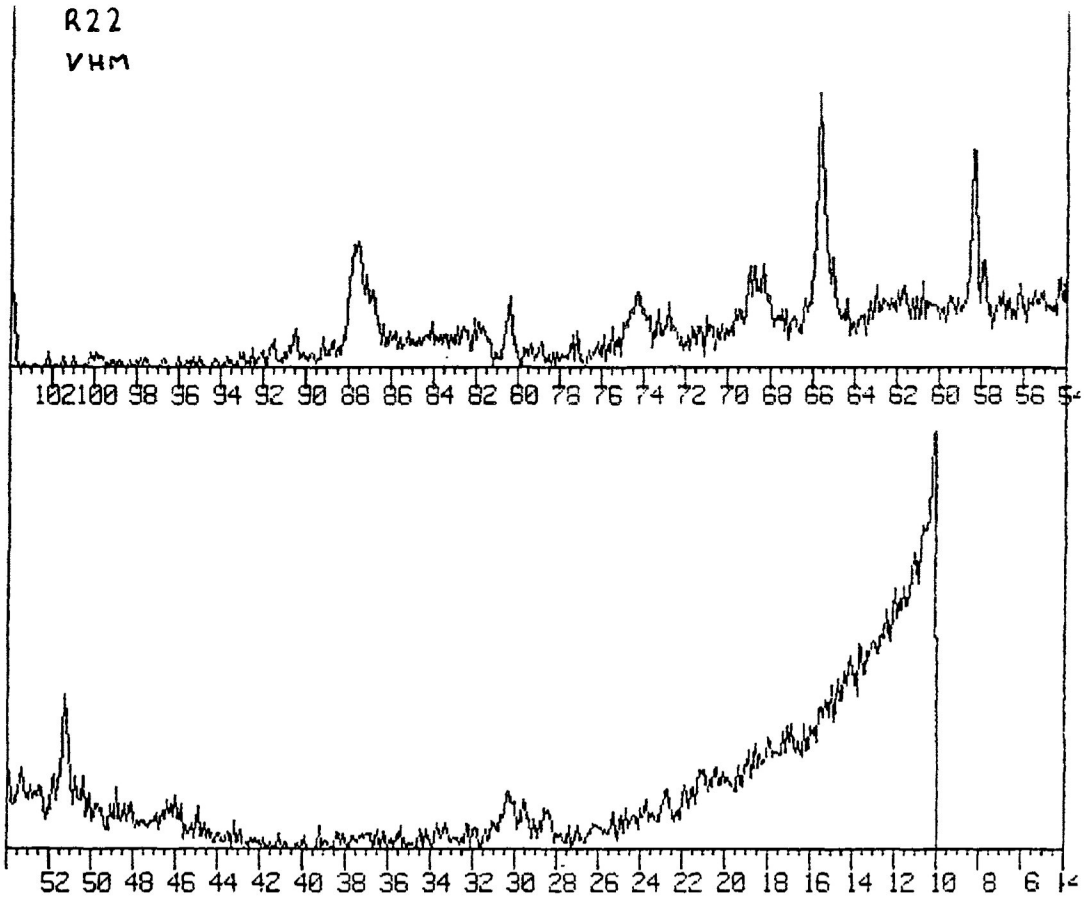
R22
VHM
102100 98 96 94 92 90 88 86 84 82 80 78 76 74 72 70 68 66 64 62 60 58 56
52 50 48 46 44 42 40 38 36 34 32 30 28 26 24 22 20 18 16 14 12 10 8 6

REFERENCES

Adams, F.D.; Bell, R.; Lane, A.C.; Leith,C.K.; Miller, W.G. and Van Hise, C.R., 1905: Report of the special committee for the Lake Superior region; J. Geol., vol. 13, p. 89-104.

Bayly, M.B., 1971: Similar folds, buckling and great-circle patterns; J. Geol., vol. 79, p. 110-118.

Bhatal, R.S., 1971: Magnetic anisotropy in rocks; Earth Sci. Rev., vol. 7, p. 227-253.

Blackburn, C.E. and Mackasey, W.O., 1977: Nature of the Quetico-Wabigoon boundary in the deCourcey-Smiley Lakes area, northwestern Ontario: Discussion; Can. J. Earth Sci., vol. 14, p.1959.

Borradaile, G.J., 1972: Variably oriented co-planar folds; Geol. Mag., vol. 109, p. 89-98.

Borradaile, G.J., 1976: "Structural Facing" (Shackleton's rule) and the Palaeozoic rocks of the Malaguide Complex near Vélez Rubio, SE Spain; Proceedings of the Koninklijke Nederlandse Akademie van Wetenschappen, Amsterdam, series B, vol. 79(5).

Borradaile, G.J., 1978: Transected folds: A study illustrated with examples from Canada and Scotland; Geol. Soc. Am. Bull., vol. 89, p. 481-493.

Borradaile, G.J., 1982: Comparison of Archean structural styles in two belts of the Canadian Superior Province; Precam. Res., vol. 19, p. 179-189.

Borradaile, G.J. and Alford, C., 1987: Relationship between magnetic susceptibility and strain in laboratory experiments; Tectonophysics, vol. 133, p. 121-135.

Borradaile, G.J. and Mothersill, J.S., 1984: Coaxial deformed and magnetic fabrics without simply correlated magnitudes of principal values; Phys. Earth Planet. Inter., vol. 35, p. 294-300.

Borradaile, G.J. and Tarling, D.H., 1981: The influence of deformation mechanisms on magnetic fabrics in weakly deformed rock. Tectonophysics, vol.77, p.151-168.

Borradaile, G.J. and Tarling, D., 1984: Strain partitioning and magnetic fabrics in particulate flow; Can. J. Earth Sci., vol. 21, p. 694-697.

Borradaile, G.J.; Mothersill, J.; Tarling, D.H. and Alford, C., 1986: Sources of magetic susceptibility in a slate; Earth Planet. Sci. Lett., vol. 76, p. 336-340.

Borradaile, G.; Keeler, W.; Alford, C. and Sarvas, P.. 1987: Anisotropy of magnetic susceptibility of some metamorphic minerals; Phys. Earth Planet. Int., vol. 48, p. 161-166.

Bouma, A.H., 1962: Sedimentology of some flysch deposits. Amstersam: Elsevier, 168 pages.

Carreras, J.; Estrada, A. and White, S., 1977: The effects of folding on the c-axis fabrics of a quartz mylonite; Tectonophysics, vol. 39, p. 3-24.

Cobbold, P.R. and Quinquis, H., 1980: Development of sheath folds in shear regimes; J. Struct. Geol., vol. 2, p. 119-126.

Cobbold, P.R. and Watkinson, A.J., 1981: Bending anisotropy: a mechanical constraint on the orientation of fold axes in an anisotropic medium; Tectonophysics, vol. 72, p. T1-T10.

Collinson, D.W., 1983: Methods in Palaeomagnetism and Rock Magnetism. London: Chapman and Hall, 500 pages.

Cummins, W.A. and Shackleton, R.M., 1955: The Ben Lui recumbent syncline (S.W. Highlands).; Geol. Mag., vol. 92, p. 353-363.

Davies, J.C., 1973: Geology of the Fort Frances area, District of Rainy River; Ont. Div. Mines, G.R. 107, 35 pages.

Dieterich, J.H., 1970: Computer experiments on mechanics of finite amplitude folds; Can. J. Earth Sci., vol. 7, p. 467-476.

Dutka, R.J.A., 1982: The structure and lithology of the Quetico metasediments in the Atikokan area; unpublished HBSc. thesis, Lakehead University, Thunder Bay, Canada.

Ellwood, B.B., 1982: Estimates of flow direction for calc-alkaline welded tuffs and palaeomagnetic data reliability from anisotropy of magnetic susceptibility measurements: central San Juan Mountains, southwest Colorado; Earth Planet. Sci. Lett., vol. 59, p. 303-314.

Fumerton, S.L., 1980: Calm Lake area, District of Rainy River. in Summary of Field Work, 1980. V.G. Milne, O.L. White, R.B. Barlow and A.C. Colvine (eds.); Ont. Geol. Surv., M.P. 96, p. 32-36.

Fumerton, S.L., 1982: Redefinition of the Quetico Fault near Atikokan, Ontario; Can. J. Earth Sci., vol. 19, p. 222-224.

Goldstein, A.G., 1980; Magnetic susceptibility of mylonites from the Lake Char mylonite zone, southeastern New England; Tectonophysics, vol. 66, p. 197-211.

Graham, J.W., 1954: Magnetic susceptibility anisotropy, and unexploited petrofabric element; Geol. Soc. Am. Bull., vol. 65, p. 1257-1258.

Graham, J.W., 1966: Significance of magnetic anisotropy in Appalachian sedimentary rocks. in The Earth beneath the Continents. J.S. Steinhart and T. Jefferson Smith (eds.). Washington D.C.: American Geophysical Union, p. 627-648.

Hamilton, N. and Rees, A.I., 1971: The anisotropy of mmagnetic susceptibility of the Franciscan rocks of the Diablo range, Central California; Geol. Rundsch., vol. 60, p. 1103-1124.

Harland, W.B., 1971: Tectonic transpression in Caledonian Spitzbergen; Geol. Mag., vol. 108, p. 27-42.

Harris, F.R., 1974: Geology of the Rainy Lake area, District of Rainy River; Ont. Div. Mines, G.R. 115, 94 pages.

Hawley, J.E., 1929: Geology of the Sapawe Lake area, with notes on some iron and gold deposits of Rainy River district; Ont. Div. Mines, vol. 38, pt. 6, p. 1-58.

Henderson, J.R., 1981: Structural analysis of sheath folds with horizontal X-axes, northeast Canada; J. Struct. Geol., vol. 3, p. 203-210.

Henry, B., 1983: Interprétation quantitative de l'anisotropie du susceptibilité magnétique (Quantitative interpretation of the magnetic susceptibility anisotropy); Tectonophysics, vol. 91, p. 165- 177.

Hobbs, B.E.; Means, W.D. and Williams, P.F., 1976: An Outline of Structural Geology. New York: John Wiley and Sons, 571 pages.

Hrouda, F., 1978: The magnetic fabric in some folds; Phys. Earth Planet. Int., vol. 17, p. 89-97.

Hrouda, F., 1983: Magnetic anisotropy of rocks and its application in geology and geophysics; Geophys. Surv., vol. 5, p. 37-82.

Hrouda, F. and Janak, F., 1976: The changes in shape of the magnetic susceptibility ellipsoid during progressive metamorphism and deformation; Tectonophysics, vol. 34, p. 135-148.

Hudleston, P.J., 1973A: Fold morphology and some geometrical implications of theories of fold development; Tectonophysics, vol. 16, p. 1-46.

Hudleston, P.J., 1973B: The analysis and interpretation of minor folds developed in the Moine rocks of Monar, Scotland; Tectonophysics, vol. 17, p. 89-132.

Hudleston, P.J., 1977: Similar folds, recumbent folds, and gravity tectonics in ice and rocks; J. Geol., vol. 85, p. 113-122.

Hudleston, P.J.; Bauer, R.L.; Southwick, D.L.; Schultz-Ela, D.D. and Bidwell, M.E., 1987: Structural geology of the boundary between Archean terranes of low-grade and high-grade rocks, northern Minnesota. in Field trip guidebook for selected areas in Precambrian geology of northeastern Minnesota. N.H. Balaban (ed.). St. Paul, Minn.: Minn. Geol. Surv., Univ. Minn. Guidebook series No. 17.

Jelinek, V., 1981: Characterization of magnetic fabric of rocks; Tectonophysics, vol. 79, p. T63-T67.

Kehlenbeck, M.M., 1976: Nature of the Quetico-Wabigoon boundary in the deCourcey-Smiley Lakes area, northwestern Ontario; Can. j. Earth Sci., vol. 13, p. 737-748.

Kennedy, M.C., 1984: The Quetico Fault in the Superior province of the Canadian Shield; unpublished MSc. thesis, Lakehead Univ., Thunder Bay, Ont.

Kligfield, R.; Lowrie, W. and Pfiffner, O.A., 1982: Magnetic properties of deformed oolitic limestones from the Swiss Alps: the correlation of magnetic anisotropy and strain; Eclog. Geol. Helv., vol. 75/1, p. 127-157.

Kuenen, P.H. and Migliorini, C., 1950: Turbidity currents as a cause of

graded bedding; J. Geol., vol. 58, p. 91-127.

Lacassin, R. and Mattauer, M., 1985: Kilometer-scale sheath fold at Mattmark and implications for transport direction in the Alps; Nature, vol. 315, p. 739-742.

Lapointe, P.; Chomyn, B.A.; Morris, W.A. and Coles, R.L., 1984: Significance of magnetic susceptibility measurements from the Lac du Bonnet Batholith, Manitoba, Canada; Geoexploration, vol. 22, p. 217-229.

Lawson, A.C., 1888: Report on the geology of the Rainy Lake Region; Geol. Nat. Hist. Surv. Can., Ann. Rept., vol. 3, pt. 1, rept. F, 183 pages.

Lawson, A.C., 1913: The Archean geology of Rainy Lake re-studied; Can. Geol. Surv., Mem. 40, 113 pages.

Lebedeva, N.B., 1982: Similarity between process of formation of axial planar cleavage and fanning cleavage. in Atlas of deformational and metamorphic rock fabrics. G.J. Borradaile, M.P. Bayly and C. McA. Powell(eds.). Berlin: Springer-Verlag. 551 pages.

Lowell, J.D., 1972: Spitsbergen Tertiary Orogenic Belt and the Spitsbergen Fracture Zone; Geol. Soc. Am. Bull., vol. 83, p. 3091-3102.

Lu, C.Y. and Wang Lee, C., 1986: The sheath folds in the Tananao Group between Tienshiang and Tailuko, east-west cross-island highway, Taiwan; Tectonophysics, vol. 125, p. 125-131.

McInnes, W., 1899: Geology of the area covered by the Seine River and Lake Shebandowan map-sheets, Rainy River and Thunder Bay districts, Ontario; Geol. Surv. Can., vol X, pt. H, 63 pages.

Milnes, A.G., 1971: A model for analyzing the strain history of folded competent layers in deeper parts of orogenic belts; Eclog. Geol. Helv., vol. 64, p. 335-342.

Minnigh, L.D., 1979: Structural analysis of sheath-folds in a meta-chert from the Western Italian Alps; J. Struct. Geol., vol. 1, p. 275-282.

Mutti, E. and Ricci Lucchi, F., 1972: Le torbiditi dell'Appennino settentrionale: introduzione all'analisi di facies; Mem. Soc. Geol. Ital., vol. 11, p. 161-199.

Noel, M., 1986: The paleomagnetism and magnetic fabric of sediments from Peak Cavern, Derbyshire; Geophys. J. Royal Astr. Soc., vol. 84, p. 445-454.

Owens, W. H., 1974: Mathematical model studies on factors affecting the magnetic anisotropy of deformed rocks; Tectonophysics, vol. 24, p. 115-131.

Owens, W.H. and Bamford, D., 1976: Magnetic, seismic, and other anisotropic properties of rock fabrics; Phil. Trans. R. Soc. Lond., A283, p. 55-68.

Owens, W.H. and Rutter, E.H., 1978: The development of magnetic susceptibility anisotropy through crystallographic preferred orientation in a calcite rock; Phys. Earth Planet. Int., vol. 16, p. 215-222.

Pettijohn, F.J.; Potter, P.E. and Siever, R., 1972: Sand and Sandstone. New York: Springer-Verlag, p. 102-292.

Pirie, J. and Mackasey, W.O., 1978: Preliminary examination of regional metamorphism in parts of Quetico metasedimentary belt, Superior province, Ontario; Geol. Surv. Can. Paper 78-10, p. 37-48.

Porath, H. and Raliegh, C.B., 1967: An origin of the triaxial basal-plane anisotropy in hematite crystals; J. Appl. Phys., vol. 38, p. 2401-2402.

Porath, H.; Stacey, F.D. and Cheam, A.S., 1966: The choice of specimen shape for magnetic anisotropy measurements of rocks; Earth Planet. Sci. Lett., vol. 1, p. 92.

Poulsen, K.H., 1980: The stratigraphy, structure and metamorphism of Archean rocks at Rainy Lake, Ontario; unpub. M.Sc. thesis, Lakehead University, Thunder Bay, Ontario.

Quinquis, H.; Audren, C.; Brun, J.P. and Cobbold, P.R., 1978: Intense progressive shear in Ile de Groix blueschists and compatibility with subduction or obduction; Nature, vol. 273, p. 43-45.

Ramdohr, P, 1969: The ore minerals and their intergrowths. Oxford. Pergamon, 1174 p.

Ramsay, J.G., 1962: The geometry and mechanisms of formation of "similar" type folds; J. Geol., vol. 70, p. 309-327.

Ramsay, J.G., 1967: Folding and fracturing of rocks. New York: McGraw-Hill, 568p.

Ramsay, J.G. and Huber, M.I., 1983: The techniques of modern structural geology. Volume One: Strain analysis. London: Academic Press, 307 p.

Rathore, J.S., 1979: Magnetic susceptibility anisotropy in the Cambrian Slate Belt of North Wales and correlation with strain; Tectonophysics, vol. 53, p. 83-97.

Rochette, P., 1987: Metamorphic control of the magnetic mineralogy of black shales in the Swiss Alps: toward the use of "magnetic isograde"; Earth Planet. Sci. Lett., vol. 84, p. 446-456.

Rochette, P. and Vialon, P., 1984: Developnent of planar and linear fabrics in Dauphinois shales and slates (French Alps) studied by magnetic anisotropy and its mineralogical control; J. Struct. Geol., vol. 6, p. 33-38.

Schwarz, E.J., 1974: Magnetic fabric in massive sulphide deposits; Can. J. Earth Sci., vol. 11, p. 1669-75.

Shackliton, R.M., 1958: Downward facing structures of the Highland border; J. Geol. Soc. Lond., vol. 113, p. 361-392.

Shklanka, R., 1972: Geology of the Steep Rock Lake area, District of Rainy River; Ont. Dept. Mines, G.R. 93, 114p.

Stephenson, A.; Sadikun, S. and Potter, D.K., 1986: A theoretical and experimental comparison of the anisotropies of magnetic susceptibility and remanence in rocks and minerals; Geophys. J. Royal Astr. Soc., vol. 84, p. 185-200.

Stewart, R. W., 1984: The structure and lothology of the Quetico metasediments in the Chub Lake-Little McCauley Lake area; unpub. H.B.Sc. thesis, Lakehead University, Thunder Bay, Ont.

Stone, D.; Kamineni, C.; Shanks, W. and Jackson, M., 1986: Geology of the Atikokan area, Map sheet C; Geol. Surv. Can., Open File 1221.

Stott, G.M. and Schwerdtner, W.M., 1981: A structual analysis of the central part of the Shebandowan metavolcanic-metasedimentary belt; Ont. Dept. Mines, Final Rept., Ont. Res. Rep. No. 5349, 44p.

Strangway, D.W., 1970: History of the Earth's magnetic field. New York: McGraw-Hill, 168p.

Stubbley, M.P., 1983: The structure and lithology of the Quetico metasediments in the Banning Lake-Seine River Area; unpub. H.B.Sc. thesis, Lakehead University, Thunder Bay, Ont.

Sullwold, H.H., 1960: Tarzana fan, deep submarine fan of late miocene age, Los Angeles county, California; Am. Assoc. Pet. Geol. Bull., vol. 44, p. 433-457.

Tanton, T.L., 1926: Recognition of the Couchiching near Steeprock Lake, Ontario; Roy. Soc. Can., Proc. and Trans., Third ser., vol. XX, pt. IV, p. 39-49.

Tarling, D.H., 1983: Palaeomagnetism: Principles and applications in geology, geophysics and archaeology. London: Chapman and Hall, 379p.

Turner;, F.J., 1981: Metamorphic petrology: Mineralogical, field and tectonic aspects. New York: McGraw-Hill, 2nd ed., 524 p.

Uyeda, S.; Fuller, M.D.; Belshe, J.C. and Girdler, R.W., 1963: Anisotropy of magnetic susceptibility of rocks and minerals; J. Geophys. Res., vol. 68, p. 279-291.

van den Ende, C., 1975: On the anisotropy of magnetic susceptibility in Permian Red Beds from the western part of the Dome de Barrot (S. France), in Progress in Geodynamics, G.J. Borradaile et. al. (eds.). Amsterdam: North Holland Publ. Co., p. 176-189.

Wagner, J.J.; Hedley, F.G.; Steen, D.; Tinkler, C. and Vaugnat, M., 1981. Magnetic anisotropy and fabric of some progressively deformed ophiolitic gabbros; J. Geophy. Res.. vol. 86, p. 307-315.

Walker, R.G., 1984: Turbidites and associated coarse clastic deposits. in Facies Models, 2nd ed. R.G. Walker(ed.); Geosci. Can. Reprint Ser. 1, p. 171-188.

Weast, R.C. and Astle, M.J.(editors), 1978: CRC Handbook of Chemistry and Physics. Palm Beach, Fla.: CRC Press Inc., 59th edition.

Wood, J., 1980: Epiclastic sedimentation and stratigraphy in the North Spirit Lake and Rainy Lake areas: a comparison; Precam. Res., vol. 12, p. 227-255.

Wood, D.S.; Oertel, G.; Singh, J. and Bennett, H.F., 1976: Strain and anisotropy in rocks; Phil. Trans. Roy. Soc. Lond., A283, p. 27-42.

Young, W.L., 1960: Geology of the Bennett-Tanner area; Ont. Dept. Mines, vol. LXIX, pt. 4, 16p.

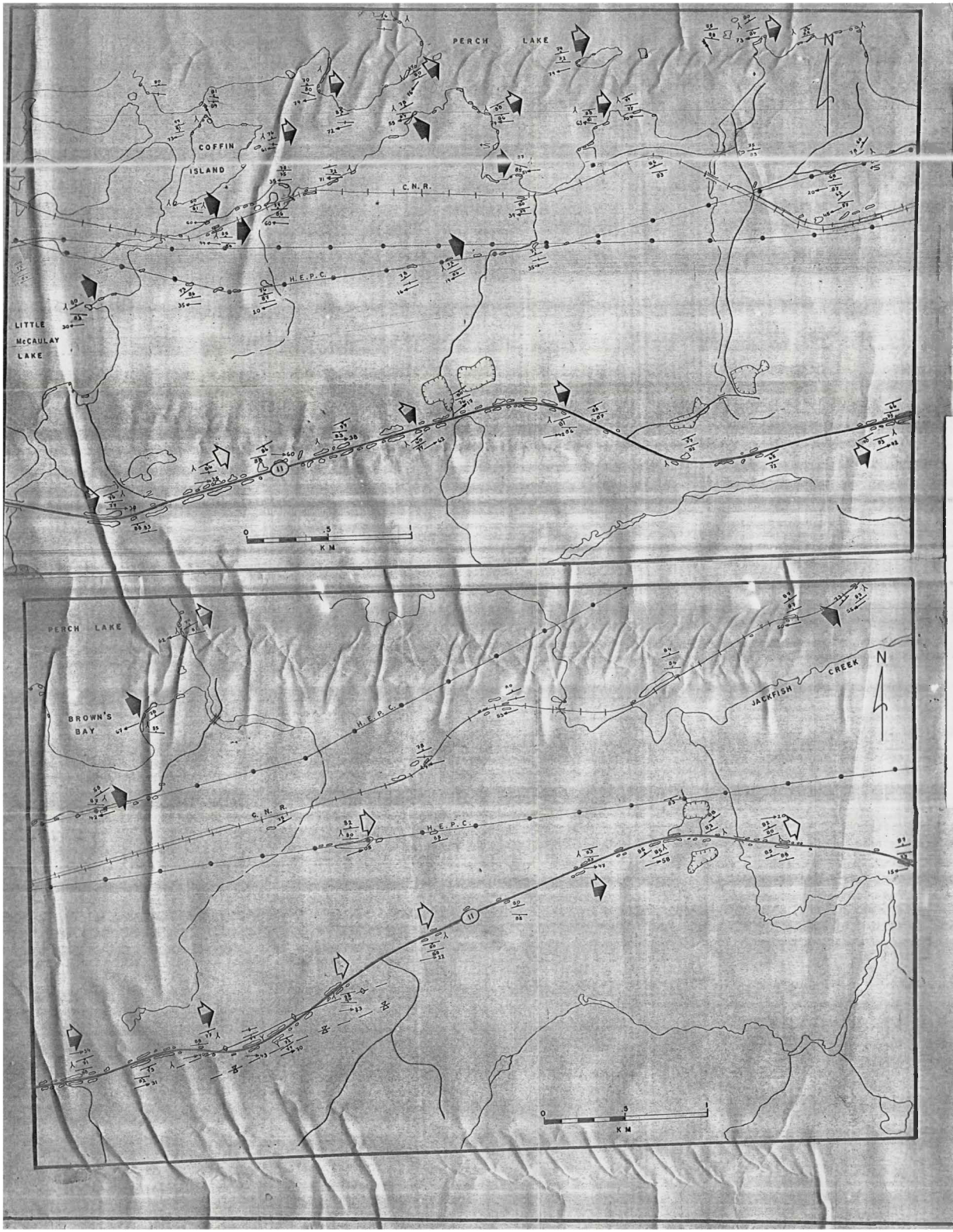

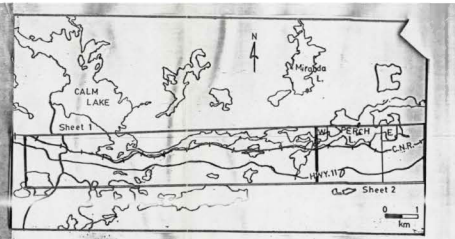

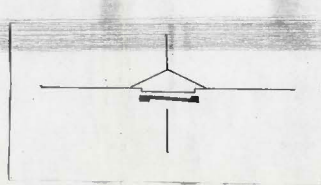

EXPLANATION OF SYMBOLS

- OUTCROP BOUNDARY
- S_0 BEDDING ORIENTATION (vertical, inclined)
- S_1 FIRST CLEAVAGE ORIENTATION (vertical, inclined)
- S_0/S_1 INTERSECTION LINEATION DIRECTION (plunge indicated)
- ASYMMETRIC MINOR FOLD (plunge of fold axis indicated)
- top — LOCAL STRATIGRAPHIC YOUNGING DIRECTION

STRUCTURAL FACING DIRECTIONS:

- UPWARD
- SIDEWAYS (±30° from horizontal)
- DOWNWARD

MAJOR FOLD AXIAL TRACES:

- SYNCLINE (delineated, inferred)
- ANTICLINE (delineated, inferred)

Perry Sarvas — Lakehead University
M.Sc. THESIS

CALM LAKE - CHUB LAKE AREA
DISTRICT OF RAINY RIVER

STRUCTURAL GEOLOGY — SHEET 2

1cm to 100m | NTS 52B/12 B 52C/9

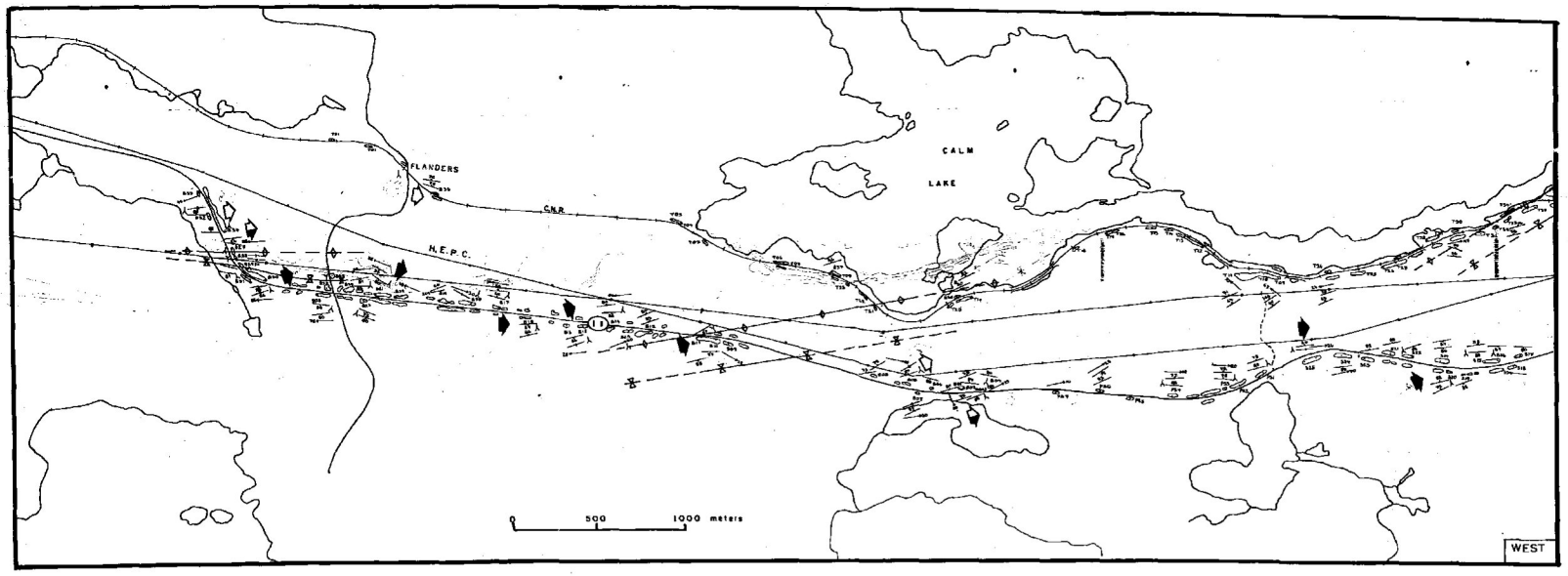

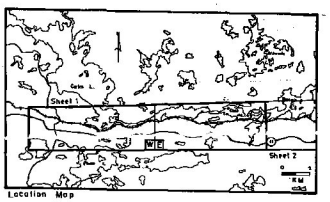

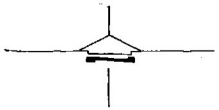

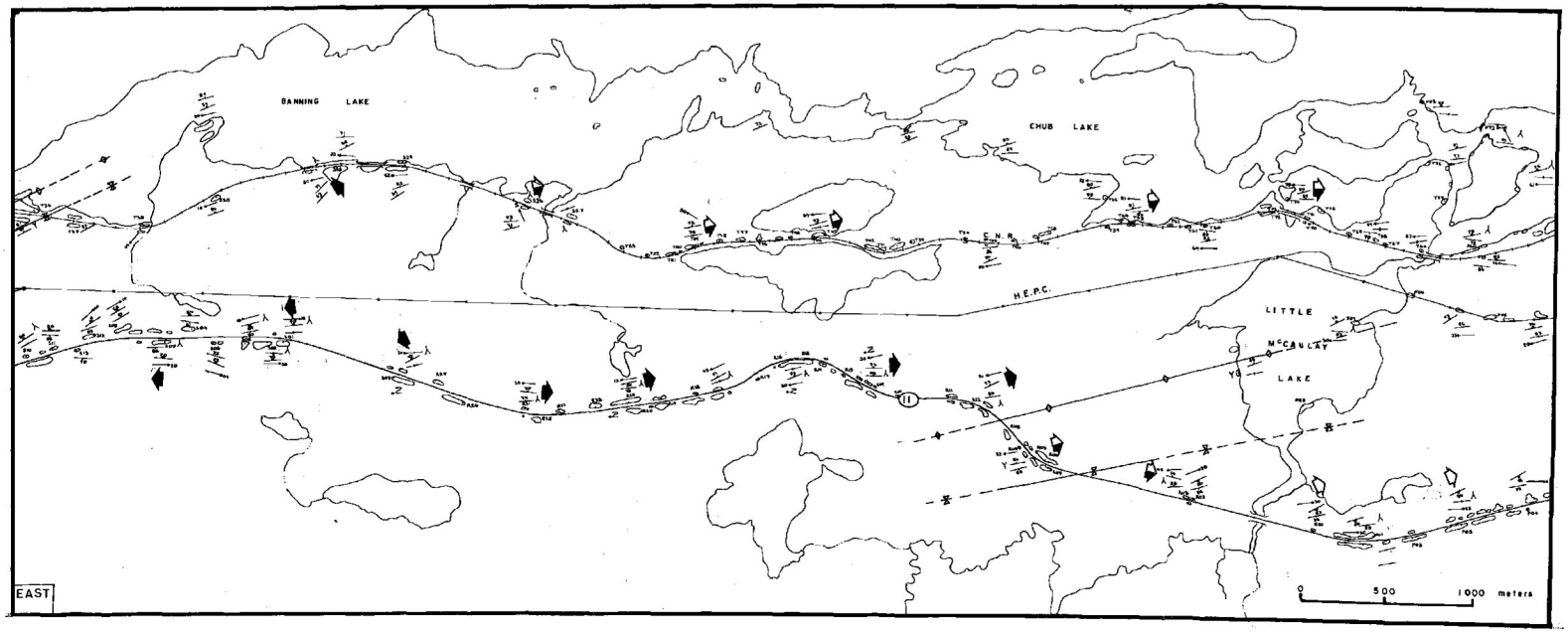

EXPLANATION OF SYMBOLS

- OUTCROP BOUNDARY
- S_0 BEDDING ORIENTATION (vertical, inclined)
- S_1 FIRST CLEAVAGE ORIENTATION (vertical, inclined)
- S_0/S_1 INTERSECTION LINEATION DIRECTION (plunge indicated)
- ASYMMETRIC MINOR FOLD (plunge of fold axis indicated)
- top LOCAL STRATIGRAPHIC YOUNGING DIRECTION

STRUCTURAL FACING DIRECTIONS:

- UPWARD
- SIDEWAYS (±30° from horizontal)
- DOWNWARD

MAJOR FOLD AXIAL TRACES:

- SYNCLINE (delineated, inferred)
- ANTICLINE (delineated, inferred)

Compiled from Borradaile(1982), Stubley(1983) and Stewart(1984)X see reference list in text), and from mapping by P. Sarvas in 1986.

Perry Sarvas — Lakehead University	
M.Sc. THESIS	
CALM LAKE - CHUB LAKE AREA	
DISTRICT OF RAINY RIVER	
STRUCTURAL GEOLOGY — SHEET 1	
1cm to 100m	NTS 52B/12 & 52C/9